



8-2007

Application of Particulate-Filled Composite (PFC) Theory to Hot-Mix Asphalt (HMA) Mixtures

Xiang Shu

University of Tennessee - Knoxville

Recommended Citation

Shu, Xiang, "Application of Particulate-Filled Composite (PFC) Theory to Hot-Mix Asphalt (HMA) Mixtures." PhD diss., University of Tennessee, 2007.

https://trace.tennessee.edu/utk_graddiss/302

This Dissertation is brought to you for free and open access by the Graduate School at Trace: Tennessee Research and Creative Exchange. It has been accepted for inclusion in Doctoral Dissertations by an authorized administrator of Trace: Tennessee Research and Creative Exchange. For more information, please contact trace@utk.edu.

To the Graduate Council:

I am submitting herewith a dissertation written by Xiang Shu entitled "Application of Particulate-Filled Composite (PFC) Theory to Hot-Mix Asphalt (HMA) Mixtures." I have examined the final electronic copy of this dissertation for form and content and recommend that it be accepted in partial fulfillment of the requirements for the degree of Doctor of Philosophy, with a major in Civil Engineering.

Baoshan Huang, Major Professor

We have read this dissertation and recommend its acceptance:

Edwin G. Burdette, Eric C. Drumm, Cheng-Xian Lin, Zukang Yao, QiuHong Zhao

Accepted for the Council:

Dixie L. Thompson

Vice Provost and Dean of the Graduate School

(Original signatures are on file with official student records.)

To the Graduate Council:

I am submitting herewith a dissertation written by Xiang Shu entitled “Application of Particulate-Filled Composite (PFC) Theory to Hot-Mix Asphalt (HMA) Mixtures”. I have examined the final electronic copy of this dissertation for form and content and recommend that it be accepted in partial fulfillment of the requirements for the degree of Doctor of Philosophy, with a major in Civil Engineering.

Baoshan Huang

Major Professor

We have read this dissertation
and recommend its acceptance:

Edwin G. Burdette

Eric C. Drumm

Cheng-Xian Lin

Zukang Yao

Qihong Zhao

Accepted for the Council:

Carolyn R. Hodges

Vice Provost and Dean of the Graduate
School

(Original signatures are on file with official student records.)

**APPLICATION OF PARTICULATE-FILLED COMPOSITE (PFC) THEORY
TO HOT-MIX ASPHALT (HMA) MIXTURES**

A Dissertation
Presented for the
Doctor of Philosophy
Degree
The University of Tennessee, Knoxville

Xiang Shu
August 2007

Copyright © 2007 by Xiang Shu
All rights reserved.

ACKNOWLEDGEMENTS

I would like to express my sincere gratitude to my advisor, Dr. Baoshan Huang, for his guidance, support, help, and encouragement throughout my doctoral study. Without his insightful suggestions on the research topics, I could not have been where I am now. I would also like to thank other professors in my doctoral committee, Dr. Edwin G. Burdette, Dr. Eric Drumm, Dr. Cheng-xian Lin, Prof. Zukang Yao, and Dr. Qihong Zhao, for taking their precious time to serve on my committee.

My thanks also go to Mr. Yip Chan for his help during sample preparation. I would like to extend my appreciation to my colleagues and friends, Mr. Randy Rainwater, Dr. Jingyao Cao, Dr. Xingwei Chen, Feng Chen, Dragon Vukosavljevic, Laura Robison, Wenbin He, Jay Bass, and Qiao Dong, for their help and friendship.

Finally, I would like to thank my wife, Zhongxin, and my daughter, Amy, for always being supportive and patient in my study. Their love and encouragement deserve special recognition.

ABSTRACT

Dynamic modulus ($|E^*|$) of HMA mixtures is one of the fundamental engineering properties measured by the Simple Performance Tester (SPT) and has been incorporated as a basic input parameter in the American Association of State Highway and Transportation Officials (AASHTO) 2002 Mechanistic-Empirical (M-E) Design Guide for flexible pavement design. Although direct laboratory testing and empirical equations (such as the Witczak model and the Hirsch model) provide two ways to obtain the values of dynamic modulus of HMA mixtures, a predictive model based on the microstructure of HMA mixtures is more desirable.

HMA mixtures consist of three phases: aggregate, asphalt binder (or mastic), and air voids. During the blending process of HMA mixtures, every aggregate particle, regardless of its size, is coated with a thin film of asphalt mastic. Therefore, the resulting mixture can be considered as a particulate-filled composite (PFC) with aggregate particles dispersed in the asphalt matrix. Consequently, the theoretical approaches for PFC can be applied to HMA mixtures.

This study presents an attempt to apply PFC models to predict the dynamic modulus of HMA mixtures. A three-dimensional two-layered model and several models from the differential method were developed and formulated. These PFC models have the ability to take into account the particular characteristics of HMA mixtures: the viscoelastic nature, aggregate gradation, and air voids.

Laboratory experiments were conducted to evaluate the applicability of the newly developed and some currently existing PFC models to HMA mixtures. Dynamic shear

rheometer (DSR) testing was conducted on asphalt binder and mastic for their dynamic shear moduli. HMA mixture was tested for its dynamic modulus.

PFC models were first applied to predict dynamic shear modulus of asphalt mastic with the measured dynamic shear modulus of asphalt binder as input parameter. The predicted dynamic shear moduli of asphalt mastic from all PFC models were fairly close to the measured results. Then, the PFC models were used to predict the dynamic modulus of HMA mixtures with dynamic shear modulus of asphalt binder or mastic as an input parameter. The predicted dynamic modulus values of HMA mixtures were found to deviate from the measured data to varying degrees.

The reasons for the discrepancy between the predicted and measured dynamic moduli were analyzed. Sensitivity analysis was conducted to explore the effects of different factors on dynamic modulus of HMA mixtures.

TABLE OF CONTENTS

CHAPTER 1	INTRODUCTION.....	1
	Research Background	1
	Importance of Dynamic Modulus in AASHTO 2002 Design Guide.....	2
	Literature Review	6
	PFC Theory	6
	Application of PFC Models to Asphalt Mastics and Mixtures and Their Limitations	14
	Latest Models for Predicting Dynamic Modulus of HMA Mixtures.....	16
	Research Objectives and Significance	21
	Arrangement of the Dissertation.....	21
CHAPTER 2	THEORETICAL BACKGROUND.....	23
	Material Properties in Linear Viscoelasticity	23
	Elastic-Viscoelastic Correspondence Principle	32
	Prony Series Representation	34
	Construction of Master Curve.....	37
CHAPTER 3	DEVELOPMENT OF THREE-DIMENSIONAL TWO-LAYERED MODEL FOR HMA MIXTURES	41
	Modeling of Three-Dimensional Two-Layered Elastic HMA Mixtures	41
	Micromechanical Model	41
	Formulation Development	43
	Complex Modulus Converted from Elastic Modulus	49

Consideration of Air Voids Effect	49
CHAPTER 4 DEVELOPMENT OF FORMULATIONS FOR PFC	
MODELS USING DIFFERENTIAL METHOD	52
Introduction.....	52
Formulation Development for Elastic and Complex Modulus Predictions	53
Formulation Development for Shear and Complex Shear Modulus Predictions.....	62
Formulation Development for Bulk and Complex Bulk Modulus Predictions	64
CHAPTER 5 LABORATORY EXPERIMENTS.....	67
Introduction.....	67
Asphalt Binder and Mastic Tests	67
Materials	67
Sample Fabrication	68
Dynamic Shear Rheometer (DSR) Testing.....	70
HMA Mixture Test	73
Materials	73
Mixture Design	75
Sample Fabrication	75
Dynamic Modulus Testing.....	77
CHAPTER 6 PREDICTION OF DYNAMIC SHEAR MODULUS	
OF ASPHALT MASTIC	81
Introduction.....	81
Determination of Input Parameter Values	82
Elastic Prediction	83

Flow Chart	83
Predictive Models	85
Prediction Results and Analyses	85
Error Analyses	94
Viscoelastic Prediction	96
Flow Chart	96
Predictive Models	96
Prediction Results and Analyses	98
Error Analyses	98
Comparison between Elastic and Viscoelastic Predictions.....	121
CHAPTER 7 PREDICTION OF DYNAMIC MODULUS OF HMA	
MIXTURE	124
Introduction.....	124
Input Parameter Values.....	126
Binder-Aggregate System Prediction	126
Flow Chart	126
Prediction Results and Analyses	130
Mastic-Aggregate System Prediction	142
Flow Chart	142
Prediction Results and Analyses	144
Analysis on Possible Reasons for Under-prediction of Dynamic Modulus	157
Sensitivity Analysis	158
Effect of Aggregate Gradation.....	161

Effect of Aggregate Modulus.....	162
Effect of Asphalt Content	163
Effect of Air Voids.....	164
CHAPTER 8 SUMMARY, CONCLUSIONS AND	
RECOMMENDATIONS.....	166
Summary	166
Research Objectives.....	166
Development of PFC Models.....	166
New Features of Proposed Models	167
Laboratory Testing.....	168
Evaluation of Proposed Models	169
Conclusions.....	169
Recommendations.....	172
REFERENCES	175
APPENDICES	183
APPENDIX A TEST DATA FOR MASTER CURVE OF ASPHALT	
 BINDER AND MASTIC	184
APPENDIX B TEST DATA FOR MASTER CURVE OF HMA MIXTURE	189
APPENDIX C EXAMPLE OF COMPUTER PROGRAM FOR PREDICTION	
 OF DYNAMIC (SHEAR) MODULI OF ASPHALT MASTIC	
 AND HMA MIXTURE.....	194
VITA	202

LIST OF FIGURES

Figure 1.1 Microstructure Schematic of HMA Mixtures.....	2
Figure 1.2 Overall Design Process for Flexible Pavements (NCHRP 2004)	4
Figure 1.3 Various Types of Micromechanical Models	7
Figure 1.4 Comparison of Different Types of Micromechanical Models	9
Figure 1.5 Hashin’s Composite Spheres Model (Christensen and Lo 1979).....	11
Figure 1.6 Christensen and Lo’s Generalized Self-Consistent Model (Christensen 1990).....	11
Figure 2.1 Stress and Strain in a Relaxation Test	25
Figure 2.2 Stress and Strain in a Creep Test.....	27
Figure 2.3 Stress and Strain in a Dynamic Modulus Test.....	29
Figure 2.4 Generalized Maxwell Model	36
Figure 2.5 Generalized Kelvin (or Voigt) Model	38
Figure 2.6 Construction of Master Curve of Dynamic Modulus	39
Figure 3.1 Three-Dimensional Two-Layered Model for HMA Mixtures	42
Figure 3.2 Air Void Size Distribution in HMA Mixture	51
Figure 3.3 Incorporation of Air Voids in Equivalent HMA mixtures	51
Figure 5.1 Particle Size Distribution of Mineral Filler	69
Figure 5.2 Microscopic Picture of Mineral Filler (400X).....	69
Figure 5.3 Asphalt Binder or Mastic Samples	70
Figure 5.4 Schematic of Dynamic Shear %Rheometer (Roberts et al. 1994).....	71
Figure 5.5 Anton Paar Physica MCR 501 Rheometer	72

Figure 5.6 Physica Rheoplus Software	73
Figure 5.7 Aggregate Gradation in HMA Mixture	74
Figure 5.8 HMA Specimens for Dynamic Modulus Test	76
Figure 5.9 Dynamic Modulus Test Setup	78
Figure 5.10 Axial Stress and Strains in Dynamic Modulus Test	78
Figure 6.1 Master Curves for Complex Shear Moduli of Asphalt Binder (25°C)	83
Figure 6.2 Flow Chart for Elastic Prediction of Dynamic Shear Modulus	84
Figure 6.3 Predicted vs. Measured Dynamic Shear Modulus of Asphalt Mastic (Model 1)	87
Figure 6.4 Predicted vs. Measured Dynamic Shear Modulus of Asphalt Mastic (Model 2)	88
Figure 6.5 Predicted vs. Measured Dynamic Shear Modulus of Asphalt Mastic (Model 3)	89
Figure 6.6 Predicted vs. Measured Dynamic Shear Modulus of Asphalt Mastic (Model 4)	90
Figure 6.7 Predicted vs. Measured Dynamic Shear Modulus of Asphalt Mastic (Model 5)	91
Figure 6.8 Predicted vs. Measured Dynamic Shear Modulus of Asphalt Mastic (Model 6)	92
Figure 6.9 Predicted vs. Measured Dynamic Shear Modulus of Asphalt Mastic (Model 7)	93
Figure 6.10 Errors in Elastic Prediction of Dynamic Shear Modulus of Asphalt Mastic	95

Figure 6.11 Flow Chart for Viscoelastic Prediction of Asphalt Mastic.....	96
Figure 6.12 Predicted vs. Measured Values of Asphalt Mastic (Model 1).....	99
Figure 6.13 Predicted vs. Measured Values of Asphalt Mastic (Model 2-1)	101
Figure 6.14 Predicted vs. Measured Values of Asphalt Mastic (Model 2-2)	103
Figure 6.15 Predicted vs. Measured Values of Asphalt Mastic (Model 3-1)	105
Figure 6.16 Predicted vs. Measured Values of Asphalt Mastic (Model 3-2)	107
Figure 6.17 Predicted vs. Measured Values of Asphalt Mastic (Model 4-1)	109
Figure 6.18 Predicted vs. Measured Values of Asphalt Mastic (Model 4-2)	111
Figure 6.19 Predicted vs. Measured Values of Asphalt Mastic (Model 5).....	113
Figure 6.20 Predicted vs. Measured Values of Asphalt Mastic (Model 6).....	115
Figure 6.21 Predicted vs. Measured Values of Asphalt Mastic (Model 7).....	117
Figure 6.22 Errors for Dynamic Shear Modulus in Viscoelastic Prediction	119
Figure 6.23 Errors for Phase Angle in Viscoelastic Prediction	120
Figure 6.24 Errors Caused by Elastic Prediction Method.....	123
Figure 6.25 Errors Caused by Elastic Prediction Method for Model 4-1	123
Figure 7.1 Schematic for Binder-Aggregate System of HMA Mixtures	125
Figure 7.2 Schematic for Mastic-Aggregate System of HMA Mixtures	125
Figure 7.3 Master Curves of Complex Shear Moduli of Asphalt Mastic at 25 v.% (25°C)	127
Figure 7.4 Flow Chart for Binder-Aggregate System Prediction	128
Figure 7.5 Relationship between Retaining Ratio and Air Voids Content	129
Figure 7.6 Predicted vs. measured $ E^* $ and ϕ of HMA mixture.....	131

Figure 7.7 Predicted vs. measured $ E^* $ and ϕ of HMA mixture (Model 1)	132
Figure 7.8 Predicted vs. measured $ E^* $ and ϕ of HMA mixture (Model 2-1)	133
Figure 7.9 Predicted vs. measured $ E^* $ and ϕ of HMA mixture (Model 2-2)	134
Figure 7.10 Predicted vs. measured $ E^* $ and ϕ of HMA mixture (Model 3-1)	135
Figure 7.11 Predicted vs. measured $ E^* $ and ϕ of HMA mixture (Model 3-2)	136
Figure 7.12 Predicted vs. measured $ E^* $ and ϕ of HMA mixture (Model 4-1)	137
Figure 7.13 Predicted vs. measured $ E^* $ and ϕ of HMA mixture (Model 4-2)	138
Figure 7.14 Predicted vs. measured $ E^* $ and ϕ of HMA mixture (Model 5)	139
Figure 7.15 Predicted vs. measured $ E^* $ and ϕ of HMA mixture (Model 6)	140
Figure 7.16 Predicted vs. measured $ E^* $ and ϕ of HMA mixture (Model 7)	141
Figure 7.17 Flow Chart for Mastic-Aggregate System Prediction	143
Figure 7.18 Predicted vs. Measured $ E^* $ and ϕ of HMA Mixture.....	145
Figure 7.19 Predicted vs. Measured $ E^* $ and ϕ of HMA Mixture (Model 1).....	146
Figure 7.20 Predicted vs. Measured $ E^* $ and ϕ of HMA Mixture (Model 2-1)	147
Figure 7.21 Predicted vs. Measured $ E^* $ and ϕ of HMA Mixture (Model 2-2)	148
Figure 7.22 Predicted vs. Measured $ E^* $ and ϕ of HMA Mixture (Model 3-1)	149
Figure 7.23 Predicted vs. Measured $ E^* $ and ϕ of HMA Mixture (Model 3-2)	150
Figure 7.24 Predicted vs. Measured $ E^* $ and ϕ of HMA Mixture (Model 4-1)	151
Figure 7.25 Predicted vs. Measured $ E^* $ and ϕ of HMA Mixture (Model 4-2)	152

Figure 7.26 Predicted vs. Measured $ E^* $ and ϕ of HMA Mixture (Model 5).....	153
Figure 7.27 Predicted vs. Measured $ E^* $ and ϕ of HMA Mixture (Model 6).....	154
Figure 7.28 Predicted vs. Measured $ E^* $ and ϕ of HMA Mixture (Model 7).....	155
Figure 7.29 Prediction Errors in Mastic-Aggregate System Prediction	156
Figure 7.30 Aggregate Gradations	159
Figure 7.31 Air Voids Size Distribution for Sensitivity Analysis	160
Figure 7.32 Effect of Aggregate Gradation	161
Figure 7.33 Effect of Aggregate Modulus	162
Figure 7.34 Effect of Asphalt Content.....	163
Figure 7.35 Effect of Air Voids	165

LIST OF TABLES

Table 1.1 Summary Statistics for the Witczak Predictive Model (Andrei et al. 1999).....	18
Table 2.1 Four Basic Viscoelastic Elements.....	35
Table 5.1 Asphalt Binder Properties.....	68
Table 5.2 Properties of Aggregates.....	74
Table 5.3 Volumetric Properties of HMA Mixture	75
Table 6.1 Values of Input Parameter in Predictive Equations	82
Table 6.2 Prony Series Constants for Relaxation Shear Modulus of Asphalt Binder	84
Table 6.3 PFC Models Used for Elastic Prediction of Asphalt Mastic	86
Table 6.4 Models Used for Viscoelastic Prediction of Asphalt Mastic	97
Table 7.1 Prony series constants for relaxation shear modulus of asphalt mastic at 25 v.%	127
Table 7.2 Input Parameters and Their Values for Sensitivity Analysis.....	160

LIST OF SYMBOLS

A	coefficient; or cross sectional area
A_1, A_2	coefficients
a	aggregate radius
a_i	radius of the opening size of the No. i sieve
a_{i+1}	radius of the opening size of the No. $(i+1)$ sieve
a_{\max}	maximum aggregate radius
a_{\min}	minimum aggregate radius
a_T	horizontal shift factor
AASHTO	American Association of State Highway and Transportation Officials
AC	asphalt content
B	coefficient
BBR	bending beam rheometer
b	aggregate radius plus thickness of asphalt mastic
C	coefficient
c	volume fraction of inclusion; or radius of equivalent medium
D	compliance; or constant
DSCM	differential self-consistent method
DSR	dynamic shear rheometer
D_g	glassy compliance
E	elastic modulus; or relaxation modulus
\bar{E}	Laplace transform of E
\tilde{E}	Carson transform of E
E'	storage modulus
E''	loss modulus
E^*	complex modulus
$ E^* $	dynamic modulus
$ E^* _{\text{air voids}}$	predicted dynamic modulus of HMA mixtures with air voids
$ E^* _{\text{no air voids}}$	predicted dynamic modulus of HMA mixtures without air voids
$ E^* _{\text{mix}}$	absolute value of mixture dynamic modulus
E_0	elastic modulus of equivalent medium
E_1	elastic modulus of asphalt mastic
E_2	elastic modulus of aggregate
E_c	elastic modulus of composite
E_c^*	complex modulus of composite
E_e	long-time equilibrium modulus
E_i	elastic modulus of inclusion
E_m	elastic modulus of matrix
E_m^*	complex modulus of matrix
F	constant

f	loading frequency
f_1	volume fraction of asphalt mastic in HMA mixture
f_2	volume fraction of aggregate in HMA mixture
f_3	volume fraction of air voids in HMA mixture
f_T	frequency at temperature T
f_{T_0}	frequency at the reference temperature T_0
G	shear modulus
G^*	complex shear modulus
$ G^* $	dynamic shear modulus
GL	gauge length
GSCM	generalized self-consistent method
$ G^* _{binder}$	absolute value of asphalt binder complex modulus
G_c	shear modulus of composite; or relaxation shear modulus of composite
G_c^*	complex shear modulus of composite
\tilde{G}_c	Carson transform of G_c
$ G^* _{elastic}$	predicted dynamic shear modulus with the elastic prediction method
G_i	shear modulus of inclusion
G_m	shear modulus of matrix; or relaxation shear modulus of matrix
\bar{G}_m	Laplace transform of G_m
\tilde{G}_m	Carson transform of G_m
G_m^*	complex shear modulus of matrix
G_{mb}	bulk specific gravity of compacted HMA mixture
G_{mm}	maximum theoretical specific gravity of loose HMA mixture
G_{sb}	bulk specific gravity of aggregate
$ G^* _{viscoelastic}$	predicted dynamic shear modulus with the viscoelastic prediction method
$H(t)$	Heaviside step function
HMA	hot-mix asphalt
i	$\sqrt{-1}$
J	creep compliance
\bar{J}	Laplace transform of J
\tilde{J}	Carson transform of J
J'	storage compliance
J''	loss compliance
J^*	complex compliance
$ J^* $	dynamic compliance
K	bulk modulus
K^*	complex bulk modulus
$ K^* $	dynamic bulk modulus
K_c	bulk modulus of composite

K_c^*	complex bulk modulus of composite
K_i	bulk modulus of inclusion
K_m	bulk modulus of matrix
K_m^*	complex bulk modulus of matrix
L	boundary at $r = c$
MTM	Mori-Tanaka method
m	number of dashpots in the generalized Maxwell model
NCHRP	National Cooperative Highway Research Program
n	number of dashpots in the generalized Kelvin model; or coefficient
\bar{P}	average loading amplitude
$P(a)$	weight fraction of aggregates with radius less than a
PAV	pressure aging vessel
p	radial stress applied at $r = c$
p_1	induced radial stress at $r = b$
p_2	induced radial stress at $r = a$
P_c	coefficient in the predictive equation of the Hirsch model by Christensen et al. (2003)
PFC	particulate-filled composite
\bar{Q}	operational relaxance
\bar{q}	polynomial in s
q_m	constant coefficient
R	retaining ratio
R^2	correlation coefficient
RTFO	rolling thin-film oven
r	radius
s	Laplace variable
SCM	self-consistent method
SPT	Simple Performance Tester
S_e	standard error of estimate
S_y	standard deviation of observed values
T	temperature
T_0	reference temperature of master curve
t_i	average time lag between peak stress and peak strain
t_p	average time for a loading cycle
\bar{U}	operational retardance
U_{mac}	strain energy when HMA is considered as a macroscopically homogeneous material
U_{mic}	strain energy when HMA is considered as a microscopically inhomogeneous material
\bar{u}	polynomial in s
u_{0b}	radial displacement of equivalent medium at $r = b$
u_{0c}	radial displacement of equivalent medium at $r = c$

u_{1a}	radial displacement of asphalt mastic at $r = a$
u_{1b}	radial displacement of asphalt mastic at $r = b$
u_{2a}	radial displacement of whole HMA mixture medium as a macroscopically homogeneous medium at $r = c$
u_c	radial displacement of aggregate at $r = a$
u_n	constant coefficient
VFA	voids filled with asphalt
VMA	voids in mineral aggregates
V_a	air void content
V_{beff}	effective bitumen content
V_i	volume fraction or concentration of inclusion
V_m	volume fraction or concentration of matrix
x	volume fraction of the lower of the first-order two constituents combined in series in the Hirsch model
x_1, x_2	coefficients; or roots of quadratic equation
$\alpha, \alpha_1 \sim \alpha_8$	coefficients
$\beta_0, \beta_1 \sim \beta_8$	coefficients
$\bar{\Delta}$	average deformation amplitude
$\delta(t)$	Dirac delta function
ε	normal strain
$\dot{\varepsilon}$	time derivative of ε
$\bar{\varepsilon}$	Laplace transform of ε
ε_0	strain amplitude
ϕ	phase angle
γ_{max}	maximum shear strain
η	bitumen viscosity
$\eta_1, \eta_2, \eta_3,$	coefficients
ρ_{34}	cumulative % retained on the 19-mm sieve
ρ_{38}	cumulative % retained on the 9.5-mm sieve
ρ_4	cumulative % retained on the 4.75-mm sieve
ρ_{200}	% passing the 0.075-mm sieve
ρ	relaxation time
σ	normal stress
$\dot{\sigma}$	time derivative of σ
$\bar{\sigma}$	Laplace transform of σ
σ_0	stress amplitude
σ_{ss}	steady state stress response
$\bar{\sigma}_{ss}$	Laplace transform of σ_{ss}
τ	retardation time
τ_{max}	maximum shear stress
ν_0	Poisson's ratio of equivalent medium

ν_1	Poisson's ratio of asphalt mastic
ν_2	Poisson's ratio of aggregate
ν_i	Poisson's ratio of inclusion
ν_m	Poisson's ratio of matrix
ω	radian frequency
ξ	coefficient

CHAPTER 1 INTRODUCTION

Research Background

Flexible pavements are widely used in the United States and all over the world. Hot mix asphalt (HMA) mixtures are commonly used in flexible pavements as surface and load carrying layers. HMA mixtures consist of asphalt cement binder, coarse and fine aggregates, and mineral filler mixed together at a high temperature and placed and compacted on the road while still hot.

During the mixing process of HMA mixtures, every aggregate particle, regardless of its size, is coated with a thin film of asphalt cement mastic (asphalt cement + mineral filler). Therefore, the resulting asphalt mixtures can be considered as a composite material with aggregate particles and air voids dispersed in the asphalt mastic matrix (Figure 1.1) (Li et al. 1999; Huang et al. 2007). Thus, HMA mixtures actually belong to a class of materials known as particulate filled composite (PFC) materials, which, by definition, consist of a single continuous phase (asphalt cement mastic) and one or more discontinuous particulate phases (aggregate particles) (Young et al. 1998).

As a composite material, the overall (or effective) behavior of HMA mixture is totally dependent on the properties and volumetric fractions of the individual constituents and their interactions. The overall properties of HMA mixture (such as effective modulus, effective strength, etc) can also be theoretically determined, provided that the properties and volumetric fractions of the individual constituents are already known.

Particulate filled composite (PFC) theory is one of the most widely used micromechanics-based modeling techniques to characterize the overall physical,

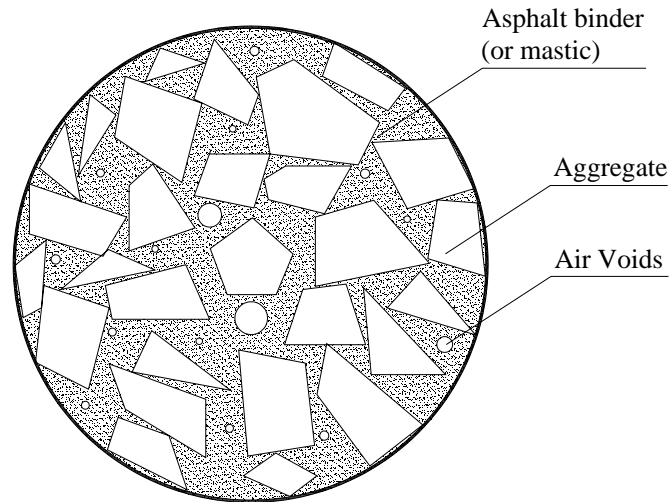


Figure 1.1 Microstructure Schematic of HMA Mixtures

mechanical, thermal, magnetic behavior of composites (Nemat-Nasser and Hori 1999). However, its application has long been limited to ceramic, metal, and polymer matrix composites other than asphalt mixtures (Christensen 1979; Nemat-Nasser and Hori 1999). In recent years, research efforts have been made to apply PFC theory to predict the mechanical properties of asphalt mastics and mixtures, such as elastic modulus, resilient modulus, dynamic (complex) modulus, and tensile strength (Lytton 1990; Buttlar and Roque 1996; Buttlar et al. 1999; Li et al. 1999; Shashidhar and Shenoy 2002; Huang et al. 2003, 2007; Kim and Little 2004; Li and Metcalf 2005).

Importance of Dynamic Modulus in AASHTO 2002 Design Guide

With the transition of flexible pavement design from empirical to mechanistic-empirical method, modulus or stiffness has long been considered one of the most important mechanical properties of HMA mixtures (Li et al. 1999; Huang 2004). In the pavement analysis with the mechanics method, modulus of HMA mixtures is a necessary

input parameter to calculate the stress and strain in the pavement layers under various traffic loadings. From the calculated stress and strain, the pavement performance can be predicted using the empirical relationships developed from long term observation and experience (Huang 2004).

However, use of an elastic stiffness parameter, such as elastic modulus or resilient modulus, cannot accurately characterize the viscoelastic properties of HMA mixtures resulting from asphalt binder. In the newly approved and implemented American Association of State Highway and Transportation Officials (AASHTO) 2002 Mechanistic-Empirical (M-E) Design Guide for new and rehabilitated pavement structures, the dynamic modulus $|E^*|$ was selected as one of the important material property input parameters for flexible pavement design. Dynamic modulus can reflect the temperature and frequency dependency of HMA mixture properties (NCHRP 2004).

In the pavement analysis according to the AASHTO 2002 M-E Design Guide, dynamic modulus value of HMA mixtures (among the other material properties needed), together with other design inputs (such as traffic loading, environmental conditions, and pavement structure) is used to predict the distress of flexible pavements with the distress prediction models and to make sure that the final designed pavement can meet all the requirements of pavement design (Figure 1.2).

Dynamic modulus $|E^*|$ is one of the fundamental engineering properties widely used to characterize the viscoelastic behavior of HMA mixtures. There are many ways available to obtain the dynamic modulus value of HMA mixtures. The most reliable one is through direct laboratory testing on HMA specimens at different loading frequencies

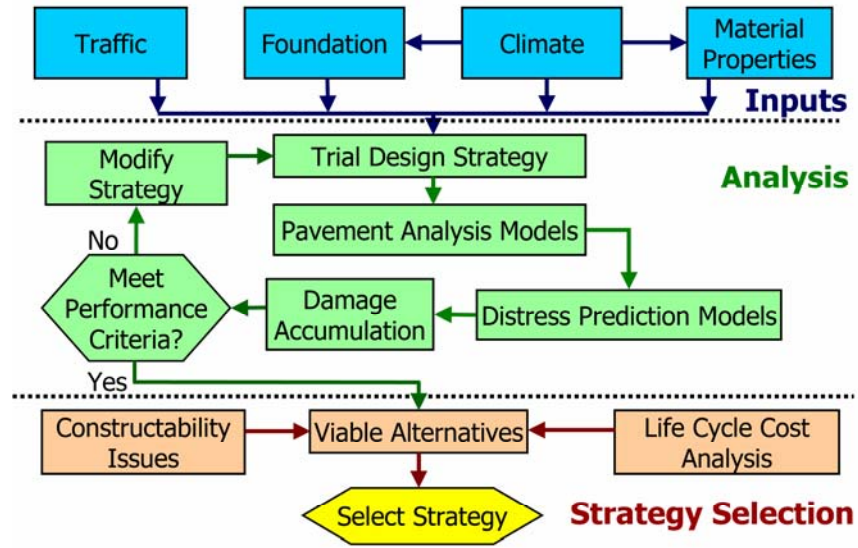


Figure 1.2 Overall Design Process for Flexible Pavements (NCHRP 2004)

and temperatures. However, dynamic modulus measurements are hard to obtain in laboratory testing under extreme conditions of temperatures or loading frequencies. Besides, laboratory testing is usually more costly and time-consuming than other methods. Currently, dynamic modulus can also be estimated using available empirical relationships, such as the Witczak model and the Hirsch model (Andrei et al. 1999; Christensen et al. 2003; Dongré et al. 2005).

The AASHTO 2002 M-E Design Guide employs the hierarchical approach for determining pavement design inputs based on the philosophy that the level of engineering efforts exerted in the pavement design process should be consistent with the relative importance, size, and cost of the design project. The hierarchical approach provides three levels of dynamic modulus input (NCHRP 2004):

- Level 1 material input provides the highest level of accuracy and requires the direct measurement of dynamic modulus of HMA mixtures through laboratory or field testing.
- Level 2 provides an intermediate level of accuracy. It does not require dynamic modulus testing. In level 2, the Witczak model is recommended to be used to predict the dynamic modulus value with laboratory measured binder stiffness or viscosity.
- Level 3 provides the lowest level of accuracy and thus does not require the laboratory testing for binder stiffness or viscosity. In level 3, the dynamic modulus predictions use the default binder properties established for all binder grades in the 2002 M-E Design Guide.

In parallel with incorporating dynamic modulus in pavement analysis and design as a basic input parameter, the dynamic modulus test has also been selected as a Simple Performance Tester (SPT) in the Superpave mixture design to provide the dynamic modulus value of HMA mixtures under the NCHRP 9-19 project: “Superpave Support and Performance Models Management” and NCHRP 9-29 project: “Simple Performance Tester for Superpave Mix Design” (NCHRP 2003; Bonaquist 2003).

However, a problem arises regarding whether accurate dynamic modulus prediction can be obtained from the empirical relationships. The empirical predictive equations can give satisfactory estimates only under conditions in which they were developed. Since there are so many types of asphalt binder and aggregates used in HMA mixtures, it is very hard, if not impossible, to establish a universal relationship that can be applied to all the HMA mixtures.

Recent studies show that PFC theory provides another possible approach for obtaining the dynamic modulus values of HMA mixtures (Huang et al 2007; Buttlar and Roque 1996; Buttlar et al. 1999; Li et al. 1999; Shashidhar and Shenoy 2002). This micromechanics approach is based on the fact that HMA mixtures are actually a composite material composed of three phases: aggregates, asphalt mastic, and air voids (Figure 1.1).

Literature Review

PFC Theory

PFC materials have been widely used in various industries due to their low production cost, ease of manufacture, and good properties (such as thermal stability, macroscopic isotropicity). Numerous particulate micromechanical models have been proposed to characterize the overall properties of PFC materials based on the properties and volume fractions of individual components and their interactions.

The parallel (or Voigt) model (Figure 1.3a) and the series (or Reuss) model (Figure 1.3b) are two commonly used micromechanical models (Paul 1960). The effective elastic modulus of the composites for the parallel and the series models can be calculated as follows:

$$E_c = E_i V_i + E_m V_m \quad (\text{Parallel model}) \quad (1.1)$$

$$\frac{1}{E_c} = \frac{V_i}{E_i} + \frac{V_m}{E_m} \quad (\text{Series model}) \quad (1.2)$$

where

E_c = effective elastic modulus of composite;

E_i = elastic modulus of inclusion;

E_m = elastic modulus of matrix;

V_i = volume fraction of inclusion; and

V_m = volume fraction of matrix.

The parallel model, in which the two component phases are subject to uniform strains, provides the upper-bound solution for the elastic modulus. Eq.(1.1) is now commonly known as the law of mixtures, or the rule of mixtures. The series model, in

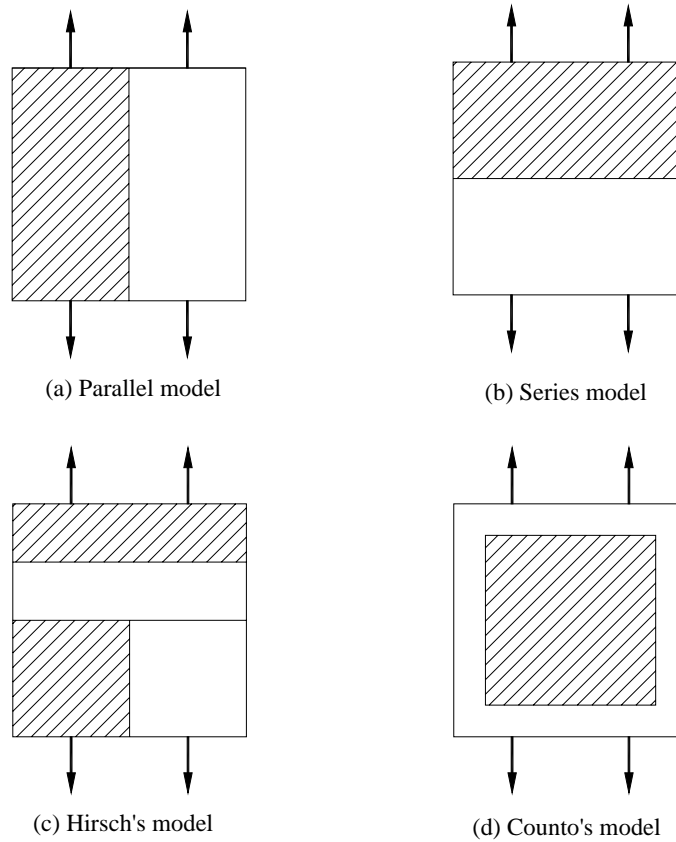


Figure 1.3 Various Types of Micromechanical Models

which the two component phases are subject to uniform stresses, provides the lower-bound solution for the elastic modulus.

These two models provide such a broad range in the prediction of elastic modulus when the constituent properties differ greatly that they actually offer no practical use but a rough estimate. Therefore, more complex composite models have been developed to give more realistic representations of particulate composites. The Hirsch model (Figure 1.3c) and the Counto model (Figure 1.3d) are two of these models (Hirsch 1961, 1962; Counto 1964). They give the following predictive equations:

$$\frac{1}{E_c} = x \frac{1}{E_i V_i + E_m V_m} + (1-x) \left(\frac{V_i}{E_i} + \frac{V_m}{E_m} \right) \quad (\text{Hirsch model}) \quad (1.3)$$

$$\frac{1}{E_c} = \frac{1 - \sqrt{V_i}}{E_m} + \frac{\sqrt{V_i}}{(1 - \sqrt{V_i})E_m + \sqrt{V_i}E_i} \quad (\text{Counto model}) \quad (1.4)$$

where

x = volume fraction of the lower of the first-order two constituents combined in series in the Hirsch model; and

$1-x$ = volume fraction of the upper of the first-order two constituents combined in series in the Hirsch model.

These four above-mentioned particulate micromechanical models are compared graphically in Figure 1.4.

In 1957, Eshelby developed an important concept of equivalent medium which forms the basis for the mechanics of composite materials (Eshelby 1957). Since then, many more sophisticated models and methods have been proposed to predict the properties of PFC. These models based on the equivalent medium can be divided into

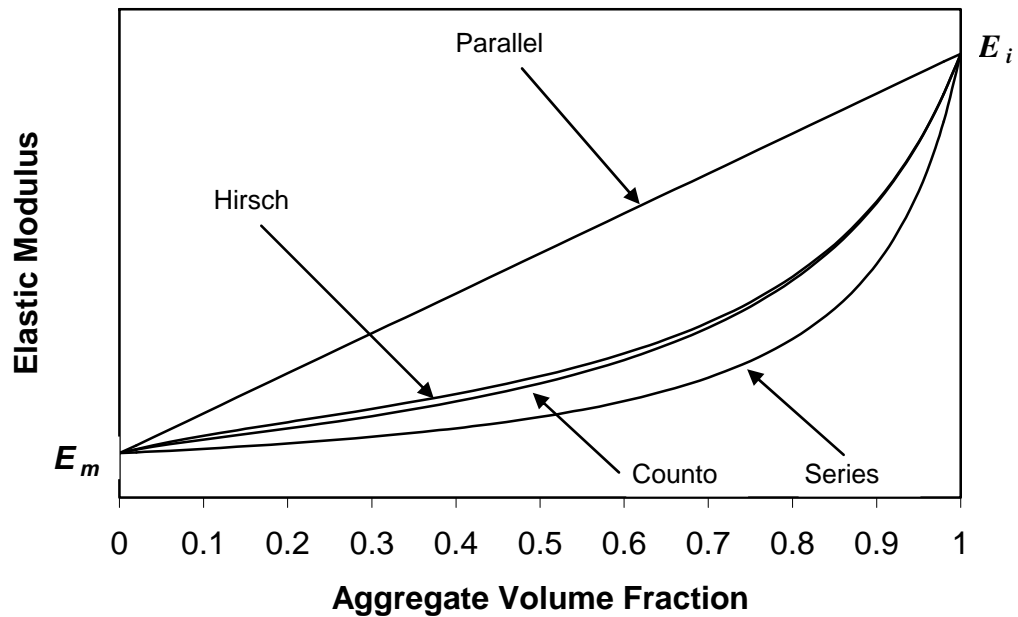


Figure 1.4 Comparison of Different Types of Micromechanical Models
 (Assuming $E_i = 10 E_m$, $x = 0.5$ for the Hirsch model)

two main categories. The first one is the dilute model with the assumption that a single inclusion is embedded in an infinite matrix subjected to a remote loading in the composites (Christensen 1979). Due to the failure to take into account the inclusion distribution and interaction between inclusion and matrix, the dilute model is not suitable for high inclusion-concentrated composites (such as HMA mixtures). To account for the inclusion interaction, many other models have been developed. Among them are the self-consistent method (SCM) (Hill 1965), the differential self-consistent method (DSCM) (McLaughlin 1977), the generalized self-consistent method (GSCM) (Christensen and Lo 1979, 1986), and Mori-Tanaka method (MTM) (Mori and Tanaka 1973). The generalized self-consistent method is a more sophisticated micromechanical approach. It is based on a

three-phase model: an inclusion is embedded in a finite matrix, which in turn is embedded in an infinite equivalent medium of the composite. Christensen gave a critical evaluation of the GSCM estimate and the corresponding DSCM and MTM estimates for the shear modulus of PFC (Christensen 1990).

In recent years, many research efforts have been directed to use the particulate micromechanical models to determine the stiffness or modulus of asphalt mastics and mixtures, among which are the Hashin's composite sphere model (Figure 1.5) and the Christensen and Lo's generalized self-consistent model (Figure 1.6). The composite sphere model proposed by Hashin (1962) consists of a series of perfectly packed spherical inclusions coated with concentric shell matrix. It is also assumed that all composite spheres have identical particle-to-matrix diameter ratios (a/b , see Figure 1.5) and are completely bounded by adjacent composite spheres. Hashin derived the exact solution to the effective bulk modulus of the model and also provided a good estimate of the effective shear modulus as follows:

$$\frac{K_c}{K_m} = 1 + \frac{3(1 - \nu_m) \left(\frac{K_i}{K_m} - 1 \right) c}{2(1 - 2\nu_m) + (1 + \nu_m) \left[\frac{K_i}{K_m} - \left(\frac{K_i}{K_m} - 1 \right) c \right]} \quad (1.5)$$

and

$$\frac{G_c}{G_m} = 1 + \frac{15(1 - \nu_m) \left(\frac{G_i}{G_m} - 1 \right) c}{7 - 5\nu_m + 2(4 - 5\nu_m) \left[\frac{G_i}{G_m} - \left(\frac{G_i}{G_m} - 1 \right) c \right]} \quad (1.6)$$

where

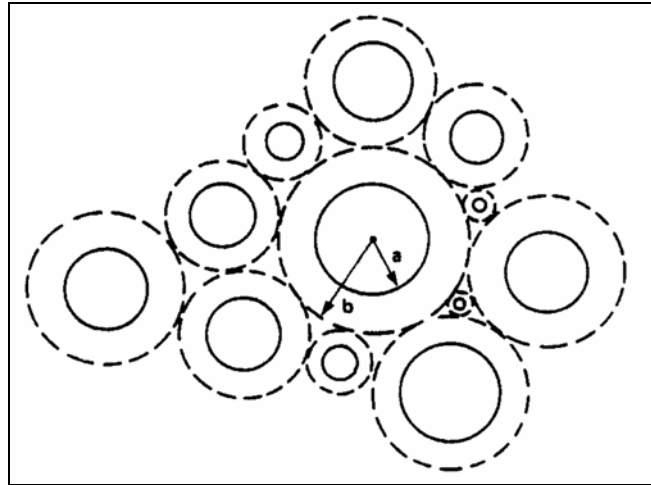


Figure 1.5 Hashin's Composite Spheres Model (Christensen and Lo 1979)

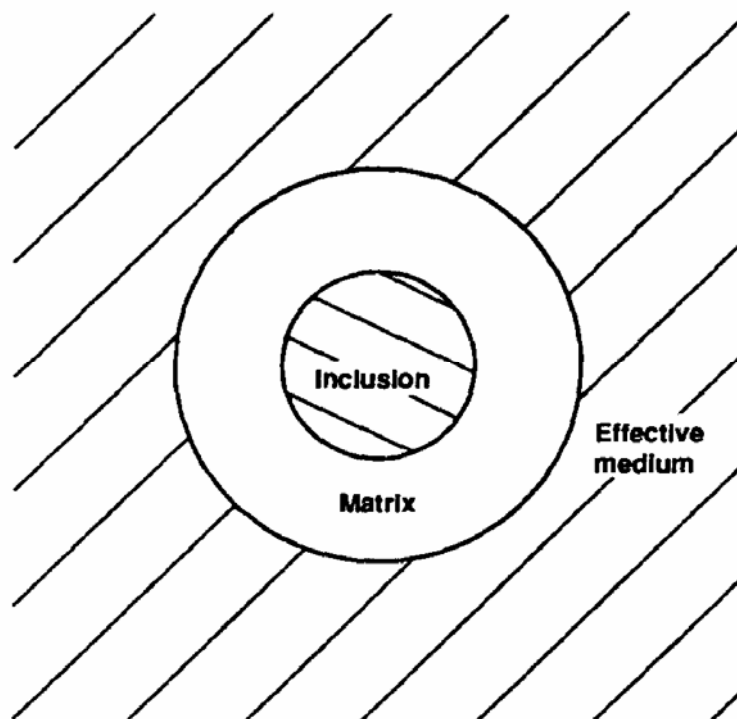


Figure 1.6 Christensen and Lo's Generalized Self-Consistent Model (Christensen 1990)

K_c = effective bulk modulus of composite;

K_i = bulk modulus of inclusion;

K_m = bulk modulus of matrix;

c = volume fraction of inclusion;

ν_m = Poisson's ratio of matrix.

G_c = effective shear modulus of composite;

G_i = shear modulus of inclusion; and

G_m = shear modulus of matrix.

The elastic (Young's) modulus, E , can be obtained by using its relationship with bulk modulus, K , shear modulus, G , and Poisson's ratio, ν :

$$E = 3(1 - 2\nu)K \quad (1.7)$$

$$E = 2(1 + \nu)G \quad (1.8)$$

$$E = \frac{9KG}{3K + G} \quad (1.9)$$

The generalized self-consistent model proposed by Christensen and Lo (1979) consists of a single composite sphere embedded in an infinite equivalent homogeneous medium of unknown properties (Figure 1.6). The exact solution to the effective shear modulus can be obtained by solving the following quadratic equation:

$$A\left(\frac{G_c}{G_m}\right)^2 + B\left(\frac{G_c}{G_m}\right) + C = 0 \quad (1.10)$$

where

$$\begin{aligned}
A = & 8 \left(\frac{G_i}{G_m} - 1 \right) (4 - 5v_m) \eta_1 c^{10/3} - 2 \left[63 \left(\frac{G_i}{G_m} - 1 \right) \eta_2 + 2\eta_1 \eta_3 \right] c^{7/3} \\
& + 252 \left(\frac{G_i}{G_m} - 1 \right) \eta_2 c^{5/3} - 50 \left(\frac{G_i}{G_m} - 1 \right) (7 - 12v_m + 8v_m^2) \eta_2 c + 4(7 - 10v_m) \eta_2 \eta_3
\end{aligned} \tag{1.11}$$

$$\begin{aligned}
B = & -4 \left(\frac{G_i}{G_m} - 1 \right) (1 - 5v_m) \eta_1 c^{10/3} + 4 \left[63 \left(\frac{G_i}{G_m} - 1 \right) \eta_2 + 2\eta_1 \eta_3 \right] c^{7/3} \\
& - 504 \left(\frac{G_i}{G_m} - 1 \right) \eta_2 c^{5/3} + 150 \left(\frac{G_i}{G_m} - 1 \right) (3 - v_m) \eta_2 v_m c + 3(15v_m - 7) \eta_2 \eta_3
\end{aligned} \tag{1.12}$$

$$\begin{aligned}
C = & 4 \left(\frac{G_i}{G_m} - 1 \right) (5v_m - 7) \eta_1 c^{10/3} - 2 \left[63 \left(\frac{G_i}{G_m} - 1 \right) \eta_2 + 2\eta_1 \eta_3 \right] c^{7/3} \\
& + 252 \left(\frac{G_i}{G_m} - 1 \right) \eta_2 c^{5/3} + 25 \left(\frac{G_i}{G_m} - 1 \right) (v_m^2 - 7) \eta_2 c - (7 + 5v_m) \eta_2 \eta_3
\end{aligned} \tag{1.13}$$

$$\eta_1 = \left(\frac{G_i}{G_m} - 1 \right) (7 - 10v_m)(7 + 5v_i) + 105(v_i - v_m) \tag{1.14}$$

$$\eta_2 = \left(\frac{G_i}{G_m} - 1 \right) (7 + 5v_i) + 35(1 - v_i) \tag{1.15}$$

$$\eta_3 = \left(\frac{G_i}{G_m} - 1 \right) (8 - 10v_m) + 15(1 - v_m) \tag{1.16}$$

where

v_i = Poisson's ratio of inclusion.

However, the above mentioned particulate micromechanical models can not be readily used to accurately predict the modulus of asphalt mixtures because they cannot

take into account the particular characteristics of HMA mixtures, such as aggregate gradation, viscoelastic effect, and air voids, etc.

Application of PFC Models to Asphalt Mastics and Mixtures and Their Limitations

Micromechanical modeling techniques have long been successfully used to characterize the overall properties using the volume fractions and properties of individual components for engineering materials such as ceramics, metals, etc. (Eshelby 1957; Christensen and Lo 1979, 1986; Hashin 1962, 1965; Mclaughlin 1977; Mori and Tanaka 1973; Hansen 1965). Not until recent years have research efforts been made to apply the micromechanical models to predict the mechanical properties of asphalt mastics and mixtures (Lytton 1990; Buttlar and Roque 1996; Buttlar et al. 1999; Li et al. 1999; Shashidhar and Shenoy 2002; Huang et al. 2003, 2007; Kim and Little 2004; Li and Metcalf 2005).

Lytton (1990) proposed a three-phase (aggregate, asphalt binder, and air voids) model to predict the modulus of HMA mixtures by considering two phases at a time from binder-air system to aggregate-binder-air system. Buttlar and Roque (1996) evaluated the applicability of four well-known modulus prediction models to HMA mixtures. Buttlar et al. (1999) also employed various micromechanical models to investigate the mastic reinforcing mechanisms and found the generalized self-consistent model (GSCM) to produce reasonable results. Li et al. (1999) developed a two-layer built-in micromechanical model and used the model to predict the elastic modulus of HMA mixtures. Compared to the conventional PFC mechanics method, Li's model has the capability of taking into account aggregate gradation and maximum aggregate particle

size of HMA mixtures. Shashidhar and Shenoy (2002) explored the applicability of PFC models in describing the dynamic mechanical behavior of asphalt mastics and simplified GSCM using an order of magnitude analysis. Using a two-phase composite model, Huang et al. (2003) developed the analytical equation to estimate the tensile strength of HMA mixtures at low temperatures. The predicted results were found to be in good agreement with the experimental data. Huang et al. (2007) also used the micromechanical model to characterize a three-layered HMA mixture produced with a type of hard and solid asphalt, Gilsonite, as an interlayer between asphalt binder and aggregate particles. Kim and Little (2004) used micromechanical models to assess the effects of filler on the performance of asphalt mastics based on the linear viscoelastic analysis and found good agreement between predicted results from traditional micromechanical models and testing data. Li and Metcalf (2005) proposed a two-step approach to predict the resilient modulus of HMA mixtures from two-phase micromechanical models and found the predicted results from appropriate models reasonably approximate the measured results.

Of all the micromechanical models mentioned previously, the predicted (elastic or resilient) modulus/stiffness results of HMA mixtures (or asphalt mastics) show varied agreement with the measured data. The discrepancy between predicted and measured moduli can be attributed to the fact that HMA mixtures possess distinctly different characteristics from the other ordinary engineering materials. Firstly, HMA mixtures exhibit time and temperature-dependent response resulting from the viscoelastic properties of asphalt cement binder. However, except for the work of Kim and Little (2004), all of the previously mentioned micromechanical models are based on the elastic analysis rather than viscoelastic analysis. Secondly, the aggregate gradation also

contributes to the discrepancy since almost all the micromechanical models can not take into account aggregate size distribution except the one developed by Li et al. (1999). Lastly, none of the micromechanical models can address the interlocking between aggregate particles, which may play an important role in the reinforcement mechanisms of HMA mixtures. Buttlar and Roque (1996) attributed the discrepancy to the incapability of the models to incorporate aggregate interlock. However, Li and Metcalf (2005) argued that there is no direct contact between large aggregates in a typical dense-graded HMA mixture (Roberts et al. 1996).

Latest Models for Predicting Dynamic Modulus of HMA Mixtures

Numerous empirical models have been proposed to predict the modulus/stiffness of HMA mixtures due to its importance in structural design of flexible pavements and the desire to reduce the amount of laboratory testing. Examples include the Heukelom and Klomp's relations (Heukelom and Klomp 1964), the relations proposed by Bonnaure et al. (1977), the SHRP SUPERPAVE™ Single-Function Power Model (Roque et al. 1994), and the Multiple-Function Power Model (Buttlar and Roque 1996).

As previously mentioned, Level 2 and 3 material inputs in the AASHTO 2002 Design Guide recommended the use of the Witczak model for predicting dynamic modulus value of HMA mixtures in terms of asphalt binder, aggregate, and mix properties. The Witczak model is expressed as (NCHRP 2004):

$$\log|E^*| = 3.750063 + 0.029232\rho_{200} - 0.001767(\rho_{200})^2 - 0.002841\rho_4 - 0.058097V_a - 0.802208\left(\frac{V_{beff}}{V_{beff} + V_a}\right) + \frac{3.871977 - 0.0021\rho_4 + 0.003958\rho_{38} - 0.000017(\rho_{38})^2 + 0.005470\rho_{34}}{1 + e^{(-0.603313 - 0.313351\log(f) - 0.393532\log(\eta))}} \quad (1.17)$$

where

$|E^*|$ = dynamic modulus, psi;

η = bitumen viscosity, 10^6 Poise;

f = loading frequency, Hz;

V_a = air void content, %;

V_{beff} = effective bitumen content, % by volume;

ρ_{34} = cumulative % retained on the 19-mm sieve;

ρ_{38} = cumulative % retained on the 9.5-mm sieve;

ρ_4 = cumulative % retained on the 4.75-mm sieve; and

ρ_{200} = % passing the 0.075-mm sieve.

The Witczak model is based on work developed by Witczak and his co-workers over nearly 30 years (Andrei et al. 1999). It is a purely empirical regression model developed from a large database of over 2700 laboratory test measurements of dynamic modulus value (Andrei et al. 1999). Table 1.1 summarizes the characteristics of the diverse set of mixtures in the database used to formulate and calibrate Eq. (1.17), as well as the relevant goodness-of-fit statistics for the model.

Another model lately developed to predict the dynamic modulus of HMA mixture is the Hirsch model (Christensen et al. 2003). The original Hirsch model was developed by Hirsch to calculate the modulus of elasticity of cement concrete or mortar in terms of one empirical constant, the aggregate modulus and cement mastic modulus, and mix proportion (Hirsch 1961, 1962). Hirsch assumed that the responses of the constituents (cement matrix, aggregate, and the composite concrete) behave in a linear elastic manner.

Table 1.1 Summary Statistics for the Witczak Predictive Model (Andrei et al. 1999).

Statistics	Value
Goodness of fit (log $ E^* $ space)	$R^2=0.96$, $Se/Sy=0.24$
Data points	2750
Temperature range	0 to 130 °F
Loading rates	0.1 to 25 Hz
	205 Total
Mixtures	171 with unmodified asphalt binders 34 with modified asphalt binders 23 Total
Binders	9 Unmodified 14 Modified
Aggregates	39
Compaction methods	Kneading and gyratory
Specimen sizes	Cylindrical 4 in. by 8 in. or 2.75 in. by 5.5 in.

Christensen developed a relatively simple version of the Hirsch model (Eq. 1.18) to predict dynamic modulus of HMA mixtures from the complex shear modulus $|G^*|$ of asphalt binder and volumetric properties of HMA mixtures. The estimated standard error reported by Christensen is 41 percent for the Hirsch model (Christensen et al. 2003).

$$|E^*|_{mix} = P_c \left[4,200,000 \left(1 - \frac{VMA}{100} \right) + 3|G^*|_{binder} \left(\frac{VFA \times VMA}{10,000} \right) \right] + \frac{1 - P_c}{\frac{1 - \frac{VMA}{100}}{4,200,000} + \frac{VMA}{3|G^*|_{binder} (VFA)}} \quad (1.18)$$

where

$$P_c = \frac{\left(20 + \frac{3|G^*|_{binder}(VFA)}{VMA} \right)^{0.58}}{650 + \left(\frac{3|G^*|_{binder}(VFA)}{VMA} \right)^{0.58}}$$

$|E^*|_{mix}$ = absolute value of mixture dynamic modulus, psi;

$|G^*|_{binder}$ = absolute value of asphalt binder complex modulus, psi;

VMA = voids in mineral aggregates, %; and

VFA = voids filled with asphalt, %.

Dongré et al. (2005) evaluated the predictive capability of the Witczak and Hirsch models by comparing the predicted dynamic modulus values to the results measured in the laboratory of the Federal Highway Administration (FHWA) Mobile Asphalt Laboratory (MATL) using asphalt mixtures from five pavement construction sites across the United States. They found that both models provide reasonable predictions of dynamic modulus within the scope of their study. The accuracy and robustness of the Witczak model was also evaluated by Schwarz (2005) through a set of sensitivity and validation studies. He found that the Witczak model may overestimate dynamic modulus, particularly at higher temperatures. His overall findings confirmed that the Witczak model can provide sufficiently accurate and robust estimates of dynamic modulus for use in mechanistic-empirical pavement performance prediction and design. Birgisson et al. (2005a) evaluated the Witczak model using 28 mixtures commonly used in the state of Florida. They found that the Witczak model appeared to work well for mixtures in Florida. However, a multiplier has to be introduced to account for the uniqueness of local mixtures. Birgisson et al. (2005b) also investigated the effects of aggregate characteristics

on dynamic modulus of HMA. They suggested to use the power-law-based aggregate gradation factors to identify and evaluate the relationships between gradation factors and dynamic modulus at higher temperatures (40°C). They also established a tentative framework to optimize the mixture gradations for dynamic modulus. Using two 25-mm Superpave mixtures with two different binder types, Mohammad et al. (2005) evaluated both Witczak and Hirsch prediction models. They found that both models can predict the dynamic modulus values from mixture properties within a reasonable reliability.

Although both the Witczak and the Hirsch models can give relatively accurate prediction of dynamic modulus, the full aggregate gradation is not taken into consideration in either model (Four representative points ρ_{34} , ρ_{38} , ρ_4 and ρ_{200} on the aggregate gradation curve are incorporated in the Witczak model; whereas the aggregate gradation characteristics are totally neglected in the Hirsch model). This implies that given the same other conditions, different aggregate gradations can lead to the same dynamic modulus value. It has been well recognized that aggregate gradation characteristics exhibit important effects on the dynamic modulus value (Birgisson et al. 2005b). Poor gradation may lead to low dynamic modulus value, which will result in poor performance of flexible pavements. In addition, these equations do not consider the internal micromechanical structure (such as air voids size distribution) of HMA mixtures. Theoretical relationships based on appropriate micromechanical models to determine the value of dynamic modulus of HMA mixtures is more desirable. The micromechanical models are also helpful in gaining insight into the mechanical behaviors of HMA mixtures from the viewpoint of their individual constituents.

Research Objectives and Significance

The objectives of this study were as follows:

1. To develop new PFC micromechanical models and modify existing PFC models for predicting dynamic modulus of asphalt mastic and mixtures;
2. To evaluate the newly developed and modified PFC models for HMA mixtures through a comparison of the predicted and laboratory measured dynamic moduli;
3. To investigate the effects of different factors (such as properties and volumetric fractions of individual constituents) on dynamic modulus of HMA mixtures.

Although there are many micromechanical models now available to determine the properties of PFC, they cannot be readily used to predict the dynamic modulus of HMA mixtures without further extension or modification. Through this proposed research, more models will be developed to better reflect the features of HMA mixtures and can be used to accurately predict the dynamic modulus value of HMA mixtures. These micromechanical models can also be helpful in promoting the understanding of the mechanical behavior of HMA mixtures and provide a basis for future substitution for expensive and time-consuming laboratory testing of HMA mixtures for dynamic modulus.

Arrangement of the Dissertation

This dissertation is divided into eight chapters. Chapter 1 introduces the research background, objectives, and literature review on some PFC models and attempts to use them in asphalt mastic and mixtures by some researchers. Chapter 2 provides the necessary theoretical background of linear viscoelasticity for the formulation of PFC

models for HMA mixtures, including the representation of viscoelastic material properties, elastic-viscoelastic correspondence principle for converting elastic modulus into complex modulus and the construction of master curve. Chapters 3 and 4 present the formulation of the three-dimensional two-layered model for HMA mixtures and the PFC models derived using the differential method. Chapter 5 describes the laboratory testing on asphalt mastic and HMA mixture to obtain the input parameters for the predictive models and to measure the dynamic modulus and phase angle values of asphalt mastic and mixture so that comparison can be made between the predicted and measured results. In Chapter 6 and 7, the proposed models in this study were used to predict the dynamic modulus and phase angle values of asphalt mastic and mixture. The proposed PFC models were also evaluated by comparing the predicted value to the measured results. Chapter 8 summarizes the conclusions from this study and recommends possible future research topics in this area.

CHAPTER 2 THEORETICAL BACKGROUND

Material Properties in Linear Viscoelasticity

In linear viscoelasticity, the relationship between the time-dependent stress and strain of a viscoelastic material can be expressed using a linear differential equation with constant coefficients (Tschoegl 1989; Ferry 1980; Park and Schapery 1999; Kim and Little 2004):

$$\sum_{n=0}^N u_n \frac{d^n \sigma(t)}{dt^n} = \sum_{m=0}^M q_m \frac{d^m \varepsilon(t)}{dt^m} \quad (2.1)$$

where

u_n and q_m = constant coefficients.

The Laplace transformation of Eq. (2.1) leads to

$$\bar{u}(s)\bar{\sigma}(s) = \bar{q}(s)\bar{\varepsilon}(s) \quad (2.2)$$

where

s = Laplace variable;

$\bar{\sigma}(s)$ = Laplace transform of stress $\sigma(t)$, i.e.,

$$\bar{\sigma}(s) = \int_0^{\infty} \sigma(t) e^{-st} dt \quad (2.3)$$

$\bar{\varepsilon}(s)$ = Laplace transform of strain $\varepsilon(t)$, i.e.,

$$\bar{\varepsilon}(s) = \int_0^{\infty} \varepsilon(t) e^{-st} dt \quad (2.4)$$

$$\bar{u}(s) = \sum_{n=0}^N u_n s^n \quad (2.5)$$

$$\bar{q}(s) = \sum_{m=0}^M q_m s^m \quad (2.6)$$

It should be noted that Eqs.(2.5) and (2.6) are valid only under the zero initial conditions. Fortunately, zero initial conditions can almost always be obtained by appropriately defining the stress and strain history (Tschoegl 1989).

Eq.(2.2) can also be expressed as:

$$\bar{\sigma}(s) = \bar{Q}(s)\bar{\varepsilon}(s) \quad (2.7)$$

or

$$\bar{\varepsilon}(s) = \bar{U}(s)\bar{\sigma}(s) \quad (2.8)$$

where

$\bar{Q}(s)$ = operational relaxance,

$$\bar{Q}(s) = \frac{\bar{q}(s)}{\bar{u}(s)} \quad (2.9)$$

$\bar{U}(s)$ = operational retardance,

$$\bar{U}(s) = \frac{\bar{u}(s)}{\bar{q}(s)} \quad (2.10)$$

Eqs.(2.7) and (2.8) are also called Hooke's law in the Laplace-transformed domain (Tschoegl 1989).

From Eq.(2.2), the following relationship holds:

$$\bar{Q}(s)\bar{U}(s) = 1 \quad (2.11)$$

The material function, $\bar{Q}(s)$ or $\bar{U}(s)$, includes all the necessary information to characterize the viscoelastic property of a material.

In order to obtain $\bar{Q}(s)$ or $\bar{U}(s)$, a relaxation or creep test can be conducted. In the relaxation test, a strain ε_0 is suddenly applied to a specimen at time $t = 0$ and then

maintained constant (Figure 2.1). Usually, the induced stress $\sigma(t)$ for a viscoelastic material to keep the constant strain is a monotonously decreasing function of time (Figure 2.1).

Thus, the strain can be expressed as:

$$\varepsilon(t) = \varepsilon_0 H(t) \quad (2.12)$$

where

$H(t)$ = Heaviside step function, i.e.,

$$H(t) = \begin{cases} 1 & t > 0 \\ 0 & t < 0 \end{cases} \quad (2.13)$$

Laplace transformation of Eq. (2.12) gives

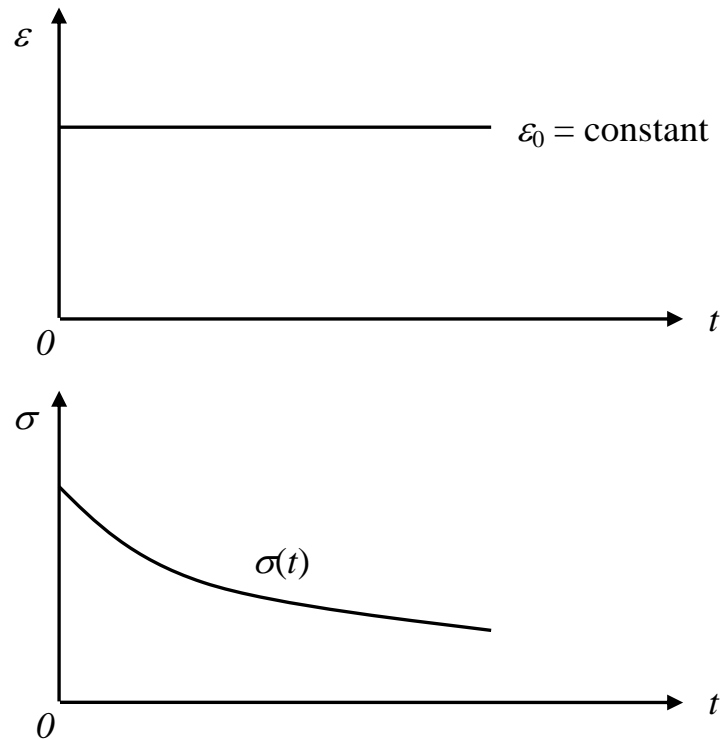


Figure 2.1 Stress and Strain in a Relaxation Test

$$\bar{\varepsilon}(s) = \frac{\varepsilon_0}{s} \quad (2.14)$$

Substituting Eq.(2.14) into Eq.(2.7), we obtain

$$\bar{\sigma}(s) = \frac{\bar{Q}(s)}{s} \varepsilon_0 \quad (2.15)$$

The inverse Laplace transformation of Eq.(2.15) gives

$$\sigma(t) = \varepsilon_0 L^{-1} \left[\frac{\bar{Q}(s)}{s} \right] \quad (2.16)$$

where

L^{-1} = inverse Laplace transformation.

Thus, we get

$$L^{-1} \left[\frac{\bar{Q}(s)}{s} \right] = \frac{\sigma(t)}{\varepsilon_0} = E(t) \quad (2.17)$$

where

$E(t)$ = relaxation modulus.

From Eq.(2.17), we obtain

$$\bar{E}(s) = \frac{\bar{Q}(s)}{s} \quad (2.18)$$

and

$$\bar{Q}(s) = s\bar{E}(s) \quad (2.19)$$

where

$\bar{E}(s)$ = Laplace transform of relaxation modulus $E(t)$, i.e.,

$$\bar{E}(s) = \int_0^{\infty} E(t) e^{-st} dt \quad (2.20)$$

In a creep test, a constant stress ε_0 is applied to a specimen and the induced strain is measured. Usually, the induced strain $\varepsilon(t)$ for a viscoelastic material under constant stress is a monotonously increasing function of time (Figure 2.2).

In a similar manner, we can obtain

$$\bar{J}(s) = \frac{\bar{U}(s)}{s} \quad (2.21)$$

and

$$\bar{U}(s) = s\bar{J}(s) \quad (2.22)$$

where

$\bar{J}(s)$ = Laplace transform of creep compliance $J(t)$, i.e.,

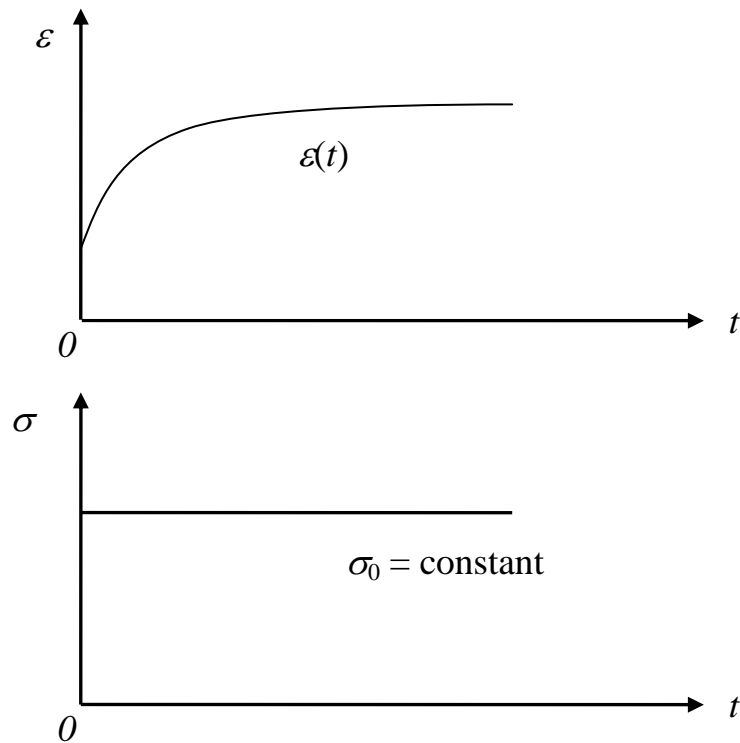


Figure 2.2 Stress and Strain in a Creep Test

$$J(t) = \frac{\varepsilon(t)}{\sigma_0} \quad (2.23)$$

and

$$\bar{J}(s) = \int_0^{\infty} J(t) e^{-st} dt \quad (2.24)$$

The Hooke's law in the Laplace-transformed domain, Eqs. (2.7) and (2.8), can then be rewritten as:

$$\bar{\sigma}(s) = s\bar{E}(s)\bar{\varepsilon}(s) = \tilde{E}(s)\bar{\varepsilon}(s) \quad (2.25)$$

and

$$\bar{\varepsilon}(s) = s\bar{J}(s)\bar{\sigma}(s) = \tilde{J}(s)\bar{\sigma}(s) \quad (2.26)$$

where

$\tilde{E}(s)$ = s -multiplied Laplace transform or Carson transform of $E(t)$, i.e.,

$$\tilde{E}(s) = s\bar{E}(s) \quad (2.27)$$

$\tilde{J}(s)$ = s -multiplied Laplace transform or Carson transform of $J(t)$, i.e.,

$$\tilde{J}(s) = s\bar{J}(s) \quad (2.28)$$

Besides the relaxation and creep tests, a dynamic modulus test is often used to obtain the viscoelastic properties of a material. In the dynamic modulus test, a sinusoidal strain is applied to a specimen and a sinusoidal steady-state stress is induced, or vice versa. Due to the viscoelastic effect, the stress always leads the strain, or the strain always lags the stress (Figure 2.3) (Tschoegl 1989; Ferry 1980).

The dynamic modulus is defined as the ratio of the axial stress amplitude to the axial strain amplitude:

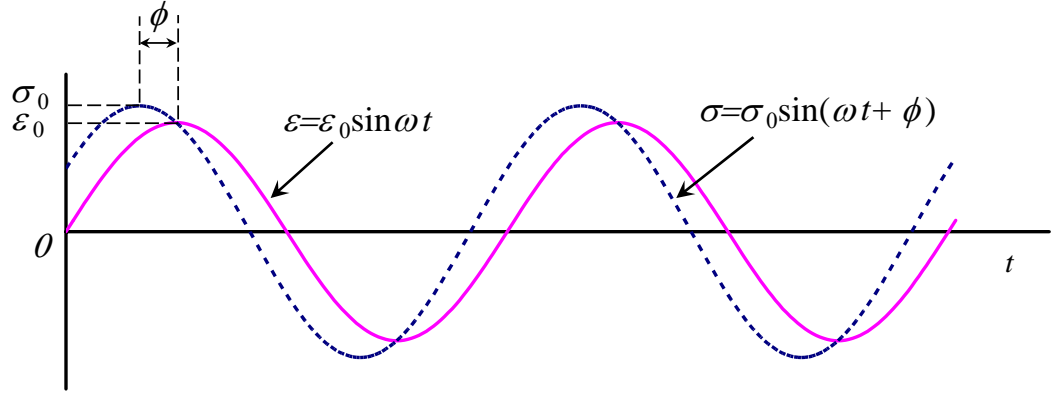


Figure 2.3 Stress and Strain in a Dynamic Modulus Test

$$|E^*| = \frac{\sigma_0}{\varepsilon_0} \quad (2.29)$$

where

$|E^*|$ = dynamic modulus;

σ_0 = axial stress amplitude; and

ε_0 = axial strain amplitude.

In the complex form, the applied sinusoidal strain $\varepsilon(t)$ can be expressed as:

$$\varepsilon(t) = \varepsilon_0 (\cos \omega t + i \sin \omega t) = \varepsilon_0 e^{i\omega t} \quad (2.30)$$

where

ω = radian frequency; and

$i = \sqrt{-1}$.

The Laplace transformation of Eq. (2.30) gives

$$\bar{\varepsilon}(s) = \frac{\varepsilon_0}{s - i\omega} \quad (2.31)$$

Substituting Eq.(2.31) into Eq.(2.7), we get

$$\bar{\sigma}(s) = \frac{\varepsilon_0 \bar{Q}(s)}{s - i\omega} \quad (2.32)$$

Thus, we have

$$\frac{\bar{\sigma}(s)}{\varepsilon_0} = \frac{\bar{Q}(s)}{s - i\omega} = \frac{\bar{q}(s)}{(s - i\omega)\bar{u}(s)} \quad (2.33)$$

Since the total stress response resulting from the sinusoidal strain excitation includes two parts: a period function of time representing the steady-state response, and a non-periodic function of time representing the transient response, Eq.(2.33) can be decomposed into two partial fractions (Tschoegl 1989):

$$\frac{\bar{\sigma}(s)}{\varepsilon_0} = \frac{A}{s - i\omega} + \frac{B(s)}{\bar{u}(s)} \quad (2.34)$$

where

A = constant; and

$B(s)$ = polynomial in s of degree one less than the degree of $\bar{u}(s)$.

The constant A can be determined using the residue theorem

$$A = \lim_{s \rightarrow i\omega} (s - i\omega) \frac{\bar{Q}(s)}{s - i\omega} = \bar{Q}(i\omega) = (i\omega)\bar{E}(i\omega) \quad (2.35)$$

For the steady state stress response, therefore, we have

$$\frac{\bar{\sigma}_{ss}(s)}{\varepsilon_0} = \frac{\bar{Q}(i\omega)}{s - i\omega} \quad (2.36)$$

where

$\bar{\sigma}_{ss}(s)$ = Laplace transform of the steady state stress response $\sigma_{ss}(t)$.

The inverse Laplace transformation of Eq.(2.36) gives

$$\sigma_{ss}(t) = \bar{Q}(i\omega)\varepsilon_0 e^{i\omega t} = \bar{Q}(i\omega)\varepsilon(t) \quad (2.37)$$

The complex modulus is defined as:

$$E^* = \frac{\sigma_{ss}(t)}{\varepsilon(t)} = \bar{Q}(i\omega) = \tilde{E}(i\omega) = (i\omega)\bar{E}(i\omega) \quad (2.38)$$

Since E^* is a complex quantity, it can be written as:

$$E^* = E' + iE'' = |E^*|(\cos\phi + i\sin\phi) = |E^*|e^{i\phi} \quad (2.39)$$

where

E' = storage modulus;

E'' = loss modulus; and

ϕ = phase angle.

From Eq.(2.39), we have

$$|E^*(\omega)| = \sqrt{[E'(\omega)]^2 + [E''(\omega)]^2} \quad (2.40)$$

and

$$\phi = \tan^{-1} \frac{E''(\omega)}{E'(\omega)} \quad (2.41)$$

Substitution of Eq.(2.39) into Eq. (2.37) leads to

$$\sigma_{ss}(t) = |E^*|e^{i\phi}\varepsilon_0 e^{i\omega t} = |E^*|\varepsilon_0 e^{i(\omega t + \phi)} \quad (2.42)$$

Let

$$|E^*|\varepsilon_0 = \sigma_0 \quad (2.43)$$

Therefore, we prove

$$|E^*| = \frac{\sigma_0}{\varepsilon_0} \quad (2.44)$$

If we use the sinusoidal stress as the excitation in dynamic modulus test, in a similar manner we can also obtain

$$|J^*| = \frac{\varepsilon_0}{\sigma_0} \quad (2.45)$$

$$J^* = \frac{\varepsilon(t)}{\sigma(t)} = \bar{U}(i\omega) = \tilde{J}(i\omega) = (i\omega)\bar{J}(i\omega) \quad (2.46)$$

$$J^* = J' - iJ'' = |J^*|[\cos(-\phi) + i\sin(-\phi)] = |J^*|e^{-i\phi} \quad (2.47)$$

$$\phi = \tan^{-1} \frac{J''(\omega)}{J'(\omega)} \quad (2.48)$$

where

$|J^*|$ = dynamic compliance;

J^* = complex compliance;

J' = storage compliance; and

J'' = loss compliance.

From Eqs.(2.11), (2.38) and (2.46), the following relationship holds between the complex modulus and compliance:

$$E^* J^* = 1 \quad (2.49)$$

Elastic-Viscoelastic Correspondence Principle

To obtain the viscoelastic properties of a composite material, the elastic-viscoelastic correspondence principle can be employed to convert the effective elastic properties derived from the PFC micromechanical models to the viscoelastic counterparts (Tschoegl 1989; Ferry 1980; Park and Schapery 1999; Kim and Little 2004).

The correspondence principle states that the viscoelastic solution in the Laplace-transformed domain can be obtained by replacing the elastic material properties in the elastic solution by the Carson-transformed material properties. It can also state that the complex moduli can be obtained by replacing the elastic moduli with the corresponding complex moduli (Tschoegl 1989; Ferry 1980; Park and Schapery 1999; Kim and Little 2004).

For example, if it is assumed that the property of aggregate in HMA mixtures is elastic and that of asphalt cement binder viscoelastic, then the effective shear modulus from the Hashin's composite spheres model, Eq. (1.6), can be converted to the Carson-transformed shear modulus by replacing G_m with $\tilde{G}_m(s)$ as follows:

$$\frac{\tilde{G}_c(s)}{\tilde{G}_m(s)} = 1 + \frac{15(1 - \nu_m) \left(\frac{G_i}{\tilde{G}_m(s)} - 1 \right) c}{7 - 5\nu_m + 2(4 - 5\nu_m) \left[\frac{G_i}{\tilde{G}_m(s)} - \left(\frac{G_i}{\tilde{G}_m(s)} - 1 \right) c \right]} \quad (2.50)$$

where

$\tilde{G}_c(s)$ = s -multiplied Laplace transform or Carson transform of $G_c(t)$;

$G_c(t)$ = relaxation shear modulus of composite (HMA mixture);

$\tilde{G}_m(s)$ = s -multiplied Laplace transform or Carson transform of $G_m(t)$; and

$G_m(t)$ = relaxation shear modulus of matrix (asphalt binder).

The inverse Laplace transformation of Eq.(2.50) gives the relaxation shear modulus of HMA mixtures as follows:

$$G_c(t) = L^{-1} \left\{ \bar{G}_m(s) + \frac{15(1-v_m) \left[\frac{G_i}{s} - \bar{G}_m(s) \right] c}{7-5v_m + 2(4-5v_m) \left[\frac{G_i}{\tilde{G}_m(s)} - \left(\frac{G_i}{\tilde{G}_m(s)} - 1 \right) c \right]} \right\} \quad (2.51)$$

In the similar manner, the complex shear modulus of HMA mixtures using the Hashin's composite spheres model can be obtained as follows by replacing G_m with $G_m^*(\omega)$:

$$G_c^*(\omega) = G_m^*(\omega) + \frac{15(1-v_m) [G_i - G_m^*(\omega)] c}{7-5v_m + 2(4-5v_m) \left\{ \frac{G_i}{G_m^*(\omega)} - \left[\frac{G_i}{G_m^*(\omega)} - 1 \right] c \right\}} \quad (2.52)$$

where

$G_c^*(\omega)$ = complex shear modulus of composite (HMA mixtures); and

$G_m^*(\omega)$ = complex shear modulus of matrix (asphalt binder).

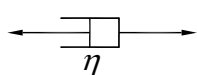
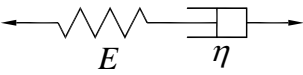
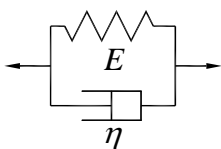
Prony Series Representation

To predict the dynamic modulus of asphalt mastics and mixtures using the PFC models developed in this study, the linear viscoelastic material properties (dynamic modulus and phase angle) of asphalt binder or mastic were obtained through the laboratory testing and used as input parameters in the predictive equations. It is desirable to fit certain rheological models to the laboratory measured data so that mathematical expression of the viscoelastic material properties can be obtained. There are many

rheological models available to describe the viscoelastic properties of materials (Tschoegl 1989; Ferry 1980). Table 2.1 presents four basic viscoelastic elements and the relaxation modulus and creep compliance associated with them. Using the interrelationship between different viscoelastic material properties, the complex modulus can also be obtained for these viscoelastic elements.

However, these viscoelastic models cannot cover the wide range of the transition zone in the master curve of dynamic modulus of HMA mixtures (Park and Kim 2001). To describe the broad band data in the measured dynamic modulus, the generalized Maxwell model (Figure 2.4) and the generalized Kelvin (or Voigt) model (Figure 2.5) are widely used. Another reason for the popularity of these two models is due to the remarkable mathematical efficiency associated with their exponential basis functions (Park and Schapery 1999; Park and Kim 2001).

Table 2.1 Four Basic Viscoelastic Elements

Element type	Schematic	$\sigma - \varepsilon$ relationship	Relaxation modulus $E(t)$	Creep compliance $J(t)$
Elastic		$\sigma = E\varepsilon$	E	$\frac{1}{E}$
Viscous		$\sigma = \eta\dot{\varepsilon}$	$\eta\delta(t)$	$\frac{t}{\eta}$
Maxwell		$\dot{\varepsilon} = \frac{\dot{\sigma}}{E} + \frac{\sigma}{\eta}$	$Ee^{-\frac{E}{\eta}t}$	$\frac{1}{E} + \frac{t}{\eta}$
Kelvin (or Voigt)		$\sigma = E\varepsilon + \eta\dot{\varepsilon}$	$E + \eta\delta(t)$	$\frac{1}{E} \left(1 - e^{-\frac{E}{\eta}t} \right)$

The mathematical expressions for the generalized Maxwell and Kelvin models are commonly referred to as ‘‘Prony’’ or ‘‘Dirichlet’’ series. The Prony series expression of the relaxation modulus in the uniaxial loading for the generalized Maxwell model in terms of E_i (Figure 2.4) can be represented as (Park and Schapery 1999; Park and Kim 2001):

$$E(t) = E_e + \sum_{i=1}^m E_i e^{-\frac{t}{\rho_i}} \quad (2.53)$$

where

E_e = long-time equilibrium modulus;

E_i = regression constants;

ρ_i = relaxation time, $\rho_i = \frac{\eta_i}{E_i}$; and

m = number of dashpots in the model.

From Eq.(2.53), the storage and loss modulus can then be expressed as

$$E'(\omega) = E_e + \sum_{i=1}^m \frac{\omega^2 \rho_i^2 E_i}{\omega^2 \rho_i^2 + 1} \quad (2.54)$$

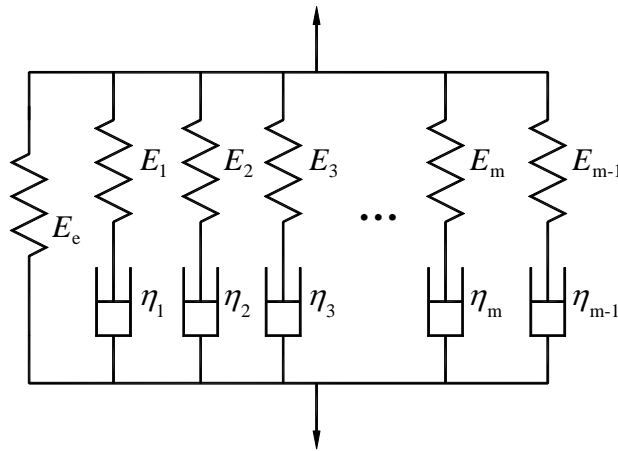


Figure 2.4 Generalized Maxwell Model

$$E''(\omega) = \sum_{i=1}^m \frac{\omega \rho_i E_i}{\omega^2 \rho_i^2 + 1} \quad (2.55)$$

The Prony series expression of the creep compliance in the uniaxial loading for the generalized Kelvin model in terms of D_j (Figure 2.5) can be written as (Park and Schapery 1999; Park and Kim 2001):

$$J(t) = D_g + \sum_{j=1}^n D_j \left(1 - e^{-\frac{t}{\tau_j}} \right) \quad (2.56)$$

where

$$D_g = \text{glassy compliance, } D_g = \frac{1}{E_g};$$

$$D_j = \text{regression constants, } D_j = \frac{1}{E_j};$$

$$\tau_j = \text{retardation time, } \tau_j = \frac{\eta_j}{E_j};$$

n = number of dashpots in the model.

From Eq.(2.56), the storage and loss compliance can then be expressed as

$$J'(\omega) = D_g + \sum_{j=1}^n \frac{D_j}{\omega^2 \tau_j^2 + 1} \quad (2.57)$$

$$J''(\omega) = \sum_{j=1}^n \frac{\omega \tau_j D_j}{\omega^2 \tau_j^2 + 1} \quad (2.58)$$

Construction of Master Curve

The master curve of different viscoelastic material properties as a function of time or frequency can be constructed by using the time-temperature superposition (Ferry

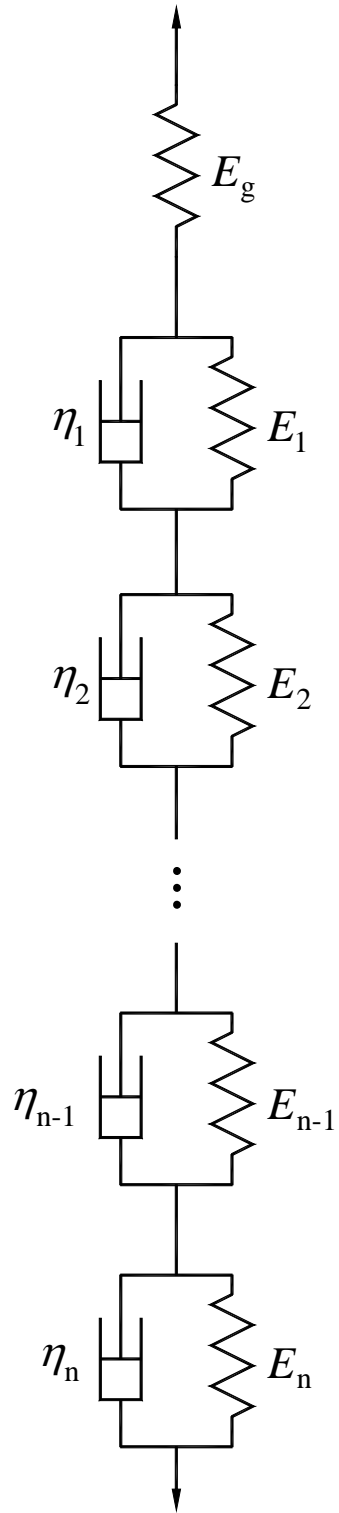


Figure 2.5 Generalized Kelvin (or Voigt) Model

1980). Test data measured at other temperatures are shifted horizontally along the time or frequency axis so that all curves form a single master curve at a reference test temperature. If the reference temperature is chosen to be in the middle of all test temperatures, then the test data measured at lower temperatures are shifted to the right, i.e. to higher frequencies until the ends of adjacent temperature curves just meet or partially overlap. In a similar manner, the test data measured at higher temperatures are shifted to the left, i.e. to low frequencies. This constructed master curve covers a much wider range of frequency than the actual experimental data. Figure 2.6 shows an example of the constructed dynamic modulus master curve of HMA mixture.

The horizontal shift factor, a_T , a constant which defines the required horizontal shift from an arbitrary test temperature, T , to the reference temperature of master curve, T_0 , can be expressed as:

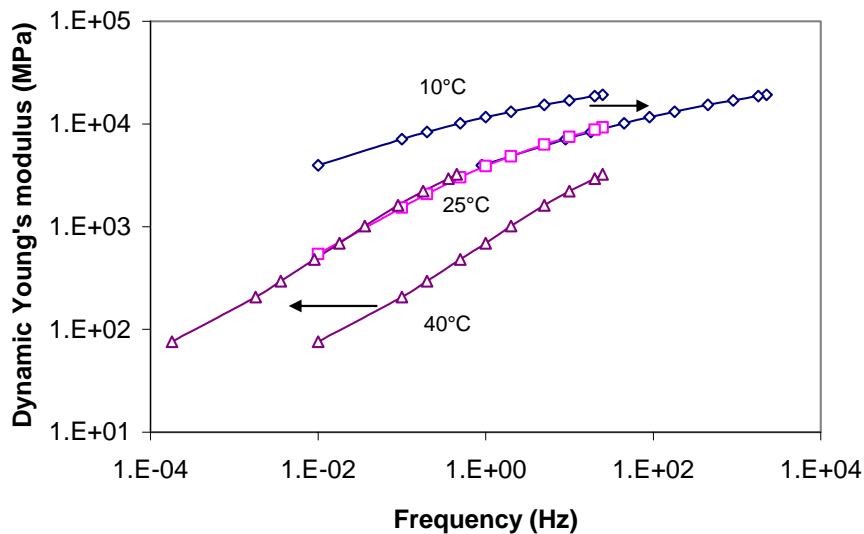


Figure 2.6 Construction of Master Curve of Dynamic Modulus

$$f_T = a_T f_{T_0} \tag{2.59}$$

where

a_T = horizontal shift factor;

f_T = frequency at a freely chosen temperature T ; and

f_{T_0} = frequency at the reference temperature T_0 .

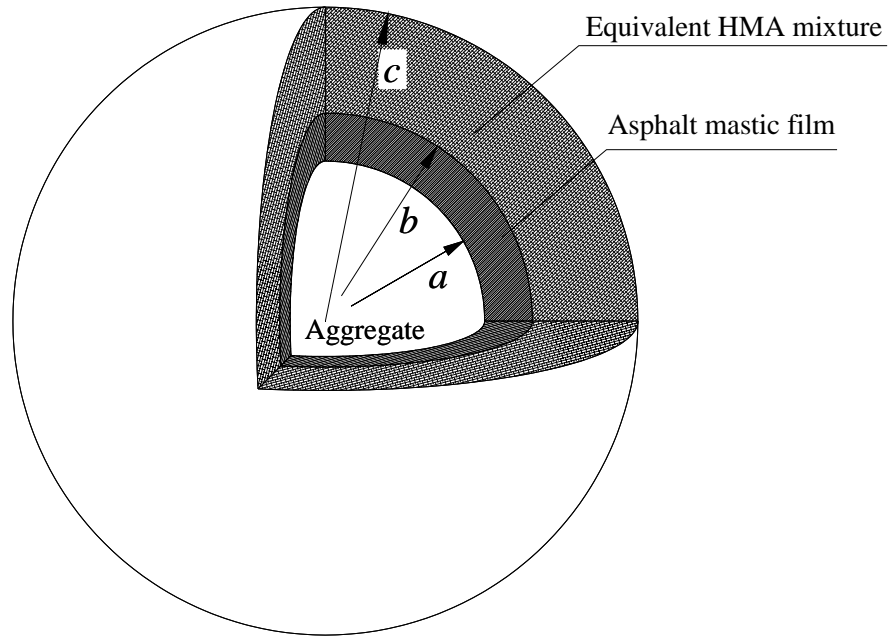
CHAPTER 3 DEVELOPMENT OF THREE-DIMENSIONAL TWO-LAYERED MODEL FOR HMA MIXTURES

Modeling of Three-Dimensional Two-Layered Elastic HMA Mixtures

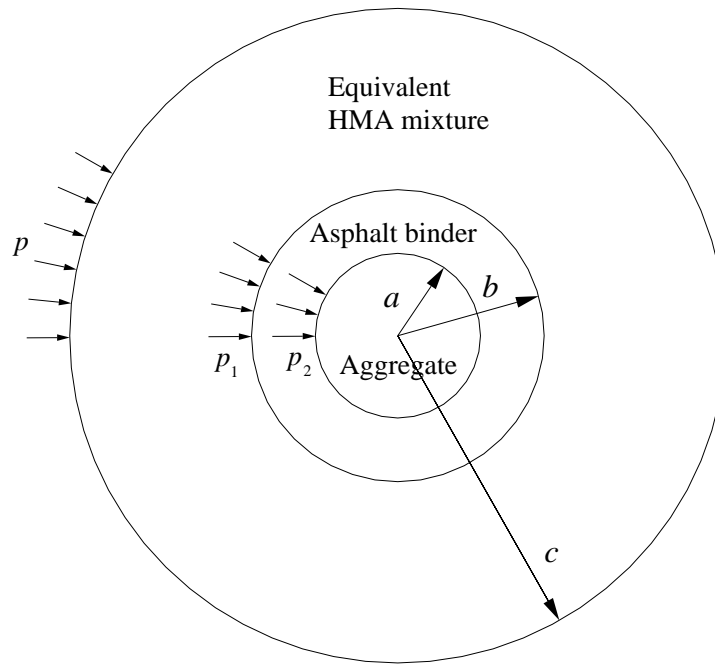
Micromechanical Model

As previously mentioned, HMA mixtures can be regarded as a composite material with aggregate particles dispersed in the asphalt mastic matrix. The same concept of equivalent medium as used by Eshelby (1957) and Christensen (1979) was employed in this study. Figure 3.1 presents the schematic drawings of the geometric model of a three-dimensional two-layered HMA mixture composite. The model consists of asphalt mastic-coated spherical aggregate particles embedded in the equivalent medium of HMA mixture with unknown effective modulus (Air voids are temporarily neglected here and will be considered later in this chapter). Thus, the micromechanically inhomogeneous HMA can now be treated as a macromechanically homogeneous composite material.

In Figure 3.1, a is the radius of aggregate, $b-a$ is the thickness of asphalt mastic film, $c-b$ is the thickness of the surrounding equivalent medium of HMA mixture, and c is the radius of the equivalent medium. Unlike an infinite equivalent medium in GSCM (Christensen and Lo 1979), a finite equivalent medium is used in the model. A uniformly distributed radial stress p is applied at the boundary $r = c$. p_1 , p_2 are the induced radial stresses at the interfaces $r = b$, $r = a$, respectively. The same loading condition was used by Li et al. (1999) and it is easy to obtain the analytical solution to the modulus of HMA mixtures. For the effect of different loading mode on dynamic modulus of HMA



(a) Three-dimensional schematic



(b) Two-dimensional schematic

Figure 3.1 Three-Dimensional Two-Layered Model for HMA Mixtures

mixtures, readers are referred to References, such as Papazian (1962), Witczak and Root (1974), Khanal and Mamlouk (1995), etc. It is assumed now that both the constituents and the equivalent medium are elastic. $E_2, \nu_2; E_1, \nu_1; E_0(a), \nu_0$ represent the elastic moduli and Poisson's ratios of aggregate, asphalt mastic, and the equivalent HMA medium, respectively. It should be pointed out that the elastic modulus of the equivalent medium is denoted as $E_0(a)$ instead of E_0 to emphasize the fact that the elastic modulus of the equivalent HMA medium is directly related to aggregate size and aggregate gradation.

Formulation Development

Based on the general assumptions of elastic bodies (isotropic and linear elasticity) for each layer, perfect bonding between neighboring layers, and uniform distribution of p at the boundary $r = c$, the radial displacements u_{0c} at the boundary $r = c$, u_{0b} and u_{1b} at the boundary $r = b$, u_{1a} and u_{2a} at the boundary $r = a$ can be obtained by applying the theory of elasticity (Timoshenko and Goodier 1970) as follows:

$$u_{0c} = \frac{1}{E_0(a)} \left[\frac{1 + \nu_0}{2} \frac{b^2 c^2 (p - p_1)}{c^2 - b^2} \frac{1}{c^2} + (1 - 2\nu_0) \frac{pc^2 - p_1 b^2}{c^2 - b^2} c \right] \quad (3.1)$$

$$u_{0b} = \frac{1}{E_0(a)} \left[\frac{1 + \nu_0}{2} \frac{b^2 c^2 (p - p_1)}{c^2 - b^2} \frac{1}{b^2} + (1 - 2\nu_0) \frac{pc^2 - p_1 b^2}{c^2 - b^2} b \right] \quad (3.2)$$

$$u_{1b} = \frac{1}{E_1} \left[\frac{1 + \nu_1}{2} \frac{a^2 b^2 (p_1 - p_2)}{b^2 - a^2} \frac{1}{b^2} + (1 - 2\nu_1) \frac{p_1 b^2 - p_2 a^2}{b^2 - a^2} b \right] \quad (3.3)$$

$$u_{1a} = \frac{1}{E_1} \left[\frac{1 + \nu_1}{2} \frac{a^2 b^2 (p_1 - p_2)}{b^2 - a^2} \frac{1}{a^2} + (1 - 2\nu_1) \frac{p_1 b^2 - p_2 a^2}{b^2 - a^2} a \right] \quad (3.4)$$

$$u_{2a} = \frac{1 - 2\nu_2}{E_2} p_2 a \quad (3.5)$$

Applying the continuity conditions at the interfaces $r = b$ and $r = a$, one obtains

$$u_{0b} = u_{1b} \quad (3.6)$$

$$u_{1a} = u_{2a} \quad (3.7)$$

Because the whole equivalent HMA mixture can be treated as a macroscopically homogeneous medium, the displacement at the boundary $r = c$ can be obtained in another form as follows:

$$u_c = \frac{1 - 2\nu_0}{E_0(a)} pa \quad (3.8)$$

For compatibility of macroscopic and microscopic treatments, the strain energy stored in the area $r \leq c$ should be the same for both cases, which is either treated as a microscopic inhomogeneous material or a macroscopic homogeneous material. According to Christensen and Lo (1979), the following relationship holds:

$$U_{mic} = U_{mac} \quad (3.9)$$

where

U_{mic} = strain energy when HMA is considered as a microscopically inhomogeneous material; and

U_{mac} = corresponding energy when HMA is considered as a macroscopically homogeneous material.

According to the theory of elasticity, the strain energy stored in the area $r \leq c$ is

$$U_{mic} = \frac{1}{2} \oint_L pu_c dl \quad (3.10)$$

$$U_{mac} = \frac{1}{2} \oint_L pu_{0c} dl \quad (3.11)$$

where

$L =$ boundary at $r = c$.

By solving Eqs (3.1) - (3.11) simultaneously, the following relationships can be obtained:

$$p_1 = p \quad (3.12)$$

$$p_2 = \alpha p_1 \quad (3.13)$$

and further, the overall elastic modulus of HMA mixture $E_0(a)$ can be expressed as

$$E_0(a) = \frac{E_1(1-2\nu_0)}{(1+\nu_1)(D-F\alpha)} \quad (3.14)$$

where

$$\alpha = \frac{A_1 B}{A_2 + A_1 C} \quad (3.15)$$

$$A_1 = \frac{1+\nu_1}{E_1} \quad (3.16)$$

$$B = \frac{\frac{1}{2} + \xi}{1-n} \quad (3.17)$$

$$C = \frac{\frac{1}{2} + \xi n}{1-n} \quad (3.18)$$

$$D = \frac{\xi + \frac{1}{2}n}{1-n} \quad (3.19)$$

$$F = \frac{\frac{1}{2}n + \xi n}{1-n} \quad (3.20)$$

$$\xi = \frac{1-2\nu_1}{1+\nu_1} \quad (3.21)$$

$$A_2 = \frac{1-2\nu_2}{E_2} \quad (3.22)$$

$$n = \frac{a^3}{b^3} \quad (3.23)$$

Substituting Eqs (3.15) ~ (3.23) into Eq. (3.14), $E_0(a)$ can be written as

$$E_0(a) = \frac{E_1(1-2\nu_0)(1-n)}{x_1 - \frac{9E_2n(1-\nu_1)^2}{4(1-2\nu_2)(1-n)E_1 + 4E_2x_2}} \quad (3.24)$$

where

$$x_1 = \frac{1}{2}n(1+\nu_1) + (1-2\nu_1) \quad (3.25)$$

$$x_2 = \frac{1}{2}(1+\nu_1) + (1-2\nu_1)n \quad (3.26)$$

From Eq. (3.24) it can be seen that the elastic modulus of the equivalent HMA composite depends not only on the elastic properties, E_i and ν_i ($i = 1, 2$), of individual constituents, but also on aggregate size, a , and the film thickness of asphalt mastic, $b-a$. $E_0(a)$ can be obtained once all the variables have been determined. The values of E_i and ν_i ($i = 1, 2$) can be acquired after the selection of raw materials (aggregates and asphalt binder) of HMA mixtures. Since the Poisson's ratio has minor effect on the predicted values (Kim and Little 2004), constant value was used in the present study for Poisson's ratio.

In order to acquire the thicknesses of asphalt mastic, $b-a$, a simplified method is usually used. In this method, it is assumed every aggregate is coated with the same

thickness of asphalt binder, regardless of the size distribution of aggregates (Li et al. 1999). Thus, the following equation can be obtained (Li et al. 1999)

$$b - a = \frac{f_1}{12f_2 \sum_{i=1}^{N+1} \frac{P(a_i) - P(a_{i+1})}{a_i + a_{i+1}}} \quad (3.27)$$

where

f_1 = volume fraction of asphalt binder in HMA mixture;

f_2 = volume fraction of aggregate in HMA mixture;

a_i = radius of the opening size of the No. i sieve when aggregates are divided into N grades by sieving;

a_{i+1} = radius of the opening size of the No. $(i+1)$ sieve;

$P(a_i)$ = volume fraction of aggregates passing through the No. i sieve; and

$P(a_{i+1})$ = volume fraction of aggregates passing the No. $(i+1)$ sieve.

For f_1, f_2 , and the volume fraction of air voids in HMA mixture f_3 , the following relationship holds

$$f_1 + f_2 + f_3 = 1 \quad (3.28)$$

For most mix designs of dense-graded HMA mixtures, $f_3 = 0.04$ (Roberts et al. 1996).

It should be noted that $P(a)$ is initially the weight fraction of aggregates with radius less than a . In this study, $P(a)$ is used as an approximate volume fraction of aggregates with the particle size below a . It describes the grain size distribution of aggregate used in HMA mixtures. For instance, for continuously graded aggregates, $P(a)$ can be represented by the following equation (Roberts et al. 1996)

$$P(a) = \left(\frac{a}{a_{\max}} \right)^{0.45} \quad (3.29)$$

where

a_{\max} = maximum aggregate radius.

A more accurate thickness of asphalt binder $b-a$ can be obtained by solving the following equation

$$\sum_{i=1}^{N+1} \left(\frac{a_i + a_{i+1}}{a_i + a_{i+1} + 2b - 2a} \right)^3 [P(a_i) - P(a_{i+1})] = \frac{f_1}{f_1 + f_2} \quad (3.30)$$

From Eq. (3.24) a predicted value of elastic modulus can be obtained corresponding to a specific single size, a , of aggregate particle. However, HMA mixtures always use different particle sizes to acquire the desirable aggregate gradation. Every aggregate of specified size makes its contribution to the elastic modulus of the equivalent HMA composite. In order to account for the size distribution of aggregate gradation, the elastic modulus of the equivalent HMA mixtures is expressed as follows:

$$E_0 = \int_{a_{\min}}^{a_{\max}} E_0(a) dP(a) \quad (3.31)$$

where

a_{\min} = minimum aggregate radius.

Integrating Eq. (3.31) is very hard, if not impossible, due to the complex expressions $E_0(a)$ and $P(a)$. Instead, Eq. (3.31) can be approximated by a numerical summation as follows

$$E_0 = \frac{1}{2} \sum_{i=1}^{N+1} [E_0(a_i) + E_0(a_{i+1})] [P(a_i) - P(a_{i+1})] \quad (3.32)$$

where

$E_0(a_i)$ = elastic moduli corresponding to aggregate radius a_i ; and

$E_0(a_{i+1})$ = elastic moduli corresponding to aggregate radius a_{i+1} .

Complex Modulus Converted from Elastic Modulus

The complex modulus of the equivalent HMA mixtures can be obtained based on the elastic-viscoelastic correspondence principle by replacing the elastic modulus of asphalt mastic with its complex modulus. Therefore, Eq. (3.24) can be expressed in the frequency domain as follows:

$$E_0^*(\omega, a) = \frac{E_1^*(\omega)(1-2\nu_0)(1-n)}{x_1 - \frac{9E_2n(1-\nu_1)^2}{4(1-2\nu_2)(1-n)E_1^*(\omega) + 4E_2x_2}} \quad (3.33)$$

where

$E_1^*(\omega)$ = complex modulus of asphalt mastic.

Considering aggregate gradation, the complex modulus of HMA mixtures can be expressed as follows:

$$E_0^*(\omega) = \frac{1}{2} \sum_{i=1}^{N+1} [E_0^*(\omega, a_i) + E_0^*(\omega, a_{i+1})] [P(a_i) - P(a_{i+1})] \quad (3.34)$$

where

$E_0^*(\omega, a_i)$ = complex modulus corresponding to aggregate radius a_i ; and

$E_0^*(\omega, a_{i+1})$ = complex modulus corresponding to aggregate radius a_{i+1} .

Consideration of Air Voids Effect

Air voids play a significant role in the determination of dynamic modulus. It is evident that mixtures with low air void content have higher moduli than mixtures with

high air voids. To better reflect the HMA mixture, it should be noted that not only the air void content, but also the air void distribution have an important influence on the mechanical properties of HMA mixtures. Unfortunately, most existing models so far do not consider air voids in their equations. The ones that do consider air voids fail to look into the air void distributions. To better characterize the HMA mixture, both air void content and air void size distribution should be incorporated in the prediction model. Figure 3.2 presents a typical air void size distribution in conventional dense-graded HMA mixtures obtained from Castelblanco et al. (2005).

To incorporate air voids into the proposed model, the above-mentioned equivalence process can be employed for the second time (Figure 3.3). The air void bubbles entrapped in HMA mixtures can be assumed to be a series of empty spheres of different sizes covered by same thickness of the first-time equivalent HMA medium. The first-time equivalent HMA medium-coated air bubbles are then embedded in the second-time equivalent medium.

Let $E_2 = 0$ in the previous equations, the elastic and complex moduli for HMA mixtures with the consideration of air voids can be obtained. The predictive equation of the elastic modulus for the three-dimensional micromechanical model can be expressed as follows:

$$E_0(a) = \frac{2E_1(1-n)(1-2\nu_0)}{n(1+\nu_1) + 2(1-2\nu_1)} \quad (3.35)$$

The mathematical expressions for the other equations in the model should also be changed accordingly.

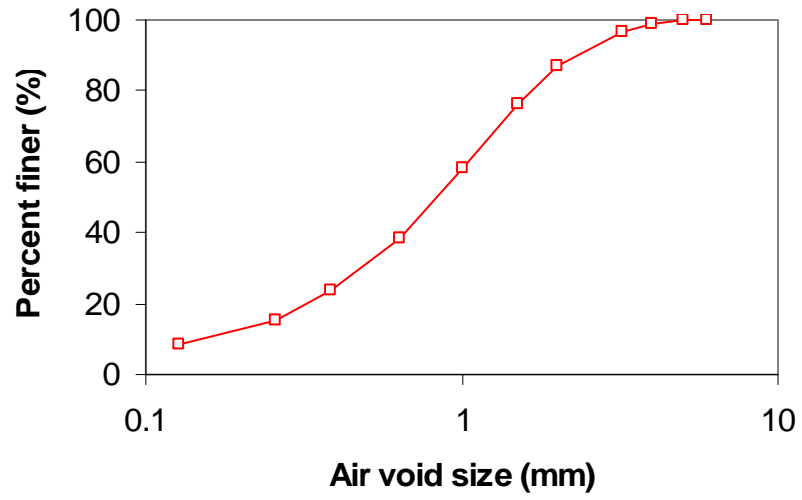


Figure 3.2 Air Void Size Distribution in HMA Mixture

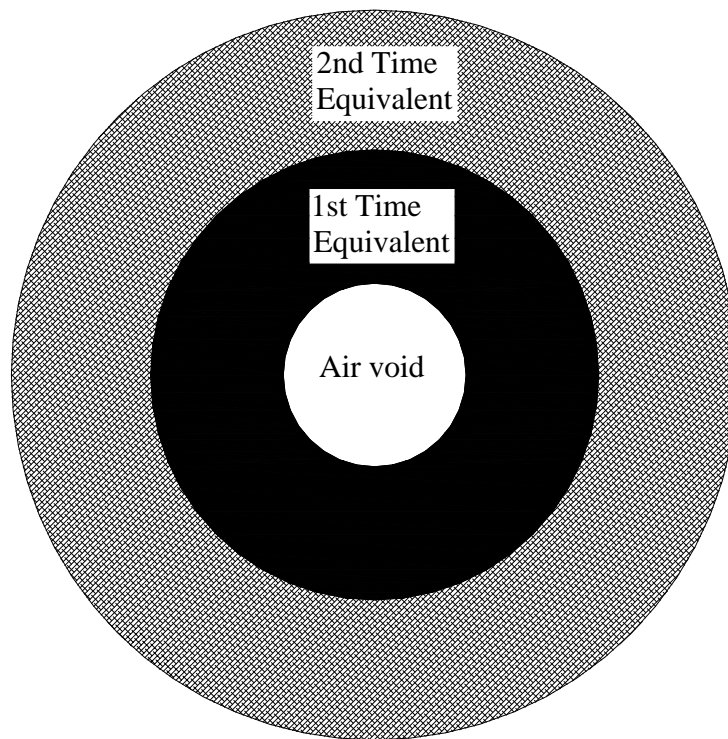


Figure 3.3 Incorporation of Air Voids in Equivalent HMA mixtures

CHAPTER 4 DEVELOPMENT OF FORMULATIONS FOR PFC MODELS USING DIFFERENTIAL METHOD

Introduction

Among various PFC micromechanical models developed to predict the modulus of composites, many can give satisfactory predictions at low to moderate volume concentrations of inclusions when the constituent materials do not differ very much in stiffness. At high concentrations, however, the predicted moduli have been observed to deviate increasingly farther from the measured values with the increase in the volume fraction of inclusion, especially when the component materials are highly different in stiffness (Pal 2005a, 2005b). The differential method used for development of PFC models shows a potential capability of accurately predicting the modulus of composites even at high volume concentrations and when there is a large mis-match in stiffness of the constituent materials (Pal 2005a, 2005b; Christensen 1990). Pal (2005a, 2005b) presented the predictive equations from the differential method for composites composed of incompressible inclusions ($\nu_i = 0.5$) embedded in incompressible matrix ($\nu_m = 0.5$). In this chapter, more general predictive equations from the differential method are given and then used to predict the dynamic modulus of HMA mixtures in the later part of this dissertation.

For the convenience and conciseness of derivation, the subscript “c” for composite is ignored and E , G , and K are used for elastic, shear, and bulk modulus of composite throughout this chapter.

Formulation Development for Elastic and Complex Modulus Predictions

The differential method starts with the predictive equations for the effective shear and bulk moduli, G and K , for an infinitely dilute suspension containing non-interacting spherical inclusions:

$$G = G_m \left[1 + \frac{15(1 - \nu_m) \left(\frac{G_i}{G_m} - 1 \right) c}{7 - 5\nu_m + 2(4 - 5\nu_m) \frac{G_i}{G_m}} \right] \quad (4.1)$$

and

$$K = K_m \left[1 + \frac{3(1 - \nu_m) \left(\frac{K_i}{K_m} - 1 \right) c}{2(1 - 2\nu_m) + (1 + \nu_m) \frac{K_i}{K_m}} \right] \quad (4.2)$$

For elastic, homogeneous, and isotropic materials, the following theoretical relationships hold between elastic modulus, E , shear modulus, G , bulk modulus, K , and Poisson's ratio, ν :

$$G = \frac{E}{2(1 + \nu)} \quad (4.3)$$

$$K = \frac{E}{3(1 - 2\nu)} \quad (4.4)$$

Substituting Eq.(4.3) into Eq.(4.1), one obtains

$$G = \frac{E_m}{2(1 + \nu_m)} \left\{ 1 + \frac{15(1 - \nu_m) \left[\frac{E_i(1 + \nu_m)}{E_m(1 + \nu_i)} - 1 \right] c}{7 - 5\nu_m + 2(4 - 5\nu_m) \frac{E_i(1 + \nu_m)}{E_m(1 + \nu_i)}} \right\} \quad (4.5)$$

Similarly, substitution of Eq.(4.4) into Eq.(4.2) gives

$$K = \frac{E_m}{3(1-2\nu_m)} \left\{ 1 + \frac{3(1-\nu_m) \left[\frac{E_i(1-2\nu_m)}{E_m(1-2\nu_i)} - 1 \right] c}{2(1-2\nu_m) + (1+\nu_m) \frac{E_i(1-2\nu_m)}{E_m(1-2\nu_i)}} \right\} \quad (4.6)$$

In the linear elasticity, the following relationship holds

$$E = \frac{9KG}{3K+G} \quad (4.7)$$

Substitution of Eqs.(4.5) and (4.6) into Eq.(4.7) leads to

$$\frac{E}{E_m} = \frac{3 \left\{ 1 + \frac{3(1-\nu_m) \left[\frac{E_i(1-2\nu_m)}{E_m(1-2\nu_i)} - 1 \right] c}{2(1-2\nu_m) + (1+\nu_m) \frac{E_i(1-2\nu_m)}{E_m(1-2\nu_i)}} \right\} \left\{ 1 + \frac{15(1-\nu_m) \left[\frac{E_i(1+\nu_m)}{E_m(1+\nu_i)} - 1 \right] c}{7-5\nu_m + 2(4-5\nu_m) \frac{E_i(1+\nu_m)}{E_m(1+\nu_i)}} \right\}}{2(1+\nu_m) \left\{ 1 + \frac{3(1-\nu_m) \left[\frac{E_i(1-2\nu_m)}{E_m(1-2\nu_i)} - 1 \right] c}{2(1-2\nu_m) + (1+\nu_m) \frac{E_i(1-2\nu_m)}{E_m(1-2\nu_i)}} \right\} + (1-2\nu_m) \left\{ 1 + \frac{15(1-\nu_m) \left[\frac{E_i(1+\nu_m)}{E_m(1+\nu_i)} - 1 \right] c}{7-5\nu_m + 2(4-5\nu_m) \frac{E_i(1+\nu_m)}{E_m(1+\nu_i)}} \right\}} \quad (4.8)$$

Eq.(4.8) can be further rewritten as

$$\frac{E}{E_m} = \frac{\left\{ 1 + \frac{3(1-\nu_m) \left[\frac{E_i}{E_m(1-2\nu_i)} - \frac{1}{1-2\nu_m} \right] c}{2 + \frac{E_i(1+\nu_m)}{E_m(1-2\nu_i)}} \right\} \left\{ 1 + \frac{15(1-\nu_m) \left[\frac{E_i}{E_m(1+\nu_i)} - \frac{1}{1+\nu_m} \right] c}{\frac{7-5\nu_m}{1+\nu_m} + \frac{2(4-5\nu_m)E_i}{(1+\nu_i)E_m}} \right\}}{1+c \left\{ \frac{2(1+\nu_m)(1-\nu_m) \left[\frac{E_i}{E_m(1-2\nu_i)} - \frac{1}{1-2\nu_m} \right]}{2 + \frac{E_i(1+\nu_m)}{E_m(1-2\nu_i)}} + \frac{5(1-\nu_m)(1-2\nu_m) \left[\frac{E_i}{E_m(1+\nu_i)} - \frac{1}{1+\nu_m} \right]}{\frac{7-5\nu_m}{1+\nu_m} + \frac{2(4-5\nu_m)E_i}{(1+\nu_i)E_m}} \right\}} \quad (4.9)$$

Using the relationship $\frac{1}{1+x} = 1 - x + O(c)$ ($|x| \ll 0$), Eq.(4.9) can be expressed

as

$$\begin{aligned}
\frac{E}{E_m} &= \left\{ 1 + \frac{3(1-v_m) \left[\frac{E_i}{E_m(1-2v_i)} - \frac{1}{1-2v_m} \right] c}{2 + \frac{E_i(1+v_m)}{E_m(1-2v_i)}} \right\} \left\{ 1 + \frac{15(1-v_m) \left[\frac{E_i}{E_m(1+v_i)} - \frac{1}{1+v_m} \right] c}{\frac{7-5v_m}{1+v_m} + \frac{2(4-5v_m)E_i}{(1+v_i)E_m}} \right\} \\
&\cdot \left\{ 1 - \frac{2(1+v_m)(1-v_m) \left[\frac{E_i}{E_m(1-2v_i)} - \frac{1}{1-2v_m} \right] c}{2 + \frac{E_i(1+v_m)}{E_m(1-2v_i)}} - \frac{5(1-v_m)(1-2v_m) \left[\frac{E_i}{E_m(1+v_i)} - \frac{1}{1+v_m} \right] c}{\frac{7-5v_m}{1+v_m} + \frac{2(4-5v_m)E_i}{(1+v_i)E_m}} + O(c) \right\} \\
&= 1 + \left\{ \frac{3(1-v_m) \left[\frac{E_i}{E_m(1-2v_i)} - \frac{1}{1-2v_m} \right]}{2 + \frac{E_i(1+v_m)}{E_m(1-2v_i)}} + \frac{15(1-v_m) \left[\frac{E_i}{E_m(1+v_i)} - \frac{1}{1+v_m} \right]}{\frac{7-5v_m}{1+v_m} + \frac{2(4-5v_m)E_i}{(1+v_i)E_m}} \right. \\
&\quad \left. - \frac{2(1+v_m)(1-v_m) \left[\frac{E_i}{E_m(1-2v_i)} - \frac{1}{1-2v_m} \right]}{2 + \frac{E_i(1+v_m)}{E_m(1-2v_i)}} - \frac{5(1-v_m)(1-2v_m) \left[\frac{E_i}{E_m(1+v_i)} - \frac{1}{1+v_m} \right]}{\frac{7-5v_m}{1+v_m} + \frac{2(4-5v_m)E_i}{(1+v_i)E_m}} \right\} c + O(c) \\
&= 1 + \left\{ 10(1+v_m) \frac{\frac{1-v_m}{1+v_i} \cdot \frac{E_i}{E_m} - \frac{1-v_m}{1+v_m}}{\frac{8-10v_m}{1+v_i} \cdot \frac{E_i}{E_m} + \frac{7-5v_m}{1+v_m}} + (1-2v_m) \frac{\frac{1-v_m}{1+v_m} \cdot \left[\frac{E_i}{E_m} - \frac{1-2v_i}{1-2v_m} \right]}{\frac{E_i}{E_m} + \frac{2-4v_i}{1+v_m}} \right\} c + O(c)
\end{aligned} \tag{4.10}$$

Neglecting the infinitesimal term of higher orders, $O(c)$, Eq.(4.10) can be rewritten as

$$\frac{E}{E_m} = 1 + \left\{ 10(1+v_m) \frac{\frac{1-v_m}{1+v_i} \cdot \frac{E_i}{E_m} - \frac{1-v_m}{1+v_m}}{\frac{8-10v_m}{1+v_i} \cdot \frac{E_i}{E_m} + \frac{7-5v_m}{1+v_m}} + (1-2v_m) \frac{\frac{1-v_m}{1+v_m} \cdot \left[\frac{E_i}{E_m} - \frac{1-2v_i}{1-2v_m} \right]}{\frac{E_i}{E_m} + \frac{2-4v_i}{1+v_m}} \right\} c \quad (4.11)$$

Let

$$\alpha_1 = \frac{1-v_m}{1+v_i} \quad (4.12)$$

$$\alpha_2 = \frac{1-v_m}{1+v_m} \quad (4.13)$$

$$\alpha_3 = \frac{8-10v_m}{1+v_i} \quad (4.14)$$

$$\alpha_4 = \frac{7-5v_m}{1+v_m} \quad (4.15)$$

$$\alpha_5 = \frac{1-2v_i}{1-2v_m} \quad (4.16)$$

$$\alpha_6 = \frac{1-2v_i}{1+v_m} \quad (4.17)$$

$$\alpha_7 = 10(1+v_m) \quad (4.18)$$

$$\alpha_8 = 1-2v_m \quad (4.19)$$

One obtains

$$\frac{E}{E_m} = 1 + \left[\alpha_7 \frac{\alpha_1 \frac{E_i}{E_m} - \alpha_2}{\alpha_3 \frac{E_i}{E_m} + \alpha_4} + \alpha_8 \frac{\alpha_2 \left(\frac{E_i}{E_m} - \alpha_5 \right)}{\frac{E_i}{E_m} + \alpha_6} \right] c \quad (4.20)$$

Thus, the predictive equation has been developed for the effective elastic modulus of an infinitely dilute suspension containing non-interacting spherical inclusions in terms of the properties of individual constituents (E_m , ν_m , E_i , and ν_i) and the volume concentration of inclusion in composite (c).

In the differential method, the composite material can be viewed as a sequence of dilute suspensions into which an increment of inclusions is added. The incremental increase in the elastic modulus, dE , resulting from the addition of the new particles can be calculated using Eq.(4.20) by treating the composite into which the new inclusions are added as an equivalent medium with elastic modulus E (Christensen 1990; Pal 2005a, 2005b). The process is continued until the finite volume concentration or fraction of inclusion is reached.

Thus from Eq.(4.20), one obtains

$$dE = E \left[\begin{array}{c} \alpha_1 \frac{E_i}{E_m} - \alpha_2 \\ \alpha_3 \frac{E_i}{E_m} + \alpha_4 \end{array} + \alpha_8 \frac{\alpha_2 \left(\frac{E_i}{E_m} - \alpha_5 \right)}{\frac{E_i}{E_m} + \alpha_6} \right] \frac{dc}{1-c} \quad (4.21)$$

Eq.(4.21) can be further written as

$$\frac{dE}{E \left[\frac{\alpha_1 \alpha_7 E_i - \alpha_2 \alpha_7 E}{\alpha_3 E_i + \alpha_4 E} + \frac{\alpha_2 \alpha_8 (E_i - \alpha_5 E)}{E_i + \alpha_6 E} \right]} = \frac{dc}{1-c} \quad (4.22)$$

and

$$\frac{(\alpha_3 E_i + \alpha_4 E)(E_i + \alpha_6 E)}{E [(\alpha_1 \alpha_7 E_i - \alpha_2 \alpha_7 E)(E_i + \alpha_6 E) + (\alpha_3 E_i + \alpha_4 E)(\alpha_2 \alpha_8 E_i - \alpha_2 \alpha_5 \alpha_8 E)]} dE = \frac{dc}{1-c} \quad (4.23)$$

The denominator of the partial fraction on the left-hand side of Eq.(4.23) can be further expressed as

$$\begin{aligned}
& E[(\alpha_1\alpha_7E_i - \alpha_2\alpha_7E)(E_i + \alpha_6E) + (\alpha_3E_i + \alpha_4E)(\alpha_2\alpha_8E_i - \alpha_2\alpha_5\alpha_8E)] \\
&= E[-(\alpha_2\alpha_6\alpha_7 + \alpha_2\alpha_4\alpha_5\alpha_8)E^2 + (\alpha_1\alpha_6\alpha_7 - \alpha_2\alpha_7 + \alpha_2\alpha_4\alpha_8 - \alpha_2\alpha_3\alpha_5\alpha_8)EE_i + (\alpha_1\alpha_7 + \alpha_2\alpha_3\alpha_8)E_i^2] \\
&= E[\beta_0(E^2 + \beta_1E_iE + \beta_2E_i^2)] \\
&= \beta_0E(E - x_1E_i)(E - x_2E_i)
\end{aligned} \tag{4.24}$$

where

$$\beta_0 = -(\alpha_2\alpha_6\alpha_7 + \alpha_2\alpha_4\alpha_5\alpha_8) \tag{4.25}$$

$$\beta_1 = \frac{\alpha_1\alpha_6\alpha_7 - \alpha_2\alpha_7 + \alpha_2\alpha_4\alpha_8 - \alpha_2\alpha_3\alpha_5\alpha_8}{\beta_0} \tag{4.26}$$

$$\beta_2 = \frac{\alpha_1\alpha_7 + \alpha_2\alpha_3\alpha_8}{\beta_0} \tag{4.27}$$

x_1 and x_2 are the roots of the following equation

$$x^2 + \beta_1x + \beta_2 = 0 \tag{4.28}$$

and thus they can be expressed as

$$x_{1,2} = \frac{-\beta_1 \pm \sqrt{\beta_1^2 - 4\beta_2}}{2} \tag{4.29}$$

The numerator of the partial fraction in the left-hand side of Eq.(4.23) can be further expressed as

$$\begin{aligned}
& (\alpha_3E_i + \alpha_4E)(E_i + \alpha_6E) \\
&= \alpha_4\alpha_6E^2 + (\alpha_4 + \alpha_3\alpha_6)EE_i + \alpha_3E_i^2
\end{aligned}$$

$$= \beta_0 (\beta_3 E^2 + \beta_4 E_i E + \beta_5 E_i^2) \quad (4.30)$$

where

$$\beta_3 = \frac{\alpha_4 \alpha_6}{\beta_0} \quad (4.31)$$

$$\beta_4 = \frac{\alpha_4 + \alpha_3 \alpha_6}{\beta_0} \quad (4.32)$$

$$\beta_5 = \frac{\alpha_3}{\beta_0} \quad (4.33)$$

Substituting Eqs.(4.24) and (4.30) into Eq.(4.23), one obtains

$$\frac{\beta_3 E^2 + \beta_4 E_i E + \beta_5 E_i^2}{E(E - x_1 E_i)(E - x_2 E_i)} dE = \frac{dc}{1-c} \quad (4.34)$$

The partial fraction of the left-hand side of Eq.(4.34) can be decomposed into three parts. The decomposition leads to

$$\left(\frac{A}{E} + \frac{B}{E - x_1 E_i} + \frac{C}{E - x_2 E_i} \right) dE = \frac{dc}{1-c} \quad (4.35)$$

where

$$A = \frac{\beta_5}{\beta_2} \quad (4.36)$$

$$B = \frac{1}{x_2 - x_1} \left[-x_1 \left(\beta_3 - \frac{\beta_5}{\beta_2} \right) + \frac{\beta_5 \beta_1}{\beta_2} - \beta_4 \right] \quad (4.37)$$

$$C = \frac{1}{x_2 - x_1} \left[x_2 \left(\beta_3 - \frac{\beta_5}{\beta_2} \right) - \frac{\beta_5 \beta_1}{\beta_2} + \beta_4 \right] \quad (4.38)$$

Integration of Eq.(4.35) with the limits $E \rightarrow E_m$ at $c \rightarrow 0$ gives

$$A \ln\left(\frac{E}{E_m}\right) + B \ln\left(\frac{E - x_1 E_i}{E_m - x_1 E_i}\right) + C \ln\left(\frac{E - x_2 E_i}{E_m - x_2 E_i}\right) = -\ln(1 - c) \quad (4.39)$$

Eq.(4.39) can be further written as

$$\left(\frac{E}{E_m}\right)^A \left(\frac{E - x_1 E_i}{E_m - x_1 E_i}\right)^B \left(\frac{E - x_2 E_i}{E_m - x_2 E_i}\right)^C = (1 - c)^{-1} \quad (4.40)$$

If the properties of the component materials (E_m , v_m , E_i and v_i) and the volume fraction of inclusion (c) are already known, Eq.(4.40) can be solved using various numerical methods to obtain the elastic modulus of a composite material.

For HMA mixtures, it is reasonable to assume that the properties of aggregate are elastic and those of asphalt binder viscoelastic. Using the elastic-viscoelastic correspondence principle, Eq.(4.40) can be converted to the frequency domain to predict the effective complex modulus of HMA mixtures

$$\left(\frac{E^*}{E_m^*}\right)^A \left(\frac{E^* - x_1 E_i}{E_m^* - x_1 E_i}\right)^B \left(\frac{E^* - x_2 E_i}{E_m^* - x_2 E_i}\right)^C = (1 - c)^{-1} \quad (4.41)$$

However, difficulty arises regarding solving Eq.(4.41) with numerical methods. Because the effective complex modulus $E^*(\omega)$ is expressed implicitly in Eq. (4.41) and the exponents A , B , and C are generally fractions, it is very hard to get the solution even using numerical methods. To facilitate the solution of Eq.(4.41), two special cases are considered in this study.

For the first case, the composites composed of incompressible inclusions ($v_i = 0.5$) embedded in incompressible matrix ($v_m = 0.5$) are considered. Then Eq.(4.41) can be reduced to

$$\left(\frac{E^*}{E_m^*}\right)\left(\frac{E^* - E_i}{E_m^* - E_i}\right)^{-2.5} = (1-c)^{-2.5} \quad (4.42)$$

Eq.(4.42) is the same as the one given by Pal (2005a).

For the second case, the Poisson's ratios $\nu_i = 0.2$ and $\nu_m = 0.2$ are used. Thus,

Eq.(4.41) can be reduced to

$$\left(\frac{E^*}{E_m^*}\right)\left(\frac{E^* - E_i}{E_m^* - E_i}\right)^{-2} = (1-c)^{-2} \quad (4.43)$$

To consider air voids effect on the effective modulus of composite, let $E_i = 0$,

from Eq. (4.11) one obtains

$$\frac{E}{E_m} = 1 - \left[\frac{10(1 - \nu_m^2)}{7 - 5\nu_m} + \frac{1 - \nu_m}{2} \right] c \quad (4.44)$$

The incremental change in the effective elastic modulus of the composite due to the incorporation of an infinitely small number of new air bubbles is

$$\frac{dE}{E} = - \left[\frac{10(1 - \nu_m^2)}{7 - 5\nu_m} + \frac{1 - \nu_m}{2} \right] \frac{dc}{1 - c} \quad (4.45)$$

On integration, one obtains

$$\ln\left(\frac{E}{E_m}\right) = \left[\frac{10(1 - \nu_m^2)}{7 - 5\nu_m} + \frac{1 - \nu_m}{2} \right] \ln(1 - c) \quad (4.46)$$

or

$$E = E_m (1 - c)^{\beta_6} \quad (4.47)$$

where

$$\beta_6 = \frac{10(1 - \nu_m^2)}{7 - 5\nu_m} + \frac{1 - \nu_m}{2} \quad (4.48)$$

For the effective complex modulus of a viscoelastic material containing air voids, Eq.(4.47) becomes

$$E^* = E_m^*(1-c)^{\beta_6} \quad (4.49)$$

Formulation Development for Shear and Complex Shear Modulus Predictions

The effective shear modulus of a composite material can be derived using the differential method in a similar manner.

The incremental increase in the effective shear modulus, dG , resulting from the incremental increase in the volume fraction of inclusion, dc , due to the addition of the new inclusion particles can be calculated from Eq.(4.1) as

$$dG = G \frac{15(1-v_m) \left(\frac{G_i}{G} - 1 \right)}{7-5v_m + 2(4-5v_m) \frac{G_i}{G}} \frac{dc}{1-c} \quad (4.50)$$

Eq.(4.50) can be further written as

$$\left[\frac{8-10v_m}{15(1-v_m)} \cdot \frac{1}{G} + \frac{1}{G_i - G} \right] dG = \frac{dc}{1-c} \quad (4.51)$$

Integration of Eq.(4.51) with the limits $G \rightarrow G_m$ at $c \rightarrow 0$ gives

$$\frac{8-10v_m}{15(1-v_m)} \ln \left(\frac{G}{G_m} \right) + \ln \left(\frac{G_i - G_m}{G_i - G} \right) = -\ln(1-c) \quad (4.52)$$

Eq.(4.52) can be further written as

$$\left(\frac{G}{G_m} \right)^{\frac{8-10v_m}{15(1-v_m)}} \left(\frac{G_i - G_m}{G_i - G} \right) = (1-c)^{-1} \quad (4.53)$$

Using the elastic-viscoelastic correspondence principle, Eq.(4.53) can be converted to the frequency domain to predict the effective complex shear modulus of a viscoelastic composite material as follows

$$\left(\frac{G^*}{G_m^*}\right)^{\frac{8-10\nu_m}{15(1-\nu_m)}}\left(\frac{G_i - G_m^*}{G_i - G^*}\right) = (1-c)^{-1} \quad (4.54)$$

To get the numerical solution of Eq.(4.54), special cases were also considered.

For the special cases $\nu_m = 0.5$ and $\nu_m = 0.2$, Eq.(4.54) becomes

$$\left(\frac{G^*}{G_m^*}\right)\left(\frac{G^* - G_i}{G_m^* - G_i}\right)^{-2.5} = (1-c)^{-2.5} \quad (4.55)$$

and

$$\left(\frac{G^*}{G_m^*}\right)\left(\frac{G^* - G_i}{G_m^* - G_i}\right)^{-2} = (1-c)^{-2} \quad (4.56)$$

To consider air voids effect on the effective shear modulus of a composite material, let $G_i = 0$, from Eq. (4.53) one obtains

$$\left(\frac{G}{G_m}\right)^{\frac{8-10\nu_m}{15(1-\nu_m)}}\left(\frac{G_m}{G}\right) = (1-c)^{-1} \quad (4.57)$$

Eq.(4.57) can be further rewritten as

$$G = G_m(1-c)^{\beta_7} \quad (4.58)$$

where

$$\beta_7 = \frac{15(1-\nu_m)}{7-5\nu_m} \quad (4.59)$$

For the effective complex shear modulus of a viscoelastic material containing air voids, Eq.(4.58) becomes

$$G^* = G_m^* (1 - c)^{\beta_7} \quad (4.60)$$

Formulation Development for Bulk and Complex Bulk Modulus Predictions

In a similar manner, the effective bulk modulus of a composite material can also be obtained from the differential method.

The incremental increase in the effective bulk modulus, dK , resulting from the incremental increase in the volume fraction of inclusion, dc , due to the addition of the new particles can be calculated from Eq.(4.2) as follows

$$dK = K \frac{3(1 - v_m) \left(\frac{K_i}{K} - 1 \right)}{2(1 - 2v_m) + (1 + v_m) \frac{K_i}{K}} \frac{dc}{1 - c} \quad (4.61)$$

Eq.(4.61) can be further written as

$$\left[\frac{1 + v_m}{3(1 - v_m)} \frac{1}{K} + \frac{1}{K_i - K} \right] dK = \frac{dc}{1 - c} \quad (4.62)$$

Integration of Eq.(4.62) with the limits $K \rightarrow K_m$ at $c \rightarrow 0$ gives

$$\frac{1 + v_m}{3(1 - v_m)} \ln \left(\frac{K}{K_m} \right) + \ln \left(\frac{K_i - K_m}{K_i - K} \right) = -\ln(1 - c) \quad (4.63)$$

Eq.(4.63) can be further written as

$$\left(\frac{K}{K_m} \right)^{\frac{1 + v_m}{3(1 - v_m)}} \left(\frac{K_i - K_m}{K_i - K} \right) = (1 - c)^{-1} \quad (4.64)$$

Based on the elastic-viscoelastic correspondence principle, to obtain the complex bulk modulus of a viscoelastic composite material, Eq.(4.64) can be converted to

$$\left(\frac{K^*}{K_m^*}\right)^{\frac{1+v_m}{3(1-v_m)}}\left(\frac{K_i - K_m^*}{K_i - K^*}\right) = (1-c)^{-1} \quad (4.65)$$

For the special cases $v_m = 0.5$ and $v_m = 0.2$, Eq.(4.65) becomes

$$\left(\frac{K^*}{K_m^*}\right)\left(\frac{K_i - K_m^*}{K_i - K^*}\right) = (1-c)^{-1} \quad (4.66)$$

and

$$\left(\frac{K^*}{K_m^*}\right)\left(\frac{K_i - K_m^*}{K_i - K^*}\right)^2 = (1-c)^{-2} \quad (4.67)$$

It is interesting to note that from Eq.(4.66) one can get

$$\frac{1}{K^*} = \frac{c}{K_i} + \frac{1-c}{K_m^*} \quad (4.68)$$

which is equivalent to the series model.

To consider air voids effect on the effective shear modulus of a composite, let

$K_i = 0$, from Eq. (4.64) one obtains

$$\left(\frac{K}{K_m}\right)^{\frac{1+v_m}{3(1-v_m)}}\left(\frac{K_m}{K}\right) = (1-c)^{-1} \quad (4.69)$$

Eq.(4.69) can be further rewritten as

$$K = K_m (1-c)^{\beta_8} \quad (4.70)$$

where

$$\beta_8 = \frac{3-3v_m}{2-4v_m} \quad (4.71)$$

For the effective complex bulk modulus of a viscoelastic material containing air voids, Eq.(4.70) becomes

$$K^* = K_m^* (1 - c)^{\beta_8} \quad (4.72)$$

CHAPTER 5 LABORATORY EXPERIMENTS

Introduction

In this study, laboratory experiments were conducted to evaluate the newly developed and modified existing PFC micromechanical models. Firstly, asphalt binder and mastic were tested to obtain their dynamic (complex) shear moduli. Then HMA mixture specimens were tested for their dynamic (complex) moduli. In the prediction of dynamic shear modulus of asphalt cement mastic with the PFC models described later in Chapter 6, the measured dynamic shear modulus and phase angle of asphalt binder were used as input parameters in the predictive equations and the predicted values of dynamic shear modulus of asphalt mastic were compared with the laboratory measured data. In the prediction of dynamic modulus of HMA mixture described later in Chapter 7, the measured complex shear moduli of asphalt binder and mastic were used as input parameters in the predictive equations and the predicted values of dynamic modulus of HMA mixtures were compared to the measured data. Through the comparison between the predicted and measured data, the PFC models and the predictive equations from them can then be evaluated to determine if they are suitable for asphalt mastics and mixtures.

Asphalt Binder and Mastic Tests

Materials

One type of conventional asphalt binder, PG 64-22, which is widely used in the state of Tennessee, was selected for asphalt binder, mastic, and mixture tests. Its properties are presented in Table 5.1 (Huang et al. 2005).

Table 5.1 Asphalt Binder Properties

Binder Status	Binder Test	Test Results	Specification	
Original binder	Rotational viscosity at 135°C, Pa*s	0.52	3 Pa*s max	
	DSR, $G^*/\sin\delta$, kPa	70°C	0.78	1.00 kPa min
64°C		1.63		
RTFO aged binder	DSR, $G^*/\sin\delta$, kPa	70°C	1.66	2.20 kPa min
		64°C	3.54	
PAV aged binder	DSR, $G^*\sin\delta$, MPa, 25°C		3725	5000 kPa max
	BBR creep stiffness S, MPa		238	300.0 MPa max
	BBR creep slope, m value		0.310	0.300 min
PG grading		64-22		

Note: RTFO = rolling thin-film oven; PAV = pressure aging vessel; DSR = dynamic shear rheometer; BBR = bending beam rheometer.

The mineral filler (aggregate fraction passing No. 200 sieve) used in this study was obtained by sieving the aggregate blend used for HMA mixture. The specific gravity of the mineral filler was 2.72 and its particle size distribution is presented in Figure 5.1. A microscopic picture indicated that mineral filler had spherical particles and smooth texture (Figure 5.2).

Sample Fabrication

To prepare the mastic samples for dynamic shear modulus testing, asphalt binder and mineral filler were preheated in an oven to 165°C. Then, they were hand-mixed in a container heated on an electric hot-plate set to a temperature of approximately 165°C. The asphalt binder and mastic were aged using the rolling thin-film oven (RTFO) aging procedure before they were poured into a silicone mold to produce the samples for the dynamic shear modulus testing. Test samples with the sizes of 1 mm thick by 25 mm in diameter or 2 mm thick by 8 mm in diameter were fabricated from the aged binder and

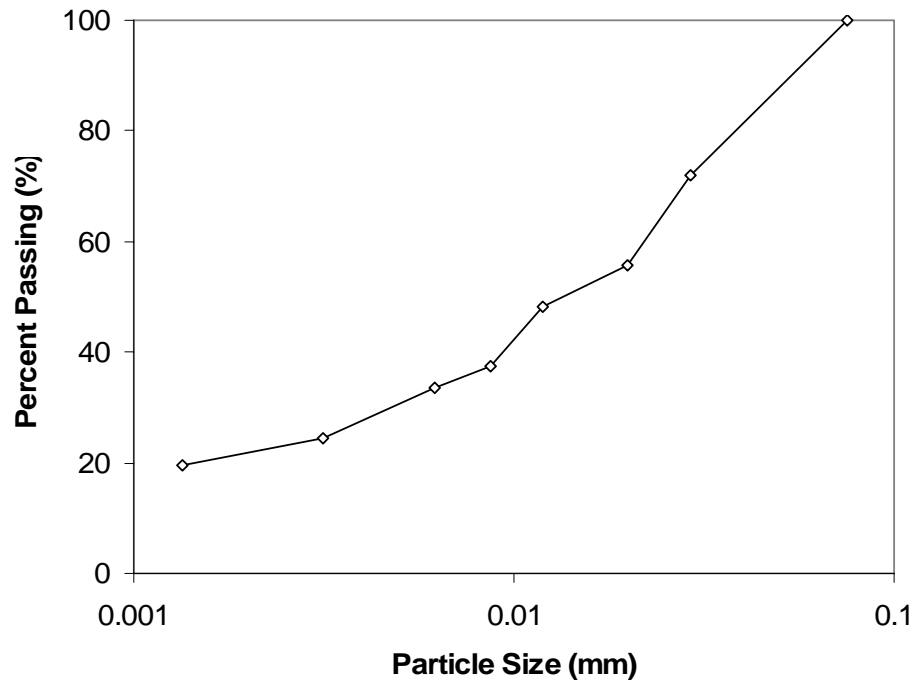


Figure 5.1 Particle Size Distribution of Mineral Filler

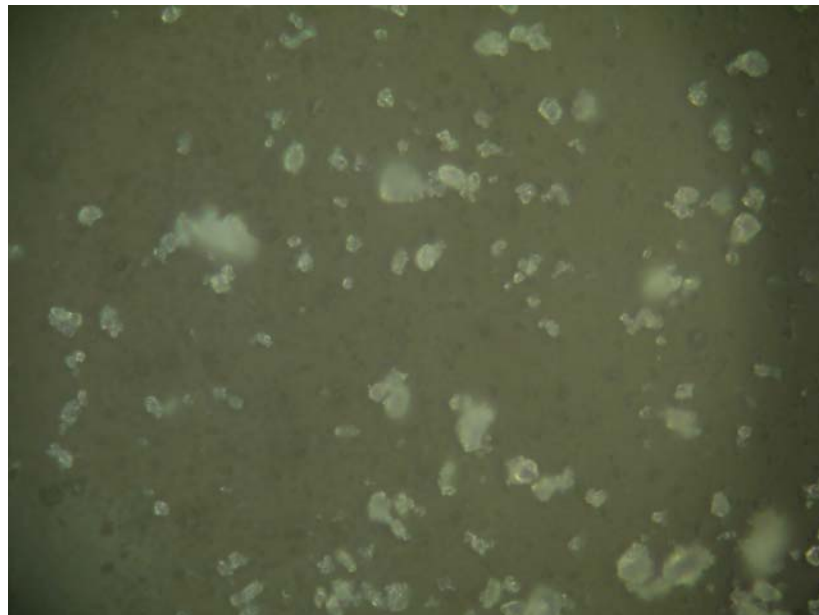


Figure 5.2 Microscopic Picture of Mineral Filler (400X)

mastic (Figure 5.3). Asphalt mastic samples were made at three volume concentrations of 20%, 35%, and 50%.

Dynamic Shear Rheometer (DSR) Testing

In this study, DSR test was performed on asphalt binder and mastic specimens to obtain the values of dynamic shear modulus and phase angle. Figure 5.4 shows a schematic of the dynamic shear rheometer (Roberts et al. 1996).

In the DSR testing, a sinusoidal shear stress or strain is applied to specimens sandwiched between a fixed plate and a plate that oscillates back and forth as shown in Figure 5.4. After some period of time, a steady state sinusoidal strain or stress response occurs. Due to the viscoelastic nature of asphalt binder, the shear strain always lags the shear stress.

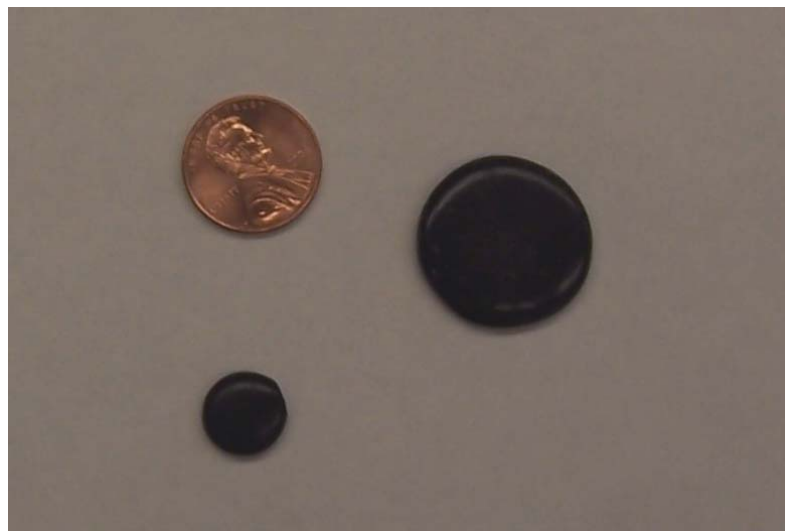


Figure 5.3 Asphalt Binder or Mastic Samples

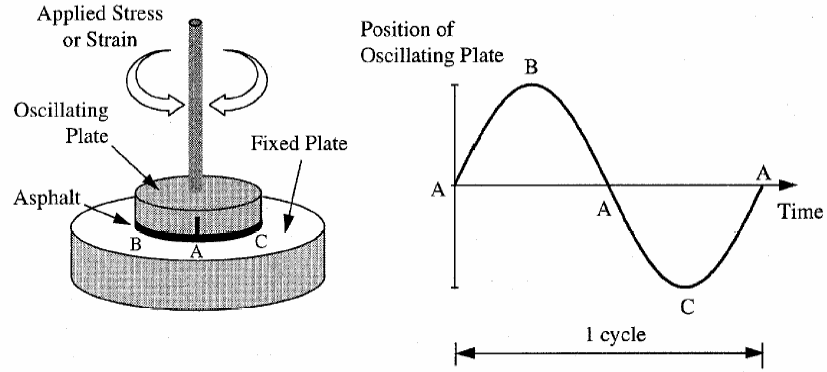


Figure 5.4 Schematic of Dynamic Shear Rheometer (Roberts et al. 1994)

The dynamic shear modulus is defined as (Roberts et al. 1996)

$$|G^*| = \frac{\tau_{\max}}{\gamma_{\max}} \quad (5.1)$$

where

$|G^*|$ = dynamic shear modulus;

τ_{\max} = maximum shear stress;

γ_{\max} = maximum shear strain.

and the lag in the phase between shear stress and strain is the phase angle ϕ .

The Anton Paar Physica MCR 501 Rheometer manufactured by the Anton Paar Germany GmbH was used to test the asphalt binder and mastic (Figure 5.5). The whole testing procedures can be automatically finished with the Physica Rheoplus Software. In this study, the DSR testing was conducted at the temperatures of 15°C, 25°C, and 35°C and at the frequencies from 0.03Hz to 25Hz. The master curves of complex shear

modulus of asphalt binder and mastic at 25°C were then constructed with the Physica Rheoplus Software. Figure 5.6 shows the interface of the Physica Rheoplus Software.

After the DSR testing, the Prony series were fitted to the measured data of complex shear modulus of asphalt binder and mastic. The Prony series representations were then obtained for relaxation shear modulus of asphalt binder and mastic. In the prediction of mastic modulus, the Prony series representation for relaxation shear modulus of asphalt binder was used as one of input parameters in the predictive equations acquired from different PFC models. In the prediction of HMA mixture modulus, the Prony series representations for asphalt binder and mastic were used as input parameters in the predictive equations. They are discussed in more detail in the later part of this dissertation.



Figure 5.5 Anton Paar Physica MCR 501 Rheometer

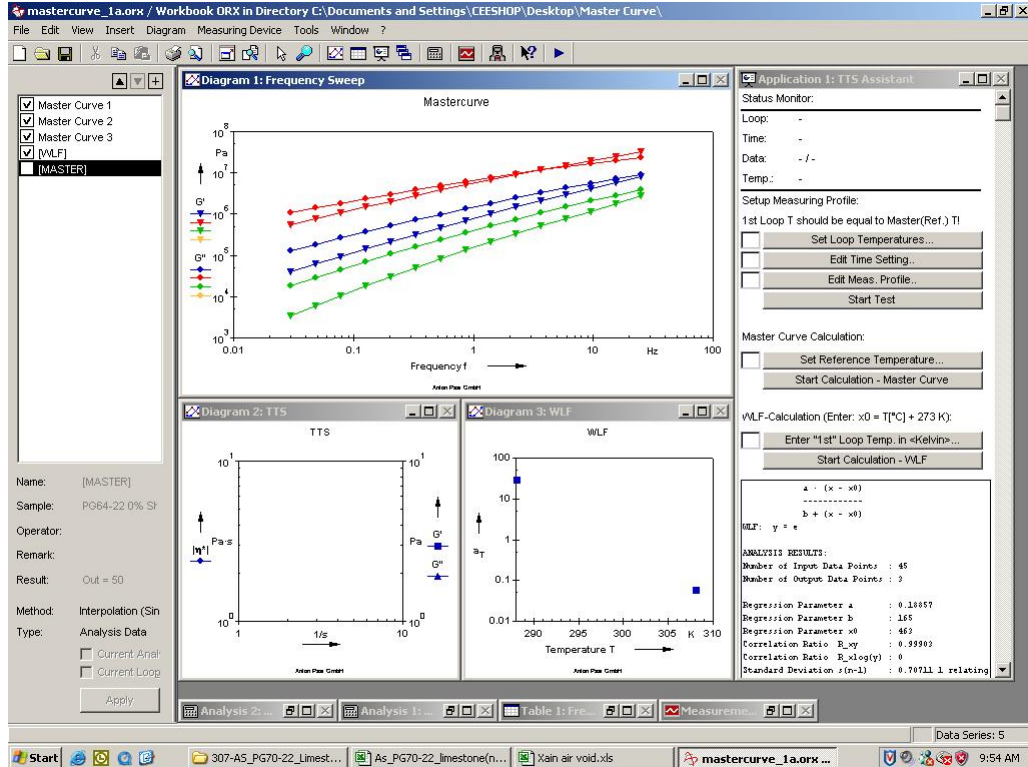


Figure 5.6 Physica Rheoplus Software

HMA Mixture Test

Materials

The same asphalt binder (PG 64-22) used in asphalt mastic test was employed in HMA mixture test. Its properties are presented in Table 5.1 (Huang et al. 2005).

The coarse aggregates used in HMA mixture test were crushed limestone with nominal maximum size of 12.5 mm. The fine aggregates consisted of the No.10 screenings, natural sand, and manufactured sand. Their gradations and other properties are presented in Table 5.2. The aggregate gradation is also shown in Figure 5.7.

Table 5.2 Properties of Aggregates

Sieve size	Limestone D-Rock	No.10 Screening	Natural Sand	Manufactured Sand
5/8"	100%	100%	100%	100%
1/2"	97%	100%	100%	100%
3/8"	70%	100%	100%	100%
#4	21%	92%	98%	99%
#8	7%	61%	93%	82%
#30	4%	29%	63%	28%
#50	3%	21%	13%	17%
#100	2.0%	20.0%	2.0%	9.0%
#200	1.8%	16.0%	1.0%	5.0%
G _{sb}	2.524	2.424	2.501	2.476

Note: G_{sb} = bulk specific gravity of aggregate.

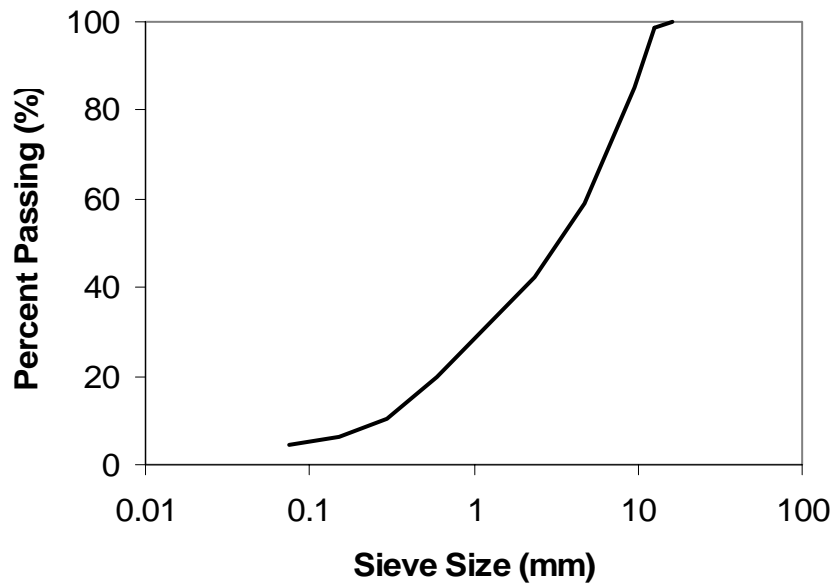


Figure 5.7 Aggregate Gradation in HMA Mixture

Mixture Design

The Marshall mix design procedure was employed to design HMA mixture. 50% limestone D-rock, 15% No.10 screenings, 25% natural sand, and 10% manufactured sand were selected for HMA mixture (Table 5.2). The optimum asphalt content was 5.0 percent. The volumetric properties of HMA mixture are listed in Table 5.3.

Sample Fabrication

The loose asphalt mixture was short-term oven aged for 4 hours at 135°C and compacted to cylindrical specimens 150 mm high by 170 mm in diameter using the Superpave Gyratory Compactor (SGC). Then, the specimens were cored in the center to a 100 mm diameter and sawed at both ends to a final height of 150 mm with smooth parallel cut faces. Figure 5.8 shows the HMA specimens at different stages. The target air voids for the control mixture were $4.0 \pm 0.5\%$. To investigate the air voids effect on dynamic modulus of HMA mixture, test specimens with air voids about 3%, 6%, and 8% were also fabricated.

Table 5.3 Volumetric Properties of HMA Mixture

AC (%)	G_{mm}	G_{mb}	Air Voids	VMA	Stability (kN)	Flow (mm)
5.0	2.456	2.356	4.0	16	11.6	2.77

Note: AC = asphalt content; G_{mm} = maximum theoretical specific gravity of loose mixture; G_{mb} = bulk specific gravity of compacted mixture; VMA = voids in mineral aggregate.



(a) SGC-compacted specimen



(b) Center-cored specimen



(c) Final specimen

Figure 5.8 HMA Specimens for Dynamic Modulus Test

Dynamic Modulus Testing

The Simple Performance Tester (SPT) manufactured by IPC global was used to run the dynamic modulus test. During the dynamic modulus testing, a cylindrical specimen is subjected to a constant lateral confining pressure and a sinusoidal vertical pressure that varies over a range of frequencies. Three linear variable differential transducers (LVDTs) mounted on studs attached to the sides of the specimen are usually used to measure the axial strain at the middle part of the specimen (Figure 5.9). In this study, the gauge length between the stud centers was 70 mm.

Test specimens were placed in an environmental chamber and allowed to equilibrate to the specified testing temperature. Prior to testing, two latex membranes were placed between the specimen ends and loading platens to reduce the end friction.

In the present study, the test was conducted under no confining pressure at three temperatures of 10°C, 25°C, and 40°C and at the frequencies from 0.01Hz to 25Hz. A contact load equal to 5 percent of the dynamic load was first applied to the specimen. A sinusoidal dynamic load was then applied to the specimen so that the induced axial strain was controlled between 75 and 125 microstrains. The dynamic load was variable from mixture to mixture depending on HMA mixture stiffness, testing temperature, and loading frequency. For each combination of testing temperature and frequency, 10 conditioning and 10 testing cycles were applied. The data from conditioning cycles were used to adjust the amount of dynamic load and those from testing cycles to calculate the values of dynamic modulus and phase angle. Figure 5.10 shows the typical axial stress and strains from the testing cycles.



(a) Studs attached to specimen



(b) Specimen placed in the confining pressure chamber



(c) Simple Performance Tester (SPT)

Figure 5.9 Dynamic Modulus Test Setup

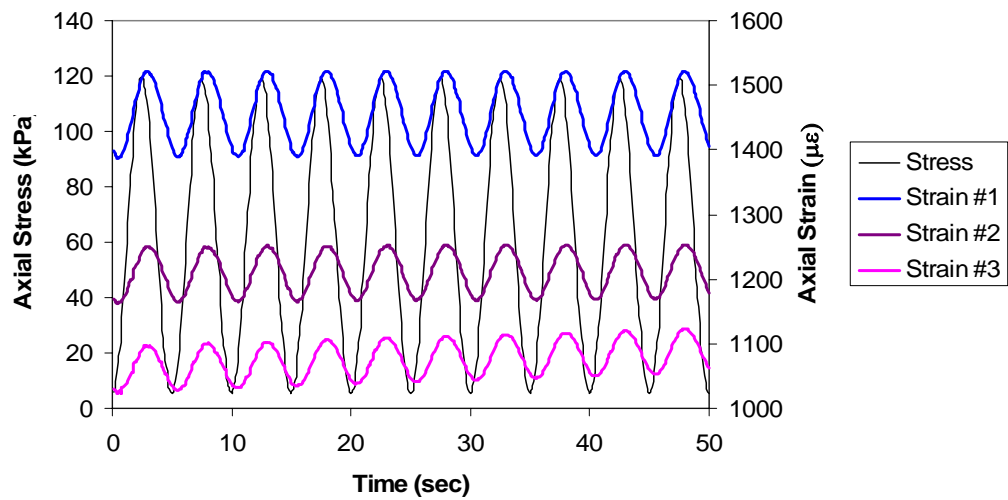


Figure 5.10 Axial Stress and Strains in Dynamic Modulus Test

The loading stress was calculated using the following equation

$$\sigma_0 = \frac{\bar{P}}{A} \quad (5.2)$$

where

σ_0 = loading stress amplitude;

\bar{P} = average loading amplitude (from best-fit sinusoid function); and

A = cross sectional area of specimen.

The recoverable axial strain was calculated as

$$\varepsilon_0 = \frac{\bar{\Delta}}{GL} \quad (5.3)$$

where

ε_0 = axial strain amplitude;

$\bar{\Delta}$ = average deformation amplitude (from best-fit sinusoid function) calculated after removal of the underlying baseline drift deformation; and

GL = gauge length.

The dynamic modulus, $|E^*|$, was then computed as

$$|E^*| = \frac{\sigma_0}{\varepsilon_0} \quad (5.4)$$

The phase angle, ϕ , was calculated using the following equation

$$\phi = \frac{t_i}{t_p} \times 360 \quad (5.5)$$

where

ϕ = phase angle (in degrees);

t_i = average time lag between the peak stress and the peak strain in seconds, calculated as the difference between the best fit load and deformation sinusoid functions; and

t_p = average time for a loading cycle in seconds.

CHAPTER 6 PREDICTION OF DYNAMIC SHEAR MODULUS OF ASPHALT MASTIC

Introduction

In this and the following chapters, the newly developed PFC models are used to predict dynamic modulus of asphalt mastic and mixture. The predicted dynamic modulus values obtained from these models are compared to the laboratory measured test results and also to the predicted values from widely used micromechanical models, such as the Hashin's composite spheres model and the Christensen and Lo's generalized self-consistent model.

There are basically two methods of applying the predictive equations from PFC models:

1. Elastic prediction method

In this method, the dynamic modulus (absolute value of complex modulus) is treated as an elastic property and used in the predictive equations. This method is relatively simple and avoids the use of the elastic-viscoelastic correspondence principle. It is also commonly used by other researchers, such as Buttlar et al. (1999). However, this method cannot predict the phase angle due to its elastic nature.

2. Viscoelastic prediction method

In this method, the complex modulus is used in the predictive equations as a real viscoelastic term. Difficulties may arise regarding solving the equations in the complex domain. In this study, special cases were considered to facilitate the solution of the equations in the complex domain. The viscoelastic method has the capability of

predicting the phase angle of viscoelastic materials because of the use of true complex terms.

Both elastic and viscoelastic methods are used to evaluate the newly proposed PFC models in this study.

Determination of Input Parameter Values

Before predicting dynamic shear modulus of asphalt mastic using the predictive equations from PFC models, the values of input parameters should be determined, such as elastic moduli and Poisson's ratios of aggregate and mineral filler, complex shear modulus and Poisson's ratio of asphalt binder. Based on the parameter values and ranges found in the literature (Huang et al. 2005; Zhou et al. 1995; Hirsch 1962; Kim and Little 2004), an elastic modulus of 50 GPa was selected for mineral filler and aggregate. Since Poisson's ratios of the constituents do not vary significantly, constant values of 0.2, 0.25, 0.3, and 0.4 were selected for the Poisson's ratios of aggregate, HMA mixture, asphalt mastic, and asphalt binder, respectively. Table 6.1 summarizes the input parameter values used for the modulus prediction.

Table 6.1 Values of Input Parameter in Predictive Equations

Material	Elastic (dynamic) modulus	Poisson's ratio
Aggregate	50 GPa	0.2
Asphalt binder	Measured	0.4
Asphalt mastic	Measured	0.3
HMA mixture	To be predicted	0.25

The complex shear modulus of asphalt binder was tested in the laboratory as an input parameter. The measured complex shear moduli are presented in Figure 6.1 together with the curves fitted with the Prony series representation. Table 6.2 presents the fitted coefficients for the Prony series representation in terms of G_i .

Elastic Prediction

Flow Chart

As mentioned previously in this chapter, the elastic prediction method used the dynamic shear modulus of asphalt binder as an elastic input parameter in the predictive

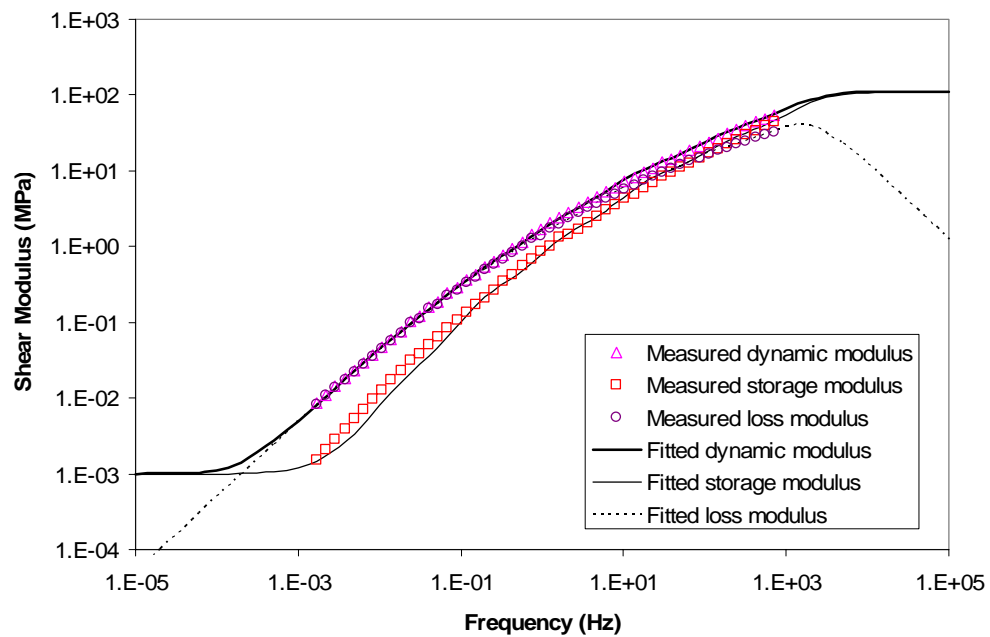


Figure 6.1 Master Curves for Complex Shear Moduli of Asphalt Binder (25°C)

Table 6.2 Prony Series Constants for Relaxation Shear Modulus of Asphalt Binder

i	ρ_i (sec)	G_i (MPa)
1	1E-04	7.601E+01
2	1E-03	2.276E+01
3	1E-02	8.418E+00
4	1E-01	1.689E+00
5	1E+00	2.752E-01
6	1E+01	1.891E-02
7	1E+02	4.451E-04

$G_e = 1.000E-03$

equations to predict dynamic shear modulus of asphalt mastic. Figure 6.2 presents the flow chart for the elastic prediction of dynamic shear modulus of asphalt mastic. To facilitate the prediction process, the dynamic (shear) moduli of asphalt mastic and mixture were calculated using the computer program developed with the Maple software (Waterloo 2006).

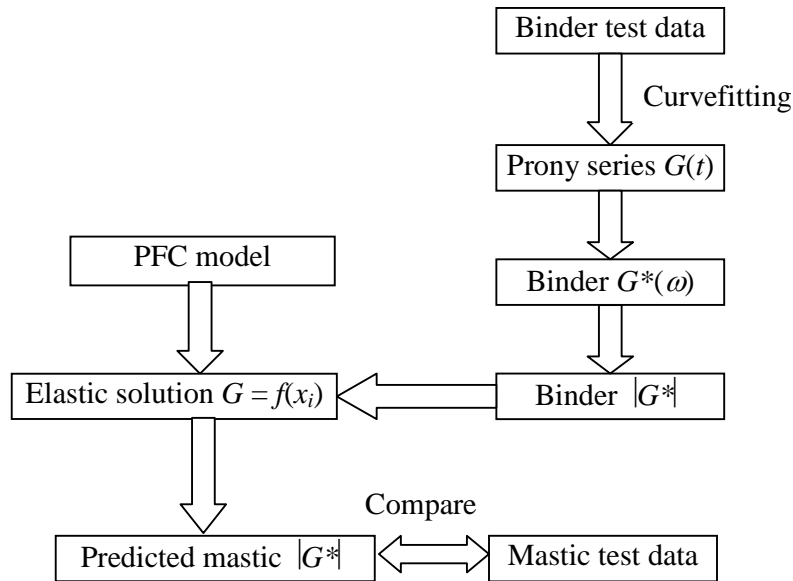


Figure 6.2 Flow Chart for Elastic Prediction of Dynamic Shear Modulus of Asphalt Mastic

Predictive Models

To evaluate the feasibility and accuracy of the new PFC models developed in the previous chapters for asphalt mastic and mixture, different forms of the predictive equations from these models were used. The newly proposed PFC models were also compared to the widely used PFC models, such as the Hashin's composite spheres model and the Christensen and Lo's generalized self-consistent model. For convenience, the predictive models for asphalt mastic are summarized in Table 6.3.

Prediction Results and Analyses

Figures 6.3 ~ 6.9 present the predicted dynamic shear modulus values of asphalt mastic along with the measured test data.

It was observed that all the predicted values of dynamic shear modulus of asphalt mastic with the PFC models summarized in Table 6.3 were generally very close to the measured test data. No significant difference in the predicted dynamic shear moduli was observed between different models.

However, it can be seen from Figure 6.3 through 6.9 that different models still gave different accuracy in predicting dynamic shear modulus of asphalt mastic at different volume concentration of mineral filler in asphalt binder. Figures 6.3, 6.6, and 6.7 showed that Models 1, 4, and 5 gave the best prediction at mineral filler concentration of 35%. For these three predictive models, the predicted dynamic shear moduli were higher than measured values at lower concentration and lower than measured values at higher concentration.

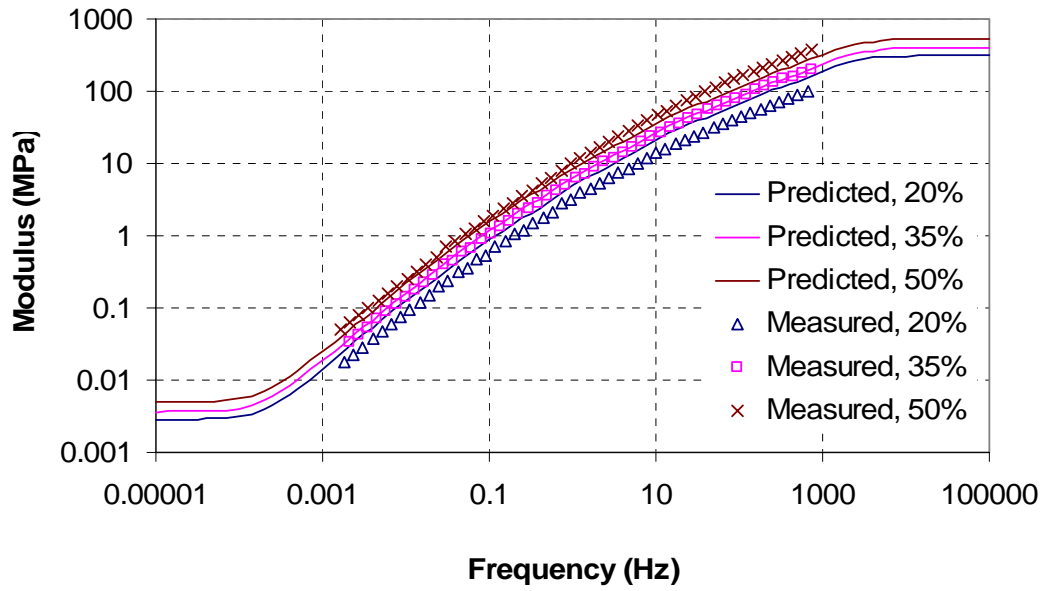
Table 6.3 PFC Models Used for Elastic Prediction of Asphalt Mastic

Model No.	Predictive equation	Equation No.
1	$E_0(a) = \frac{E_1(1-2\nu_0)(1-n)}{x_1 - \frac{9E_2n(1-\nu_1)^2}{4(1-2\nu_2)(1-n)E_1 + 4E_2x_2}}$	3.24
2	$\left(\frac{E_c}{E_m}\right)^A \left(\frac{E_c - x_1E_i}{E_m - x_1E_i}\right)^B \left(\frac{E_c - x_2E_i}{E_m - x_2E_i}\right)^C = (1-c)^{-1}$	4.40
3	$\left(\frac{G_c}{G_m}\right)^{\frac{8-10\nu_m}{15(1-\nu_m)}} \left(\frac{G_i - G_m}{G_i - G_c}\right) = (1-c)^{-1}$	4.53
4	$\left(\frac{K_c}{K_m}\right)^{\frac{(1+\nu_m)}{3(1-\nu_m)}} \left(\frac{K_i - K_m}{K_i - K_c}\right) = (1-c)^{-1}$	4.64
5	$\frac{K_c}{K_m} = 1 + \frac{3(1-\nu_m) \left(\frac{K_i}{K_m} - 1\right) c}{2(1-2\nu_m) + (1+\nu_m) \left[\frac{K_i}{K_m} - \left(\frac{K_i}{K_m} - 1\right) c \right]}$	1.5
6	$\frac{G_c}{G_m} = 1 + \frac{15(1-\nu_m) \left(\frac{G_i}{G_m} - 1\right) c}{7 - 5\nu_m + 2(4 - 5\nu_m) \left[\frac{G_i}{G_m} - \left(\frac{G_i}{G_m} - 1\right) c \right]}$	1.6
7	$A \left(\frac{G_c}{G_m}\right)^2 + B \left(\frac{G_c}{G_m}\right) + C = 0$	1.10

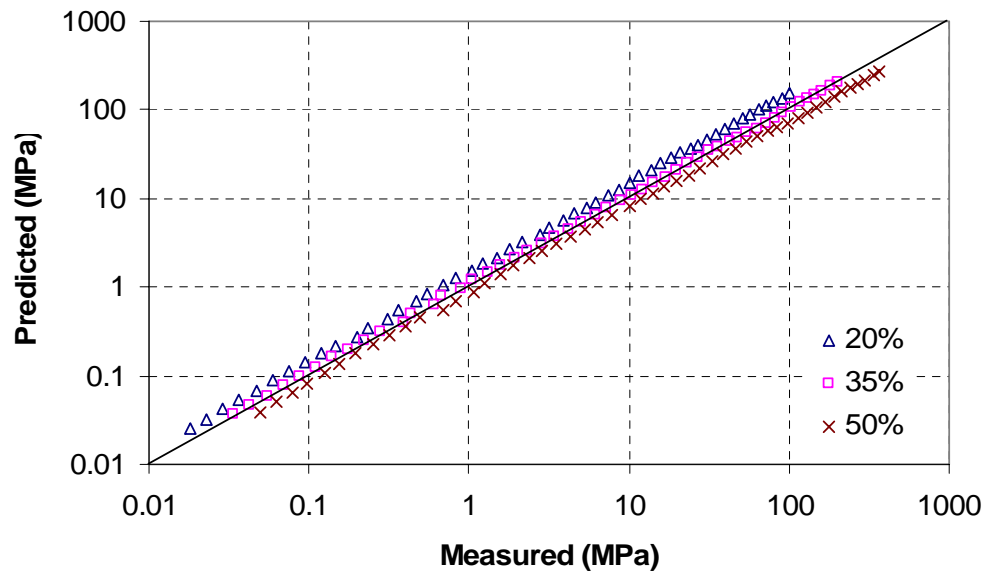
Note: 1. The first four predictive models were developed in this study. The last three

models were given by Hashin (1962) and Christensen and Lo (1979).

2. The final predicted results were converted to dynamic shear modulus if the models are not expressed in terms of dynamic shear modulus.

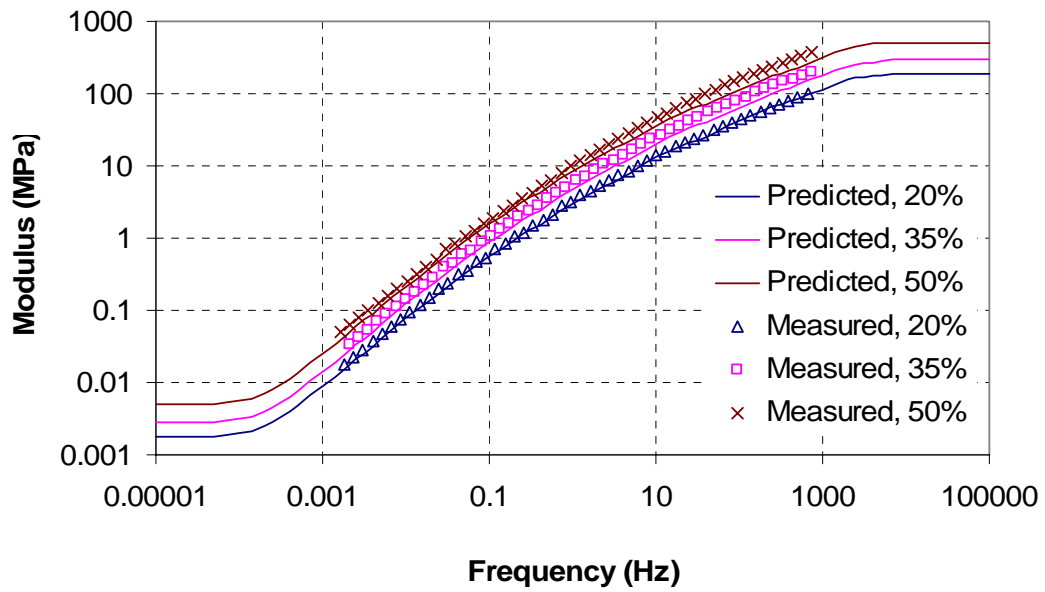


(a) Modulus vs. frequency

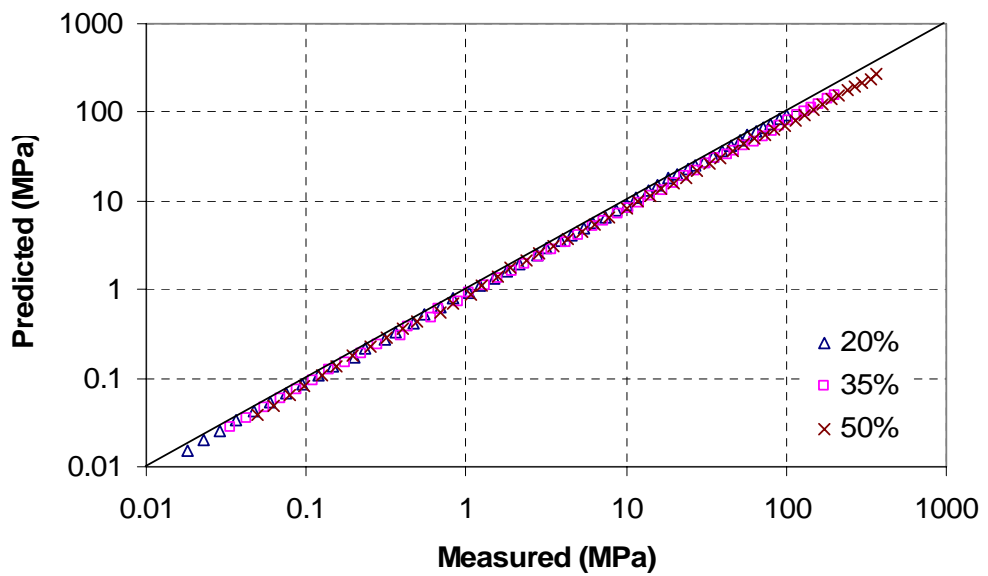


(b) Predicted vs. measured modulus

Figure 6.3 Predicted vs. Measured Dynamic Shear Modulus of Asphalt Mastic (Model 1)



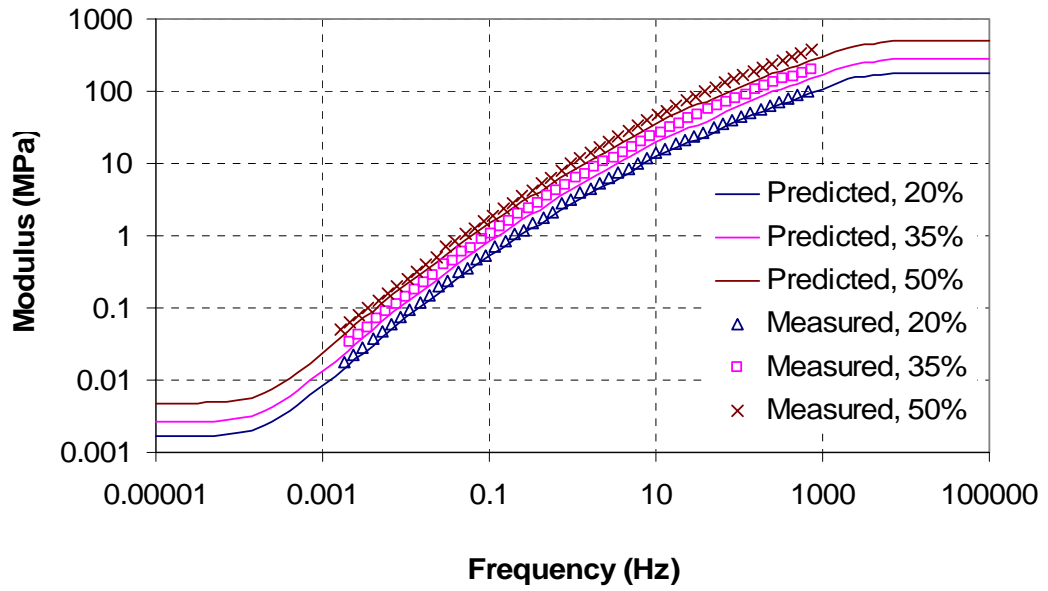
(a) Modulus vs. frequency



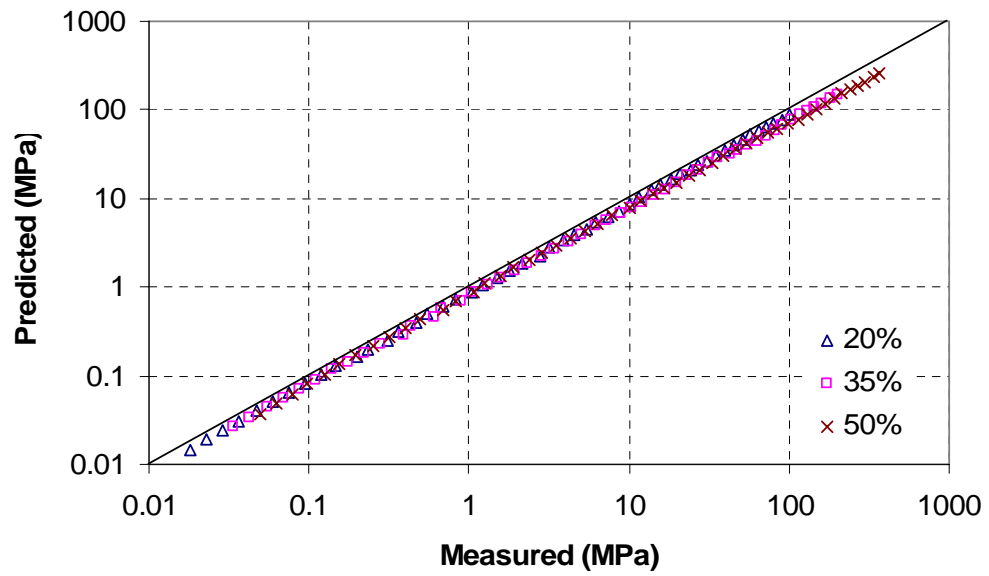
(b)

Predicted vs. measured modulus

Figure 6.4 Predicted vs. Measured Dynamic Shear Modulus of Asphalt Mastic (Model 2)

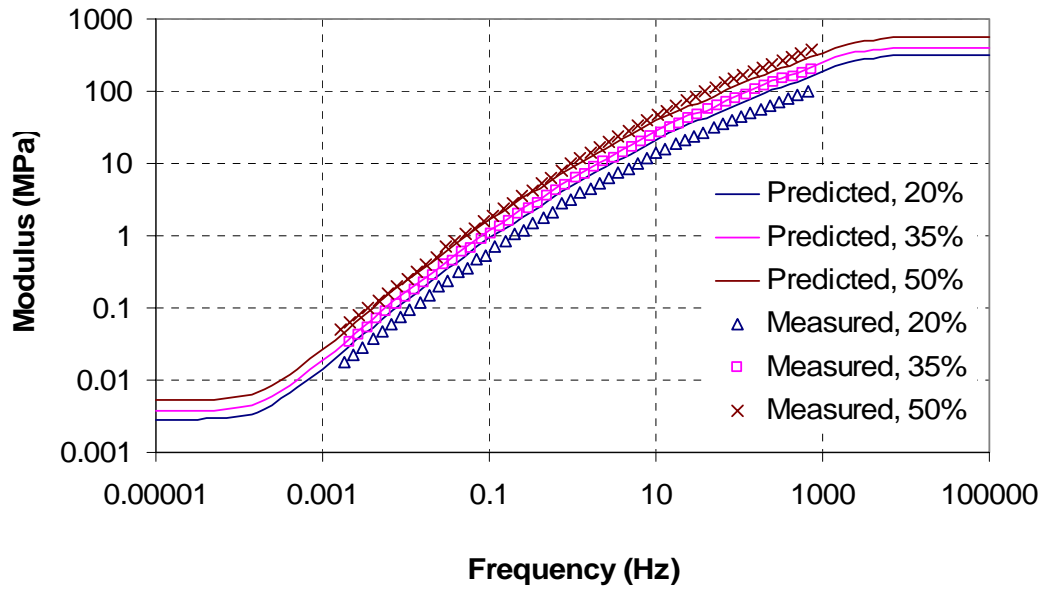


(a) Modulus vs. frequency

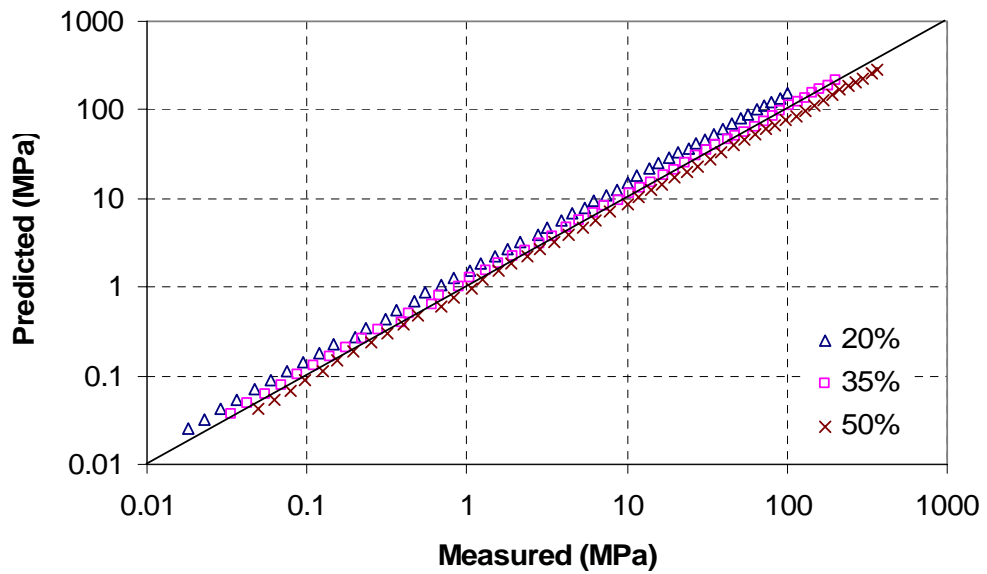


(b) Predicted vs. measured modulus

Figure 6.5 Predicted vs. Measured Dynamic Shear Modulus of Asphalt Mastic (Model 3)

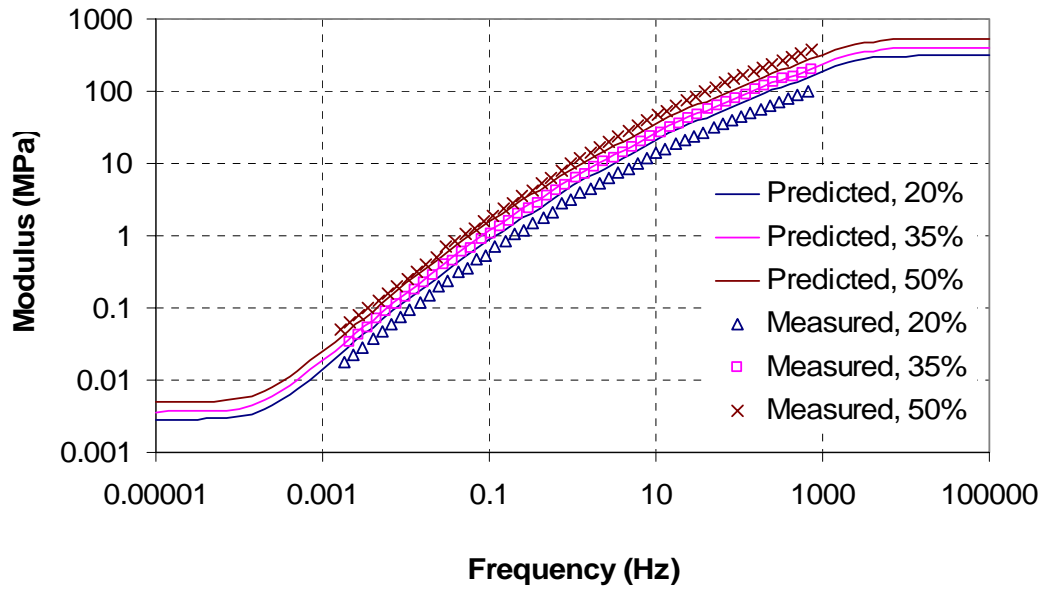


(a) Modulus vs. frequency

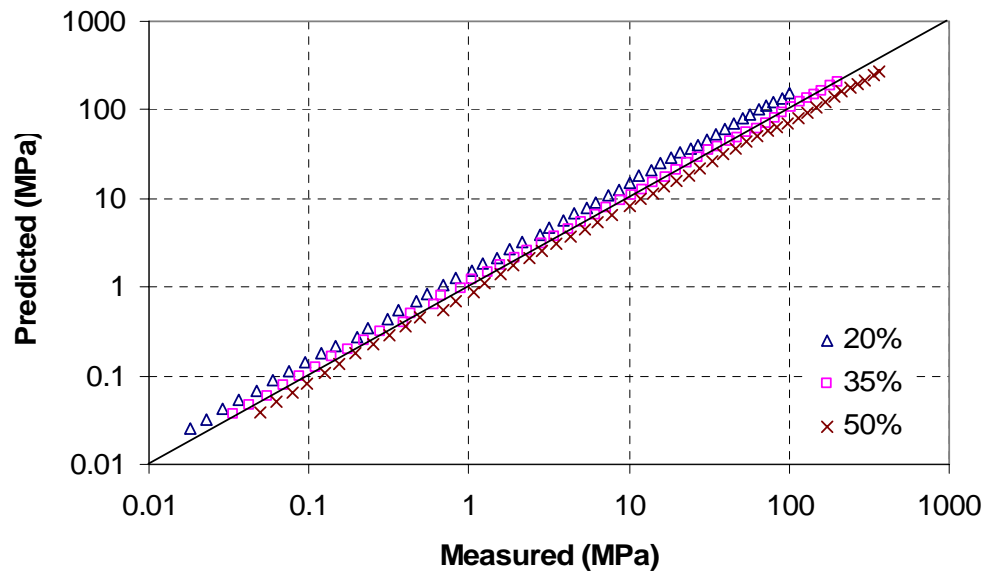


(b) Predicted vs. measured modulus

Figure 6.6 Predicted vs. Measured Dynamic Shear Modulus of Asphalt Mastic (Model 4)

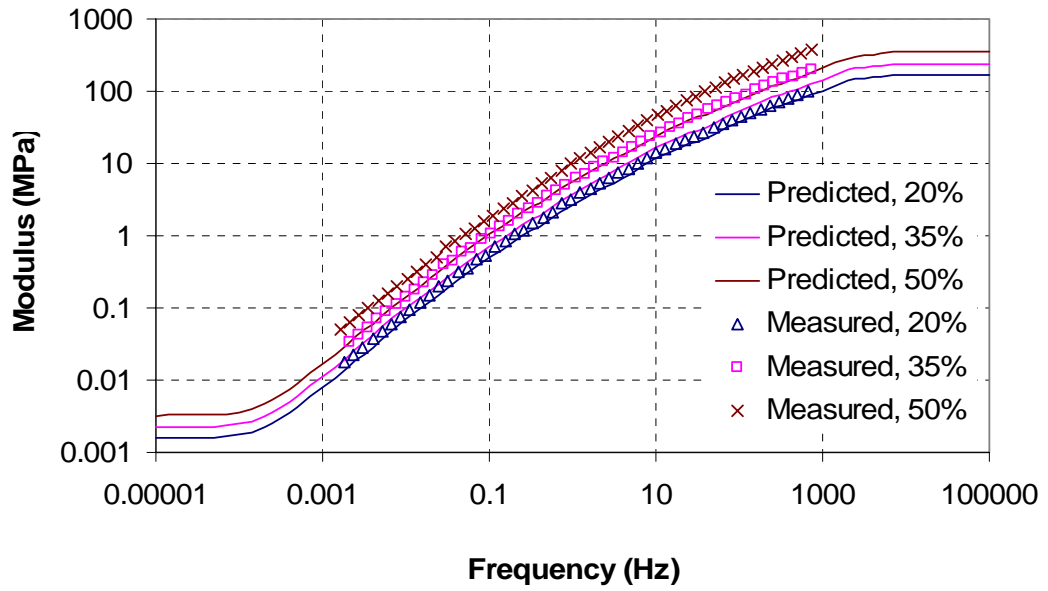


(a) Modulus vs. frequency

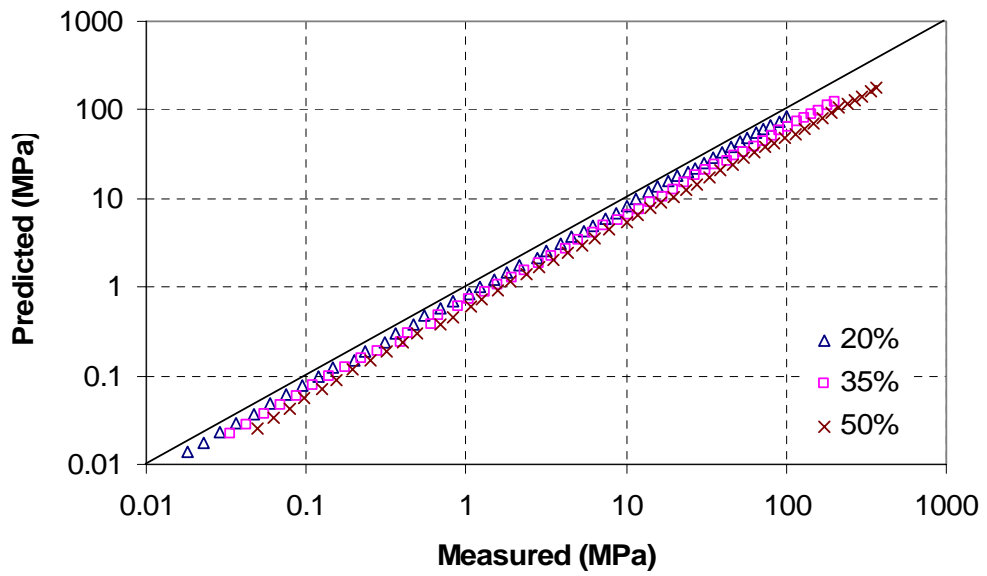


(b) Predicted vs. measured modulus

Figure 6.7 Predicted vs. Measured Dynamic Shear Modulus of Asphalt Mastic (Model 5)



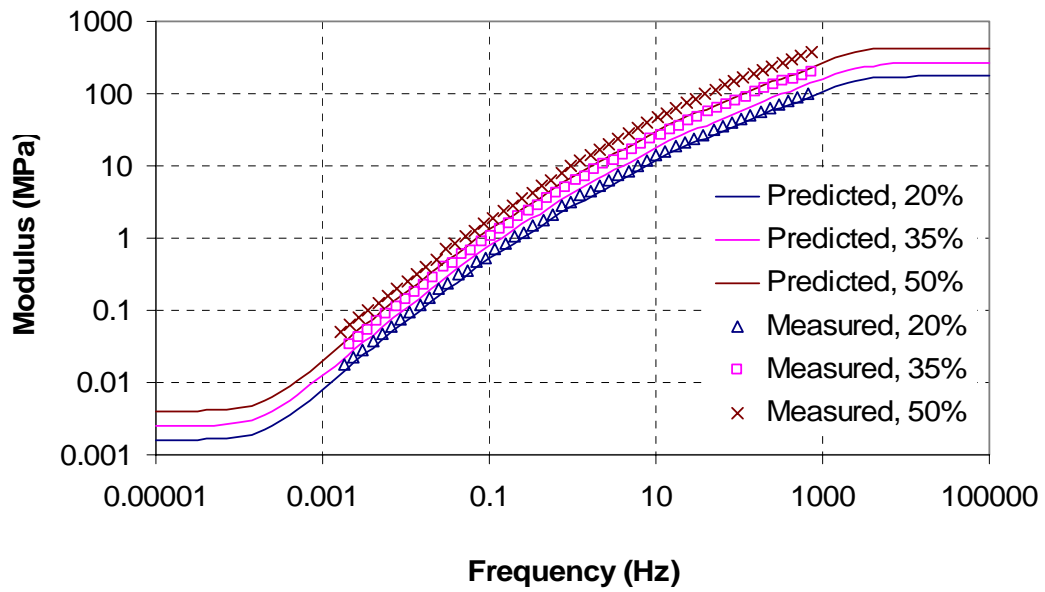
(a) Modulus vs. frequency



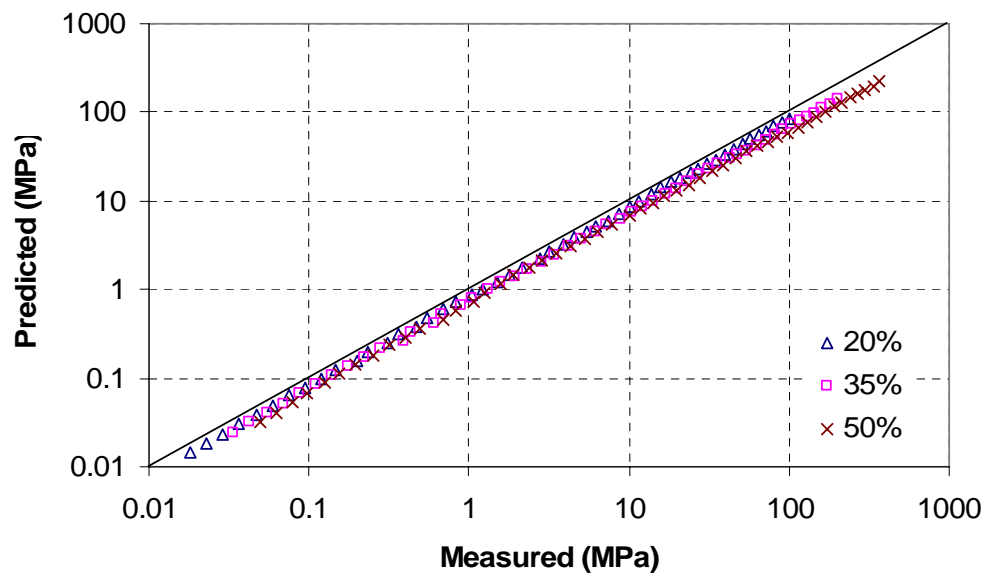
(b)

Predicted vs. measured modulus

Figure 6.8 Predicted vs. Measured Dynamic Shear Modulus of Asphalt Mastic (Model 6)



(a) Modulus vs. frequency



(b) Predicted vs. measured modulus

Figure 6.9 Predicted vs. Measured Dynamic Shear Modulus of Asphalt Mastic (Model 7)

From Figures 6.4, 6.5, 6.8, and 6.9 it was seen that Models 2, 3, 6, and 7 generally slightly under-predicted the dynamic shear modulus of asphalt mastic, regardless of mineral filler concentration. But, the predicted dynamic shear moduli with Models 6 and 7 deviated farther away from measured data than with Models 2 and 3.

Error Analyses

The prediction accuracy of different PFC models can be evaluated through error analysis. The relative error in the prediction of dynamic shear modulus of asphalt mastic was calculated in percent using the following equation:

$$\text{Error} = \frac{|G^*|_{\text{predicted}} - |G^*|_{\text{measured}}}{|G^*|_{\text{measured}}} \times 100 \quad (6.1)$$

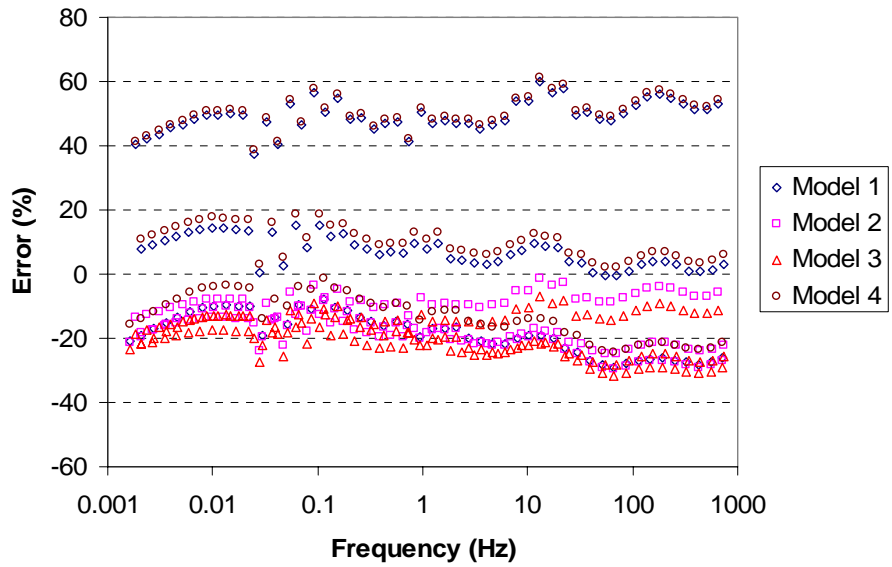
where

Error = relative error, %;

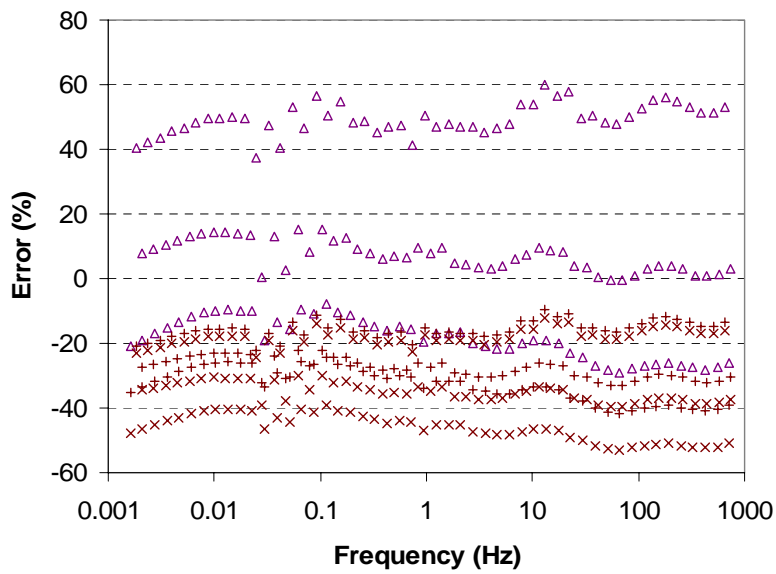
$|G^*|_{\text{predicted}}$ = predicted dynamic shear modulus; and

$|G^*|_{\text{measured}}$ = measured dynamic shear modulus.

Figure 6.10 presents the plots of prediction error vs. frequency for different PFC models. Generally, almost all the prediction errors were within the range of $\pm 60\%$. For the models developed in this study (Models 1 through 4), most of the prediction errors were within the range of $\pm 40\%$ (Figure 6.10a), while the predictive equations from the Hashin model and the Christensen and Lo's GSCM model (Models 5 through 7) gave a larger prediction error scatter (Figure 6.10b).



(a) Models developed in this study



(b) Currently existing models

Figure 6.10 Errors in Elastic Prediction of Dynamic Shear Modulus of Asphalt Mastic

Viscoelastic Prediction

Flow Chart

In the viscoelastic prediction of dynamic shear modulus of asphalt mastic, the complex shear modulus of asphalt binder was used in the form of true complex term as an input parameter in the predictive equations so that the complex shear modulus of asphalt mastic could be calculated and both dynamic shear modulus and phase angle could be predicted. Figure 6.11 presents the flow chart for the viscoelastic prediction of dynamic shear modulus of asphalt mastic.

Predictive Models

As mentioned previously in Chapter 4, to numerically solve the predictive equations from the differential method, special cases of $\nu_m = \nu_i = 0.5$ and $\nu_m = \nu_i = 0.2$ were considered for the viscoelastic prediction ($\nu_m =$ Poisson ratio of asphalt binder, $\nu_i =$ Poisson ratio of aggregate). Totally, there were 10 predictive models used for the viscoelastic prediction of asphalt mastic, as summarized in Table 6.4.

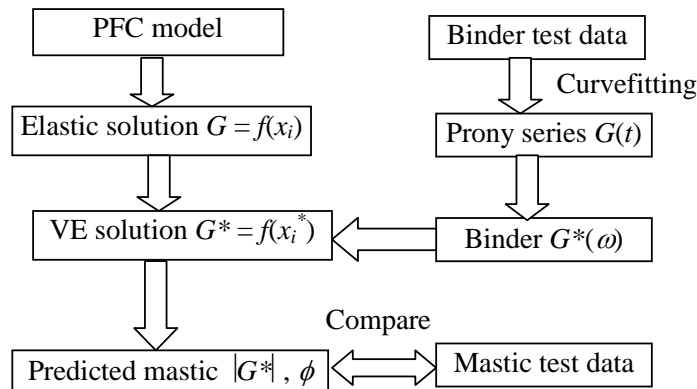


Figure 6.11 Flow Chart for Viscoelastic Prediction of Asphalt Mastic

Table 6.4 Models Used for Viscoelastic Prediction of Asphalt Mastic

Model No.	Predictive Equation	Equation No.
1	$E_0^*(\omega, a) = \frac{E_1^*(\omega)(1-2\nu_0)(1-n)}{x_1 - \frac{9E_2n(1-\nu_1)^2}{4(1-2\nu_2)(1-n)E_1^*(\omega) + 4E_2x_2}}$	3.33
2-1	$\left(\frac{E_c^*}{E_m^*}\right)\left(\frac{E_c^* - E_i}{E_m^* - E_i}\right)^{-2.5} = (1-c)^{-2.5}$	4.42
2-2	$\left(\frac{E_c^*}{E_m^*}\right)\left(\frac{E_c^* - E_i}{E_m^* - E_i}\right)^{-2} = (1-c)^{-2}$	4.43
3-1	$\left(\frac{G_c^*}{G_m^*}\right)\left(\frac{G_c^* - G_i}{G_m^* - G_i}\right)^{-2.5} = (1-c)^{-2.5}$	4.55
3-2	$\left(\frac{G_c^*}{G_m^*}\right)\left(\frac{G_c^* - G_i}{G_m^* - G_i}\right)^{-2} = (1-c)^{-2}$	4.56
4-1	$\left(\frac{K_c^*}{K_m^*}\right)\left(\frac{K_i - K_m^*}{K_i - K_c^*}\right) = (1-c)^{-1}$	4.66
4-2	$\left(\frac{K_c^*}{K_m^*}\right)\left(\frac{K_i - K_m^*}{K_i - K_c^*}\right)^2 = (1-c)^{-2}$	4.67
5	$\frac{K_c^*}{K_m^*} = 1 + \frac{3(1-\nu_m)\left(\frac{K_i}{K_m^*} - 1\right)c}{2(1-2\nu_m) + (1+\nu_m)\left[\frac{K_i}{K_m^*} - \left(\frac{K_i}{K_m^*} - 1\right)c\right]}$	1.5
6	$\frac{G_c^*}{G_m^*} = 1 + \frac{15(1-\nu_m)\left(\frac{G_i}{G_m^*} - 1\right)c}{7-5\nu_m + 2(4-5\nu_m)\left[\frac{G_i}{G_m^*} - \left(\frac{G_i}{G_m^*} - 1\right)c\right]}$	1.6
7	$A\left(\frac{G_c^*}{G_m^*}\right)^2 + B\left(\frac{G_c^*}{G_m^*}\right) + C = 0$	1.10

Note: 1. The first seven predictive equations were developed in this study (Model 2-1 was also given in Pal (2005a). The last three equations were given by the Hashin model and the Christensen and Lo model.
 2. All the final prediction results were converted to dynamic shear modulus and phase angle of asphalt mastic.

Prediction Results and Analyses

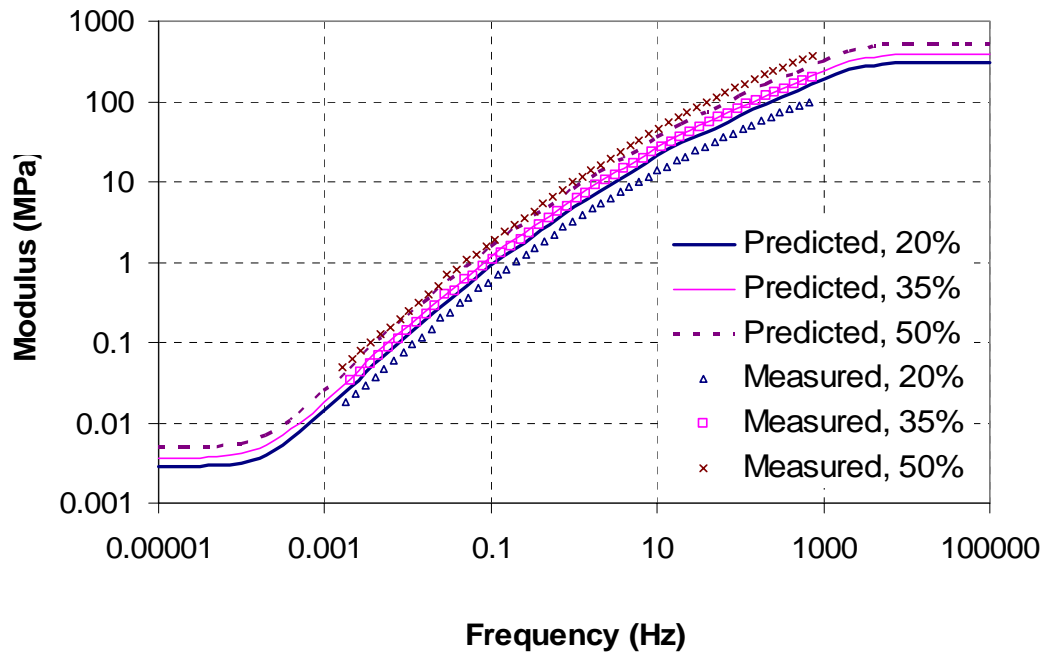
Figures 6.12 ~ 6.21 present the predicted values for dynamic shear modulus and phase angle of asphalt mastic along with the measured test data.

As in the elastic prediction, different models provided different accuracy in predicting dynamic shear modulus of asphalt mastic using the viscoelastic method. It was observed that among all the models, Model 4-2 was the only one that slightly over-predicted dynamic shear modulus at all three volume concentrations (Figure 6.18). Predicted dynamic shear moduli from Models 1, 4-1, 5 were higher than measured data at lower concentration of mineral filler and lower than measured data at high concentration (Figures 12, 17, and 19). Models 2-1 and 3-1 gave very good predictions at all three volume concentrations of mineral filler (Figures 13 and 15), while Models 2-2, 3-2, 6, and 7 slightly under-predicted the dynamic shear modulus of asphalt mastic, regardless of the volume concentration of mineral filler (Figures 14, 16, 20, and 21).

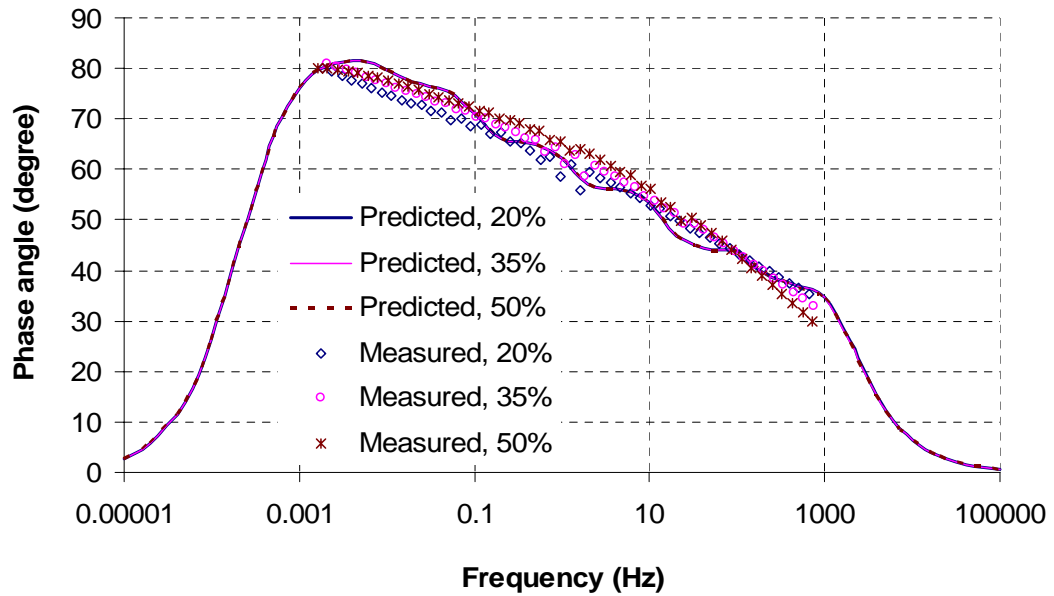
As for the predicted values of phase angle, it was observed that all the models gave almost same plots of predicted phase angle vs. frequency at all three mineral filler concentrations. This was verified by the fact that no significant difference in the measured phase angle was observed between mastics with different mineral filler concentrations.

Error Analyses

Figures 6.22 and 23 present the prediction errors for dynamic shear modulus and phase angle in the viscoelastic analysis. It was observed that the prediction errors for dynamic shear modulus were mostly within the range between – 40% and 80%. For the

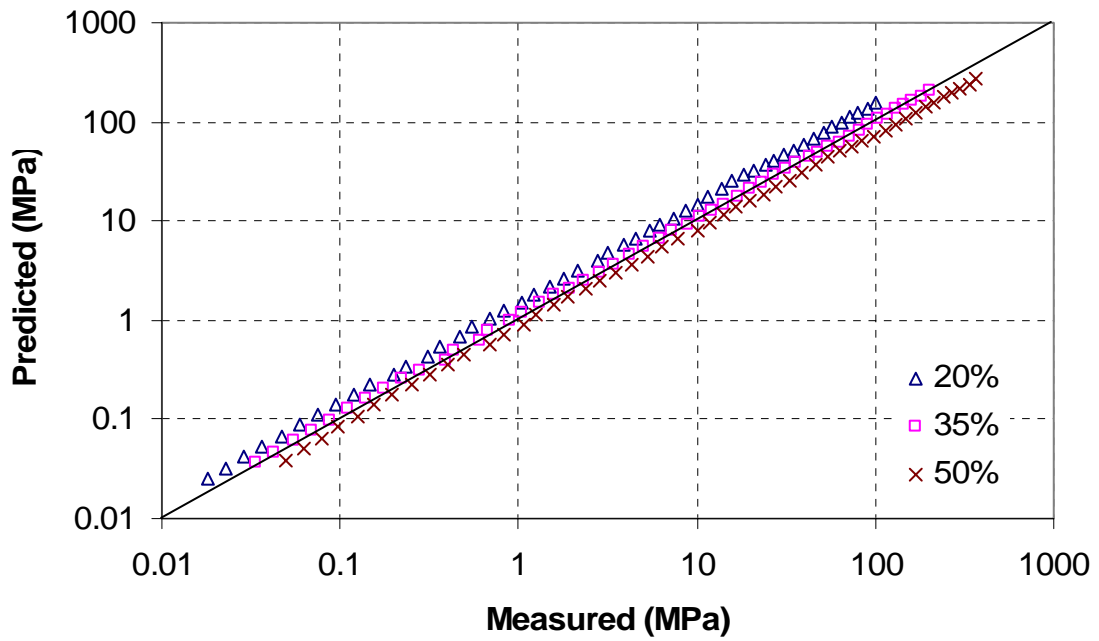


(a) Modulus vs. frequency

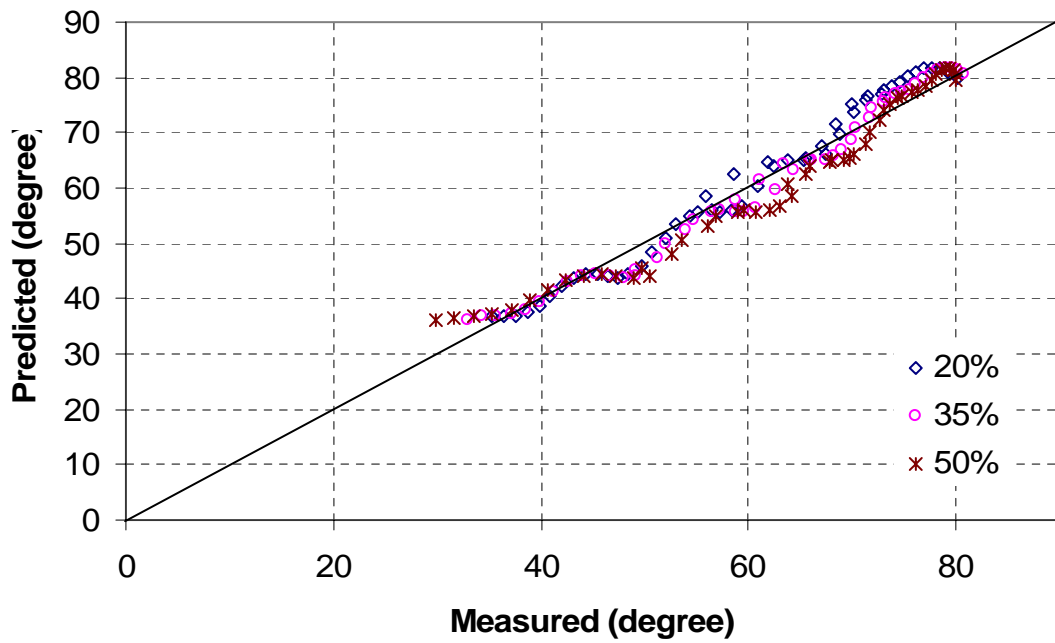


(b) Phase angle vs. frequency

Figure 6.12 Predicted vs. Measured Values of Asphalt Mastic (Model 1)

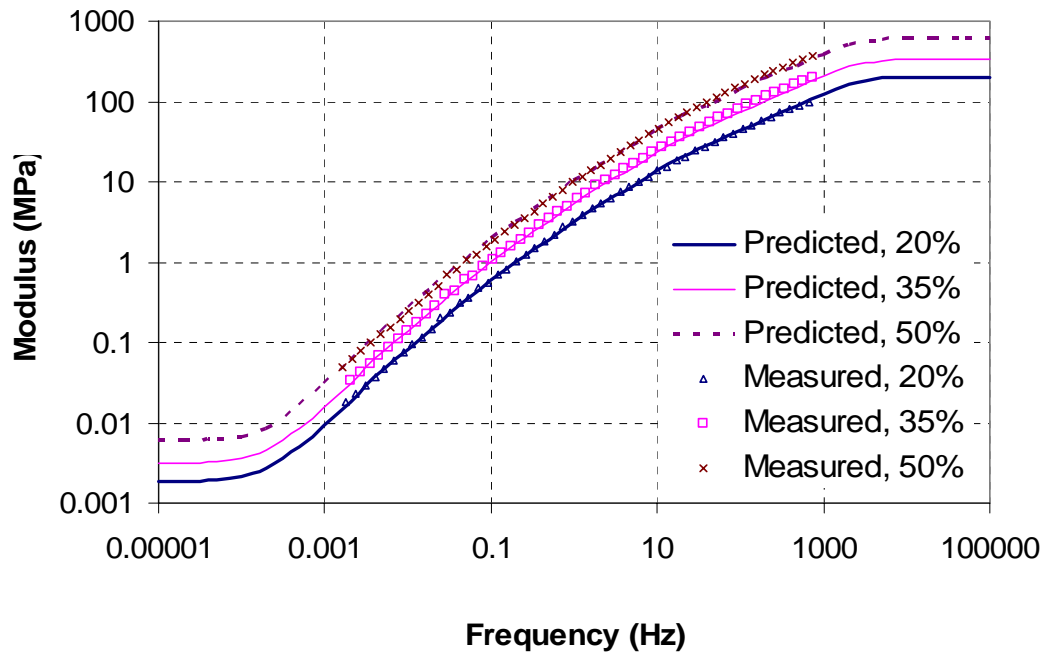


(c) Predicted vs. measured modulus

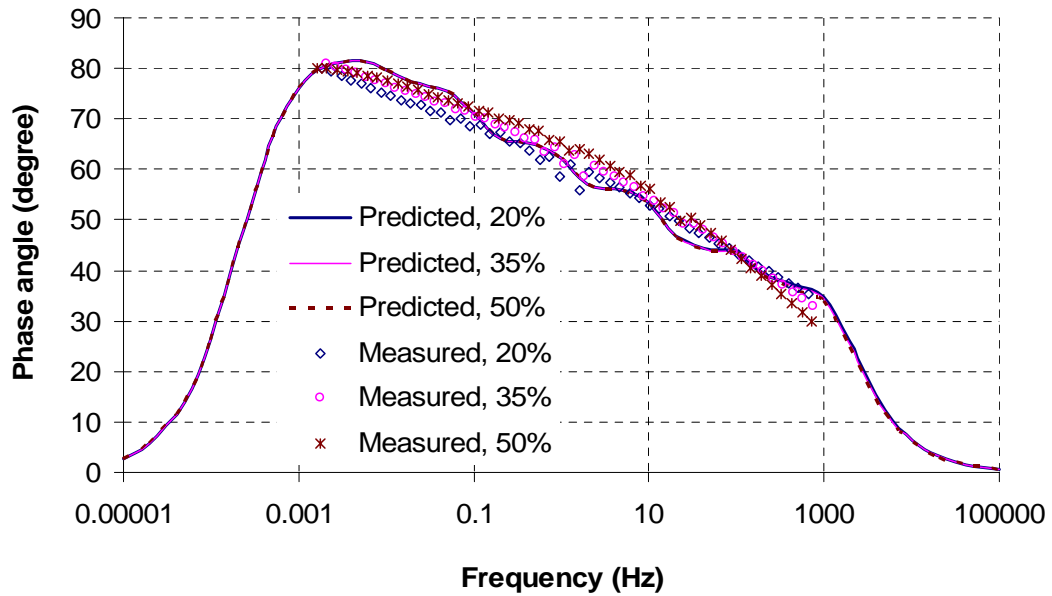


(d) Predicted vs. measured phase angle

Figure 6.12 Predicted vs. Measured Values of Asphalt Mastic (Model 1) (Contd.)

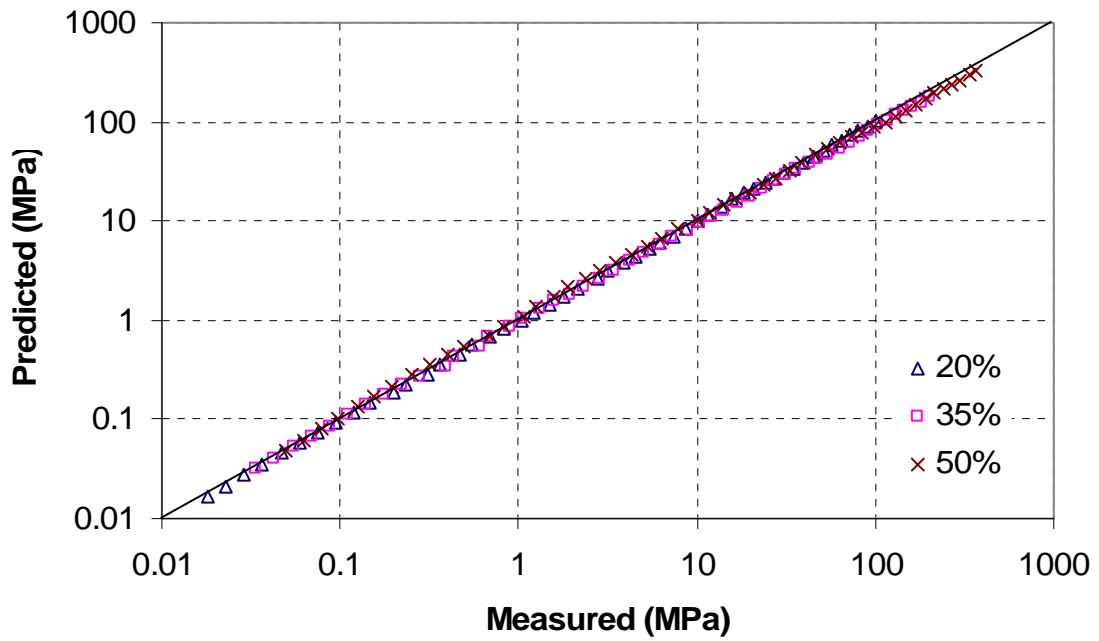


(a) Modulus vs. frequency

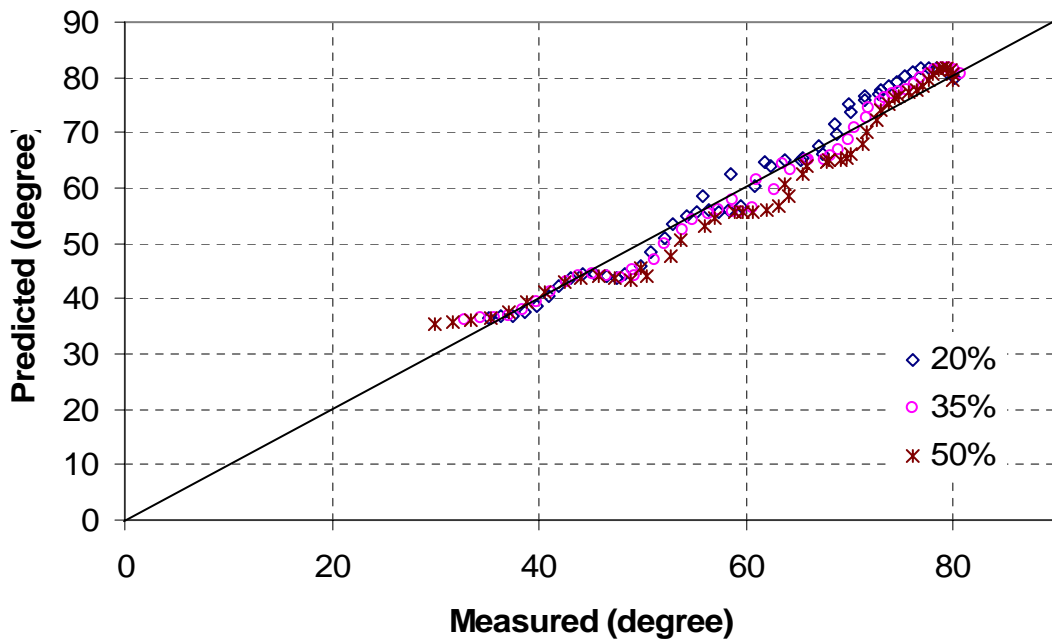


(b) Phase angle vs. frequency

Figure 6.13 Predicted vs. Measured Values of Asphalt Mastic (Model 2-1)

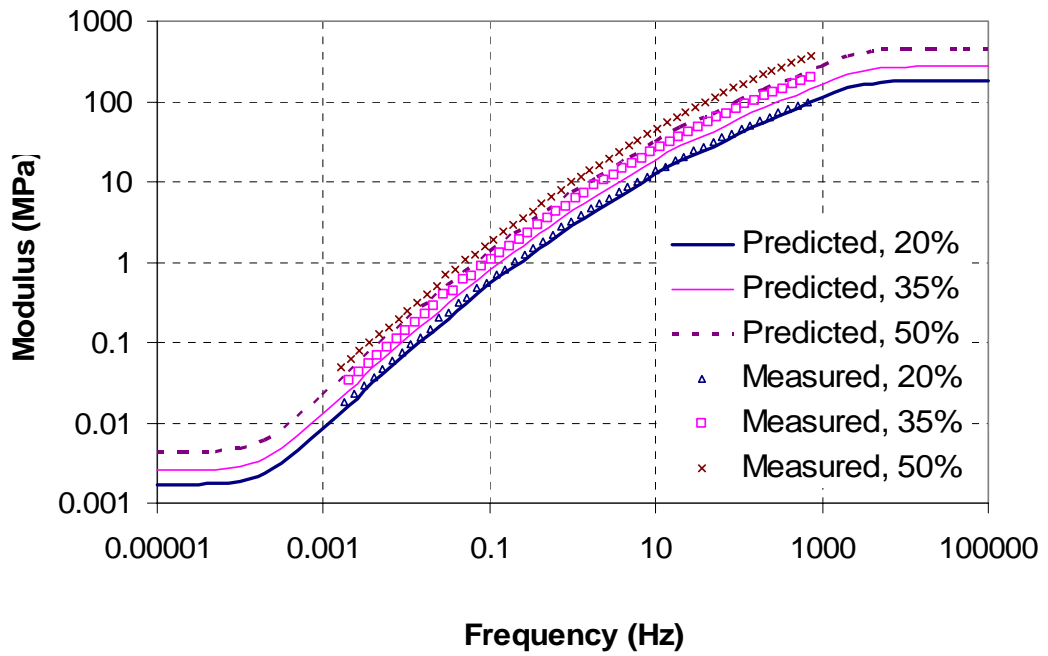


(c) Predicted vs. measured modulus

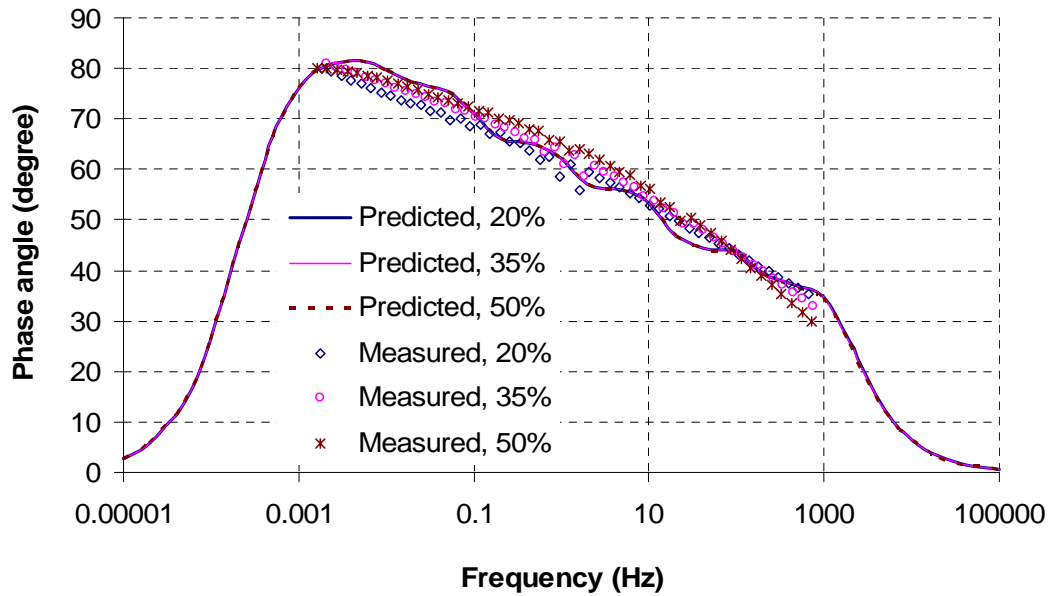


(d) Predicted vs. measured phase angle

Figure 6.13 Predicted vs. Measured Values of Asphalt Mastic (Model 2-1) (Contd.)

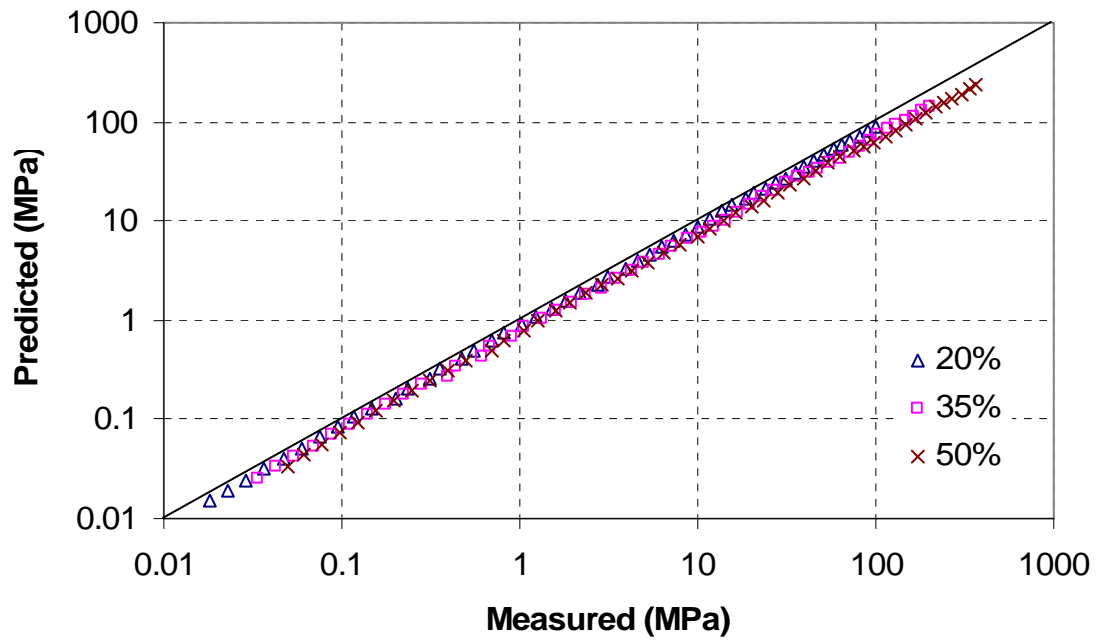


(a) Modulus vs. frequency

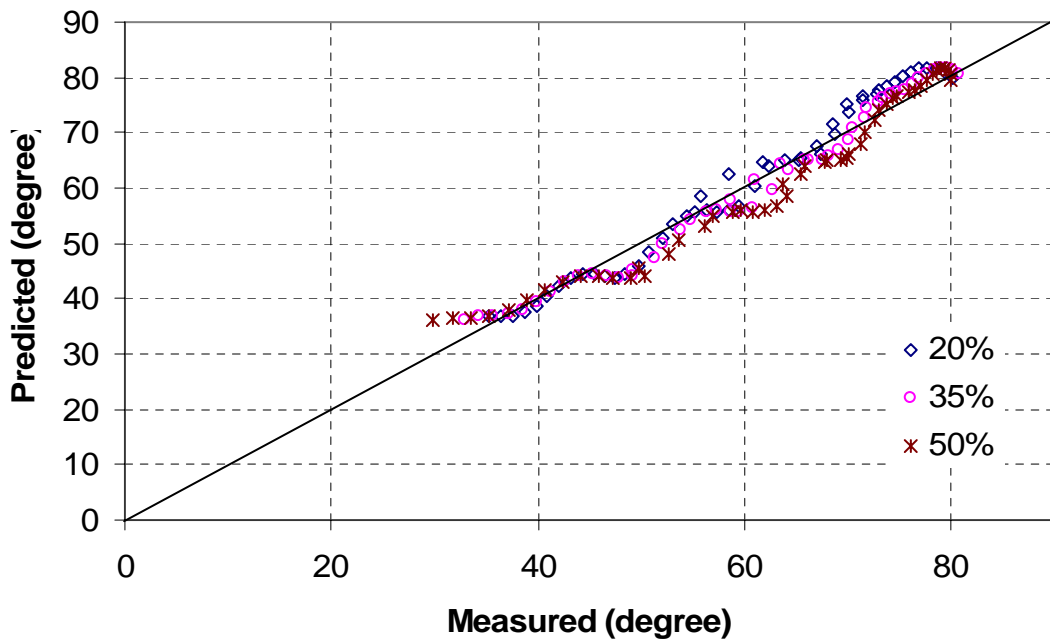


(b) Phase angle vs. frequency

Figure 6.14 Predicted vs. Measured Values of Asphalt Mastic (Model 2-2)

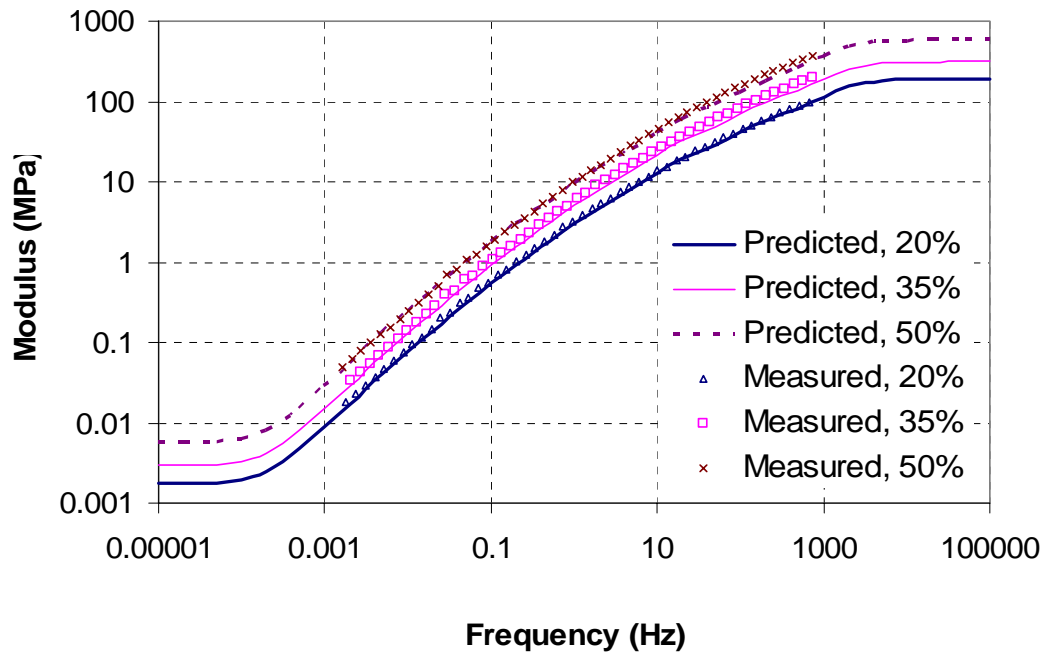


(c) Predicted vs. measured modulus

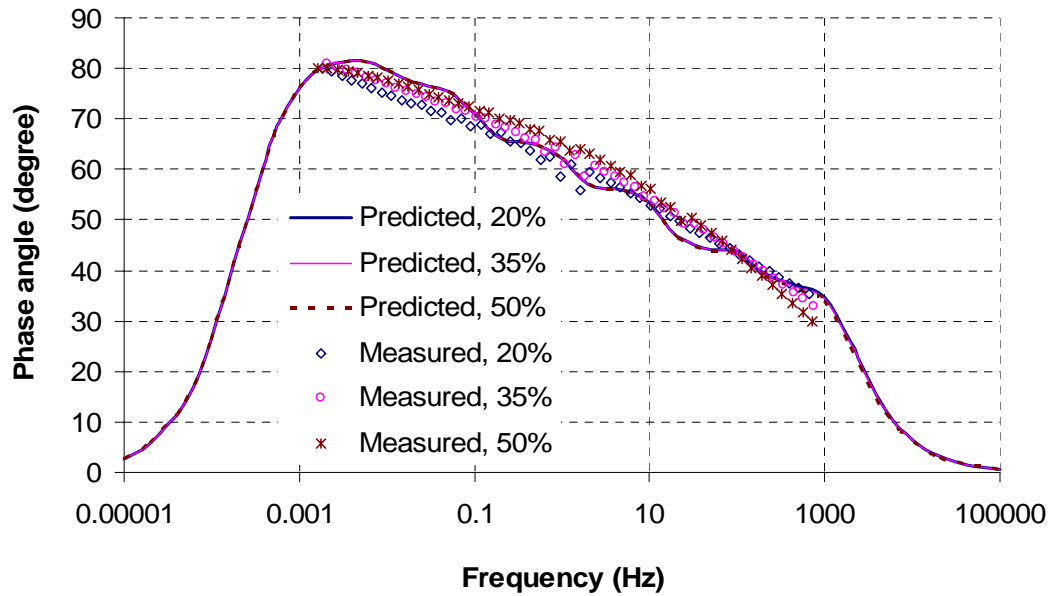


(d) Predicted vs. measured phase angle

Figure 6.14 Predicted vs. Measured Values of Asphalt Mastic (Model 2-2) (Contd.)

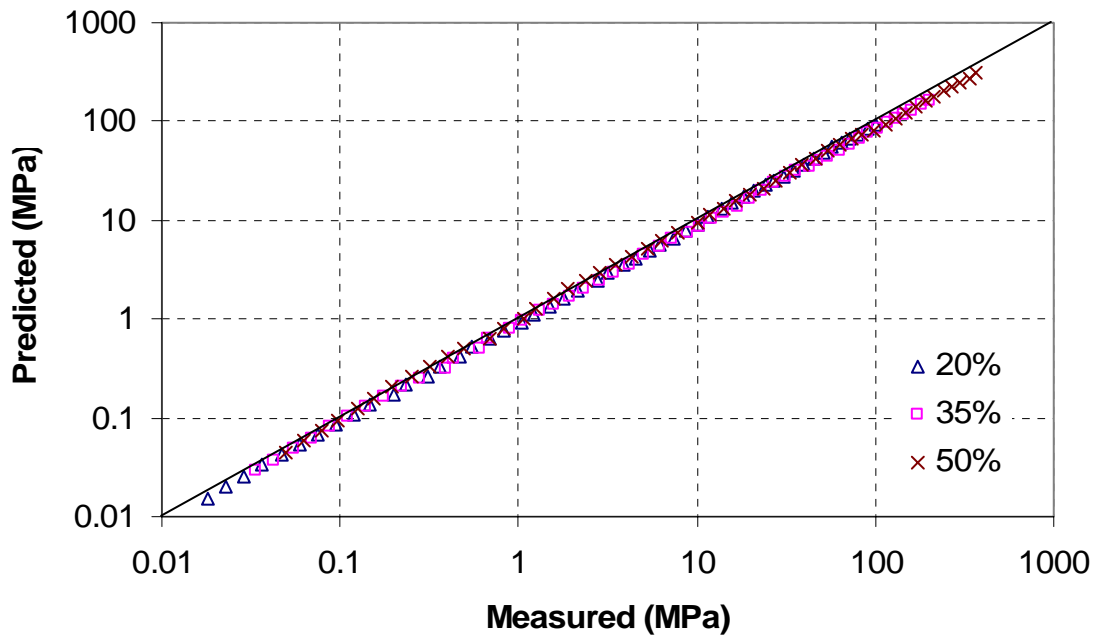


(a) Modulus vs. frequency

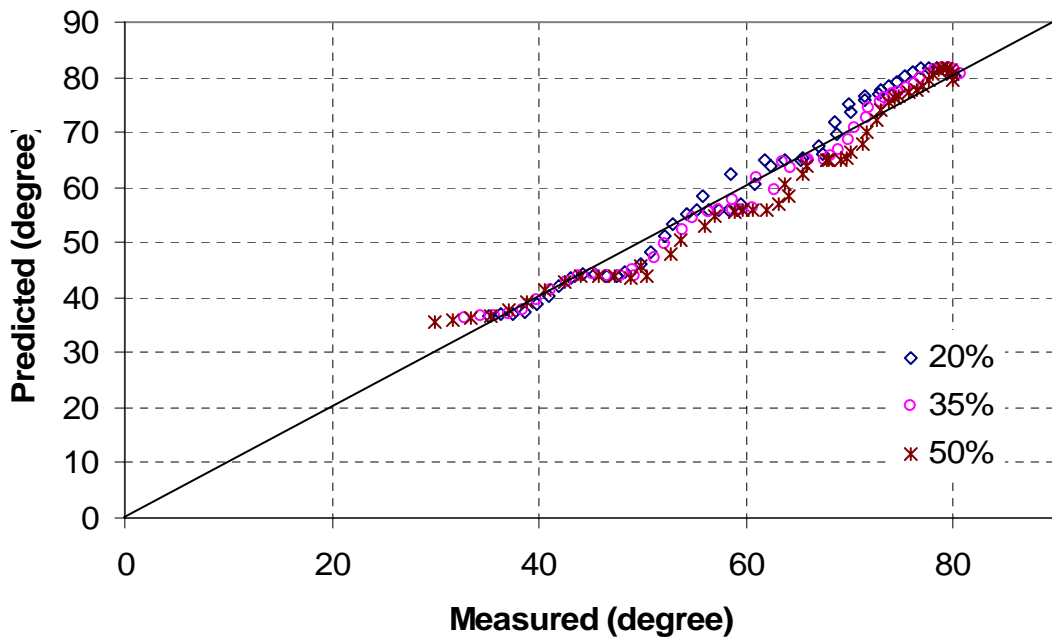


(b) Phase angle vs. frequency

Figure 6.15 Predicted vs. Measured Values of Asphalt Mastic (Model 3-1)

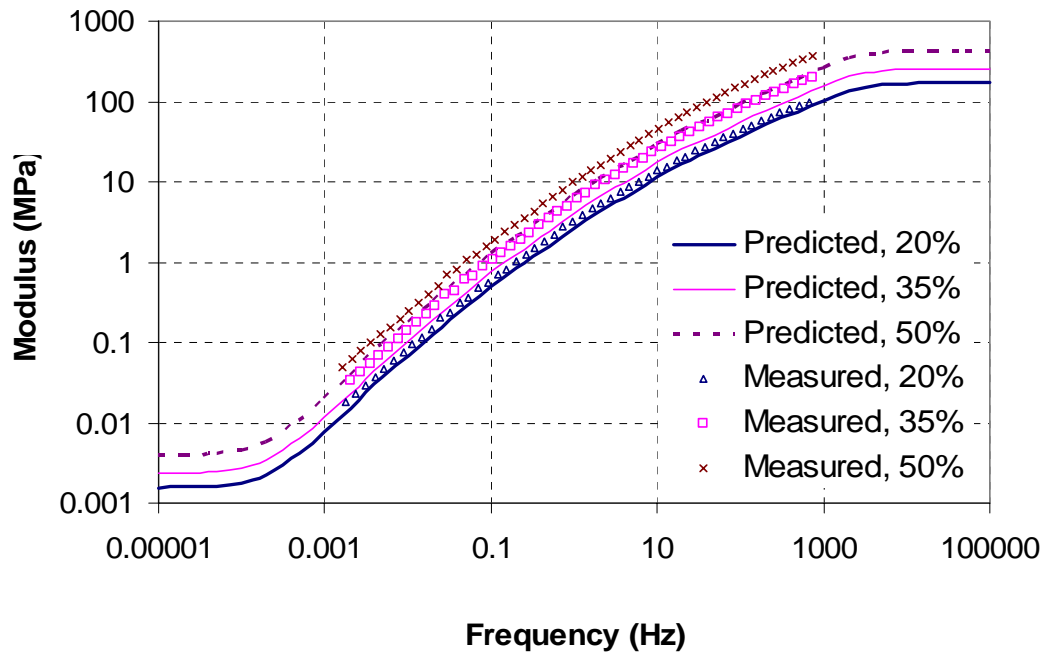


(c) Predicted vs. measured modulus

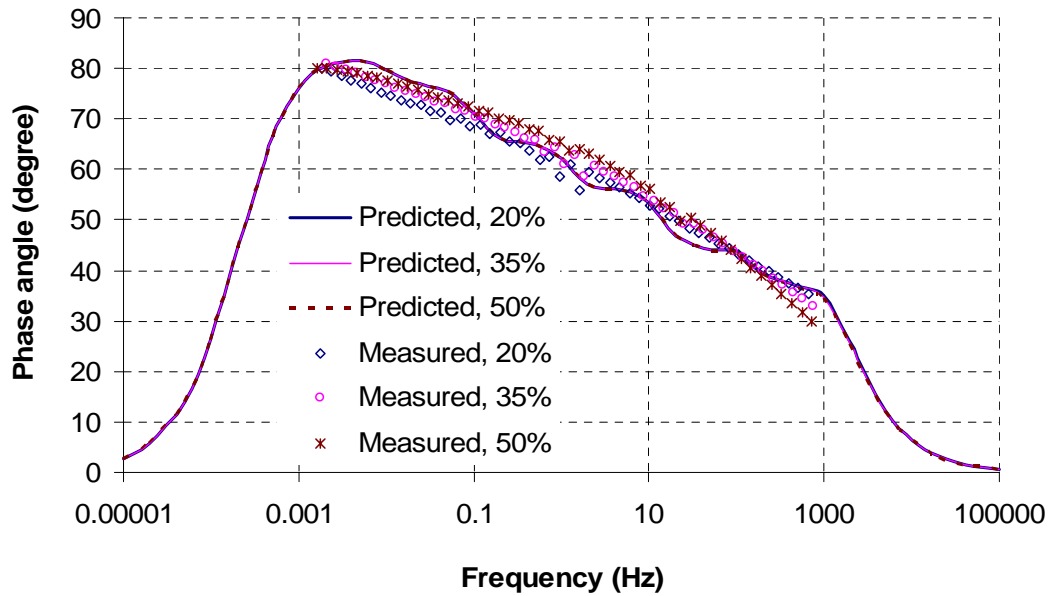


(d) Predicted vs. measured phase angle

Figure 6.15 Predicted vs. Measured Values of Asphalt Mastic (Model 3-1) (Contd.)

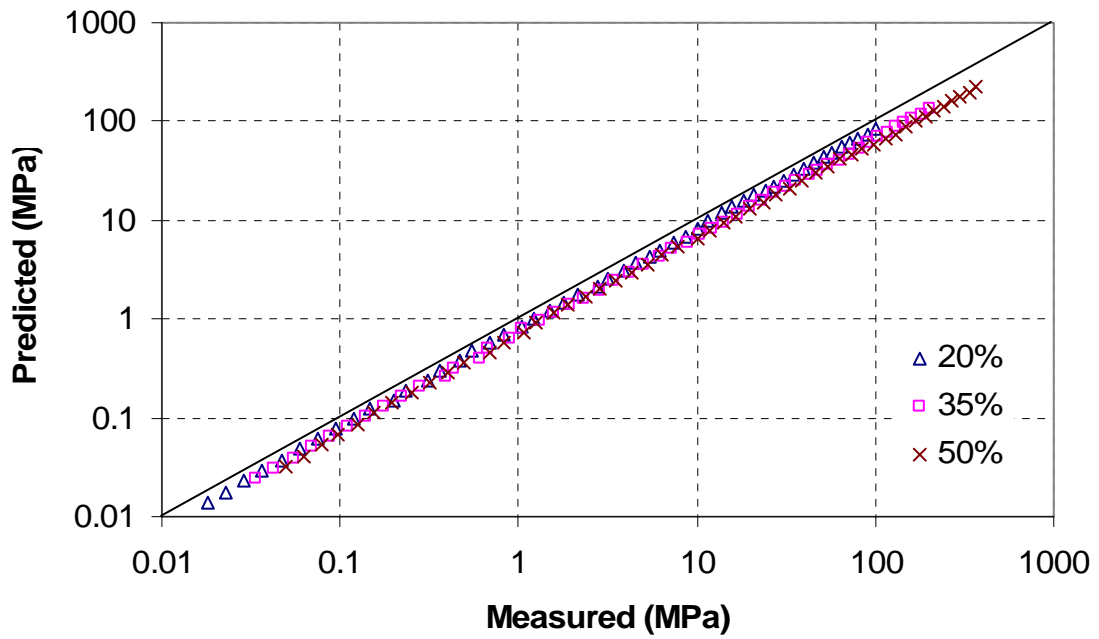


(a) Modulus vs. frequency

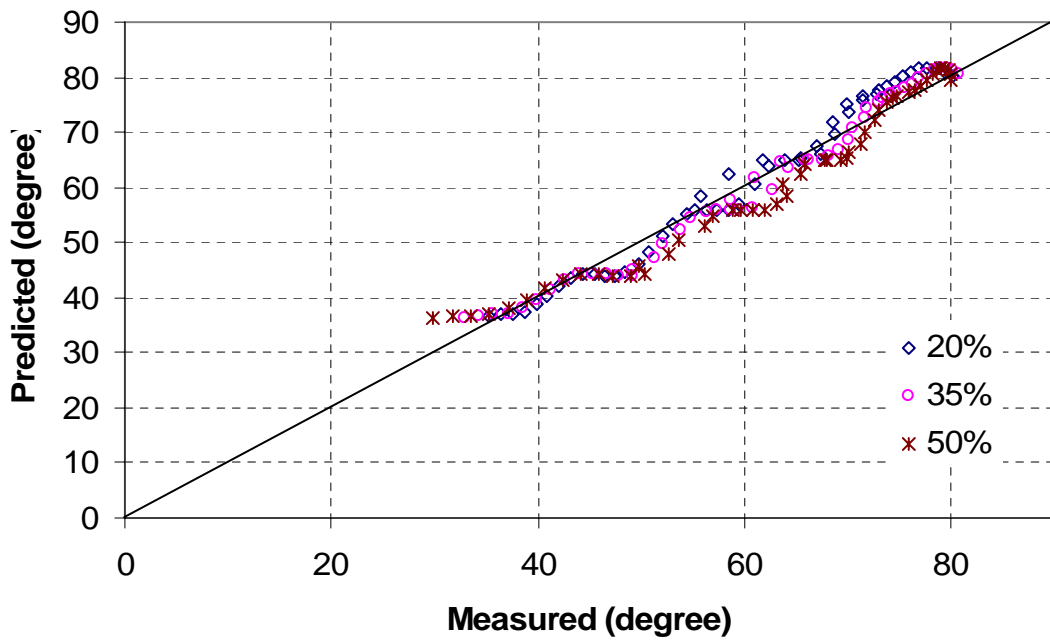


(b) Phase angle vs. frequency

Figure 6.16 Predicted vs. Measured Values of Asphalt Mastic (Model 3-2)

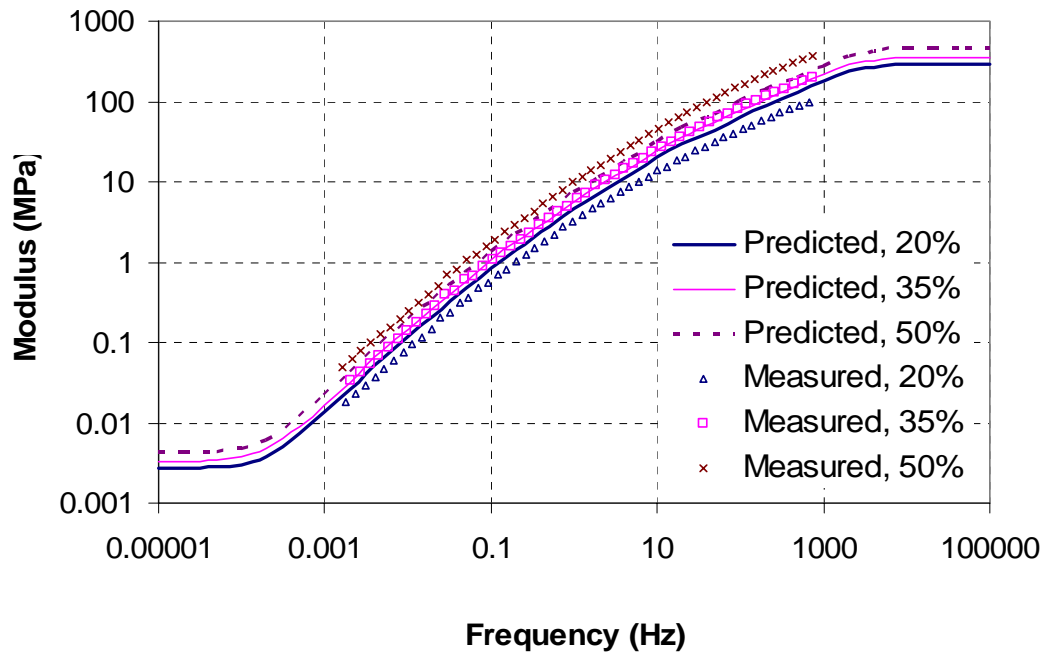


(c) Predicted vs. measured modulus

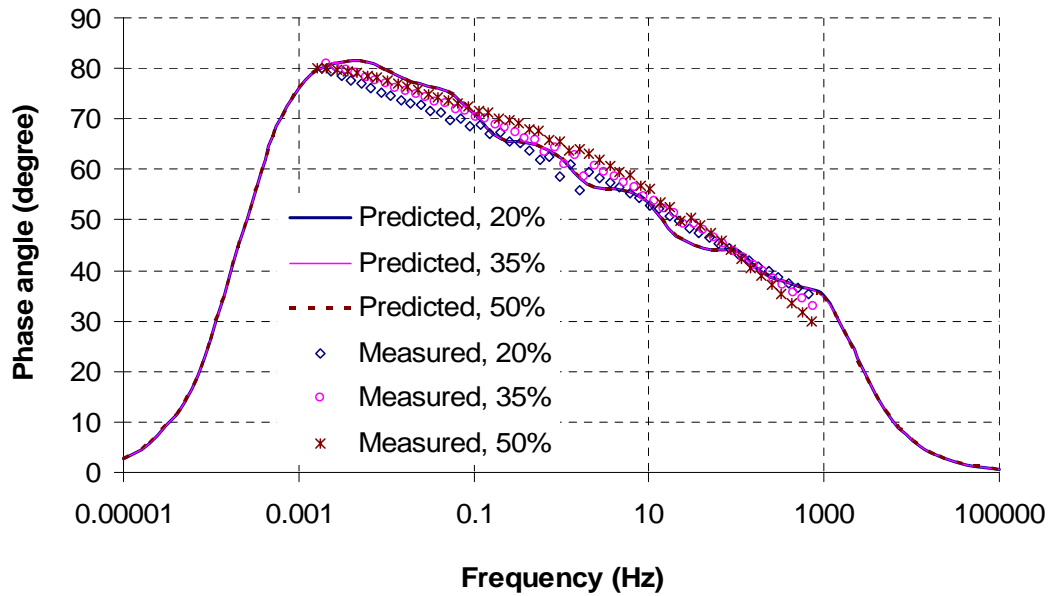


(d) Predicted vs. measured phase angle

Figure 6.16 Predicted vs. Measured Values of Asphalt Mastic (Model 3-2) (Contd.)

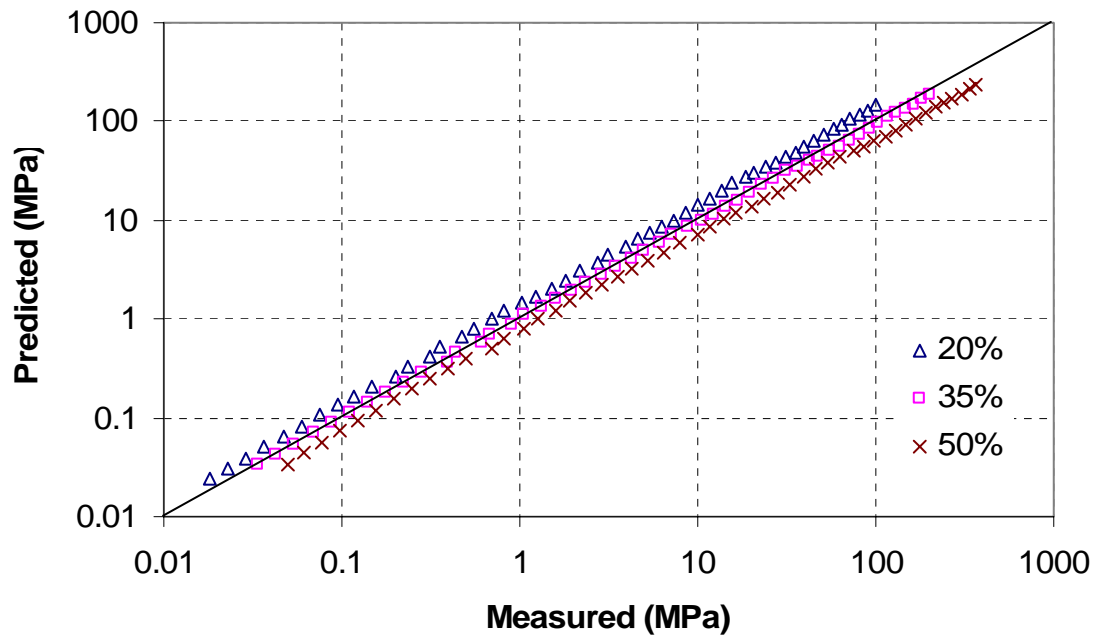


(a) Modulus vs. frequency

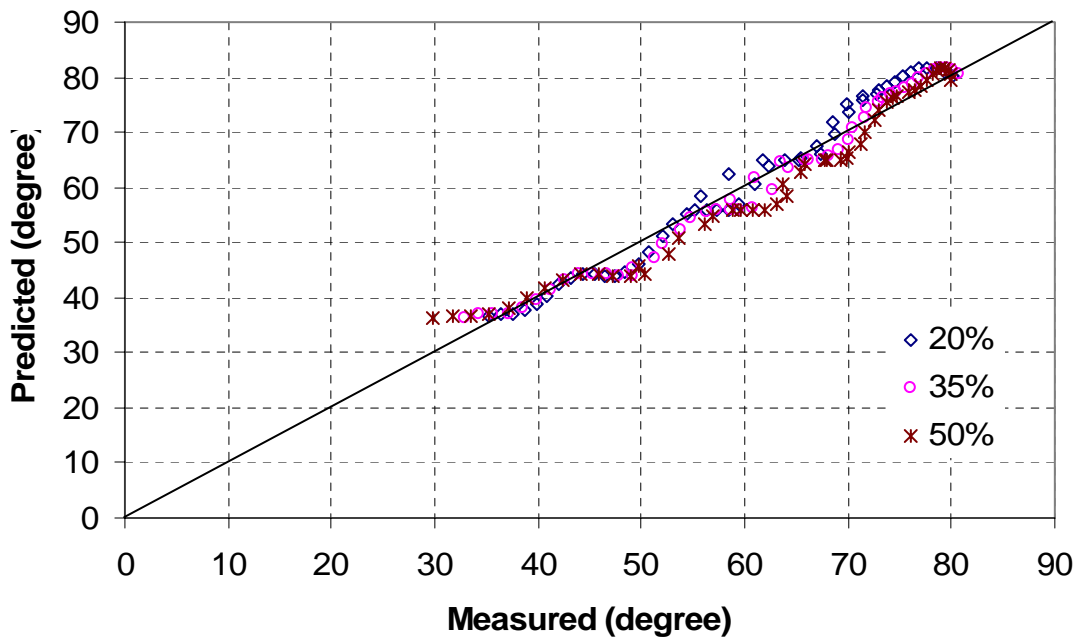


(b) Phase angle vs. frequency

Figure 6.17 Predicted vs. Measured Values of Asphalt Mastic (Model 4-1)

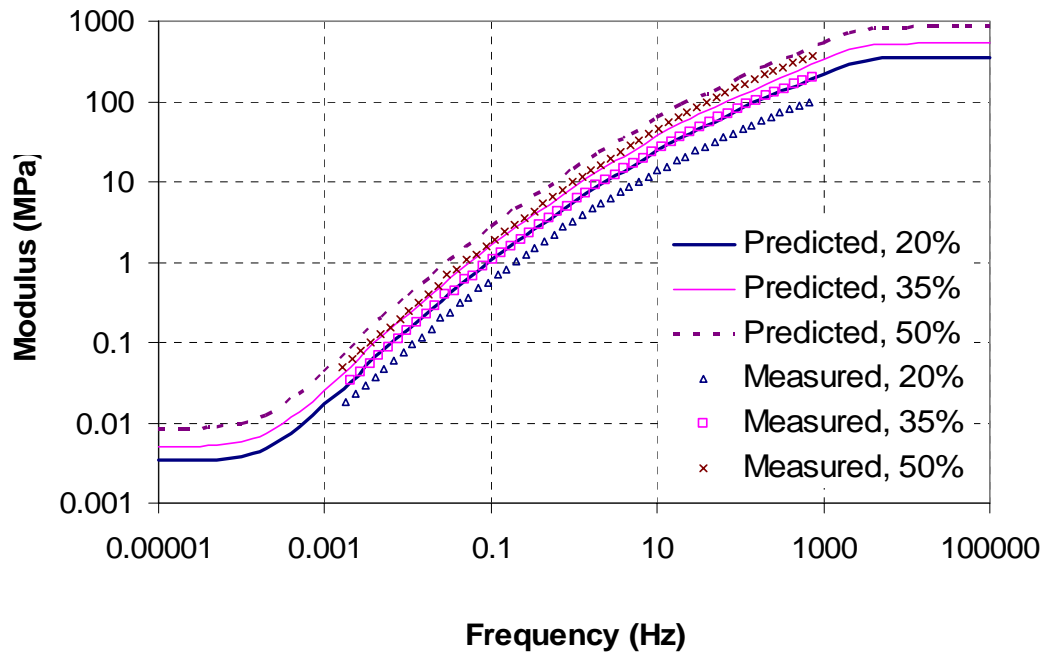


(c) Predicted vs. measured modulus

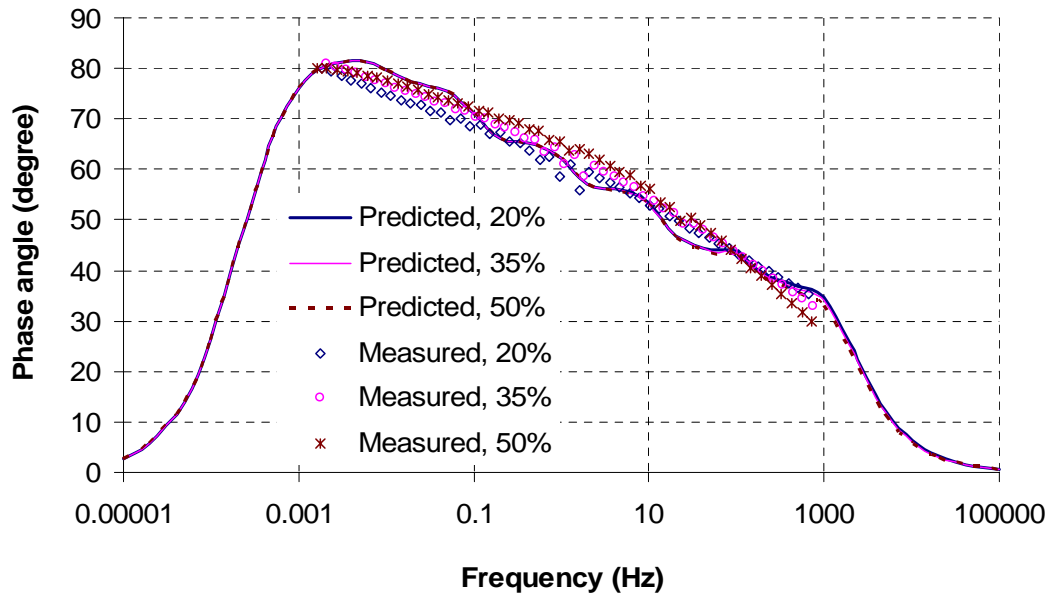


(d) Predicted vs. measured phase angle

Figure 6.17 Predicted vs. Measured Values of Asphalt Mastic (Model 4-1) (Contd.)

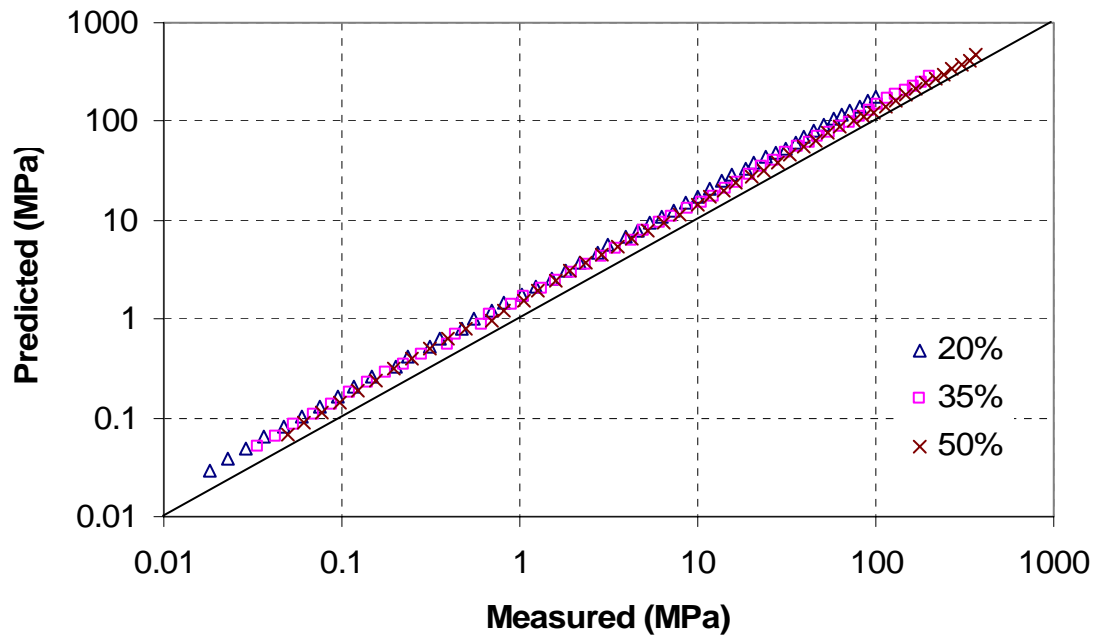


(a) Modulus vs. frequency

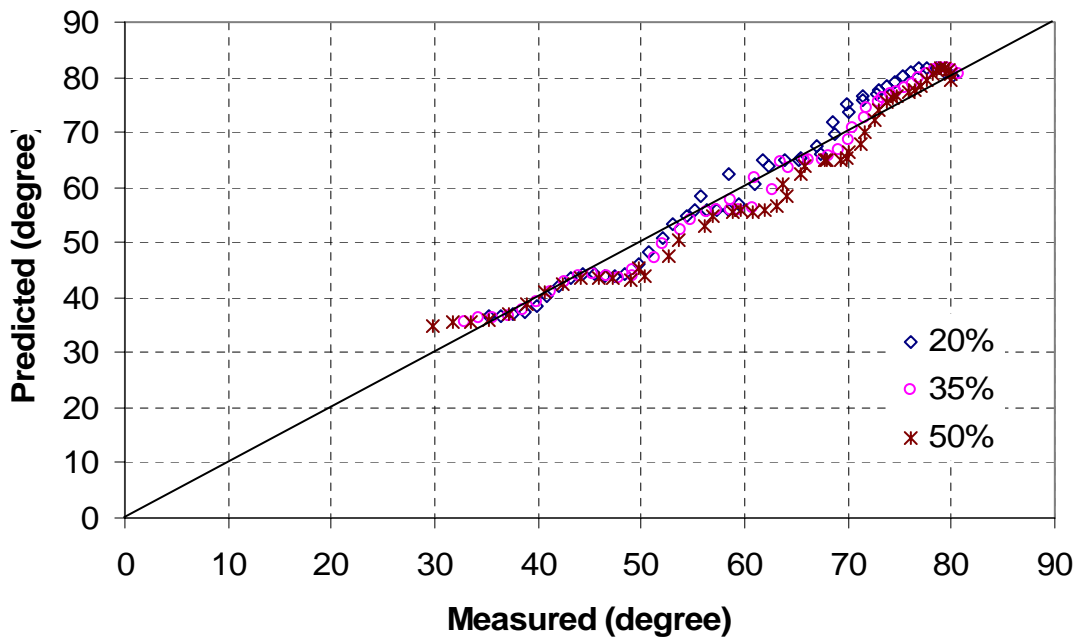


(b) Phase angle vs. frequency

Figure 6.18 Predicted vs. Measured Values of Asphalt Mastic (Model 4-2)

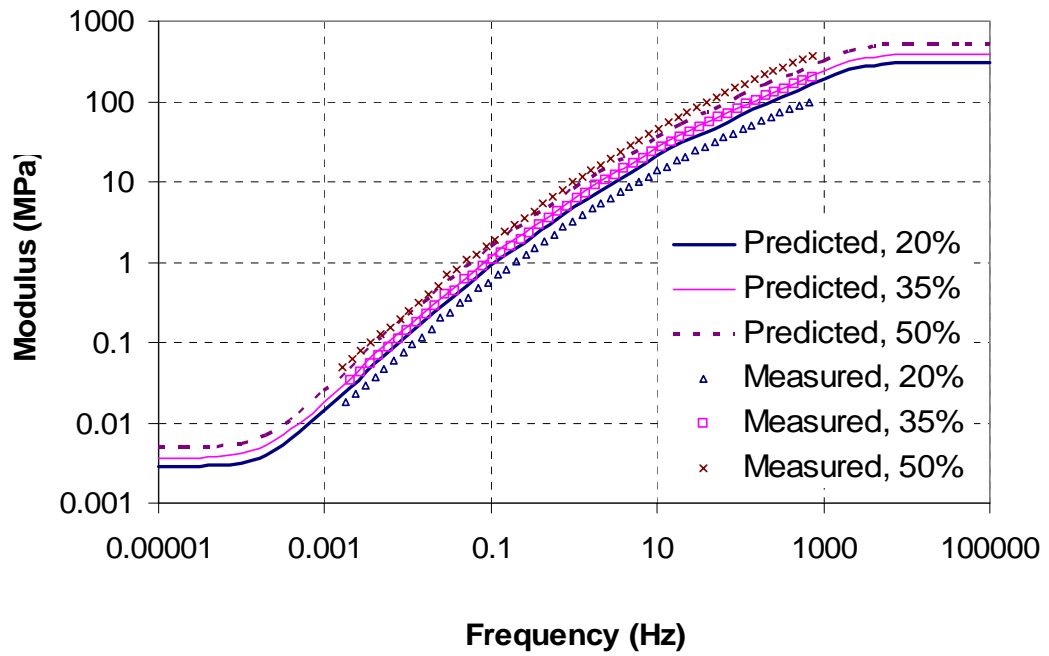


(c) Predicted vs. measured modulus

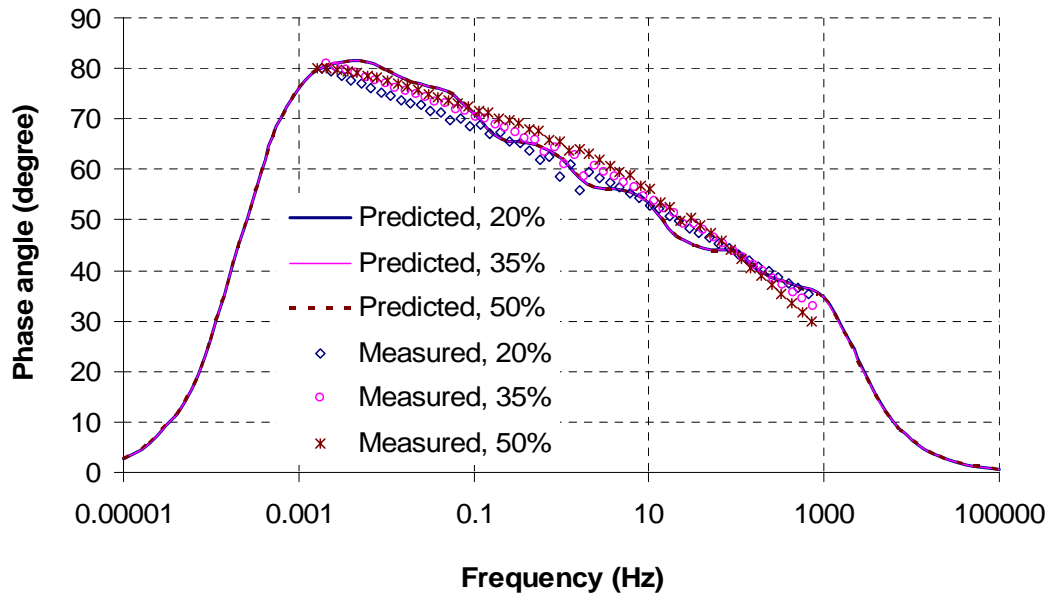


(d) Predicted vs. measured phase angle

Figure 6.18 Predicted vs. Measured Values of Asphalt Mastic (Model 4-2) (Contd.)

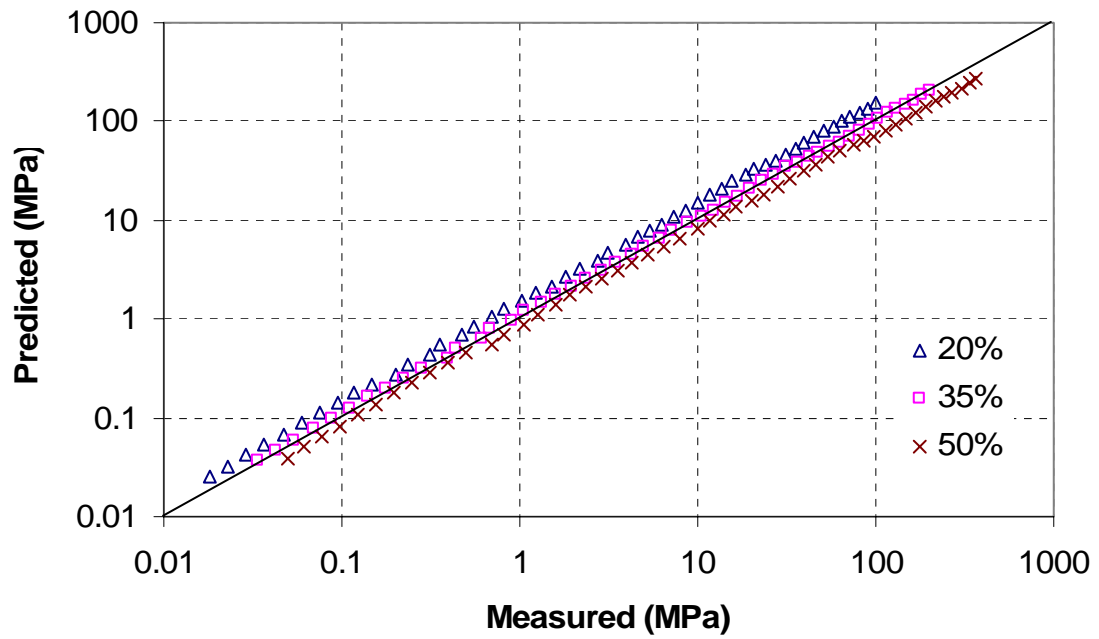


(a) Modulus vs. frequency

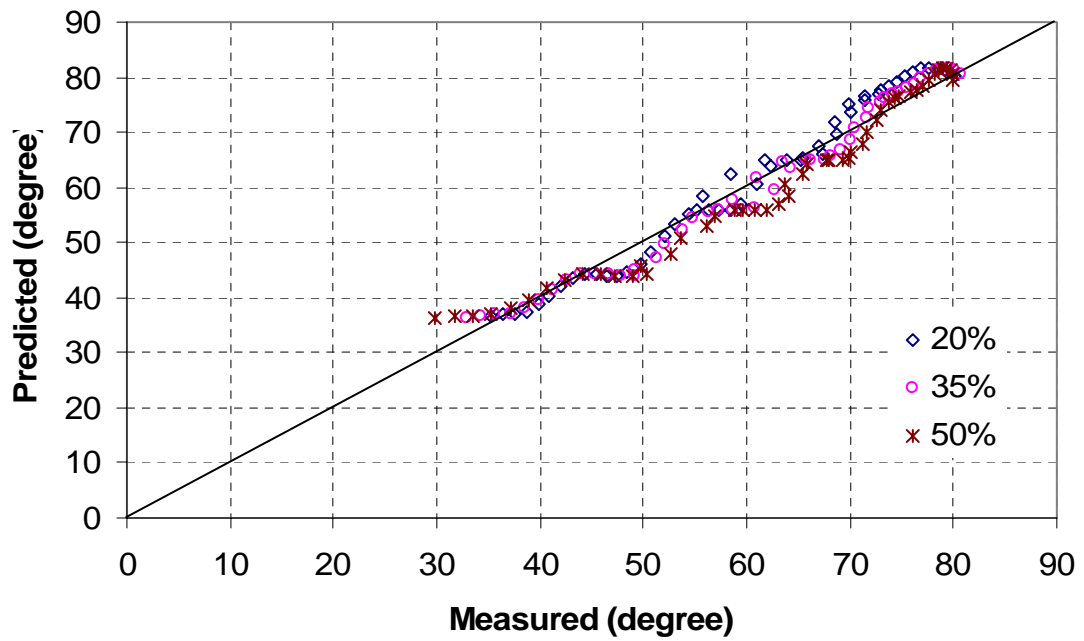


(b) Phase angle vs. frequency

Figure 6.19 Predicted vs. Measured Values of Asphalt Mastic (Model 5)

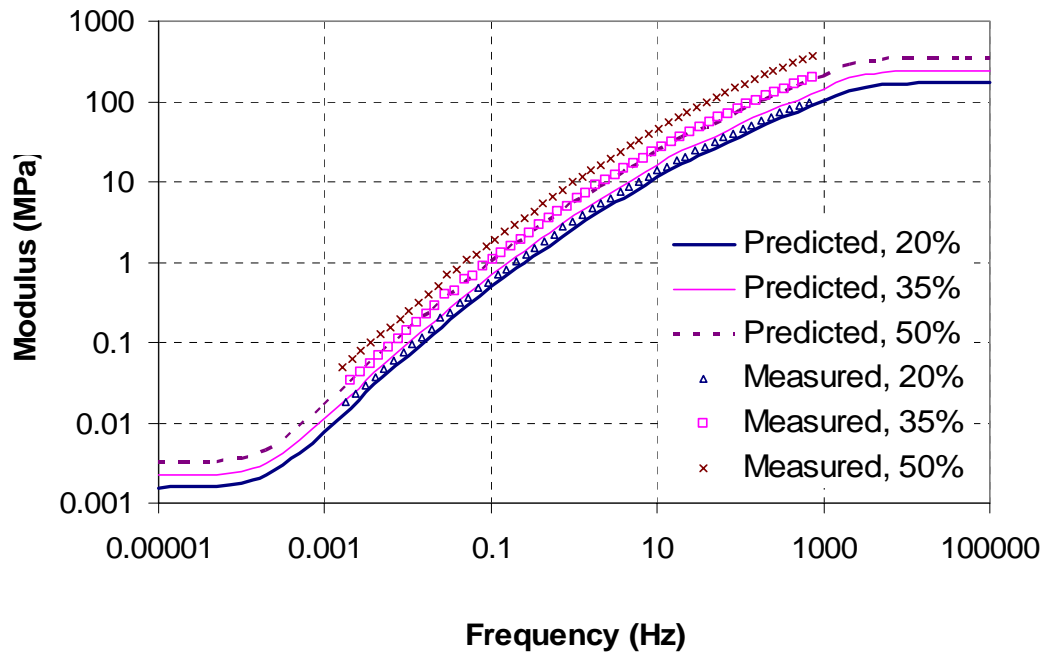


(c) Predicted vs. measured modulus

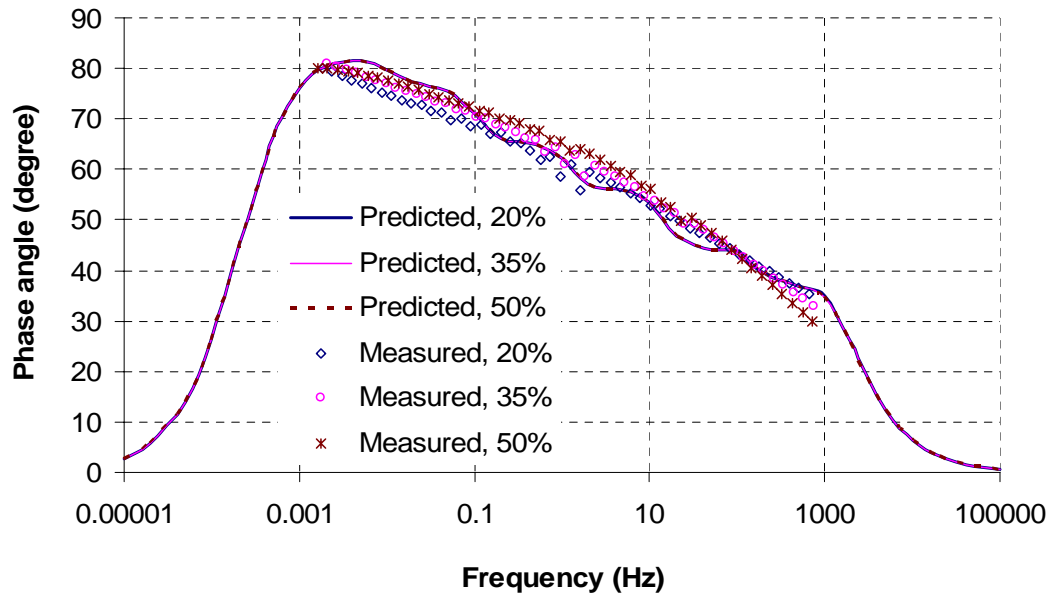


(d) Predicted vs. measured phase angle

Figure 6.19 Predicted vs. Measured Values of Asphalt Mastic (Model 5) (Contd.)

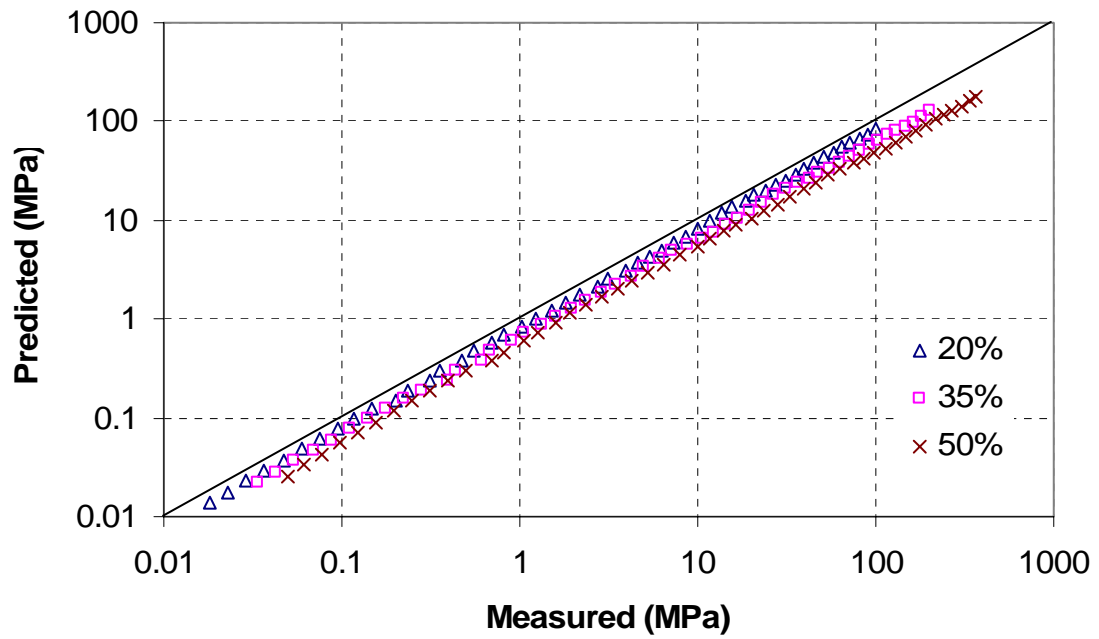


(a) Modulus vs. frequency

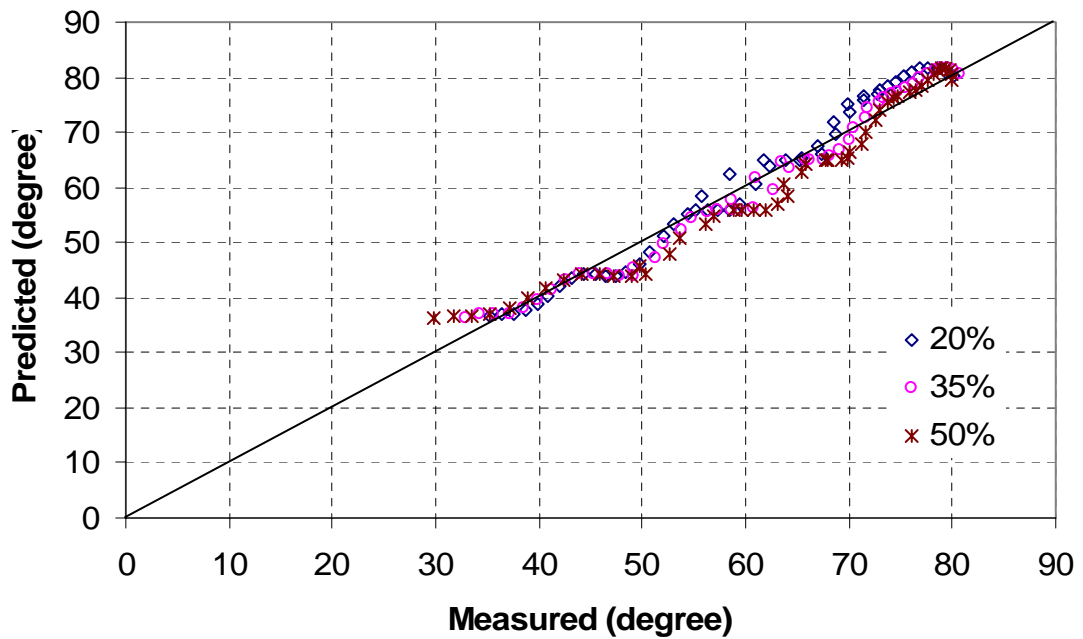


(b) Phase angle vs. frequency

Figure 6.20 Predicted vs. Measured Values of Asphalt Mastic (Model 6)

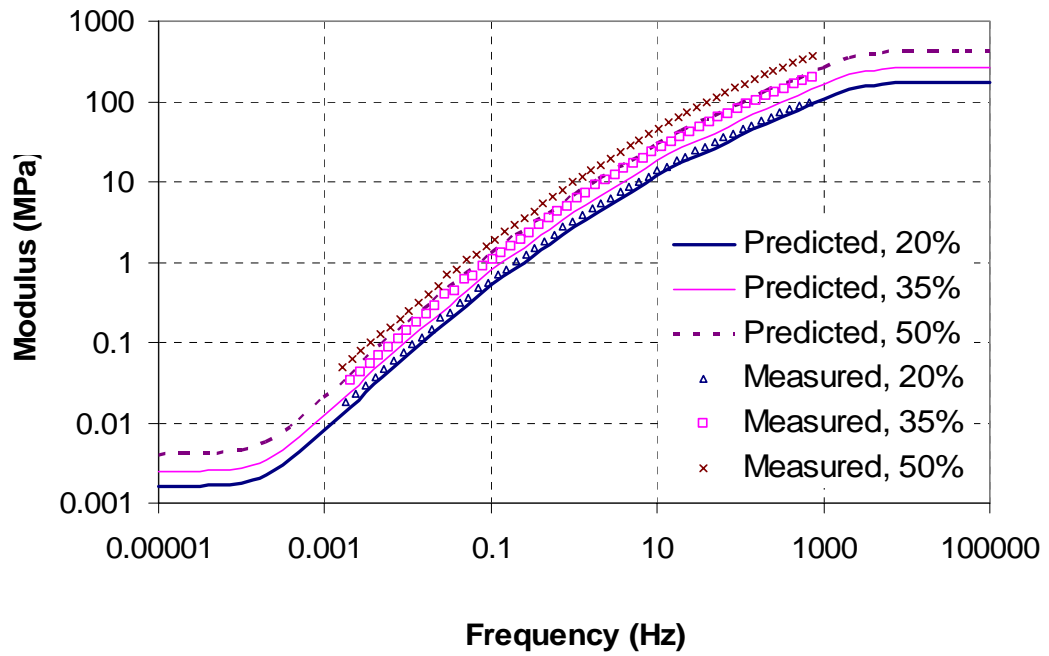


(c) Predicted vs. measured modulus

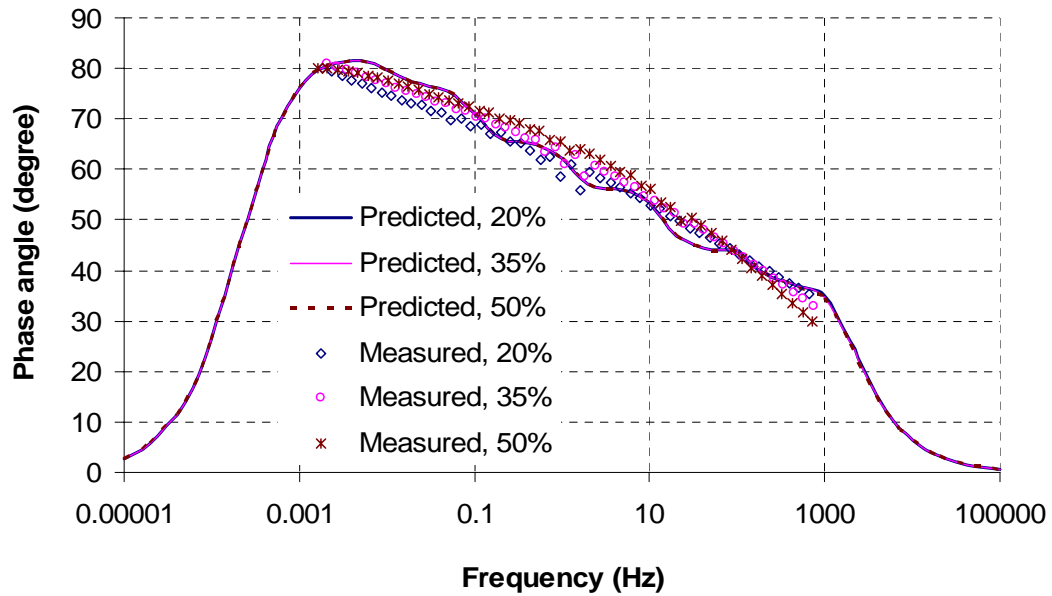


(d) Predicted vs. measured phase angle

Figure 6.20 Predicted vs. Measured Values of Asphalt Mastic (Model 6) (Contd.)

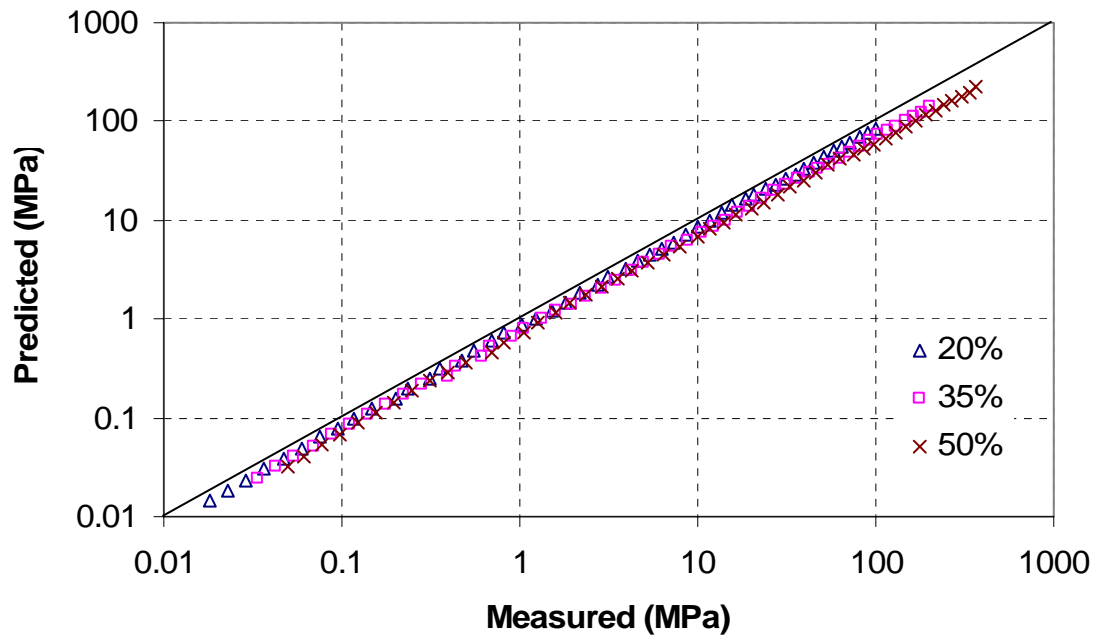


(a) Modulus vs. frequency

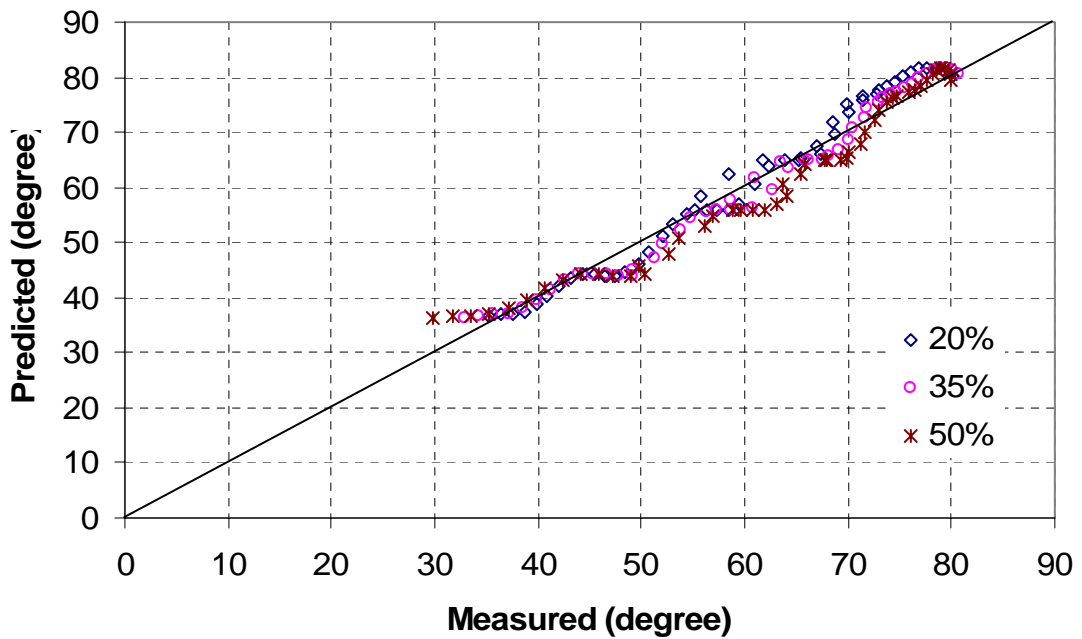


(b) Phase angle vs. frequency

Figure 6.21 Predicted vs. Measured Values of Asphalt Mastic (Model 7)

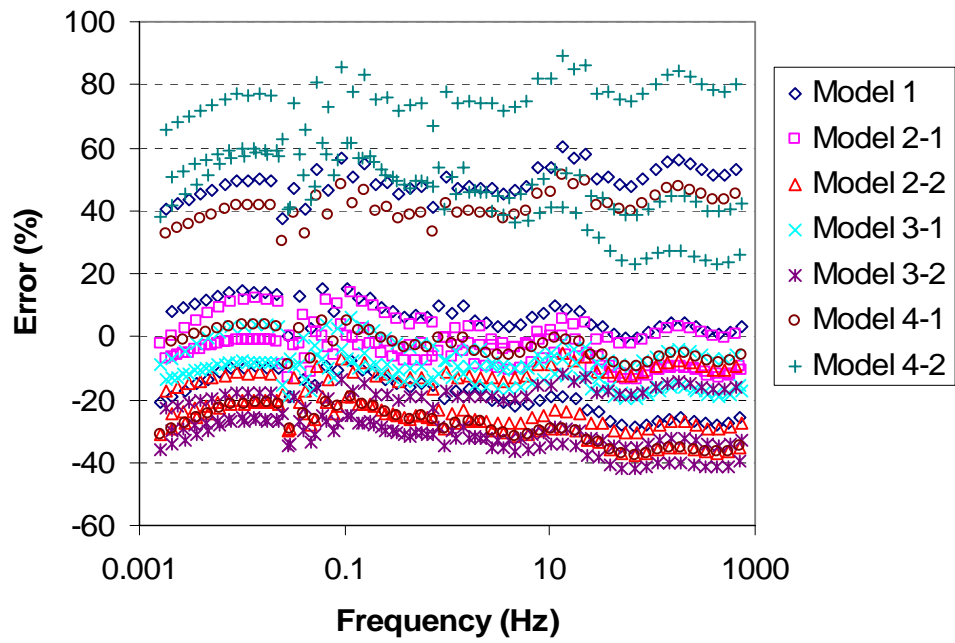


(c) Predicted vs. measured modulus

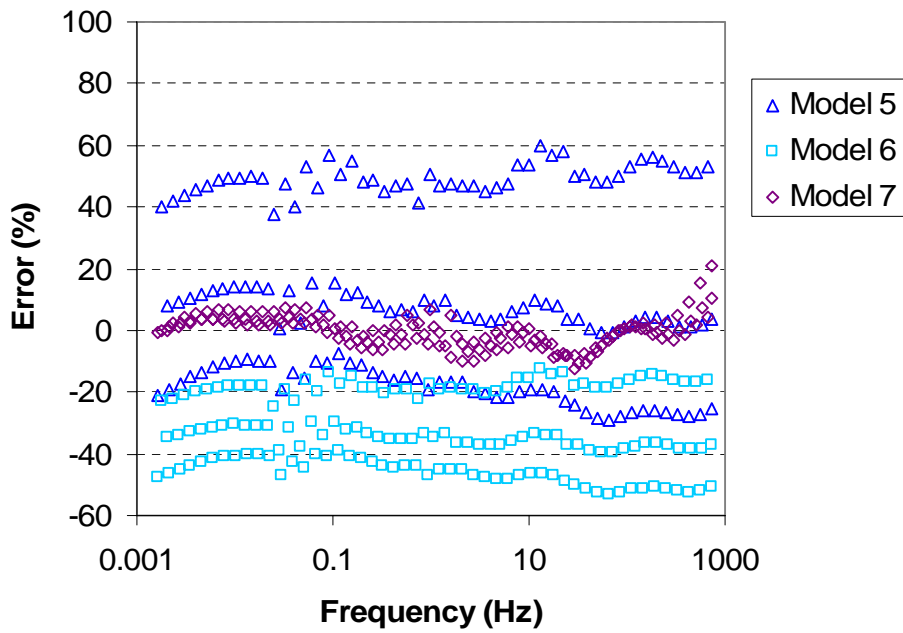


(d) Predicted vs. measured phase angle

Figure 6.21 Predicted vs. Measured Values of Asphalt Mastic (Model 7) (Contd.)

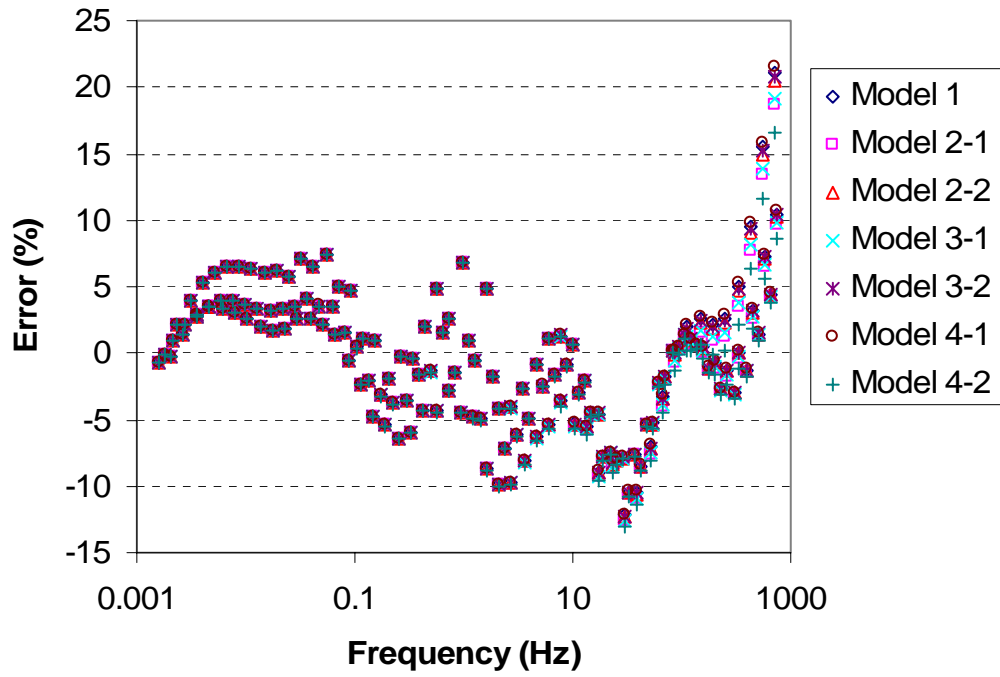


(a) Models developed in this study

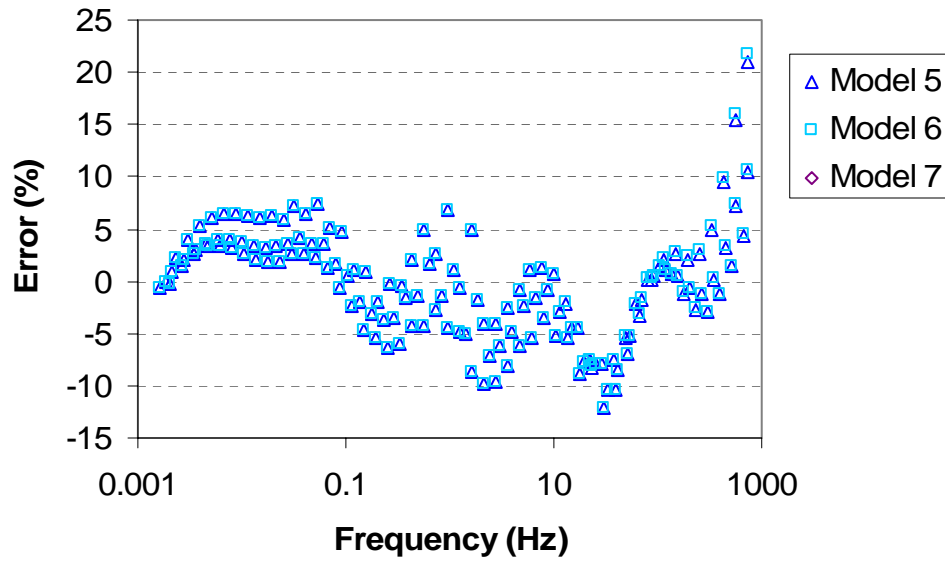


(b) Currently existing models

Figure 6.22 Errors for Dynamic Shear Modulus in Viscoelastic Prediction



(a) Models developed in this study



(b) Currently available models

Figure 6.23 Errors for Phase Angle in Viscoelastic Prediction

models developed in this study, more than half of the prediction errors were distributed within the range between – 40% and 20%. For the predictive equations from the Hasin model and the Christensen and Lo’s GSCM model, the prediction errors were mainly within the range between – 60% and 20%.

For phase angle, different models gave similar prediction errors, as presented in Figure 6.23. The prediction errors were mostly within the range of $\pm 10\%$, especially at low to intermediate frequencies. No significant difference in the predicted phase angle was observed between different PFC models.

Comparison between Elastic and Viscoelastic Predictions

To evaluate the difference in the predicted dynamic shear modulus between elastic and viscoelastic prediction methods and potential of replacing viscoelastic with elastic method in predicting the dynamic (shear) modulus of asphalt mastic and mixture, the predicted results from these two methods are compared. The difference in the predicted moduli from these two methods was evaluated using the following equation:

$$\text{Error} = \frac{|G^*|_{\text{elastic}} - |G^*|_{\text{viscoelastic}}}{|G^*|_{\text{viscoelastic}}} \times 100 \quad (6.2)$$

where

Error = relative error, %;

$|G^*|_{\text{elastic}}$ = predicted dynamic shear modulus from elastic prediction method; and

$|G^*|_{\text{viscoelastic}}$ = predicted dynamic shear modulus from viscoelastic prediction method.

Figure 6.24 presents the predicted errors in dynamic shear modulus of asphalt mastics at three different concentrations (20%, 35% and 50%) caused by using elastic prediction methods. It should be noted that Poisson's ratios of 0.5 and 0.2 were used for both methods so that the error caused by different value of Poisson ratio could be eliminated. It was observed that at the three volume concentrations used in this study (20%, 35% and 50%), the error due to the use of elastic method was really small. All the prediction errors were within the range between - 1% and 4%. Among all the models used in this study, Model 4-1 gave the largest prediction scatter and it also showed the trend that prediction error increased with the increase in the volume concentration of mineral filler in asphalt mastic.

Figure 6.25 presents the plots of prediction errors vs. frequency for Model 4-1 at different volume concentrations. It can be seen that even at the mineral filler volume concentration of up to 70%, the prediction error caused by the use of elastic method was still below 10%. This indicated that at low to mediate volume concentrations, it was possible to use elastic method instead of viscoelastic method to predict dynamic shear modulus of asphalt mastic. The prediction error due to the replacement of viscoelastic with elastic model was pretty small. Large prediction errors were only observed at very high volume concentrations and high frequencies.

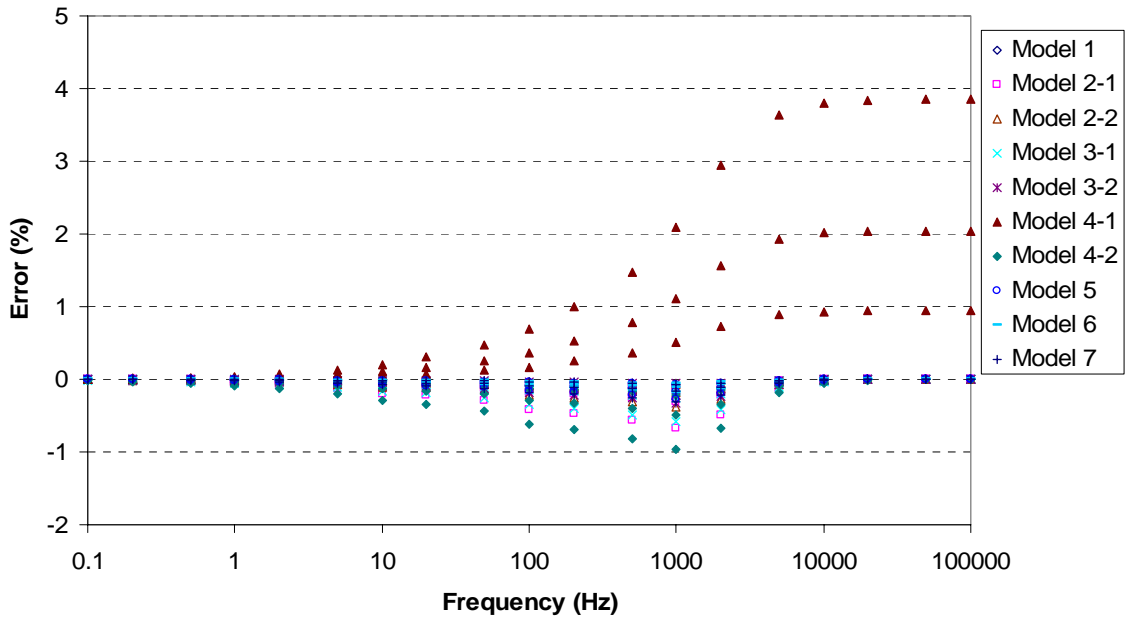


Figure 6.24 Errors Caused by Elastic Prediction Method

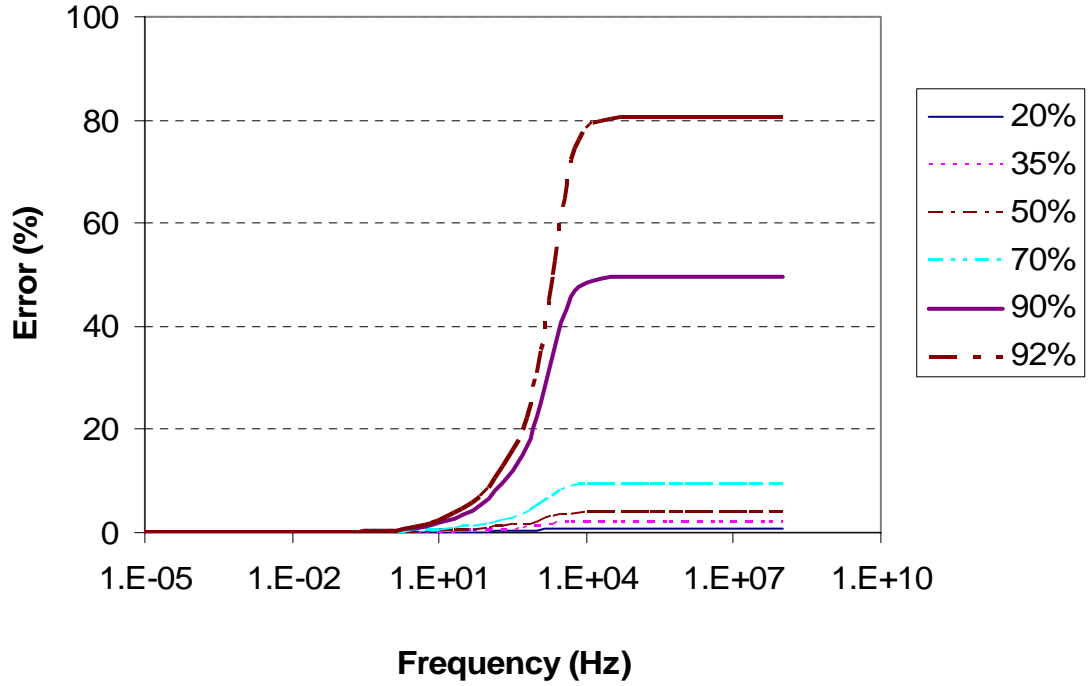


Figure 6.25 Errors Caused by Elastic Prediction Method for Model 4-1

CHAPTER 7 PREDICTION OF DYNAMIC MODULUS OF HMA MIXTURE

Introduction

This chapter presents the application of various PFC models developed in this study to predicting the dynamic modulus of HMA mixtures. The prediction accuracy of the PFC models in predicting the dynamic modulus was evaluated through the comparison between the predicted results and the measured test data.

In order to simulate the microstructure of the asphalt-aggregate composite system of HMA mixtures, two different methods were used in this study. In the first method, HMA was regarded as a composite material with aggregate particles and mineral fillers dispersed in the asphalt cement binder matrix (Figure 7.1). This method was named “binder-aggregate system” method in this study. In this method, mineral filler particles were treated as aggregate, no matter how small they are. Because it is impossible to obtain the whole aggregate particle size distribution over the range from the minimum mineral filler (nearly zero) to the maximum aggregate size, this method could not consider the aggregate gradation and its effect on the viscoelastic properties of HMA mixtures. The volumetric property of HMA mixtures used in this method was the volume concentration of inclusion (aggregate) in the matrix, as in the prediction of asphalt mastic modulus. In the second method, HMA was considered as a mixture of aggregate particles bonded with asphalt mastic. The asphalt mastic was then made of asphalt binder and mineral filler. Each aggregate particle, regardless of its size, was coated with an asphalt mastic film of same thickness (Figure 7.2). Therefore, the second method was named “mastic-aggregate system” method in this study. Since the aggregate particle size

distribution can be readily acquired, this method has the capability of taking into account aggregate gradation in the prediction and evaluating its effect on the properties of HMA mixtures. Both methods were employed to predict the viscoelastic properties of HMA mixtures and to evaluate their applicability to HMA mixtures.

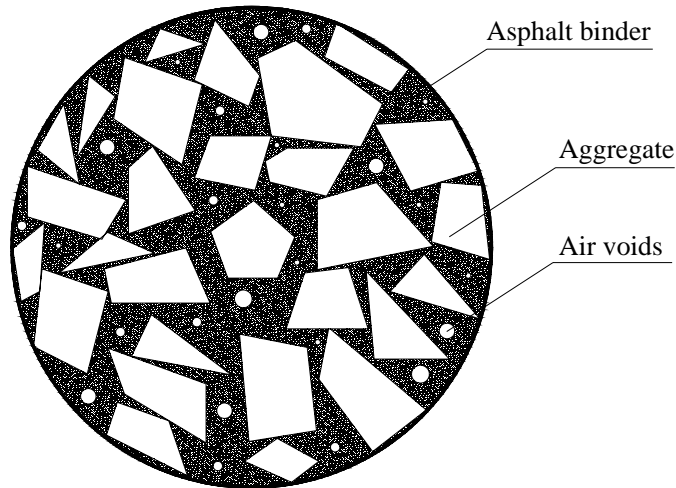


Figure 7.1 Schematic for Binder-Aggregate System of HMA Mixtures

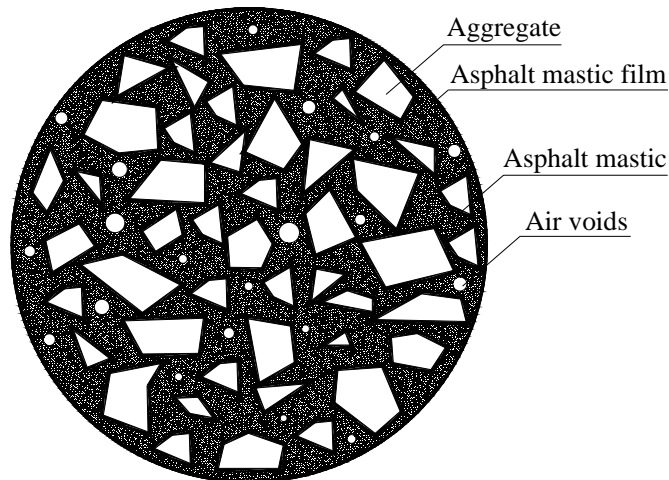


Figure 7.2 Schematic for Mastic-Aggregate System of HMA Mixtures

Input Parameter Values

Part of the input parameter values necessary for both the binder-aggregate system and mastic-aggregate system methods are presented in Table 6.1 in Chapter 6. To employ the mastic-aggregate system method, the complex (shear) modulus of asphalt mastic was also needed as an input parameter in the predictive models and should be determined before the prediction.

The complex (shear) modulus of asphalt mastic in laboratory-prepared HMA mixtures can be determined using the following procedures. From the aggregate gradation and the asphalt cement content used in the laboratory-prepared HMA mixture (Table 5.2), the volume concentration of mineral filler in asphalt mastic was determined to be 25%. From the test data of asphalt mastic at 20% and 35% volume concentrations, the complex shear modulus values of asphalt mastic were determined at 25% volume concentration using the interpolation method. The interpolated complex shear moduli of asphalt mastic at the volume concentration of 25% are presented in Figure 7.3 along with the curves fitted with the Prony series representation. Table 7.1 presents the fitted coefficients for the Prony series representation in terms of G_i .

Binder-Aggregate System Prediction

Flow Chart

Figure 7.4 presents the flow chart for the prediction of dynamic modulus and phase angle of HMA mixtures using the binder-aggregate system method.

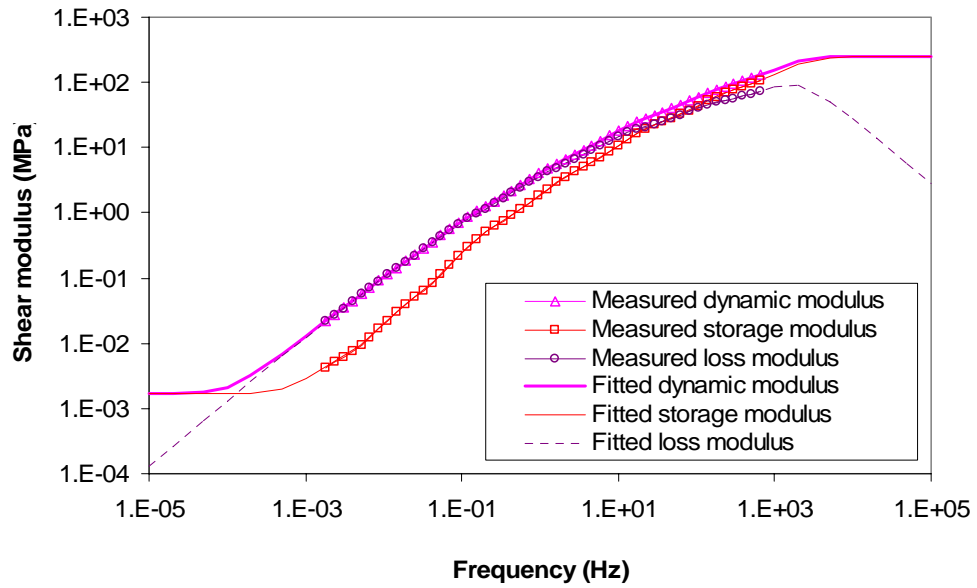


Figure 7.3 Master Curves of Complex Shear Moduli of Asphalt Mastic at 25 v.% (25°C)

Table 7.1 Prony series constants for relaxation shear modulus of asphalt mastic at 25 v.%

i	ρ_i (sec)	G_i (MPa)
1	1E-04	1.718E+02
2	1E-03	5.881E+01
3	1E-02	2.088E+01
4	1E-01	3.991E+00
5	1E+00	6.338E-01
6	1E+01	4.114E-02
7	1E+02	3.565E-03

$$G_e = 1.667E-03$$

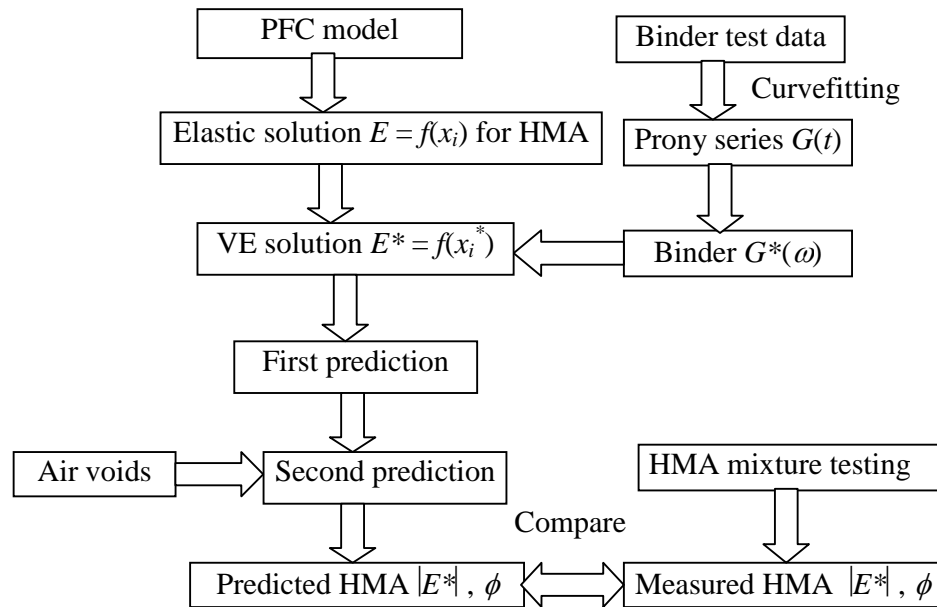


Figure 7.4 Flow Chart for Binder-Aggregate System Prediction

It should be noted that in the predicting process, two-step method was used to take into account air voids effect on HMA mixtures, as described in Chapter 3. In the first step, HMA was assumed to a mixture without air voids in it. The predicted viscoelastic properties were for HMA mixture containing no air voids. In the second step, the effect of air voids on the properties of HMA mixtures was investigated by treating air voids as a series of air bubbles with zero modulus. With more air voids entrapped in HMA mixtures, larger reduction was observed in the predicted dynamic modulus of asphalt mastic and mixtures. In order to characterize the effect of air voids on the modulus of HMA mixtures, the retaining ratio was defined as follows

$$R = \frac{|E^*|_{\text{air voids}}}{|E^*|_{\text{no air voids}}} \quad (7.1)$$

where

R = retaining ratio due to the incorporation of air voids in HMA mixtures, $R = 0 \sim 1$;

$|E^*|_{\text{air voids}}$ = predicted dynamic modulus of HMA mixtures with air voids entrapped in them; and

$|E^*|_{\text{no air voids}}$ = predicted dynamic modulus of HMA mixtures without air voids.

Figure 7.5 presents the plots of retaining ratio vs. air voids content for Model 1 through Model 7 (Table 6.3). It can be seen that Model 6 (the Hashin model) had the highest retaining ratio among all the models used in this study. In other words, the Hashin model gave the smallest reduction due to incorporation of air voids in HMA mixtures. Model 4 showed the lowest retaining ratio, which indicated that the predicted modulus from Model 4 was the smallest among all the predicted modulus values. Other models showed moderate decrease in modulus caused by air voids.

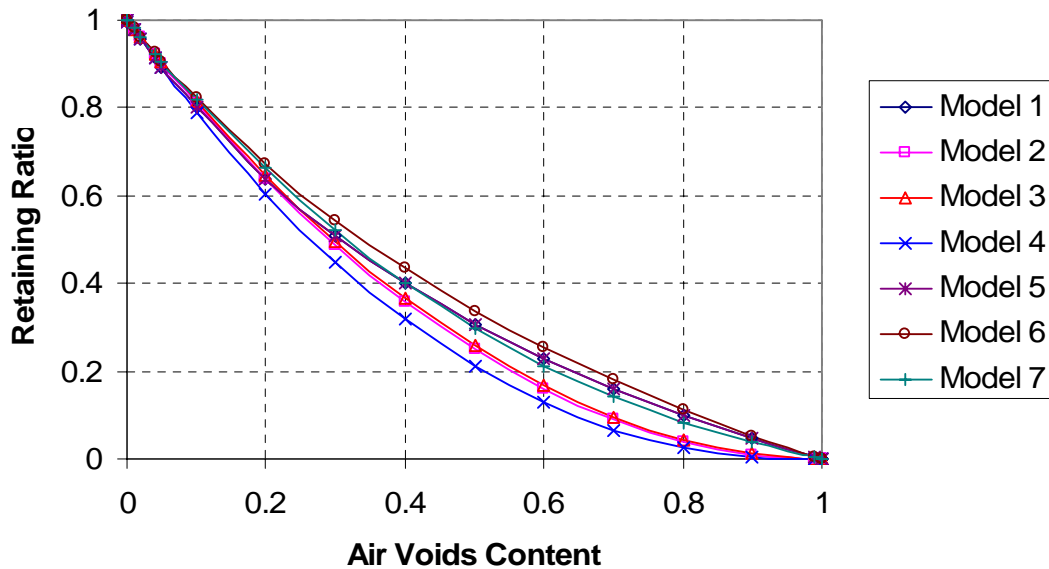


Figure 7.5 Relationship between Retaining Ratio and Air Voids Content

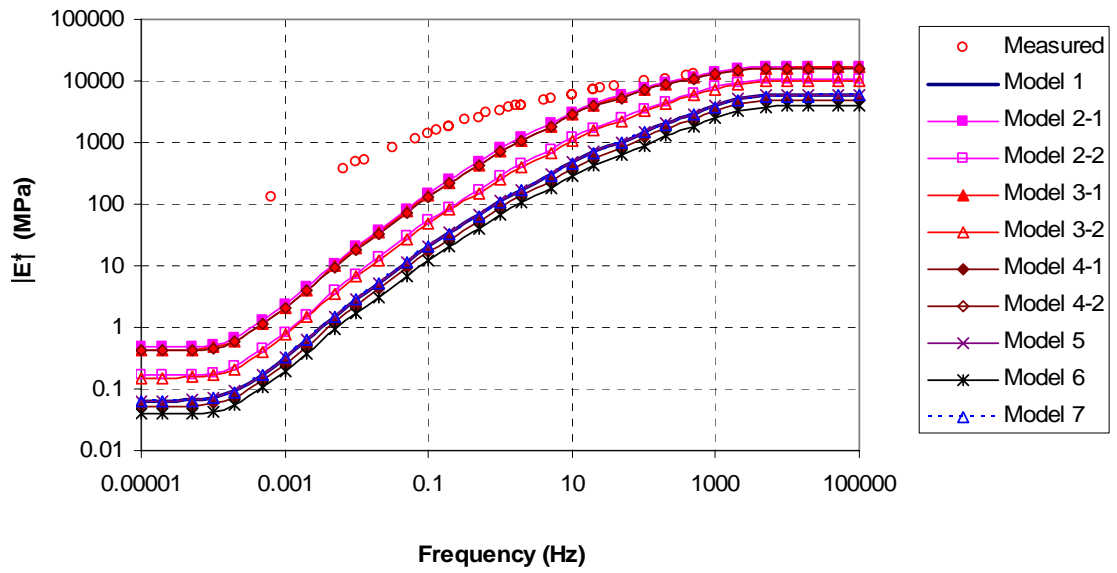
Prediction Results and Analyses

Figures 7.6 ~ 7.16 show the predicted dynamic moduli of HMA mixture from the predictive models presented in Table 6.4. The measured dynamic moduli were also included in these figures in comparison to the predicted values.

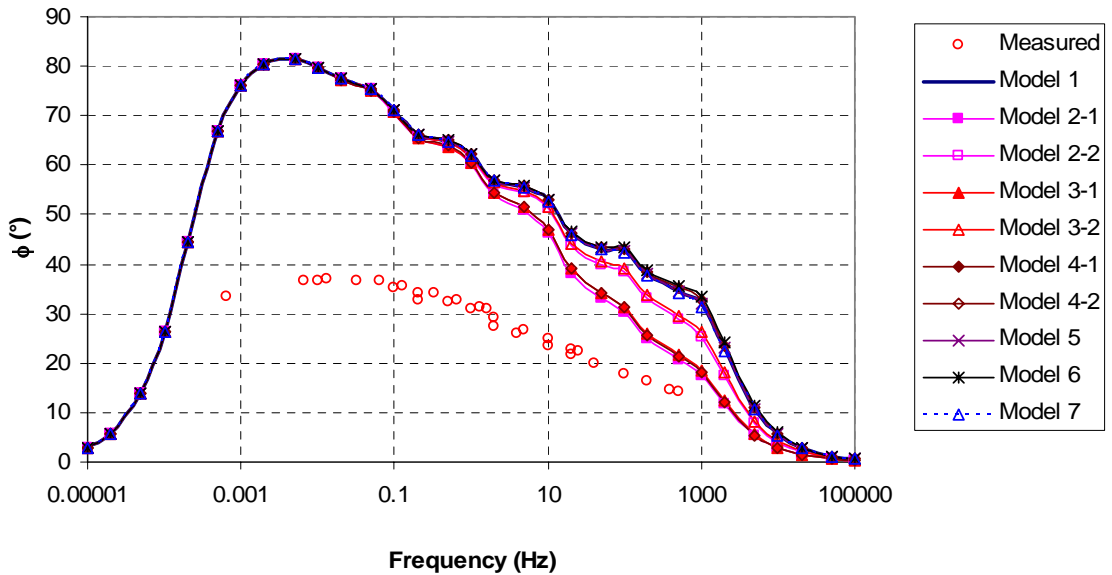
From Figures 7.6 through 7.16, it was observed that the predicted values followed the general pattern of dynamic modulus of HMA mixtures, i.e., the higher the frequency, the higher the dynamic modulus value. All the plots of predicted modulus vs. frequency exhibited the sigmoidal shape, which could be attributed to the viscoelastic nature of HMA mixtures.

However, when compared to the measured dynamic moduli, the predicted values from all the models were unfavorably lower, which indicated that all the models under-predicted dynamic modulus of HMA mixtures. This under-prediction phenomenon of PFC models in estimating the modulus of asphalt mastic and mixtures was also observed in studies by other researchers (Buttlar and Roque 1996; Buttlar et al. 1999; Li and Metcalf 2005).

Different PFC models gave different prediction errors in estimating the dynamic modulus of HMA mixtures. Among all the models, Model 2-1 gave the highest predicted dynamic moduli, which were closest to the measured values. Model 6 (the Hashin model) gave the lowest prediction results, deviating farthest from the measured data. From these figures, it was observed that with the increase in the loading frequency, the predicted dynamic moduli approached the measured values increasingly closer. The predicted dynamic moduli were much closer to the measured values at higher frequencies than at low frequencies. This phenomenon can be attributed to the fact that with the increase in

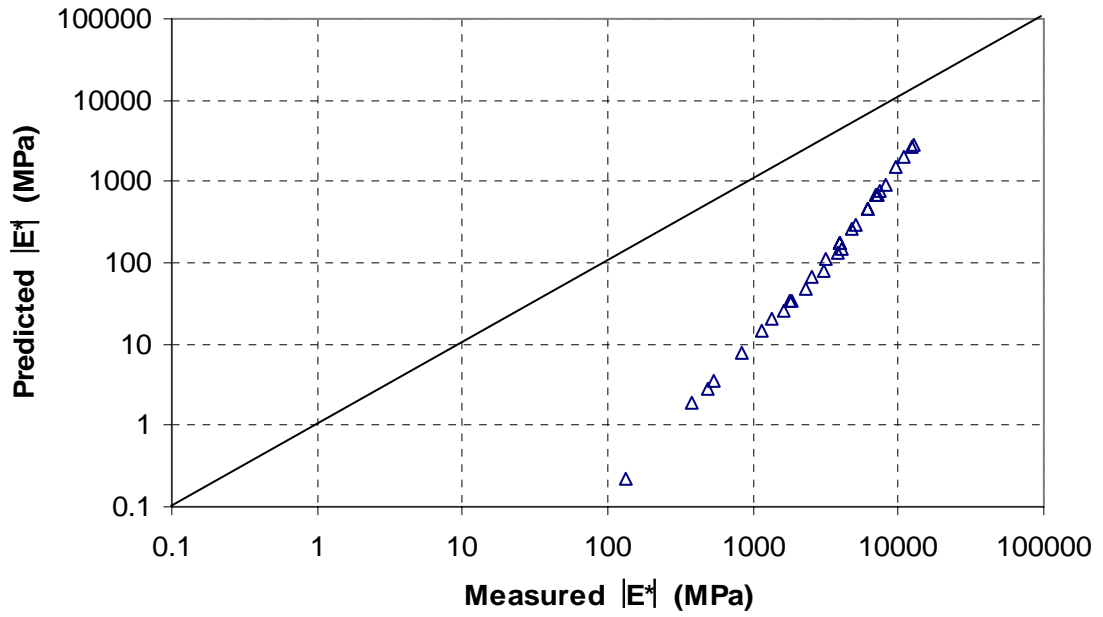


(a) Dynamic modulus $|E^*|$

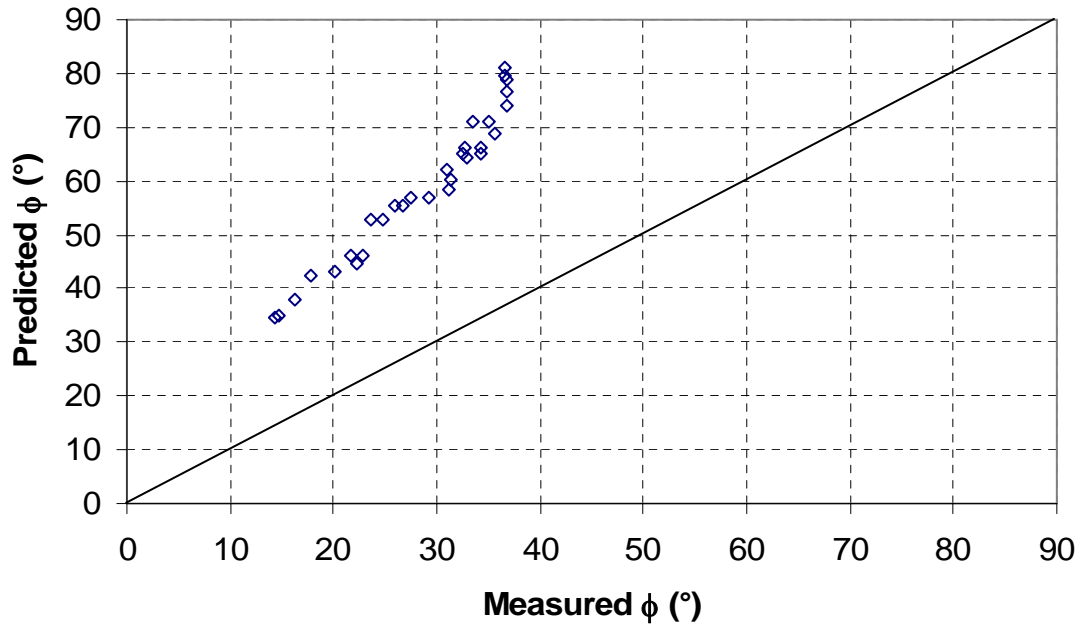


(b) Phase angle ϕ

Figure 7.6 Predicted vs. measured $|E^*|$ and ϕ of HMA mixture

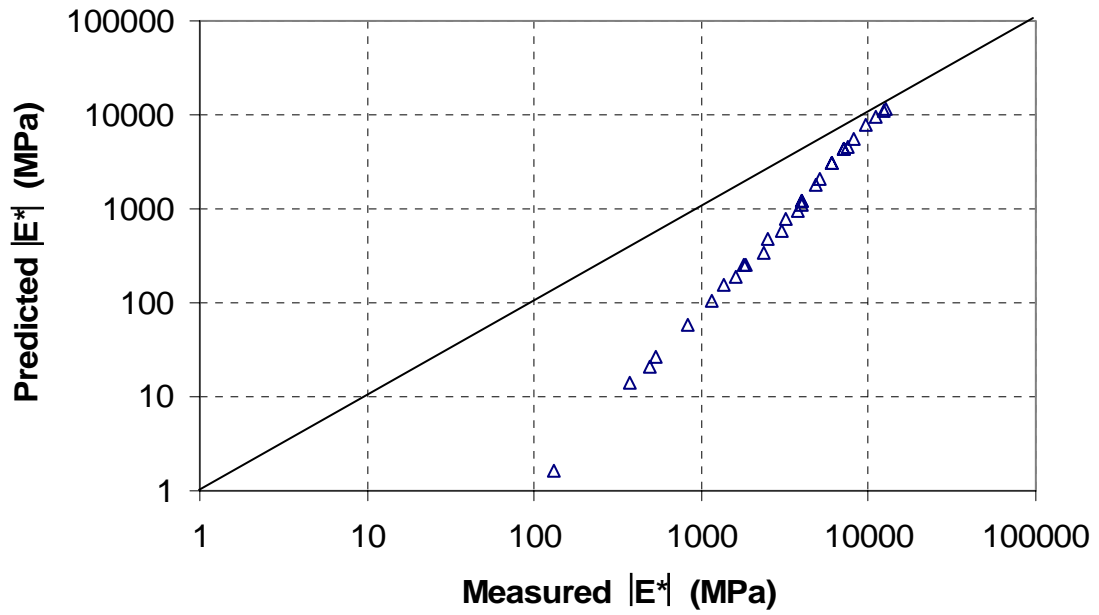


(a) Predicted vs. measured dynamic modulus

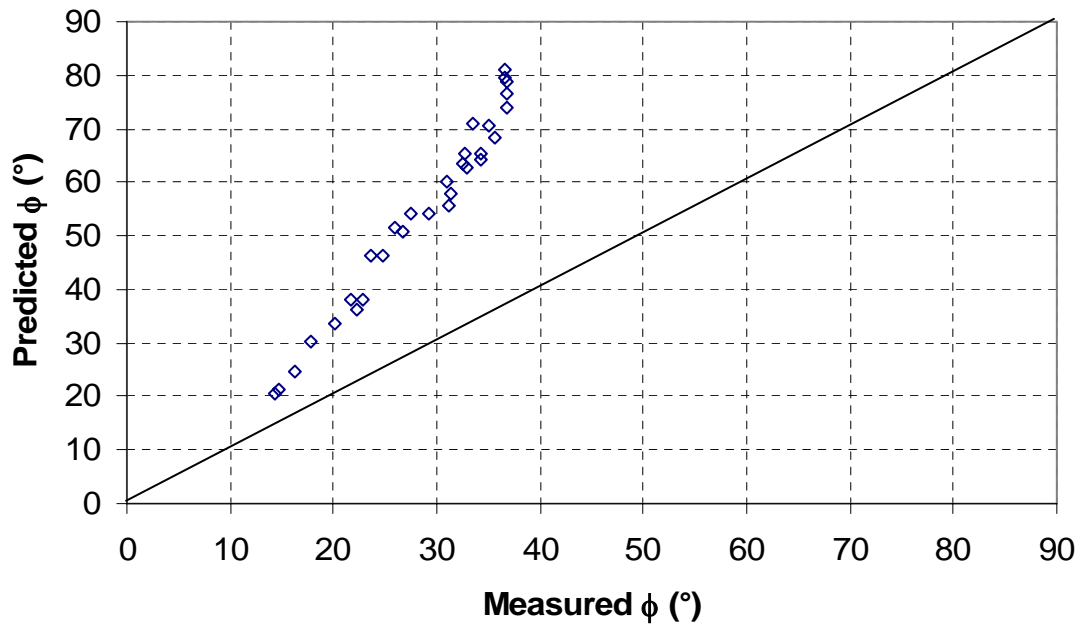


(b) Predicted vs. measured phase angle

Figure 7.7 Predicted vs. measured $|E^*|$ and ϕ of HMA mixture (Model 1)

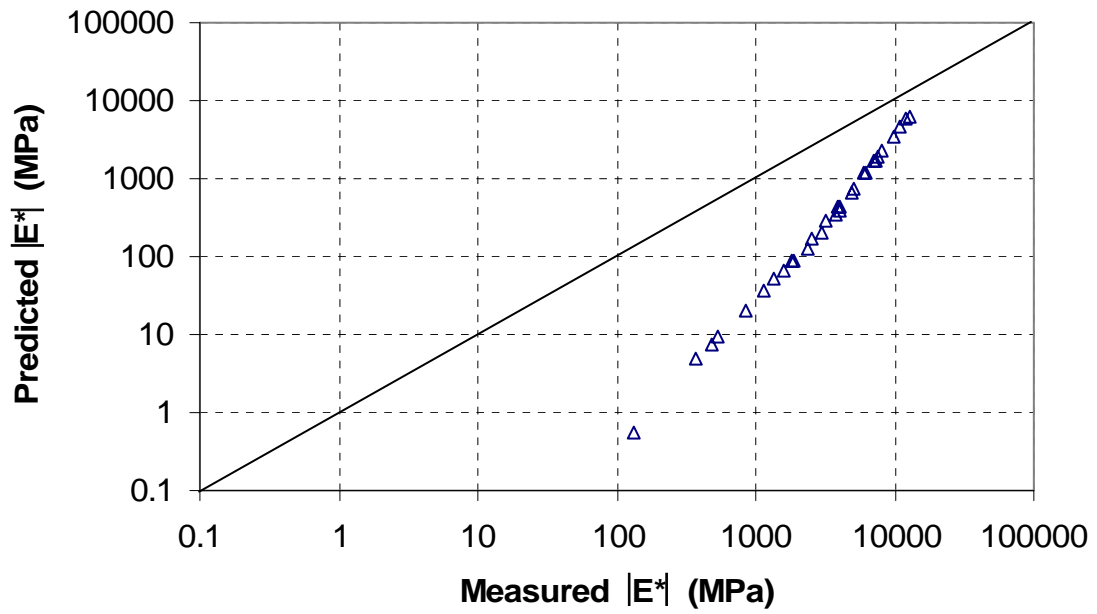


(a) Predicted vs. measured dynamic modulus

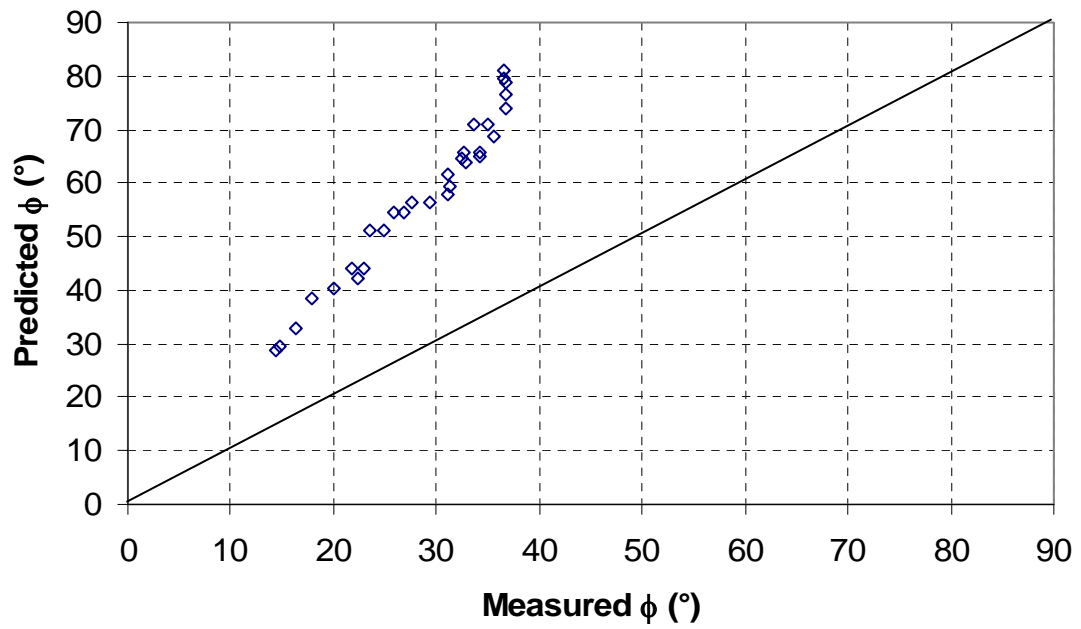


(b) Predicted vs. measured phase angle

Figure 7.8 Predicted vs. measured $|E^*|$ and ϕ of HMA mixture (Model 2-1)

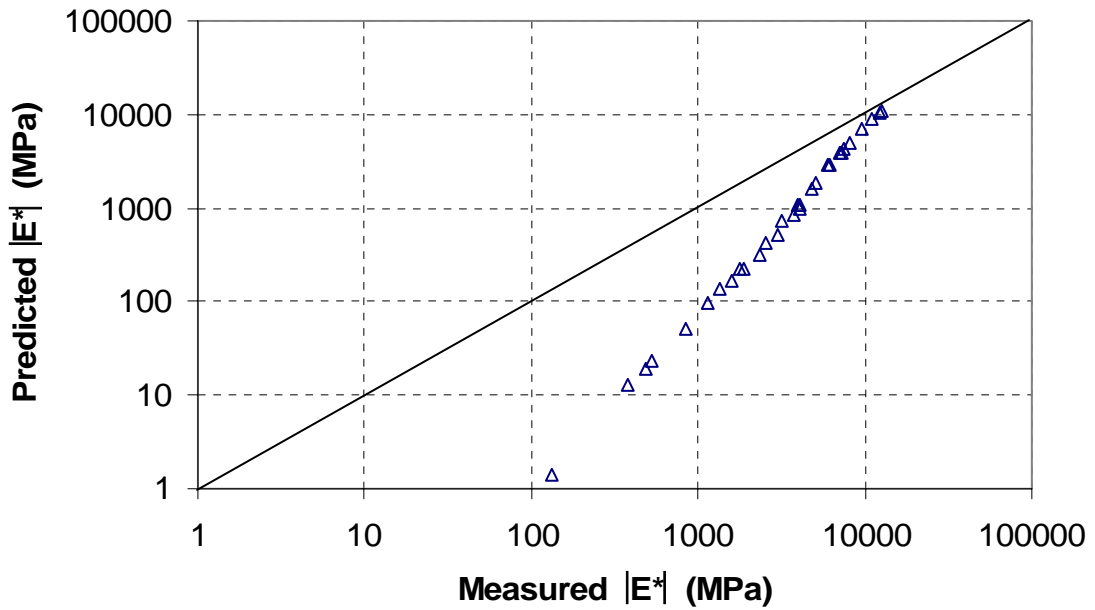


(a) Predicted vs. measured dynamic modulus

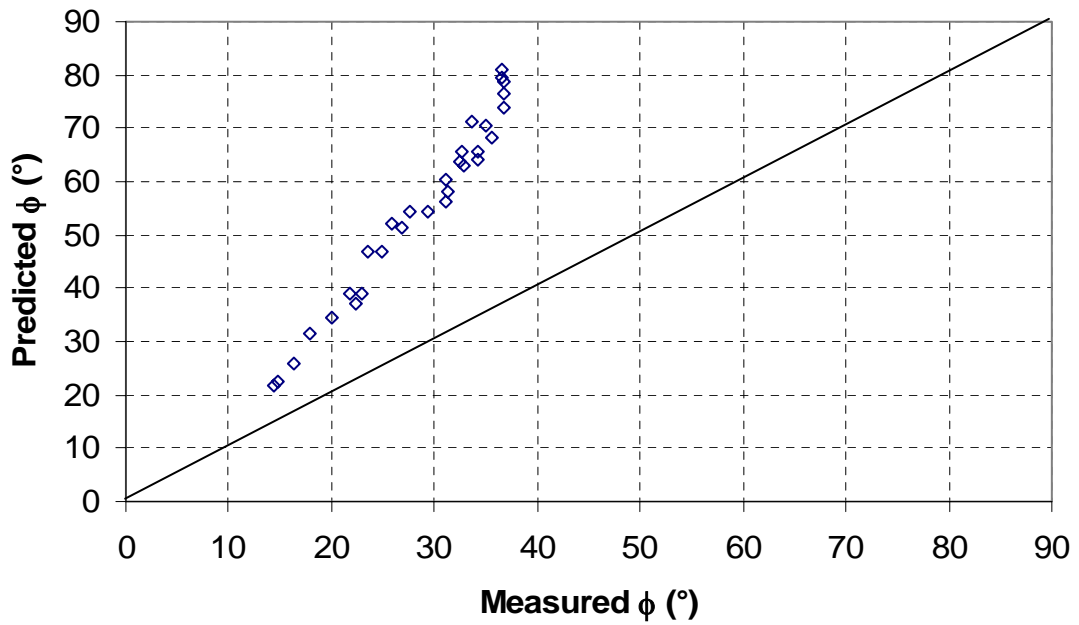


(b) Predicted vs. measured phase angle

Figure 7.9 Predicted vs. measured $|E^*|$ and ϕ of HMA mixture (Model 2-2)

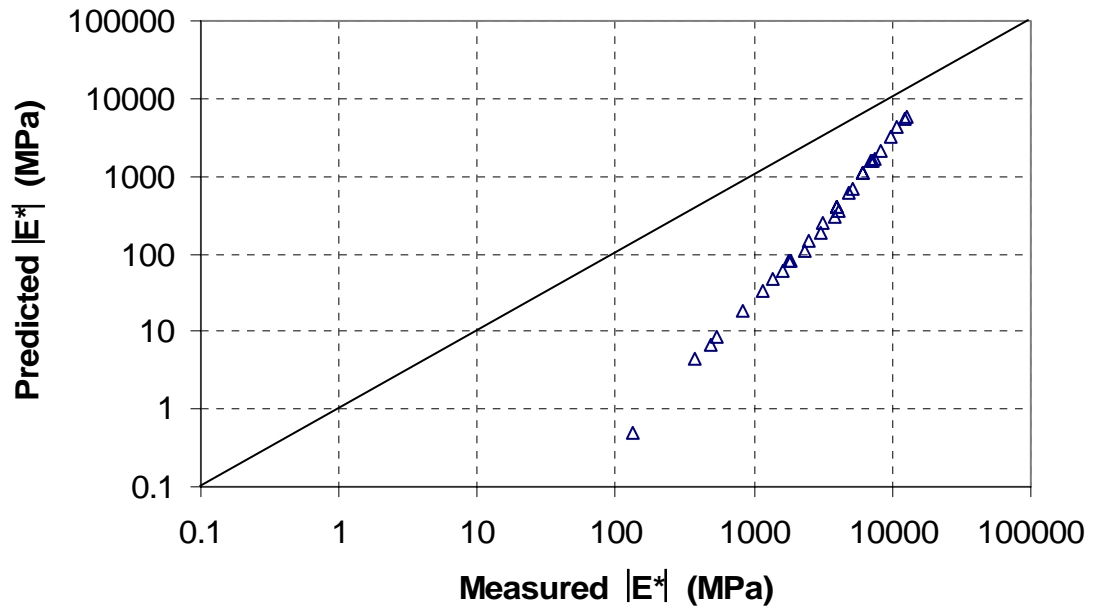


(a) Predicted vs. measured dynamic modulus

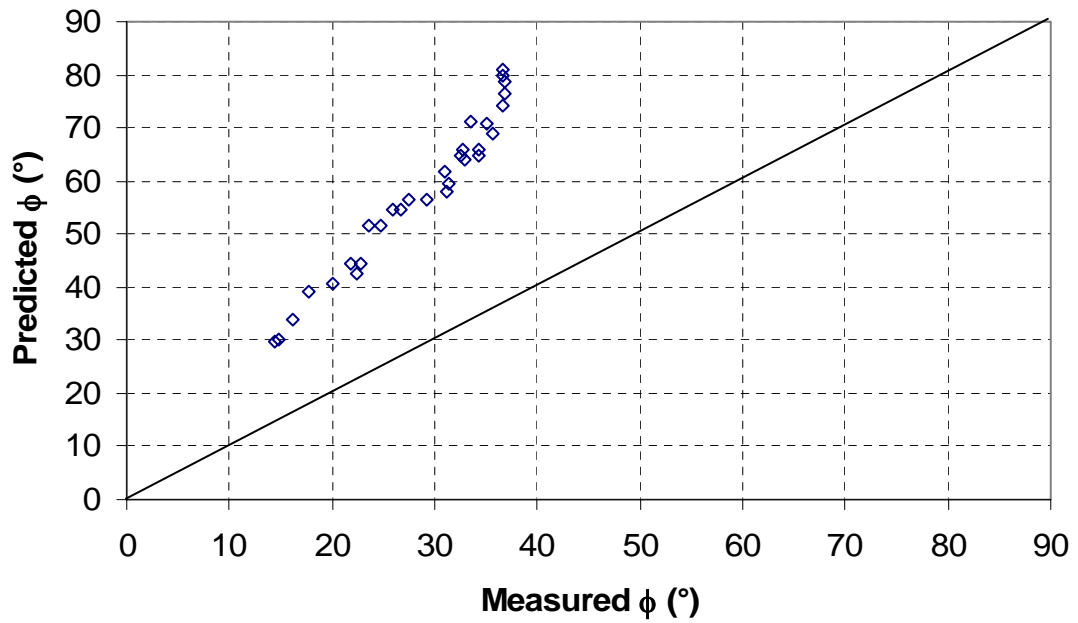


(b) Predicted vs. measured phase angle

Figure 7.10 Predicted vs. measured $|E^*|$ and ϕ of HMA mixture (Model 3-1)

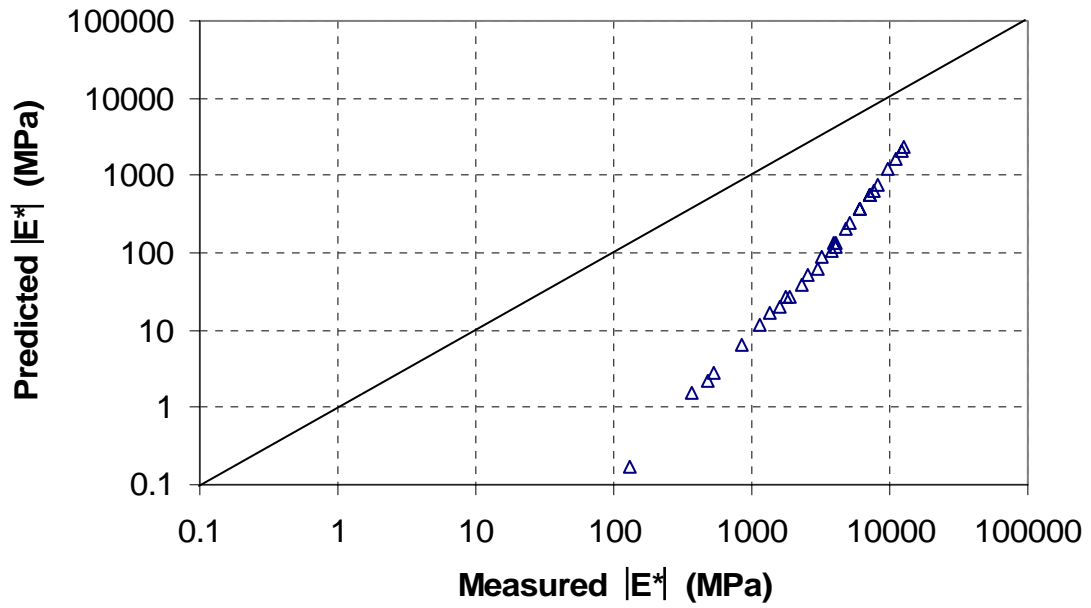


(a) Predicted vs. measured dynamic modulus

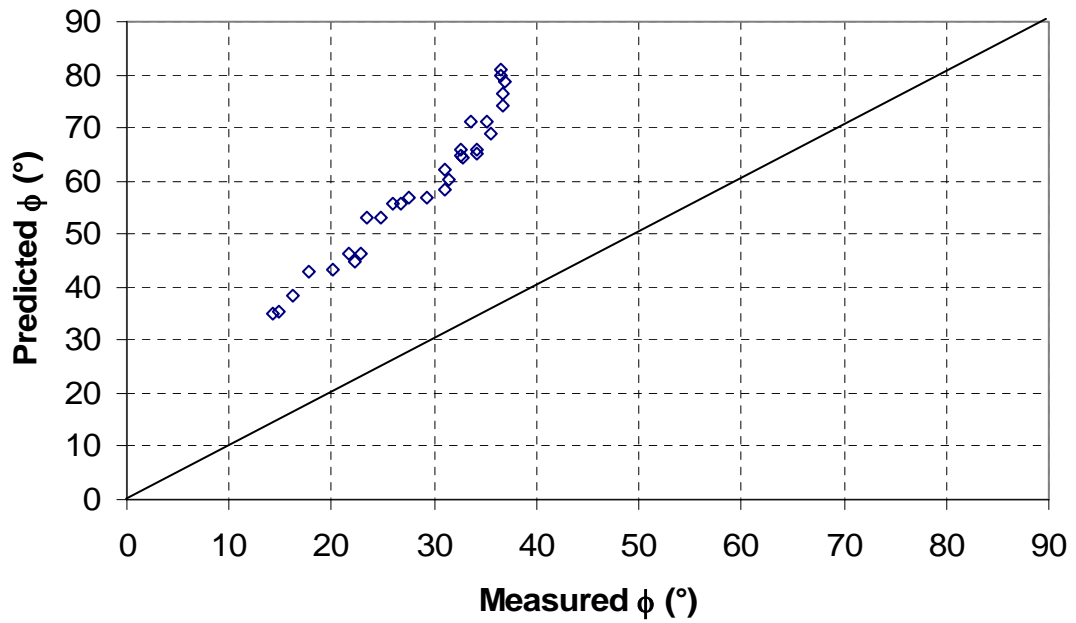


(b) Predicted vs. measured phase angle

Figure 7.11 Predicted vs. measured $|E^*|$ and ϕ of HMA mixture (Model 3-2)

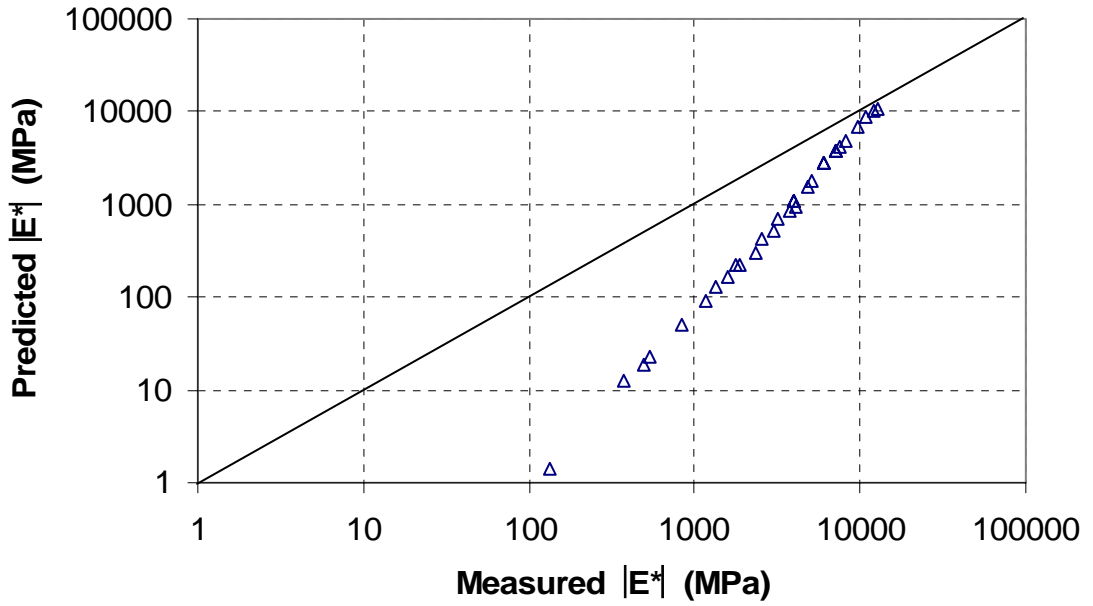


(a) Predicted vs. measured dynamic modulus

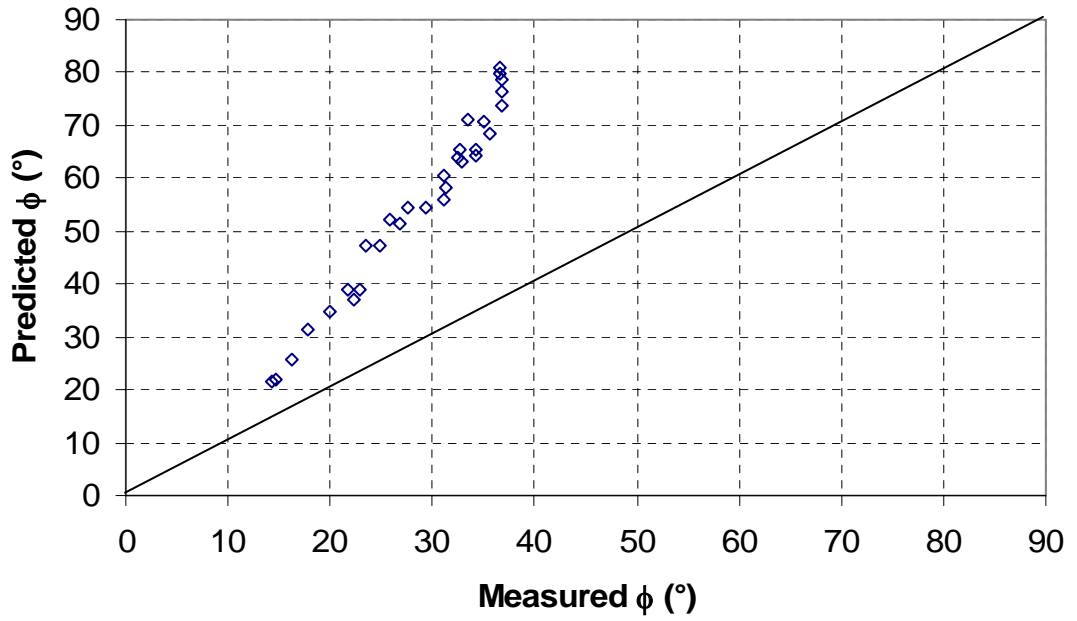


(b) Predicted vs. measured phase angle

Figure 7.12 Predicted vs. measured $|E^*|$ and ϕ of HMA mixture (Model 4-1)

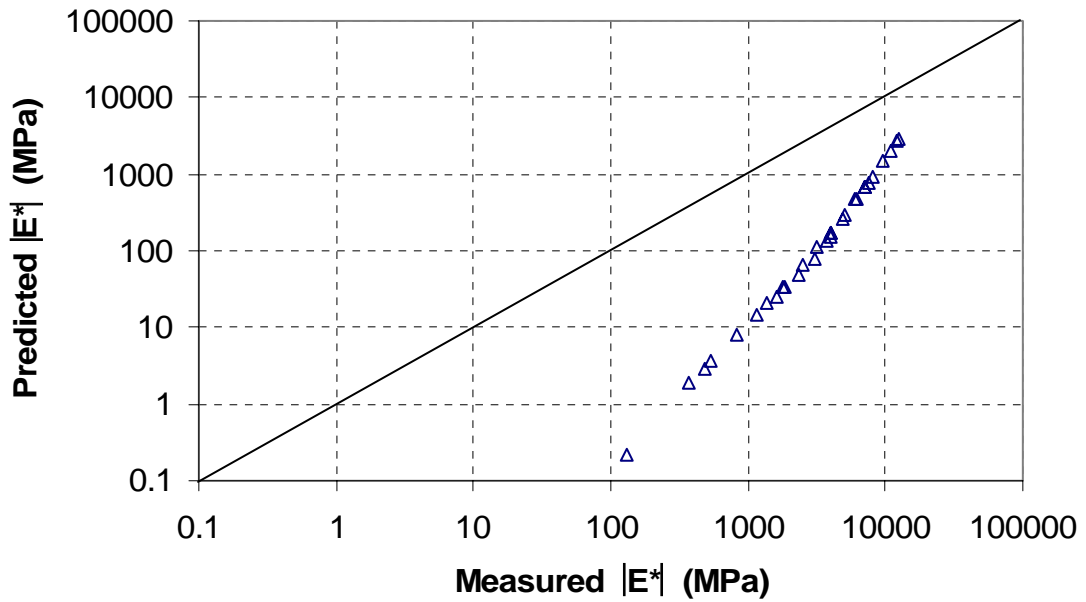


(a) Predicted vs. measured dynamic modulus

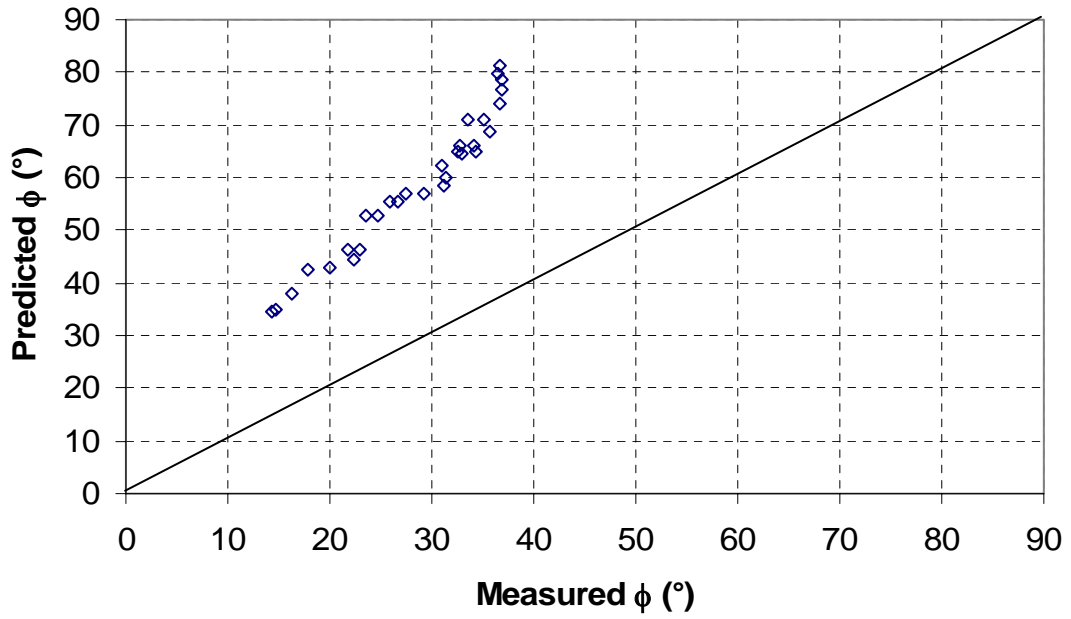


(b) Predicted vs. measured phase angle

Figure 7.13 Predicted vs. measured $|E^*|$ and ϕ of HMA mixture (Model 4-2)

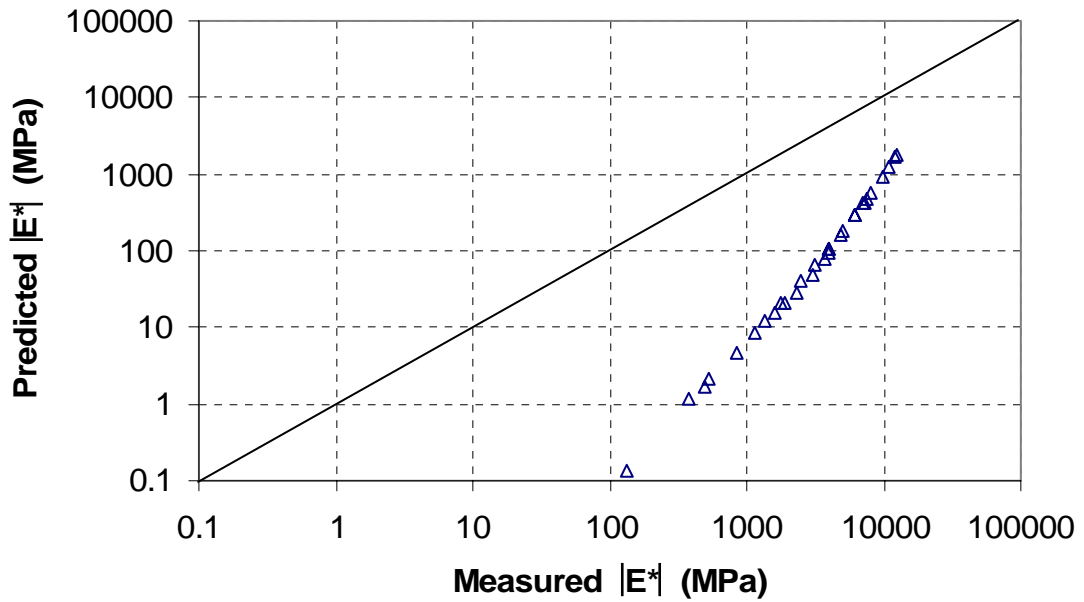


(a) Predicted vs. measured dynamic modulus

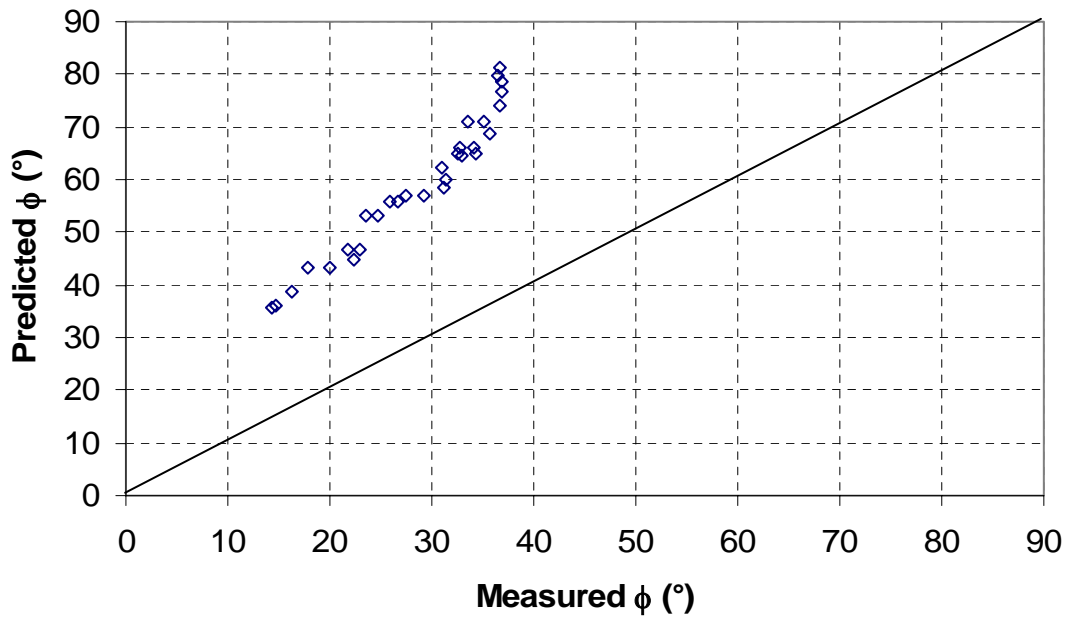


(b) Predicted vs. measured phase angle

Figure 7.14 Predicted vs. measured $|E^*|$ and ϕ of HMA mixture (Model 5)

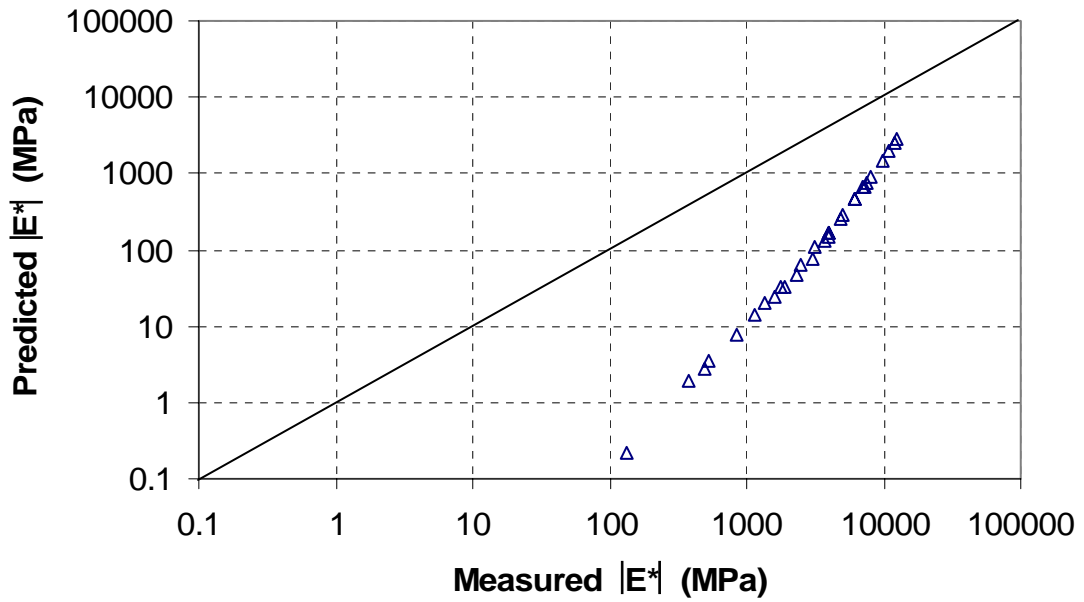


(a) Predicted vs. measured dynamic modulus

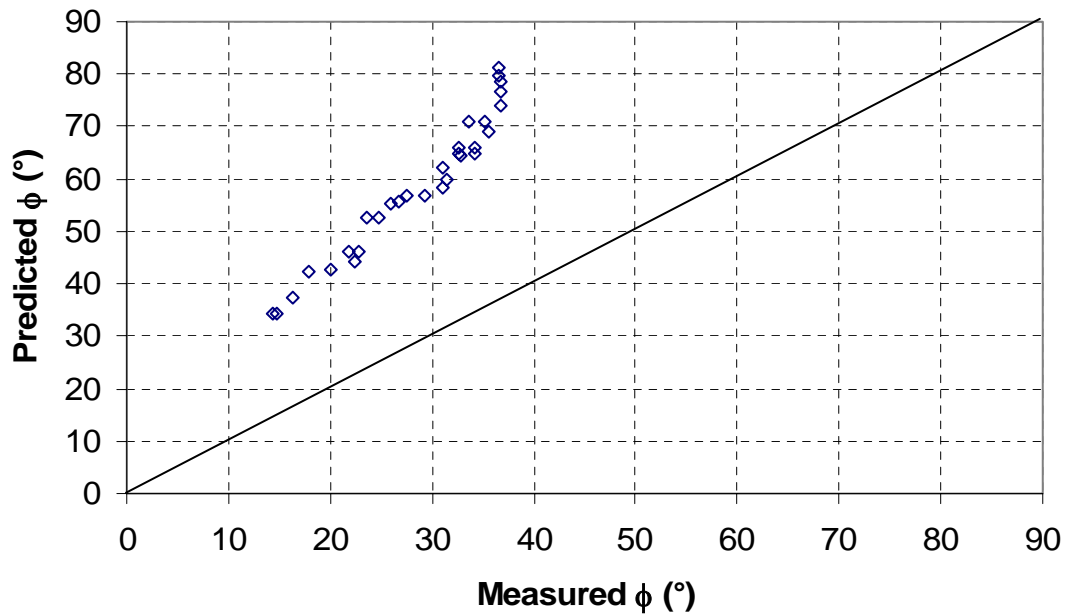


(b) Predicted vs. measured phase angle

Figure 7.15 Predicted vs. measured $|E^*|$ and ϕ of HMA mixture (Model 6)



(a) Predicted vs. measured dynamic modulus



(b) Predicted vs. measured phase angle

Figure 7.16 Predicted vs. measured $|E^*|$ and ϕ of HMA mixture (Model 7)

the loading frequency, dynamic modulus of asphalt binder increased and subsequently the difference in modulus between asphalt binder and aggregate decreased. The reduced mismatch in the properties of different constituents in a composite material helps the PFC models give better and closer predictions.

From Figures 7.6 through 7.16, it can be seen that the predicted phase angle values were lower than the measured data. The predicted phase angles were roughly half the predicted values, depending on predictive model and loading frequency.

When compared to the prediction results for asphalt mastic from these models, it can be seen that the prediction errors increased dramatically for HMA mixtures. This indicated that HMA mixtures are much more complicated than asphalt mastic due to the addition of aggregate particles of different sizes. More work need to be done to obtain better prediction results from PFC models for HMA mixtures.

Mastic-Aggregate System Prediction

Flow Chart

Since all the HMA mixtures use aggregates of different particle sizes to obtain the desirable aggregate gradation and stable aggregate structure under traffic loading, each portion of aggregate with specified size makes its own contribution to the dynamic modulus of HMA mixtures. It is very important to take into account the aggregate gradation used in HMA mixtures. The under-prediction of the binder-aggregate system method is due in part to its inability to incorporate the aggregate gradation of HMA mixtures in its predicting procedures.

In the mastic-aggregate system prediction, the aggregate particle size distribution was considered in the predictive procedures as described in Chapter 3. It should be pointed out that this method used to consider the aggregate gradation in HMA mixture was not limited to the three-dimensional two-layered HMA model developed in Chapter 3, the procedures for the incorporation of aggregate gradation and air voids can be employed in all the PFC models in this study. Figure 7.17 presents the flow chart for the prediction of dynamic modulus and phase angle of HMA mixtures using the mastic-aggregate system method. As shown in Figure 7.17, aggregate gradation was considered in the first prediction process. In the second prediction process, air voids content and its

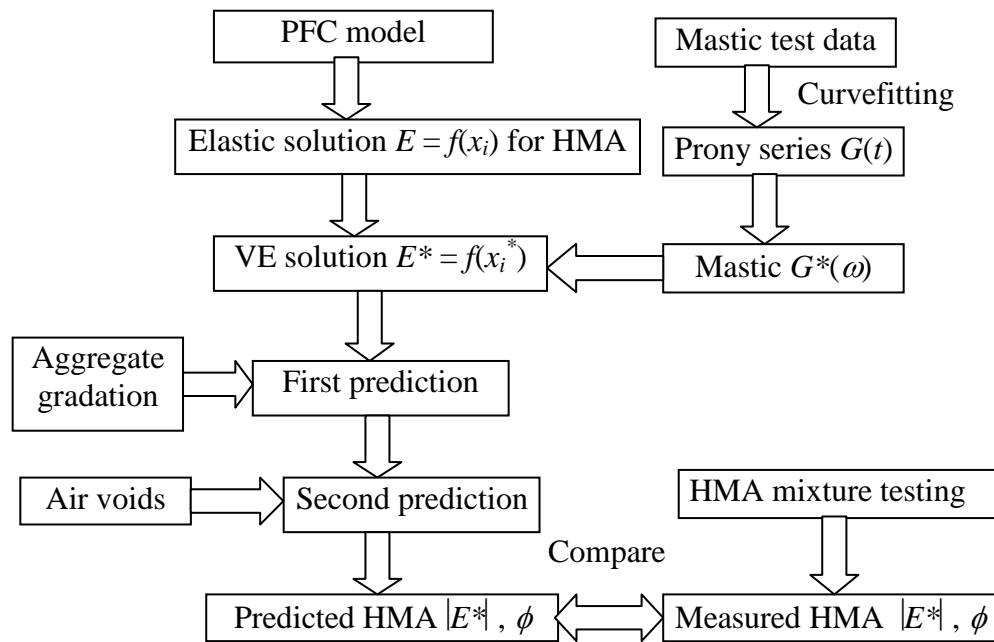


Figure 7.17 Flow Chart for Mastic-Aggregate System Prediction

size distribution were taken into account in the same manner as the one used for aggregate gradation. The detailed predicting procedures and the associated equations can be found in Chapter 3.

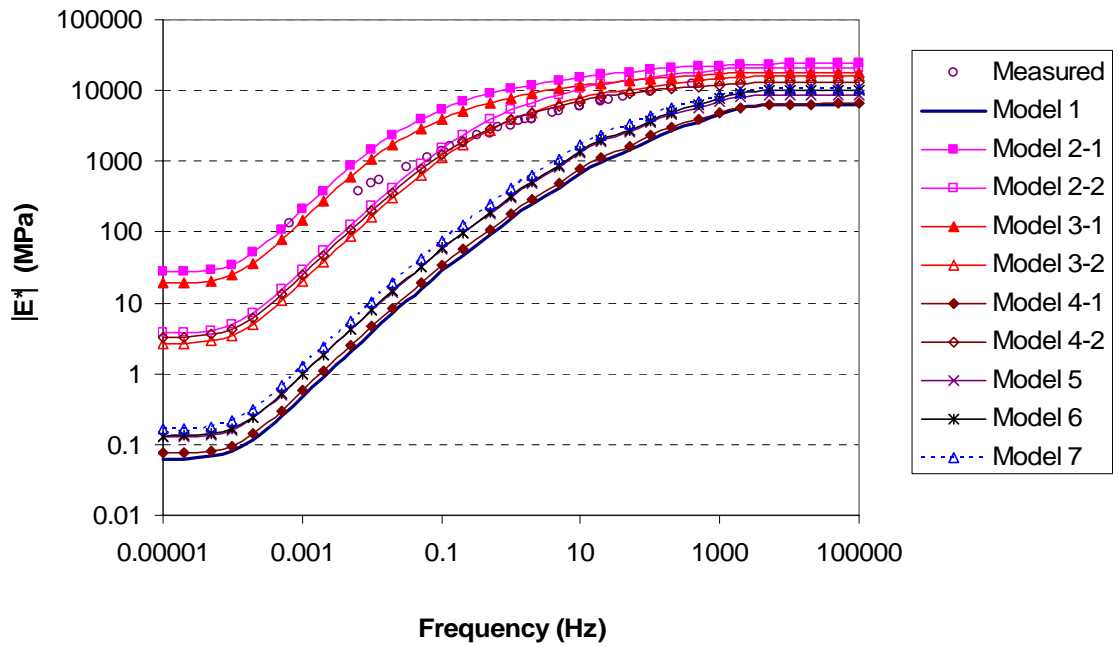
Prediction Results and Analyses

Figures 7.18 ~ 7.28 present the predicted dynamic modulus and phase angle values of HMA mixture using the mastic-aggregate system method along with the measured results.

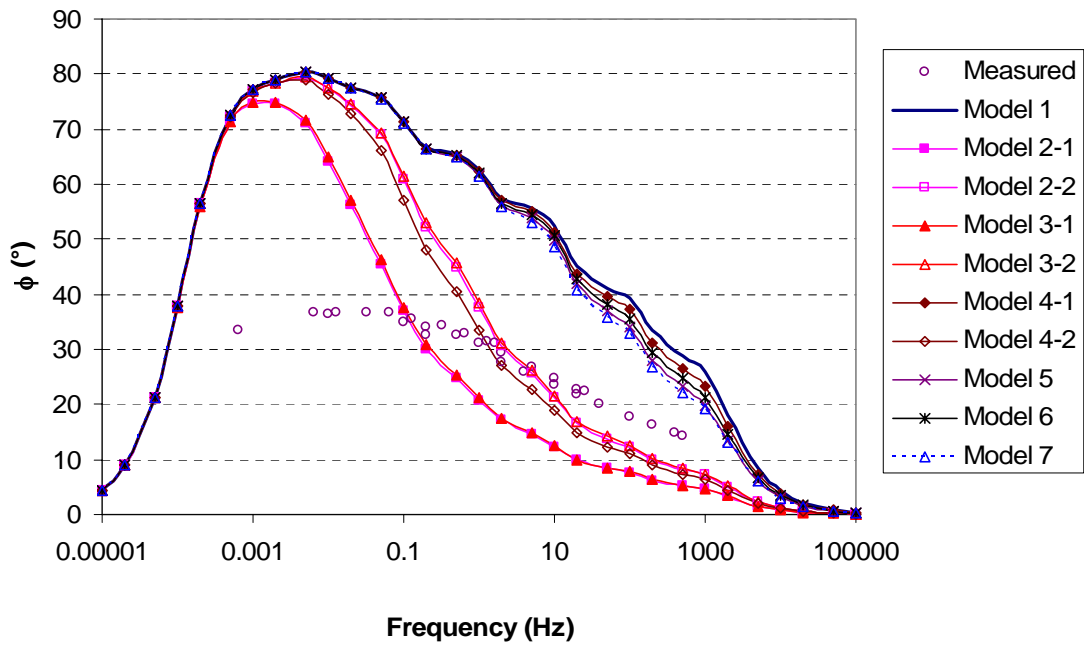
The prediction shown in Figures 7.18 through 7.28 suggests that the mastic-aggregate system produces better results for dynamic modulus and phase angle values than the binder-aggregate system method (Figures 6 to 16). The mastic-aggregate system method obviously improved the predicted results for all the PFC models due to the consideration of aggregate gradation in the predicting procedures, although the plot of dynamic modulus vs. frequency followed the similar sigmoidal shape.

Among all the models, Model 2-1 gave the highest predicted dynamic moduli as in the binder-aggregate system prediction. However, Model 2-1 slightly over-predicted the dynamic modulus in the mastic-aggregate system method, compared to the under-prediction in the binder-aggregate system prediction. The three-dimensional two-layered model (Model 1 developed in Chapter 3) gave the lowest of the predicted dynamic modulus values from all the models, deviating farthest from the measured data.

Among the models used in this study, three models, Models 2-2, 3-2, and 4-2, gave the best prediction results of dynamic modulus, especially at higher frequencies. Figure 7.29 presents the prediction errors for these three models in the mastic-aggregate

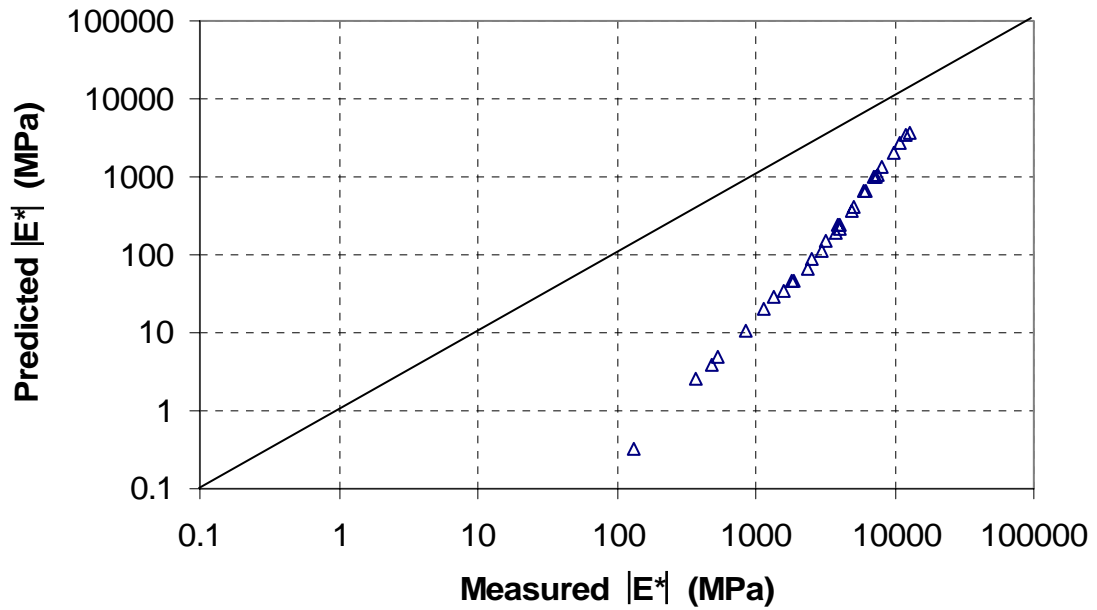


(a) Dynamic modulus $|E^*|$

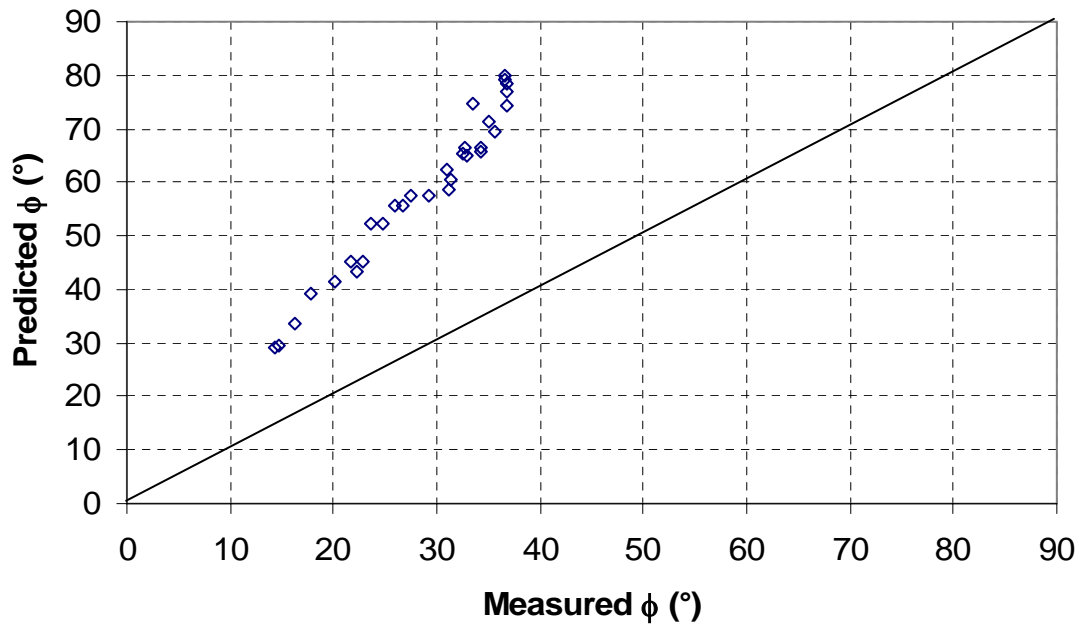


(b) Phase angle ϕ

Figure 7.18 Predicted vs. Measured $|E^*|$ and ϕ of HMA Mixture

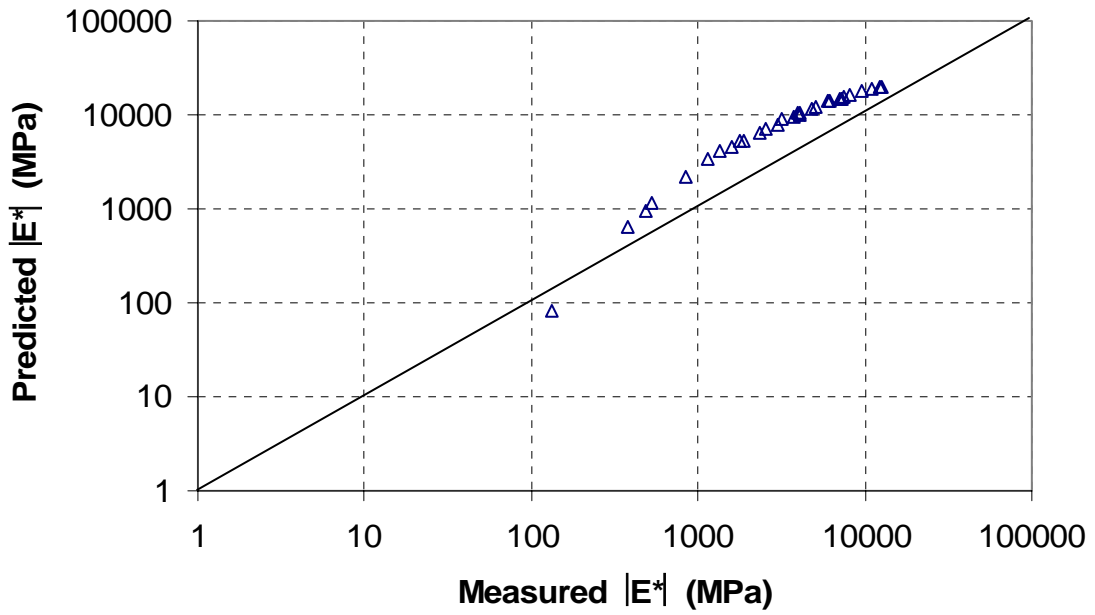


(a) Predicted vs. measured dynamic modulus

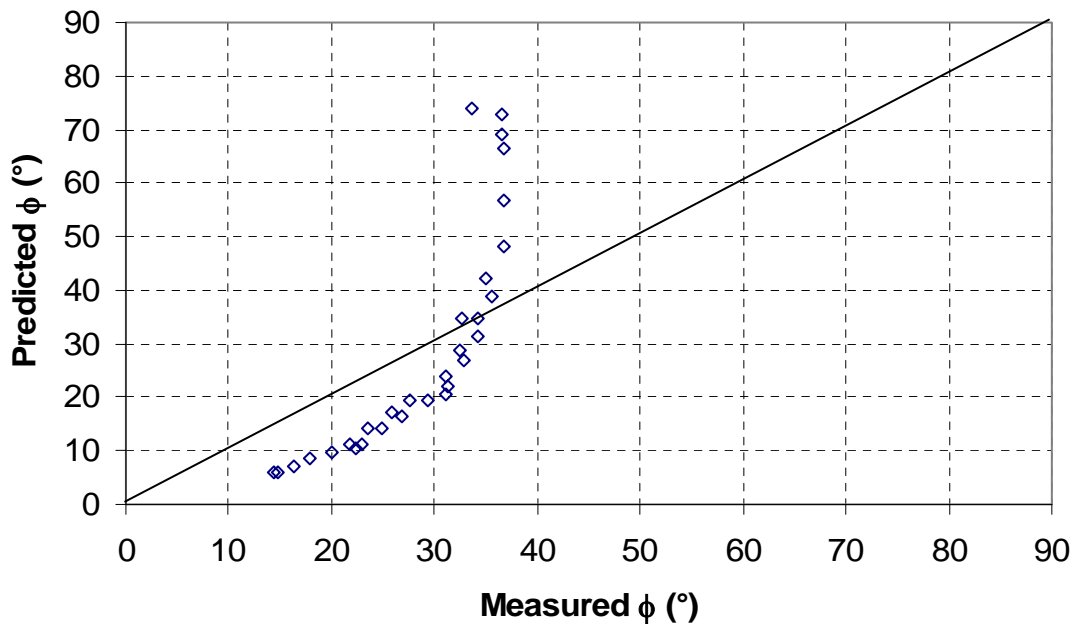


(b) Predicted vs. measured phase angle

Figure 7.19 Predicted vs. Measured $|E^*|$ and ϕ of HMA Mixture (Model 1)

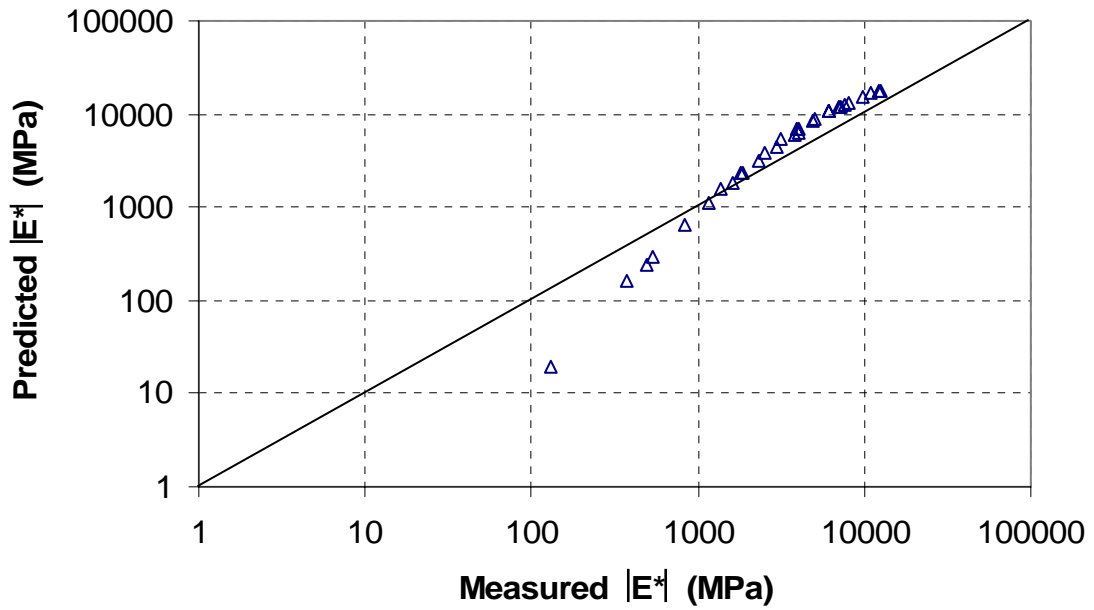


(a) Predicted vs. measured dynamic modulus

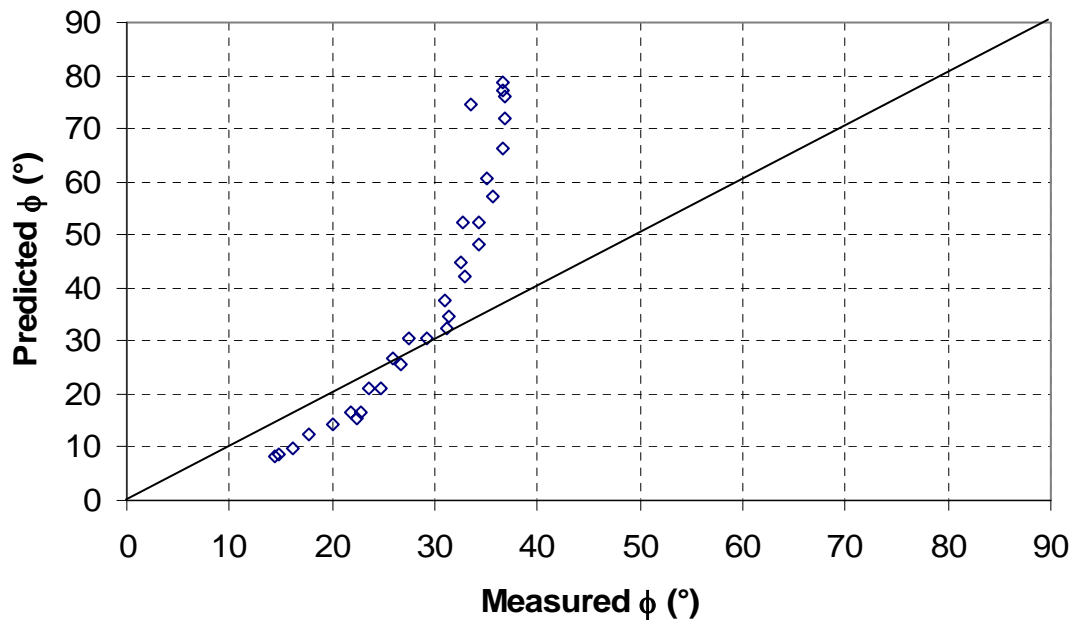


(b) Predicted vs. measured phase angle

Figure 7.20 Predicted vs. Measured $|E^*|$ and ϕ of HMA Mixture (Model 2-1)

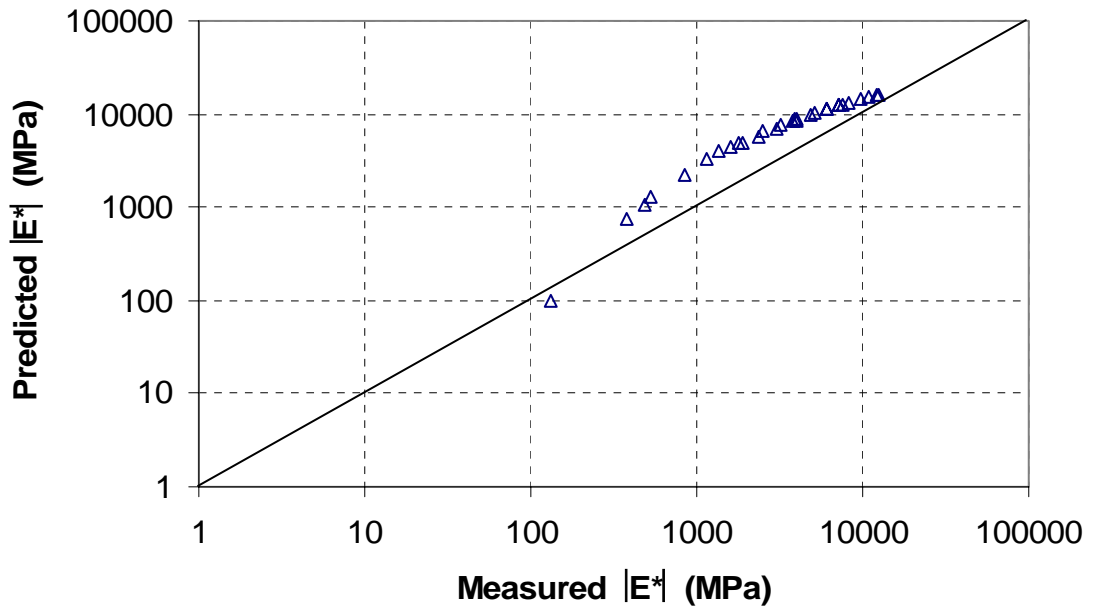


(a) Predicted vs. measured dynamic modulus

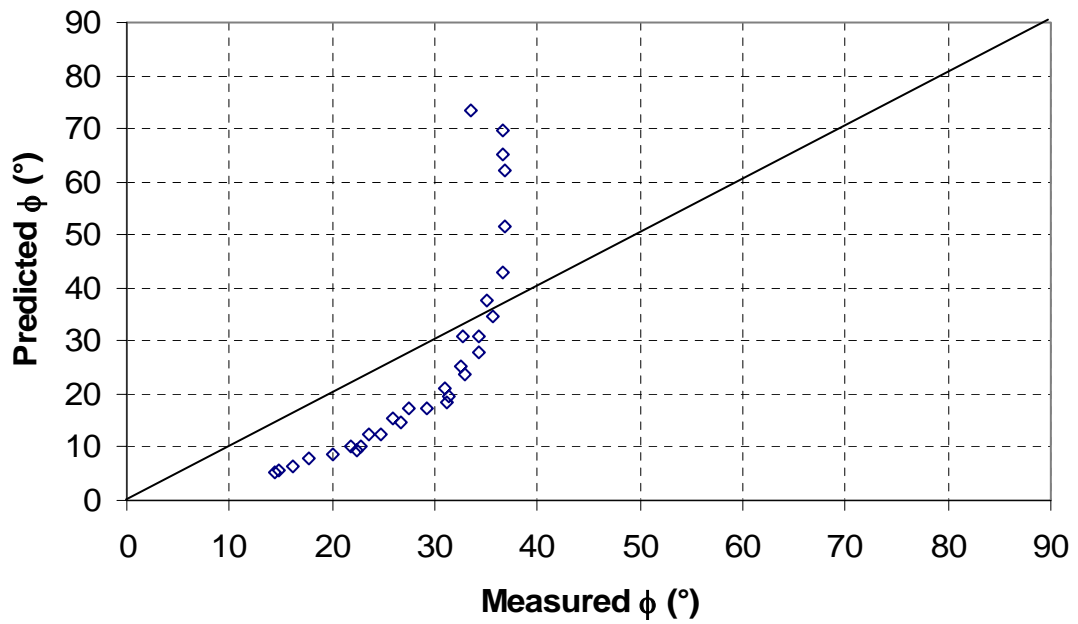


(b) Predicted vs. measured phase angle

Figure 7.21 Predicted vs. Measured $|E^*|$ and ϕ of HMA Mixture (Model 2-2)

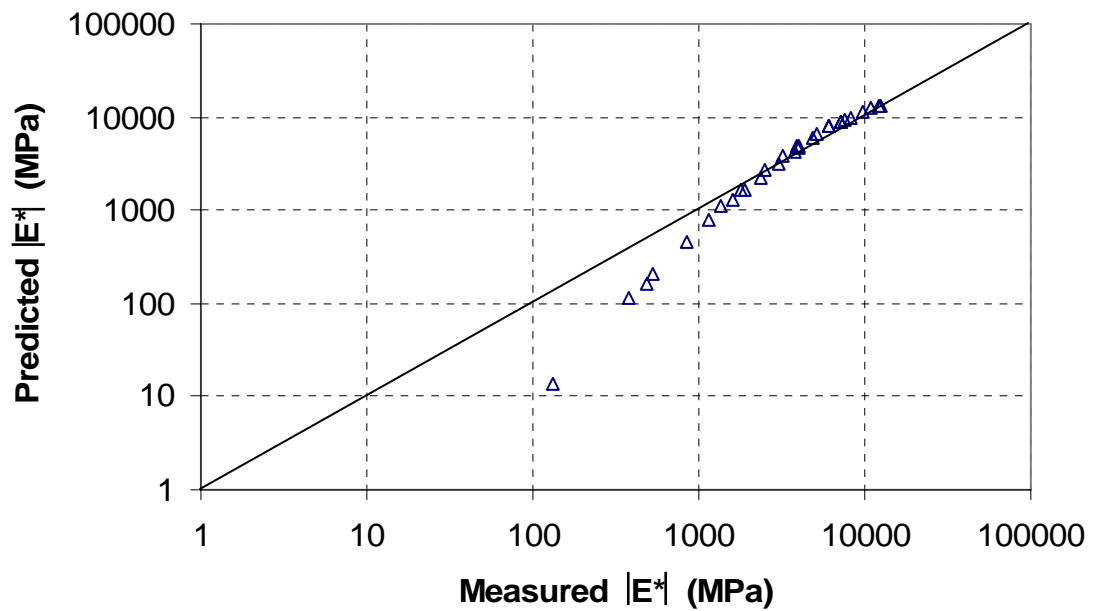


(a) Predicted vs. measured dynamic modulus

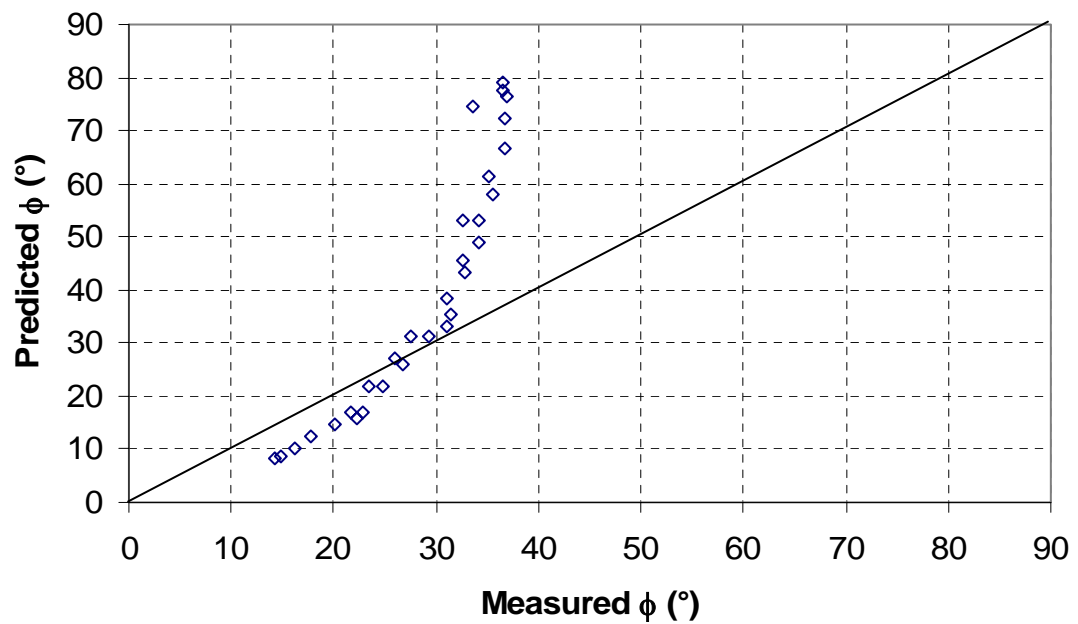


(b) Predicted vs. measured phase angle

Figure 7.22 Predicted vs. Measured $|E^*|$ and ϕ of HMA Mixture (Model 3-1)

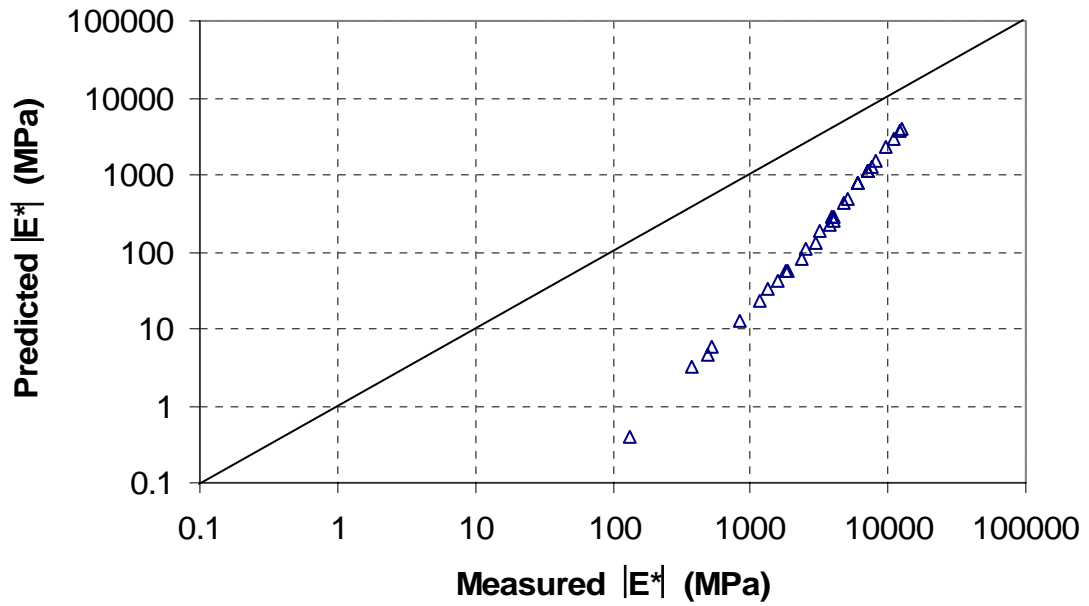


(a) Predicted vs. measured dynamic modulus

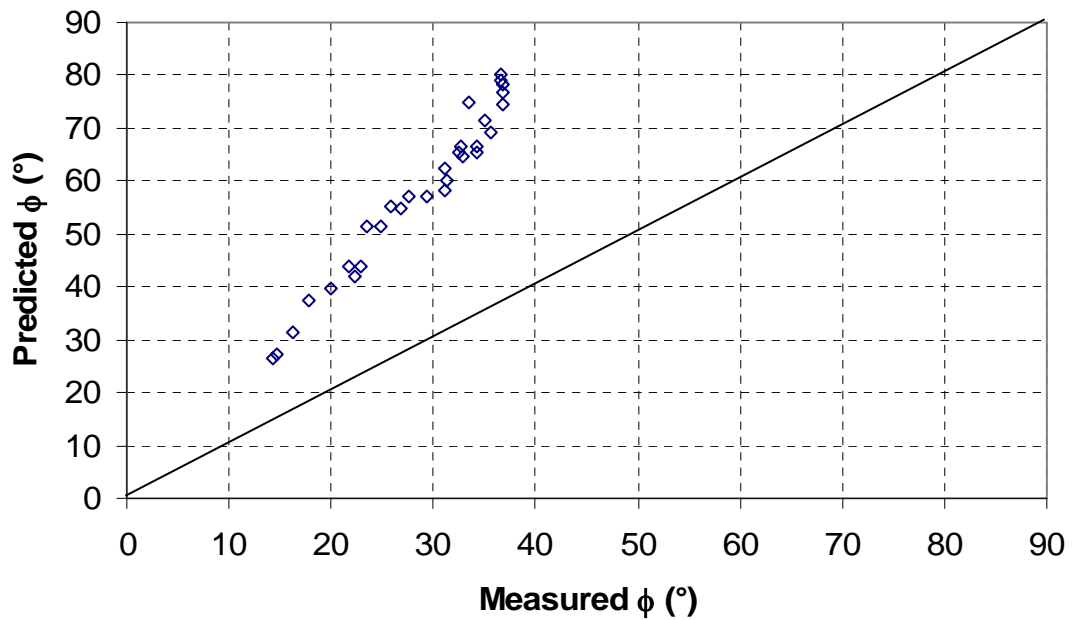


(b) Predicted vs. measured phase angle

Figure 7.23 Predicted vs. Measured $|E^*|$ and ϕ of HMA Mixture (Model 3-2)

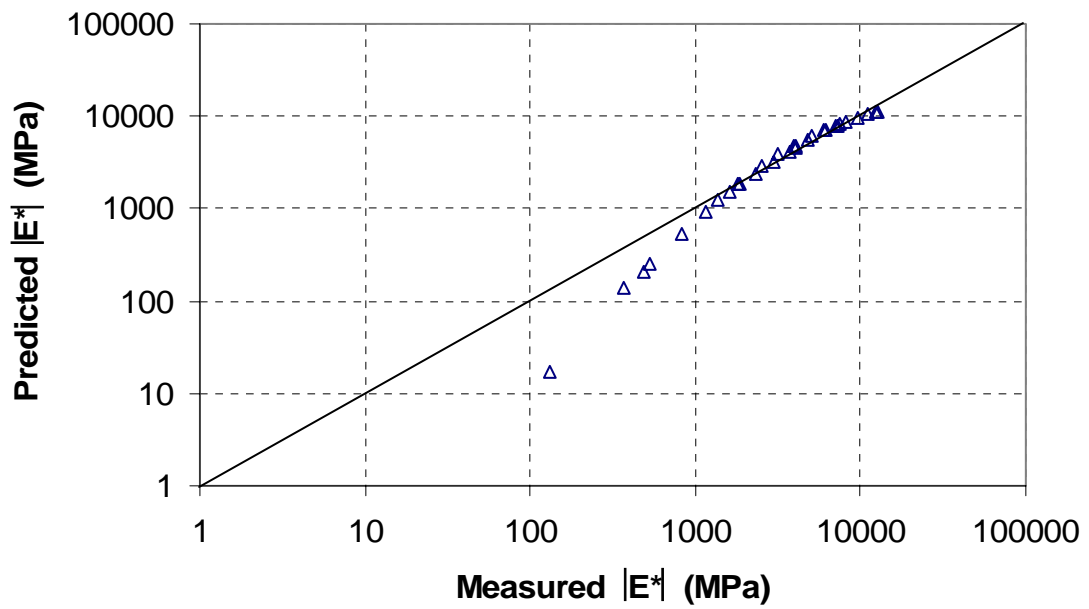


(a) Predicted vs. measured dynamic modulus

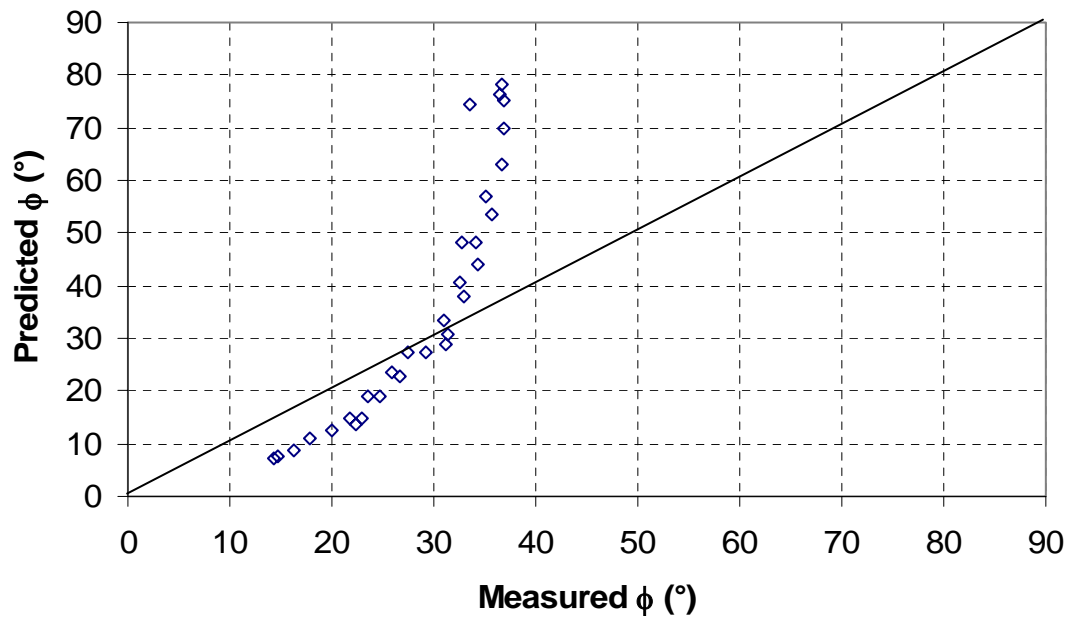


(b) Predicted vs. measured phase angle

Figure 7.24 Predicted vs. Measured $|E^*|$ and ϕ of HMA Mixture (Model 4-1)

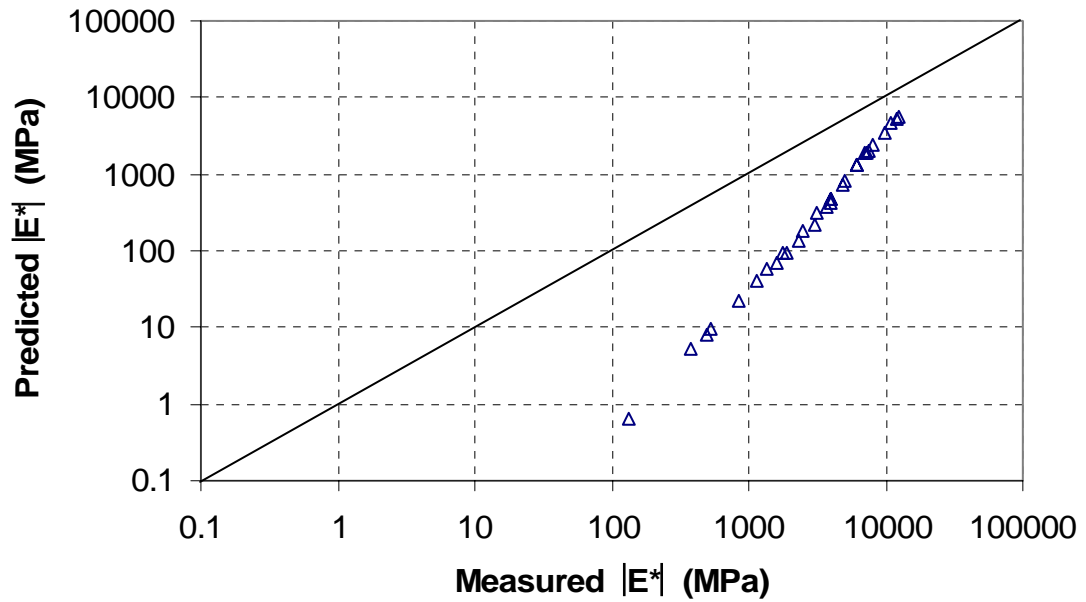


(a) Predicted vs. measured dynamic modulus

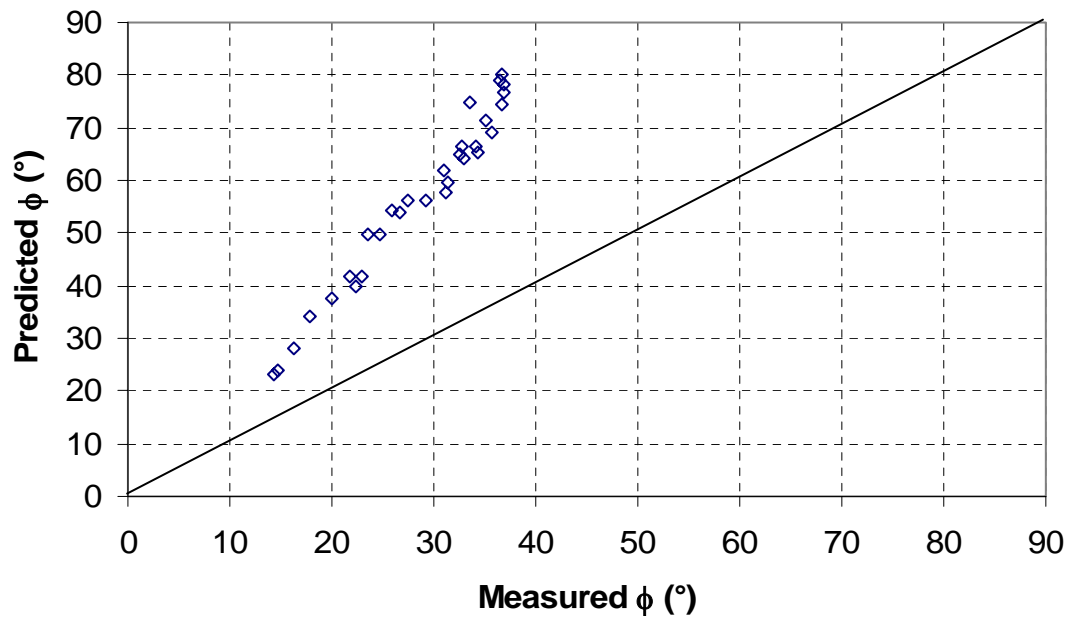


(b) Predicted vs. measured phase angle

Figure 7.25 Predicted vs. Measured $|E^*|$ and ϕ of HMA Mixture (Model 4-2)

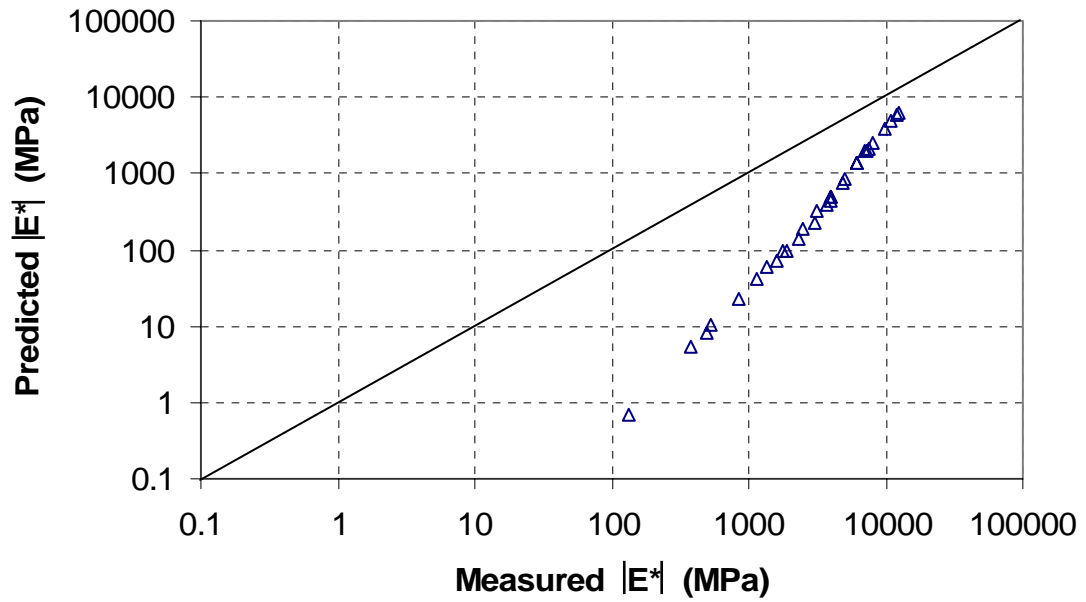


(a) Predicted vs. measured dynamic modulus

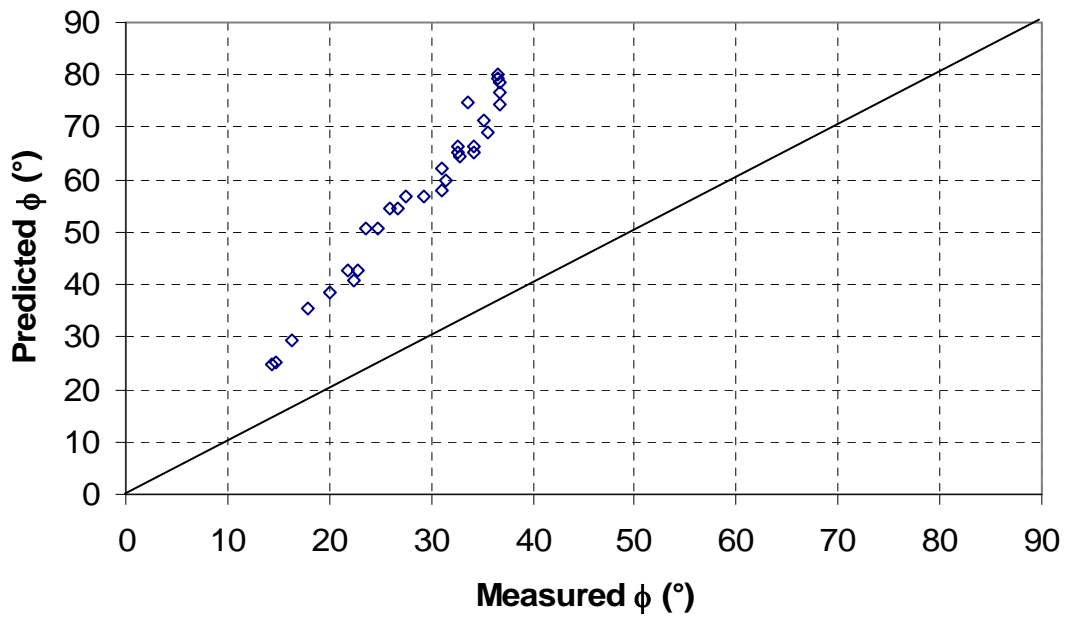


(b) Predicted vs. measured phase angle

Figure 7.26 Predicted vs. Measured $|E^*|$ and ϕ of HMA Mixture (Model 5)

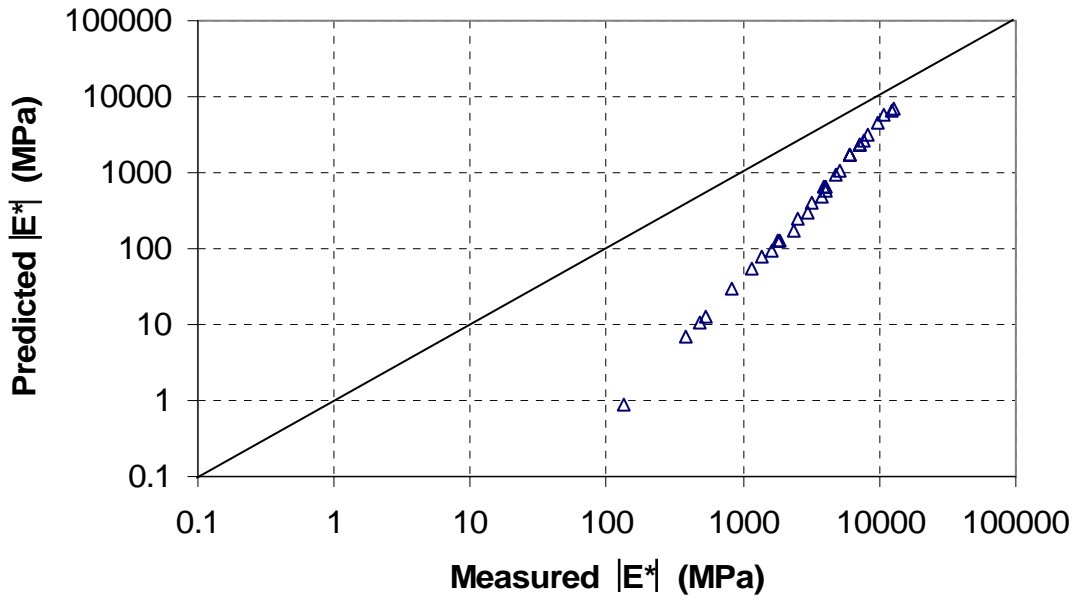


(a) Predicted vs. measured dynamic modulus

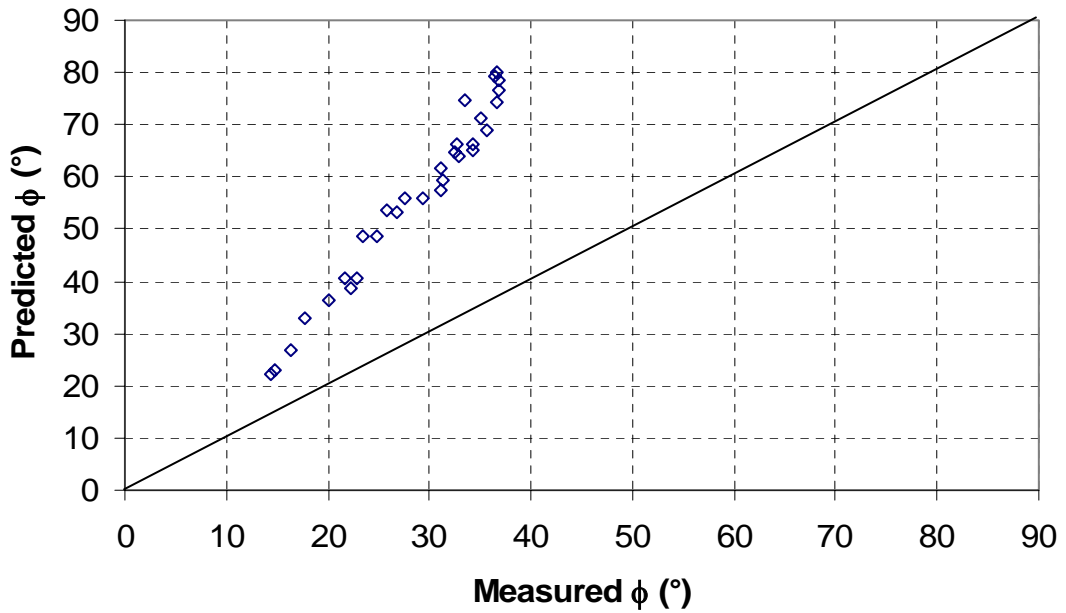


(b) Predicted vs. measured phase angle

Figure 7.27 Predicted vs. Measured $|E^*|$ and ϕ of HMA Mixture (Model 6)



(a) Predicted vs. measured dynamic modulus



(b) Predicted vs. measured phase angle

Figure 7.28 Predicted vs. Measured $|E^*|$ and ϕ of HMA Mixture (Model 7)

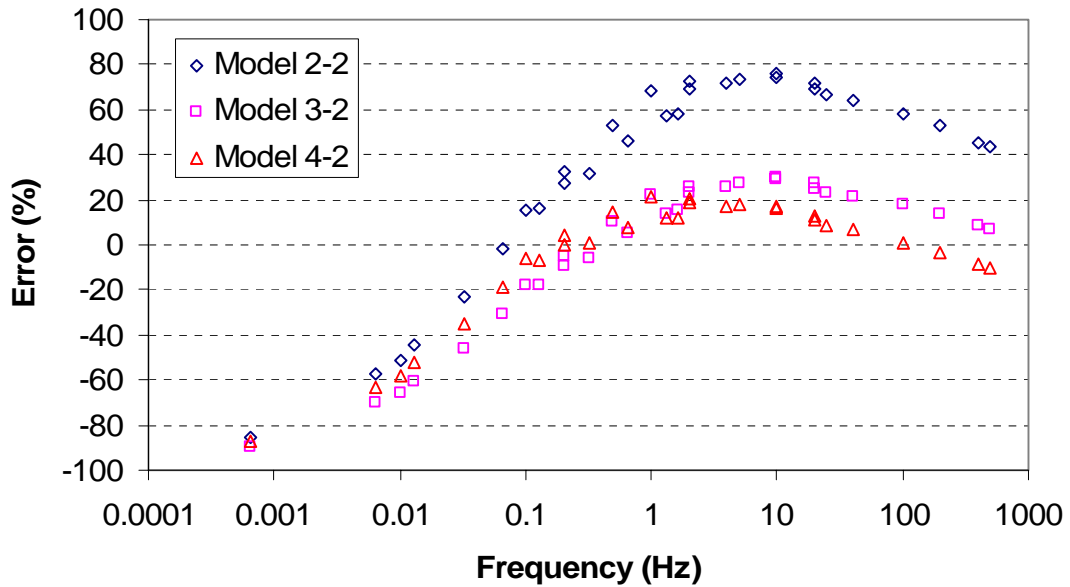


Figure 7.29 Prediction Errors in Mastic-Aggregate System Prediction

system prediction. It can be seen that most of the prediction errors lied within the range between -80% and $+80\%$, while Model 4-2 could give prediction with errors within the range between -20% and $+20\%$ over the frequency range from 0.1 Hz to 1000 Hz.

The predicted phase angle values from the mastic-aggregate system method also showed difference from those obtained from the binder-aggregate system method. It was observed that Models 2-1, 2-2, 3-1, 3-2 and 4-2 predicted phase angle values lower than measured results at low frequencies, but higher than measured ones at higher frequencies. The remaining other models still over-predicted the phase angle values over the whole frequency range, as in the prediction of binder-aggregate system.

Analysis on Possible Reasons for Under-prediction of Dynamic Modulus

In general, most of the PFC models used in this study under-predicted the dynamic modulus of HMA mixtures, whether using the binder-aggregate system method or the mastic-aggregate system method. The reasons for under-prediction could be attributed to the discrepancy between these PFC models and real HMA mixtures. First of all, the real aggregates are composed of particles with various shapes rather than the spherical shape used for all the PFC models in this study. The assumption of spherical particles lowered the total surface area of aggregate and subsequently increased the calculated film thickness of asphalt mastic around aggregate particles. This eventually resulted in the lower predicted dynamic modulus of HMA mixtures. Another issue associated with aggregate shape is the interlocking between coarse aggregate particles. Aggregate interlocking plays an important role in the reinforcement mechanisms of HMA mixtures. It is critical for aggregates to develop and sustain a stable structure and withstand traffic loading. However, spherical shape does not provide any interlocking at all. Aggregate particles with spherical shape are liable to the shear deformation under traffic loading. The lack of consideration of interlocking between large aggregate particles could further lower the value of dynamic modulus of HMA mixtures, as suggested by some researchers (such as Buttlar and Roque 1996). However, it has been shown that there is literally no direct contact between large aggregates in a typical dense-graded HMA mixture (Roberts et al. 1996). Li and Metcalf (2005) argued that large aggregates mainly float in and interact with the surrounding mastic, and the direct aggregate interaction or interlocking effect does not exist in dense-graded HMA mixtures.

From Figures 7.6(a) and 7.18(a), it was observed that the under-predictive models gave closer prediction results at high frequencies than at low frequencies, which meant frequency (namely the loading rate) had different effect on the measured dynamic modulus than on the predicted dynamic modulus. This indicated that the viscoelastic properties of asphalt mastic in HMA mixtures were somewhat changed when coarse aggregates were introduced into the asphalt mastic matrix. This property change of asphalt mastic should be attributed to the physico-chemical effect between asphalt mastic matrix and coarse aggregate inclusion (Buttlar et al. 1999). The physico-chemical effect could stiffen the composite system by interfacial effects between mastic matrix and coarse aggregate particles, including absorption, adsorption, and selective sorption, and thus lower the frequency dependency of HMA mixtures.

Sensitivity Analysis

To gain better understanding of the effects of different factors on the dynamic modulus of HMA mixtures, the following sensitivity analysis was performed by changing one of the parameters and keeping others constant.

In order to investigate the effect of aggregate gradation on dynamic modulus of HMA mixtures, three more aggregate gradations were employed in the sensitivity analysis in addition to the aggregate gradation used in HMA mixture for the laboratory testing. These three aggregate gradations can be represented by Eq.(3.29) and maximum aggregate sizes of $2a_{\max} = 19, 9.5, \text{ and } 4.75 \text{ mm}$ (namely $a_{\max} = 9.5, 4.75, \text{ and } 2.38 \text{ mm}$) were used in Eq.(3.29) to examine the effect of aggregate gradation. The aggregate

gradations are shown in Figure 7.30 along with the aggregate gradation used in the laboratory testing.

Two air voids distributions were used to analyze the effect of air voids on dynamic modulus of HMA mixtures (Figure 7.31). Distribution 1 was calculated from Castelblanco et al. (2005) and represents the general air voids size distribution in conventional dense-graded HMA mixtures. Distribution 2 is an arbitrary coarse air voids size distribution and was used in this study to investigate the effect of coarse distribution on the dynamic modulus.

The input parameters evaluated and their values used in the sensitivity analysis are summarized in Table 7.2. In Table 7.2, the entry “varying range” means the range in which the input parameter varies in order to evaluate its effect and “fixed value” means to keep the value fixed during the evaluation of other input parameters.

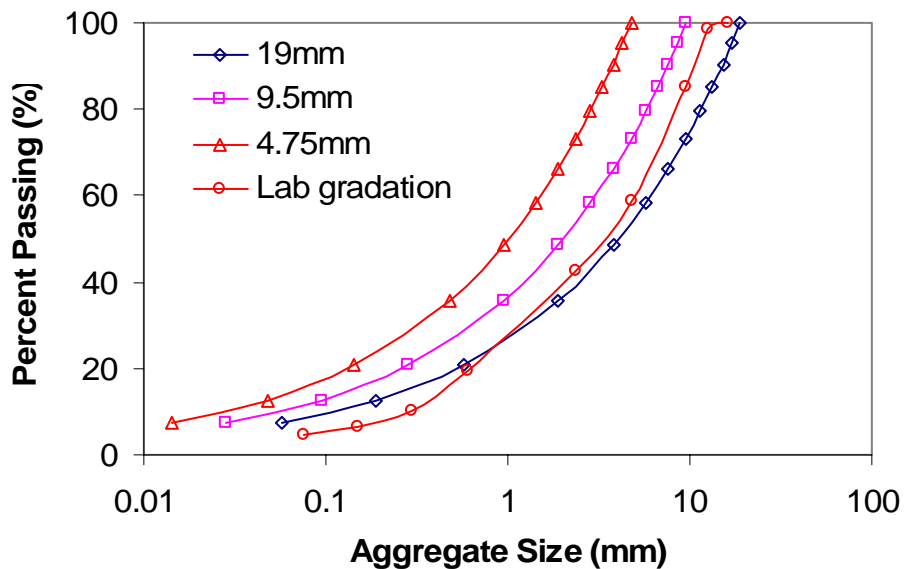


Figure 7.30 Aggregate Gradations

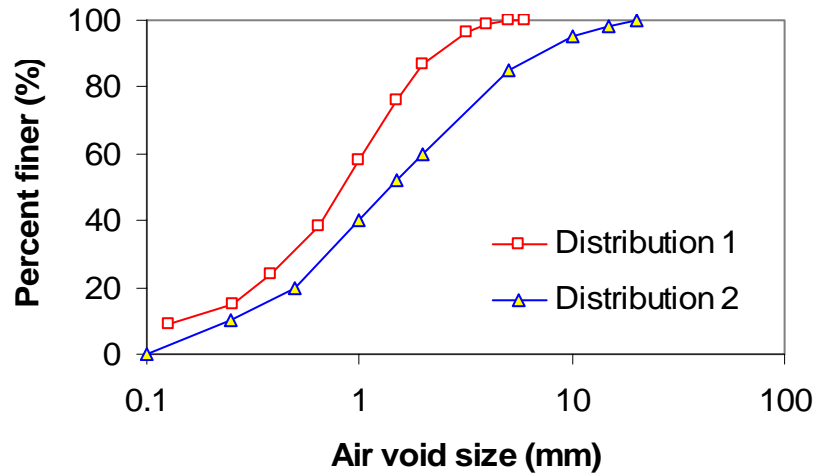


Figure 7.31 Air Voids Size Distribution for Sensitivity Analysis

Table 7.2 Input Parameters and Their Values for Sensitivity Analysis

Parameter	Unit	Varying Range	Fixed Value
Aggregate gradation	N/A	$P(a) = \left(\frac{a}{a_{\max}} \right)^{0.45}$ $(a_{\max} = 9.5, 4.75, \text{ and } 2.36 \text{ mm})$ and laboratory gradation	laboratory gradation
Air voids distribution	N/A	Distributions 1 and 2	Distribution 1
Aggregate modulus	MPa	10 ~ 1000000	50000
Asphalt content	wt. %	2 ~ 10	5
Air voids content	v. %	0 ~ 20	4

Since Model 4-2 was one of the best models that can accurately predict the dynamic modulus of HMA mixtures, it was chosen for the sensitivity analysis.

Effect of Aggregate Gradation

Figure 7.32 presents the effect of aggregate gradation on the dynamic modulus of HMA mixtures. It was observed that the aggregate gradation with maximum particle size 19 mm exhibited the highest dynamic modulus, while the aggregate gradation with maximum particle size 4.75 mm gave the lowest value of dynamic modulus at the given frequency. This indicated that use of coarse aggregate gradation would increase the dynamic modulus of dense-graded HMA mixture. To produce high modulus asphalt mixture, one of the feasible options was to select coarse aggregate gradation.

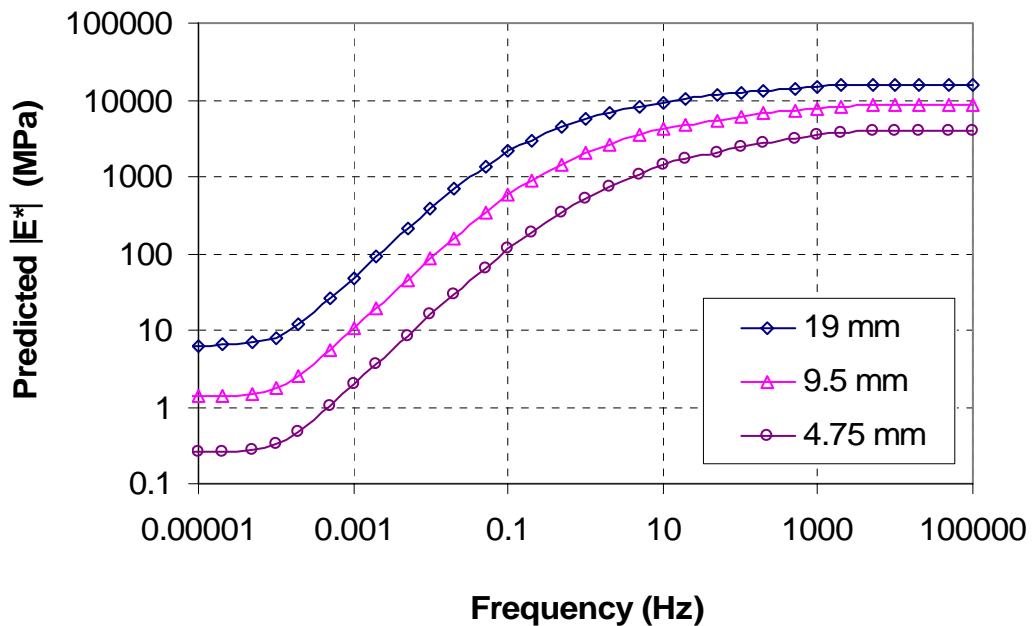


Figure 7.32 Effect of Aggregate Gradation

Effect of Aggregate Modulus

The influence of aggregate modulus on the dynamic modulus value of HMA mixtures is shown in Figure 7.33. In Figure 7.33 the dynamic modulus of HMA mixtures increased with the increase in aggregate modulus. However, at low frequency (such as 0.1 Hz) the magnitude of the increase in dynamic modulus was comparably small after aggregate modulus reached certain value. This meant that the contribution of aggregate to dynamic modulus improvement is limited at low frequency, given the fixed portion of aggregate. The reason for this phenomenon is that the dynamic modulus of asphalt mixture is usually controlled by the softest constituent (asphalt binder), not by aggregate. In practice, use of stiffer aggregate may not effectively increase the dynamic modulus of HMA mixtures.

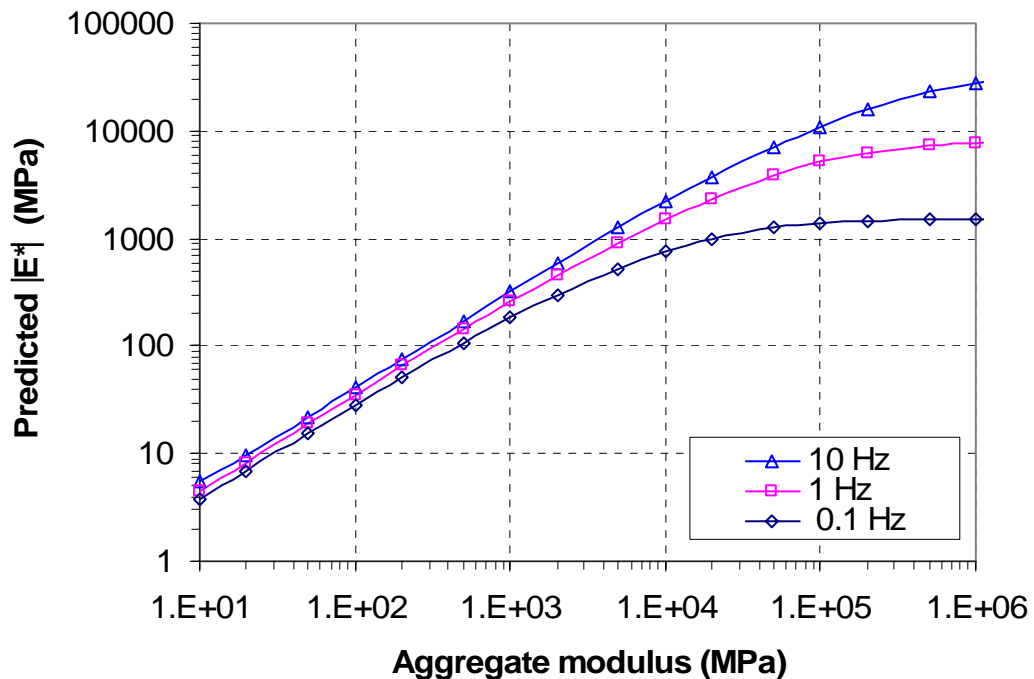


Figure 7.33 Effect of Aggregate Modulus

Effect of Asphalt Content

Asphalt content plays an important role in the dynamic modulus of HMA mixtures. Figure 7.34 shows that higher asphalt content would result in a lower dynamic modulus of HMA mixtures. On the other hand, too much asphalt would overlubricate the HMA mixture and subsequently increase the permanent deformation of flexible pavements. One effective way to obtain a higher dynamic modulus would be to keep asphalt content at low level.

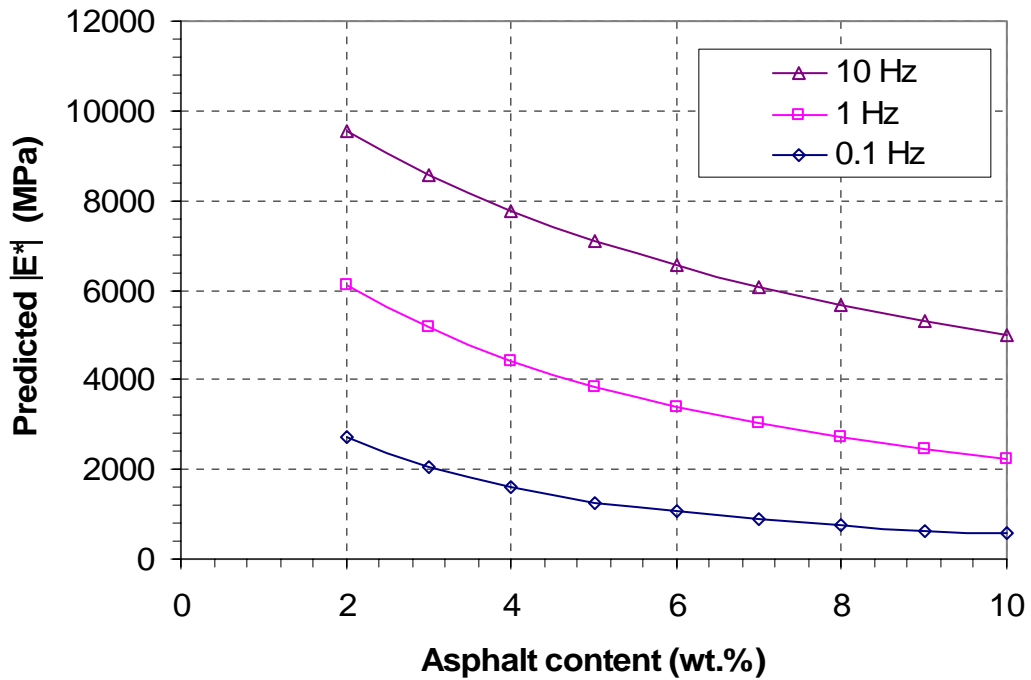
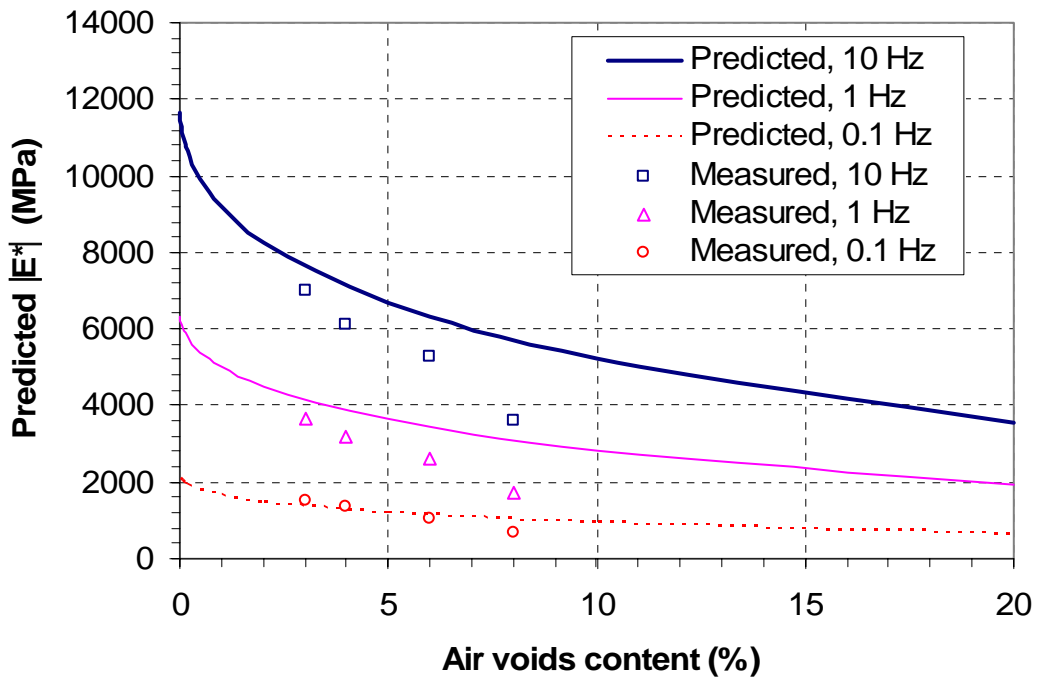


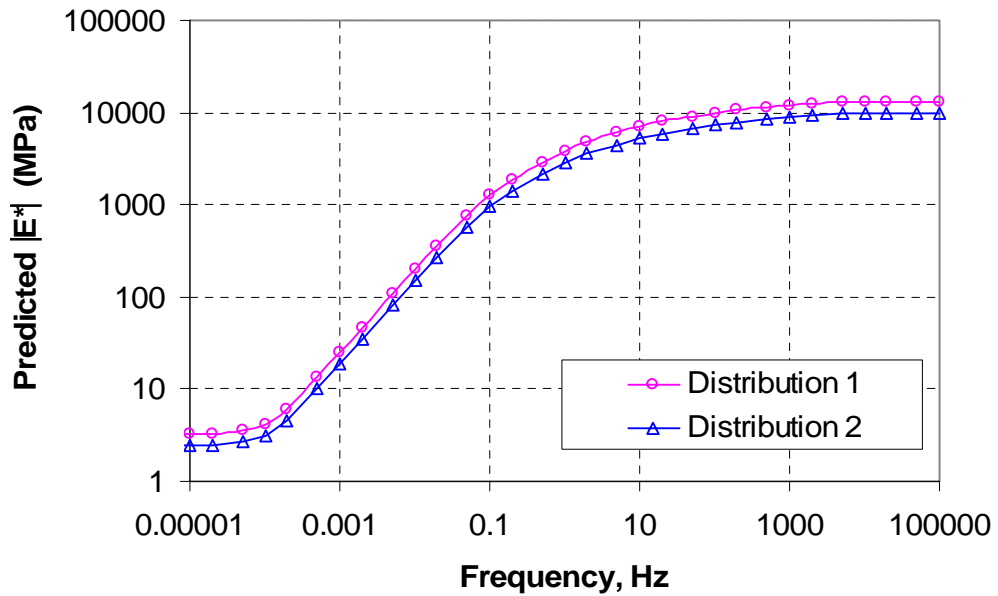
Figure 7.34 Effect of Asphalt Content

Effect of Air Voids

As previously mentioned, air voids content, as well as air voids size distribution, plays an important role in the dynamic modulus of HMA mixtures. The effects of air voids content and size distribution are shown in Figure 7.35. It was obvious from Figure 7.35(a) that higher air voids content resulted in lower dynamic modulus of HMA mixtures. Since Distribution 2 is more coarse than Distribution 1 (Figure 7.31), Figure 7.35(b) showed that HMA mixture with coarser air voids size distribution exhibited a lower dynamic modulus than with fine distribution. In other words, larger air bubbles entrapped in asphalt mixtures did more harm to dynamic modulus than smaller bubbles. Gaining better control of air void content and air voids size distribution provides another effective way to improve the dynamic modulus of HMA mixtures.



(a) Air voids content



(b) Air voids size distribution

Figure 7.35 Effect of Air Voids

CHAPTER 8 SUMMARY, CONCLUSIONS AND RECOMMENDATIONS

Summary

Research Objectives

The primary objective of this study was to develop and apply PFC models to predict the dynamic modulus of HMA mixtures. This included:

- To develop new PFC micromechanical models and modify existing PFC models for predicting the dynamic modulus of asphalt mastic and mixtures;
- To evaluate the newly developed and modified PFC models for HMA mixtures through the comparison between the predicted dynamic moduli with the laboratory measured data;
- To investigate the effects of different factors (such as properties and volumetric fractions of individual constituents) on the dynamic modulus of HMA mixtures.

Development of PFC Models

- Based on the two-dimensional two-layer built-in micromechanical model developed by Li et al. (1999), a three-dimensional two-layered model was developed and closed-form equations were derived to predict dynamic modulus of HMA mixtures.
- Using the differential method, three predictive equations were derived to predict the elastic, shear, and bulk modulus of asphalt mixtures. To convert these three equations for complex (shear or bulk) modulus prediction, special cases were

considered for Poisson's ratios of 0.5 and 0.2. This resulted in totally six predictive models.

- Three representative currently existing PFC models from the Hashin's composite spheres model and Christensen and Lo's generalized self-consistent model, one for bulk modulus and two for shear modulus, were modified and extended to be suitable for predicting dynamic modulus of HMA mixtures.

New Features of Proposed Models

The proposed PFC models in this study, including the newly developed and those modified ones, had the capability of taking into account the particular characteristics of HMA mixtures, i.e., the viscoelastic nature, aggregate gradation, and air voids:

- Using the elastic-viscoelastic correspondence principle, the elastic solution obtained from these models for elastic modulus prediction were converted into the complex domain to predict the dynamic modulus and phase angle of HMA mixtures.
- Using the aggregate gradation to approximately represent the volume fraction distribution of aggregate, the dynamic modulus of HMA mixtures could be calculated by summing the modulus contribution from each portion of aggregate over the whole aggregate gradation.
- Assuming air voids entrapped in HMA mixtures to be a series of spherical air bubbles with different sizes, the effect of air voids content and size distribution were investigated in a manner similar to the one used for aggregate gradation. To obtain the dynamic modulus of HMA mixtures containing air voids, two-step

method was employed. In the first step, the dynamic modulus of HMA mixture with no air voids was predicted with the consideration of aggregate gradation. In the second step, dynamic modulus of HMA mixture containing air voids was calculated with the account of air voids content and size distribution.

Laboratory Testing

Laboratory tests were performed on asphalt binder, mastic, and mixture to acquire the values for input parameters and to obtain the measured dynamic moduli, to which the predicted dynamic modulus and phase angle values of asphalt mastic and mixture from PFC models were compared.

- Asphalt mastic was produced in the laboratory by mixing asphalt binder (PG 64-22) with mineral filler at three volume concentrations (20%, 35%, and 50%). DSR testing was performed on samples from short-term aged asphalt binder and mastic at three temperatures (15°C, 25°C, and 35°C) and at the loading frequency range from 0.01 to 25 Hz to obtain their dynamic shear modulus and phase angle values using the Anton Paar Physica MCR 501 Rheometer. The master curves of dynamic shear modulus at 25°C for asphalt binder and mastic were constructed using the Physica Rheoplus Software.
- HMA mixture samples for dynamic modulus test were cored and cut from SGC-compacted specimens. The test was conducted under no confining pressure at three temperatures of 10°C, 25°C, and 40°C and at the loading frequencies ranging from 0.01Hz to 25Hz using the Simple Performance Tester (SPT). The

master curve of dynamic modulus of HMA mixture at 25°C was constructed manually.

Evaluation of Proposed Models

The applicability of the proposed PFC models to asphalt mastic and HMA mixtures was evaluated by comparing the predicted dynamic modulus and phase angle values with the measured results.

Conclusions

Based on this study, the following conclusions can be drawn:

- Totally, seven new PFC models were developed and three currently available models were modified to predict the dynamic modulus and phase angle of HMA mixtures. Closed-form predictive equations were formulated for these models. These models were capable of taking into account the particular characteristics of HMA mixtures: viscoelastic nature, aggregate gradation, and air voids.
- The procedures developed to incorporate viscoelastic nature, aggregate gradation, and air voids were not limited to these proposed models in this study. They could be used in other PFC models so that these models could be modified to be suitable for prediction of dynamic modulus of HMA mixtures.
- When used to predict the dynamic shear modulus of asphalt mastic, all the models gave reasonable prediction results, using either elastic or viscoelastic method. The prediction results from these two methods did not show much difference in the dynamic shear modulus of asphalt mastic. In practice, the errors caused by use of

elastic instead of viscoelastic model were small for the prediction of dynamic shear modulus of asphalt mastic.

- The predicted dynamic shear moduli of asphalt mastic from all the models were also close to the measured results.
- When used to predict the dynamic modulus of HMA mixtures, the proposed models showed different accuracy in the prediction, regardless of the binder-aggregate system prediction or the mastic-aggregate system prediction used in this study. The difference in the prediction error between the applications of these models to asphalt mastic and HMA mixtures indicated that HMA mixture was a much more complicated composite material than asphalt mastic due to the addition of large aggregate particles.
- In the binder-aggregate system prediction method for HMA mixtures, all the models under-predicted dynamic modulus and over-predicted phase angle to varying degrees. Model 2-1 (the predictive equation for dynamic modulus from the differential method with the assumption of $\nu_m = \nu_i = 0.5$) gave the highest predicted dynamic moduli, which were closest to the measured values. Model 6 (the Hashin's composite spheres model for shear modulus) gave the lowest prediction results, deviating farthest from the measured results.
- Due to the incorporation of aggregate gradation, the mastic-aggregate system method gave improved prediction results for dynamic modulus and phase angle than the binder-aggregate system method. Model 2-1 still gave the highest predicted values and slightly over-predicted the dynamic moduli. Model 1 (the

three-dimensional two-layered model) gave the lowest of the predicted dynamic modulus values, deviating farthest from the measured data. Among all the models, Models 2-2, 3-2, and 4.3, gave the best prediction results of dynamic modulus, especially at higher frequencies.

- In the mastic-aggregate system prediction, Models 2-1, 2-2, 3-1, 3-2 and 4-2 predicted phase angle values lower than measured results at low frequencies, but predicted phase angles higher than measured ones at higher frequencies. The remaining other models over-predicted the phase angle values over the whole frequency range.
- The possible reasons for the under-prediction of dynamic modulus of HMA mixtures by PFC models were explored. The major reason for the discrepancy between predicted and measured results is due to the assumption of spherical shape for aggregate particles. The spherical shape lowered the total surface area and increased the calculated film thickness of asphalt mastic coated around aggregate particles, thus decreasing the dynamic modulus of HMA mixtures. The spherical shape could not provide any aggregate interlocking at all, which was believed to be an important factor affecting the stability of aggregate structure. However, some researchers argued that interlocking does not exist in dense-graded HMA mixtures. The change in the viscoelastic properties of asphalt mastic due to the physico-chemical effect caused by the addition of large aggregates may also be responsible for the discrepancy.

- The sensitivity analysis was performed by changing one of input parameters and keeping others constant. From the sensitivity analysis, the following conclusions can be obtained:
 - Coarse aggregate gradation resulted in high dynamic modulus for dense-graded HMA mixtures.
 - Use of stiff aggregate resulted in high dynamic modulus of HMA mixtures. However, increasing aggregate modulus may not be an effective way to increase the dynamic modulus of HMA mixtures.
 - Use of too much asphalt binder contributed to low dynamic modulus of HMA mixtures. Keeping asphalt content at low level was effective in obtaining high modulus HMA.
 - Both air voids content and air voids size distribution had influence on dynamic modulus of HMA mixtures. Too much air voids and too large air cavity would result in reduced dynamic modulus of HMA mixtures.

Recommendations

This study focuses on developing new and modifying currently existing PFC models so that they can be used to predict the dynamic modulus and phase angle of HMA mixtures. Limited laboratory experiments were performed to evaluate the feasibility of these PFC models to HMA mixtures. Future research work was recommended as follows:

- In general, the prediction results from the PFC models are much better for asphalt mastics than for HMA mixtures. This implies that HMA mixture is far more complicated than asphalt mastic and there are still some more factors that need to

be identified and incorporated in the PFC models. All these models need to be further refined and verified before they can be put into practical use.

- These PFC models have to be evaluated with many more measured dynamic modulus data from various HMA mixtures before they can be put into practical use. Different sources and types of asphalt binder, aggregate should be used to produce HMA mixtures. Different mixing process and compaction type should also be included in future study.
- Although all the PFC micromechanical models are fundamental in characterizing the effective properties of HMA mixtures and they do not need any calibration for the predictive equations, the question still exists as to which model is best suitable for which type of HMA mixture due to the difference in the microstructure of HMA mixtures and the assumptions used in each PFC model.
- The input parameter values for the PFC models need to be refined. The influence and interaction between the constituents of HMA mixtures need to further investigated. The effect of this interaction on the properties of asphalt should be examined. The real material properties of asphalt binder or mastic and the detailed microstructure should be accurately determined to improve the prediction results.
- This study focuses on the analytical approach to the dynamic modulus prediction of HMA mixtures. With the recent advance in digital image processing technique, the numerical modeling method (such as finite element method and discrete element method) provides another promising tool in better understanding and modeling HMA mixtures with the help of digital image process in determining

the internal structure of HMA mixtures. Much research work can be done using the numerical modeling techniques.

REFERENCES

- Andrei, D., Witczak, M. W., and Mirza, M. W. (1999). "Development of a Revised Predictive Model for the Dynamic (Complex) Modulus of Asphalt Mixtures." NCHRP 1-37A Inter Team Report, University of Maryland, College Park, MD.
- Birgisson, B., and Roque, R. (2005a). "Evaluation of Gradation Effect on Dynamic Modulus," *Proc., Annual Meeting*, Transportation Research Board, Washington, D.C.
- Birgisson, B., Sholar, G., and Roque, R. (2005b). "Evaluation of Predicted D Dynamic Modulus for Florida Mixtures," *Proc., Annual Meeting*, Transportation Research Board, Washington, D.C.
- Bonaquist, R. (2003). *Simple Performance Tester for Superpave Mix Design*, Quarterly Progress Report (Appendix B), National Cooperative Highway Research Program (NCHRP) Project 9-29, Sterling, VA.
- Bonnaure, F., Gest, G., Gravois, A., and Uge, P. (1977). "A new method of predicting the stiffness of asphalt paving mixtures." *Proc., Assn. of Asphalt Paving Technologists*, Assn. of Asphalt Paving Technologists, San Antonio, TX, 46, 64–100.
- Buttlar, W. G., Bozkurt, D., Al-Khateeb, G. G., and Waldhoff, A. S. (1999). "Understanding asphalt mastic behavior through micromechanics." *Transportation Research Board 1681*, Transportation Research Board, Washington, D. C., 157-169.
- Buttlar, W. G., and Roque, R. (1996). "Evaluation of empirical and theoretical models to determine asphalt mixtures stiffnesses at low temperature." *J. of Assn. of Asphalt Paving Technologists*, 65, 99 -141.
- Castelblanco, A., Masad, E., and Birgisson, B. (2005). "HMA Moisture Damage as a Function of Air Void Size Distribution, Pore Pressure and Bond Energy." *Proc., Annual Meeting*, Transportation Research Board, Washington, D.C.

- Christensen, D., Pellinen, T., and Bonaquist, R. (2003). "Hirsch Model for estimating the Modulus of Asphalt Concrete." *J. Assoc. Asphalt Paving Technol.*, 72, 97–121.
- Christensen, R. M. (1979). *Mechanics of composite materials*, Wiley, New York.
- Christensen, R.M. (1990). "A critical evaluation for a class of micromechanics models." *J. Mech. Phys. Solids*, 38, 379-404.
- Christensen, R.M., and Lo, K.H. (1979). "Solutions for effective shear properties of three phase sphere and cylinder models." *J. Mech. Phys. Solids*, 27, 315–330.
- Christensen, R.M., and Lo, K.H. (1986). "Erratum: Solutions for effective shear properties of three phase sphere and cylinder models." *J. Mech. Phys. Solids*, 34, 639–639.
- Dongré, R., Myers, L., D'Angelo, J., Paugh, C., and Gudimettla, J. (2005). "Field Evaluation of Witczak and Hirsch Models for Predicting Dynamic Modulus of Hot-Mix Asphalt." *J. Assoc. Asphalt Paving Technol.*, Vol. 74, 381–442.
- Eshelby, J. D. (1957). "The determination of the elastic field of an ellipsoidal inclusion, and related problems." *Proc. R. Soc. London, Ser. A*, 241, 376–396.
- Ferry, J. D. (1980). *Viscoelasticity properties of polymers*, 3rd Ed., Wiley, New York.
- Hansen, T.C. (1965). "Influence of aggregate and voids on modulus of elasticity of concrete, cement mortar, and cement paste." *J. Am. Concr. Inst.*, 62(2), 193–216.
- Hashin, Z. (1962). "The elastic moduli of heterogeneous materials." *J. Appl. Mech.*, 143–150.
- Hashin, Z. (1965). "Viscoelastic behavior of heterogeneous materials." *J. Appl. Mech.*, 630–636.

- Heukelom, Z. and Klomp, A.J.G. (1964). "Road design and dynamic loading." *Proc., Assn. of Asphalt Paving Technologists*, Assn. of Asphalt Paving Technologists, St. Paul, Minn., 33, 92–165.
- Hill, R. (1965). "A self-consistent mechanics of composite materials." *J. Mech. Phys. Solids*, 13, 213–222.
- Hirsch, T. J. (1961). The Effects of the Elastic Moduli of the Cement Paste Matrix and Aggregate on the Modulus of Elasticity of Concrete, Ph. D. Thesis, Agricultural and Mechanical College of Texas (Texas A & M), College Station Texas, January 1961, pp. 105.
- Hirsch, T. J. (1962). "Modulus of elasticity of concrete affected by elastic moduli of cement paste matrix and aggregate." *J. Am. Concr. Inst.*, 59(3), 427–452.
- Huang, B., Li, G., and Mohammad, L. N. (2003). "Analytical Modeling and Experimental Study of Tensile Strength of Asphalt Concrete Composite at Low Temperatures." *Composites Part B: Engineering*, 34(8), 705–714.
- Huang, B., Li, G., Vukosavljevic, D., Shu, X., and Egan, B. K. (2005). "Laboratory Investigation of mixing HMA with RAP." *Transportation Research Record 1929*, Transportation Research Board, Washington, D.C., 37 – 45.
- Huang, B., Shu, X., Li, G., and Chen, L. (2007). "Analytical modeling of three-layered HMA mixtures." *International Journal of Geomechanics*, 7(2), 140 – 148.
- Huang, Y. H (2004). *Pavement Analysis and Design*, 2nd Ed., Pearson Prentice Hall, Upper Saddle River, New Jersey.
- Khanal, P. P. and Mamlouk, M. S. (1995). "Tensile versus compressive moduli of asphalt concrete." *Transportation Research Record 1492*, 144–150.

- Kim, Y., and Little, D. N. (2004). "Linear Viscoelastic Analysis of Asphalt Mastics." *ASCE Journal of Materials in Civil Engineering*, 16(2), 236–241.
- Li, G., Li, Y., Metcalf, J. B., and Pang, S. S. (1999). "Elastic Modulus Prediction of Asphalt Concrete." *ASCE Journal of Materials in Civil Engineering*, 11(3), 236–241.
- Li, Y., and Metcalf, J. B. (2005). "Two-step approach to prediction of asphalt concrete modulus from two-phase micromechanical models." *ASCE Journal of Materials in Civil Engineering*, 17(4), 407–415.
- Lytton, R. (1990). "Materials property relationships for modeling the behavior of asphalt aggregate mixtures in pavements." *International Memorandum, Strategic Highway Research Program*, Washington, D. C.
- Mclaughlin, R. (1977). "A study of the differential scheme for composite materials." *Int. J. Eng. Sci.*, 15, 237–244.
- Mohammad, L. N., Z. Wu, Z., Myers, L., Cooper, S., and Abadie, C. (2005). "A Practical Look at the Simple Performance Tests: Louisiana's Experience," *J. Assoc. Asphalt Paving Technol.*, Vol.74 , 557-600.
- Mori, T., and Tanaka, K. (1973). "Average stress in matrix and average elastic energy of materials with misfitting inclusions." *Acta Metallurgica*, 21(5), 571–574.
- National Cooperative Highway Research Program (2003). *Simple Performance Test for Superpave Mix Design*, NCHRP 9-19, Interim Report, National Research Council.
- National Cooperative Highway Research Program (2004). *Development of the 2002 Guide for the Design of New and Rehabilitated Pavement Structures*, NCHRP 1-37A, Final Report, National Research Council.

- Nemat-Nasser, S. and Hori, M. (1999). *Micromechanics : overall properties of heterogeneous materials*, 2nd Ed., North-Holland, Amsterdam.
- Pal, R. (2005a). “Modeling viscoelastic behavior of particulate composites with high volume of fraction of filler.” *Materials Science & Engineering A*, 412(1-2), 71–77.
- Pal, R. (2005b). “New models for effective Young’s modulus of particulate composites.” *Composites Part B: Engineering*, 36, 513–523.
- Papazian, H. S. (1962). “The response of linear viscoelastic materials in the frequency domain with emphasis on asphaltic concrete.” (1st) International Conference on the Structural Design of Asphalt Pavements, 454–463.
- Park, S. W. and Kim, Y. R. (2001). “Fitting Prony-Series Viscoelastic Models with Power-Law Presmoothing.” *ASCE Journal of Materials in Civil Engineering*, 13(1), 26–32.
- Park, S. W. and Schapery, R. A. (1999). “Methods of interconversion between linear viscoelastic material functions. Part I-A numerical method based on Prony series.” *Int. J. Solids and Struct.*, 36(11), 1653–1675.
- Paul, B. (1960). “Prediction of elastic constants of multiphase materials.” *Trans. ASME*, 218, 36–48.
- Roberts, F.L., Kandhal, P. S., Brown, E. R., Lee, D. Y., and Kennedy, T. W. (1996). *Hot mix asphalt materials, mixture design, and construction*, 2nd Ed., NAPA Education Foundation, Lanham, MD.
- Roque, R., Hiltunen, D. R., Buttlar, W. G., and Farwana, T. (1994). “Development of the SHRP SUPERPAVE™ mixture specification test method to control thermal

- cracking performance of pavements.” *Proc., Symp. On Engineering Properties of Asphalt Mixtures and Relation to Performance*, ASTM, West Conshohocken, Pa.
- Schwartz, C. W. (2005). “Evaluation of the Witczak Dynamic Modulus Prediction Model,” *Proc., Annual Meeting*, Transportation Research Board, Washington, D.C.
- Shashidhar, N., and Romero, P. (1998). “Factors affecting the stiffening potential of mineral fillers.” *Transportation Research Record*. 1638, Transportation Research Board, Washington, D.C., 94-100.
- Shashidhar, N., and Shenoy, A. (2002). “On using micromechanical models to describe dynamic mechanical behavior of asphalt mastics.” *Mech. Mater.*, 34, 657-669.
- Tschoegl, N. W. (1989). *The phenomenological theory of linear viscoelastic behavior*, Springer, Berlin.
- Timoshenko, P.S., and Goodier, J. N. (1970). *Theory of elasticity*, 3rd Ed., McGraw-Hill, New York.
- van der Poel. (1954). “A General System Describing the Viscoelastic Properties of Bitumens and Its Relation to Routine Test Data.” *J. Appl. Chem.*, 4, 221–236.
- Waterloo Maple Inc. (2006). Maple 10 [Computer Software]. <http://www.maplesoft.com/>. Accessed October 15, 2006.
- Witczak, M. W. and Root, R. E. (1974). “Summary of complex modulus laboratory test procedures and results.” *STP 561*, American Society for Testing and Materials, 67–94.
- Young, J.F., Mindess, S. Gray, R.J., and Bentur, A. (1998). *The Science and Technology of Civil Engineering Materials*, Prentice Hall, Upper Saddle River, New Jersey.

Zhou, F.P., Lydon, F. D., and Barr, B.I.G. (1995). "Effect of Coarse Aggregate on Elastic Modulus and Compressive Strength of High Performance Concrete." *Cement and Concrete Res.*, 20, 177–186.

APPENDICES

**APPENDIX A TEST DATA FOR MASTER CURVE OF ASPHALT BINDER
AND MASTIC**

$c = 0$

Temperature [°C]	Frequency [Hz]	Phase Angle [°]	Dynamic Modulus [Pa]	Storage Modulus [Pa]	Loss Modulus [Pa]
25	0.00170	79.8	8.55E+03	1.52E+03	8.42E+03
25	0.00221	79.0	1.10E+04	2.09E+03	1.08E+04
25	0.00288	78.2	1.41E+04	2.87E+03	1.38E+04
25	0.00375	77.4	1.80E+04	3.92E+03	1.76E+04
25	0.00488	76.6	2.30E+04	5.33E+03	2.24E+04
25	0.00635	75.8	2.93E+04	7.19E+03	2.84E+04
25	0.00827	75.0	3.72E+04	9.66E+03	3.59E+04
25	0.0108	74.1	4.73E+04	1.29E+04	4.55E+04
25	0.0140	73.3	5.99E+04	1.72E+04	5.74E+04
25	0.0183	72.5	7.58E+04	2.28E+04	7.22E+04
25	0.0238	72.6	1.04E+05	3.11E+04	9.89E+04
25	0.0310	70.9	1.20E+05	3.91E+04	1.13E+05
25	0.0404	71.3	1.60E+05	5.13E+04	1.51E+05
25	0.0526	69.5	1.86E+05	6.53E+04	1.75E+05
25	0.0685	69.9	2.43E+05	8.33E+04	2.28E+05
25	0.0892	68.1	2.85E+05	1.06E+05	2.65E+05
25	0.116	68.6	3.65E+05	1.33E+05	3.40E+05
25	0.151	66.7	4.30E+05	1.70E+05	3.95E+05
25	0.197	67.3	5.39E+05	2.08E+05	4.97E+05
25	0.257	65.1	6.40E+05	2.69E+05	5.80E+05
25	0.334	62.9	7.72E+05	3.52E+05	6.87E+05
25	0.435	63.6	9.39E+05	4.18E+05	8.41E+05
25	0.567	61.1	1.14E+06	5.50E+05	9.97E+05
25	0.739	62.0	1.45E+06	6.82E+05	1.28E+06
25	0.962	58.6	1.66E+06	8.63E+05	1.41E+06
25	1.25	60.3	2.05E+06	1.02E+06	1.78E+06
25	1.63	56.3	2.38E+06	1.32E+06	1.98E+06
25	2.12	58.9	2.84E+06	1.47E+06	2.43E+06
25	2.77	58.5	3.26E+06	1.70E+06	2.78E+06
25	3.60	57.6	3.85E+06	2.06E+06	3.25E+06
25	4.69	56.6	4.47E+06	2.46E+06	3.73E+06
25	6.11	55.3	5.33E+06	3.03E+06	4.38E+06
25	7.96	54.6	6.07E+06	3.52E+06	4.94E+06
25	10.4	53.3	7.24E+06	4.33E+06	5.81E+06
25	13.5	52.5	8.15E+06	4.96E+06	6.47E+06
25	17.6	51.4	9.71E+06	6.05E+06	7.59E+06
25	22.9	50.5	1.08E+07	6.89E+06	8.34E+06
25	29.8	49.0	1.29E+07	8.48E+06	9.74E+06
25	38.9	48.3	1.42E+07	9.45E+06	1.06E+07
25	50.6	47.3	1.62E+07	1.10E+07	1.19E+07
25	65.9	46.3	1.85E+07	1.28E+07	1.34E+07
25	85.8	45.2	2.11E+07	1.48E+07	1.50E+07
25	112	44.2	2.39E+07	1.72E+07	1.67E+07
25	146	43.1	2.71E+07	1.98E+07	1.85E+07
25	190	42.1	3.06E+07	2.27E+07	2.05E+07
25	247	41.0	3.45E+07	2.60E+07	2.26E+07
25	322	39.9	3.88E+07	2.98E+07	2.49E+07
25	419	38.8	4.36E+07	3.40E+07	2.73E+07
25	546	37.6	4.90E+07	3.88E+07	2.99E+07
25	711	36.4	5.49E+07	4.42E+07	3.26E+07

$c = 20\%$

Temperature [°C]	Frequency [Hz]	Phase Angle [°]	Dynamic Modulus [Pa]	Storage Modulus [Pa]	Loss Modulus [Pa]
25	0.00182	80.1	1.80E+04	3.10E+03	1.77E+04
25	0.00236	79.3	2.28E+04	4.23E+03	2.24E+04
25	0.00307	78.5	2.90E+04	5.77E+03	2.84E+04
25	0.00399	77.7	3.68E+04	7.83E+03	3.60E+04
25	0.00518	76.9	4.68E+04	1.06E+04	4.55E+04
25	0.00672	76.1	5.91E+04	1.42E+04	5.74E+04
25	0.00873	75.3	7.46E+04	1.89E+04	7.22E+04
25	0.0113	74.5	9.41E+04	2.51E+04	9.07E+04
25	0.0147	73.8	1.18E+05	3.31E+04	1.14E+05
25	0.0191	73.0	1.48E+05	4.35E+04	1.42E+05
25	0.0248	72.8	2.01E+05	5.97E+04	1.92E+05
25	0.0322	71.5	2.35E+05	7.44E+04	2.23E+05
25	0.0418	71.4	3.10E+05	9.90E+04	2.94E+05
25	0.0543	69.9	3.58E+05	1.23E+05	3.36E+05
25	0.0705	70.1	4.69E+05	1.60E+05	4.41E+05
25	0.0916	68.5	5.45E+05	1.99E+05	5.07E+05
25	0.119	68.8	6.98E+05	2.53E+05	6.51E+05
25	0.154	67.0	8.20E+05	3.20E+05	7.55E+05
25	0.201	67.4	1.03E+06	3.96E+05	9.52E+05
25	0.260	65.5	1.22E+06	5.07E+05	1.11E+06
25	0.338	65.3	1.50E+06	6.26E+05	1.36E+06
25	0.439	63.8	1.79E+06	7.93E+05	1.61E+06
25	0.570	61.8	2.17E+06	1.03E+06	1.91E+06
25	0.740	62.4	2.77E+06	1.28E+06	2.45E+06
25	0.961	58.5	3.16E+06	1.65E+06	2.70E+06
25	1.25	60.9	3.89E+06	1.89E+06	3.40E+06
25	1.62	55.8	4.58E+06	2.57E+06	3.78E+06
25	2.10	59.4	5.37E+06	2.74E+06	4.62E+06
25	2.73	58.4	6.24E+06	3.27E+06	5.32E+06
25	3.55	57.3	7.36E+06	3.97E+06	6.20E+06
25	4.61	56.4	8.58E+06	4.75E+06	7.14E+06
25	5.98	55.2	1.01E+07	5.79E+06	8.31E+06
25	7.77	54.3	1.16E+07	6.78E+06	9.43E+06
25	10.1	53.0	1.38E+07	8.29E+06	1.10E+07
25	13.1	52.1	1.56E+07	9.59E+06	1.23E+07
25	17.0	50.7	1.84E+07	1.17E+07	1.43E+07
25	22.1	49.8	2.07E+07	1.34E+07	1.58E+07
25	28.7	48.3	2.44E+07	1.62E+07	1.82E+07
25	37.3	47.5	2.71E+07	1.83E+07	2.00E+07
25	48.4	46.5	3.09E+07	2.13E+07	2.24E+07
25	62.8	45.4	3.52E+07	2.47E+07	2.51E+07
25	81.6	44.3	3.99E+07	2.86E+07	2.79E+07
25	106	43.1	4.52E+07	3.30E+07	3.09E+07
25	138	42.0	5.10E+07	3.79E+07	3.42E+07
25	179	40.9	5.74E+07	4.34E+07	3.76E+07
25	232	39.8	6.45E+07	4.95E+07	4.13E+07
25	301	38.7	7.21E+07	5.63E+07	4.50E+07
25	391	37.5	8.06E+07	6.39E+07	4.91E+07
25	508	36.4	8.97E+07	7.22E+07	5.32E+07
25	659	35.2	9.97E+07	8.15E+07	5.76E+07

$c = 35\%$

Temperature [°C]	Frequency [Hz]	Phase Angle [°]	Dynamic Modulus [Pa]	Storage Modulus [Pa]	Loss Modulus [Pa]
25	0.00207	80.8	3.39E+04	5.42E+03	3.35E+04
25	0.00268	80.2	4.29E+04	7.29E+03	4.23E+04
25	0.00348	79.6	5.44E+04	9.81E+03	5.35E+04
25	0.00452	79.0	6.91E+04	1.32E+04	6.78E+04
25	0.00587	78.3	8.77E+04	1.77E+04	8.58E+04
25	0.00762	77.6	1.11E+05	2.37E+04	1.08E+05
25	0.0099	76.9	1.40E+05	3.16E+04	1.36E+05
25	0.0128	76.2	1.76E+05	4.20E+04	1.71E+05
25	0.0167	75.5	2.22E+05	5.54E+04	2.15E+05
25	0.0217	74.8	2.78E+05	7.30E+04	2.69E+05
25	0.0281	74.2	3.93E+05	1.07E+05	3.78E+05
25	0.0365	73.3	4.38E+05	1.26E+05	4.19E+05
25	0.0474	73.0	6.07E+05	1.78E+05	5.81E+05
25	0.0616	71.9	6.78E+05	2.11E+05	6.45E+05
25	0.0799	71.6	9.03E+05	2.85E+05	8.57E+05
25	0.104	70.4	1.05E+06	3.50E+05	9.86E+05
25	0.135	70.0	1.32E+06	4.53E+05	1.24E+06
25	0.175	69.0	1.58E+06	5.66E+05	1.47E+06
25	0.227	68.2	1.94E+06	7.21E+05	1.80E+06
25	0.295	67.5	2.35E+06	9.01E+05	2.17E+06
25	0.383	66.1	2.87E+06	1.16E+06	2.62E+06
25	0.497	65.9	3.46E+06	1.41E+06	3.16E+06
25	0.646	63.5	4.24E+06	1.89E+06	3.79E+06
25	0.838	64.3	5.01E+06	2.17E+06	4.52E+06
25	1.09	61.0	6.19E+06	3.00E+06	5.41E+06
25	1.41	62.7	7.23E+06	3.32E+06	6.42E+06
25	1.83	58.7	8.89E+06	4.62E+06	7.59E+06
25	2.38	60.7	1.04E+07	5.11E+06	9.10E+06
25	3.09	59.5	1.22E+07	6.17E+06	1.05E+07
25	4.02	58.7	1.43E+07	7.43E+06	1.22E+07
25	5.22	57.3	1.68E+07	9.08E+06	1.41E+07
25	6.77	56.4	1.96E+07	1.09E+07	1.64E+07
25	8.79	54.8	2.31E+07	1.33E+07	1.89E+07
25	11.4	53.9	2.68E+07	1.58E+07	2.16E+07
25	14.8	52.1	3.15E+07	1.93E+07	2.48E+07
25	19.2	51.2	3.62E+07	2.27E+07	2.82E+07
25	25.0	49.1	4.25E+07	2.79E+07	3.21E+07
25	32.4	49.2	4.76E+07	3.11E+07	3.60E+07
25	42.1	47.9	5.47E+07	3.67E+07	4.06E+07
25	54.7	46.6	6.25E+07	4.30E+07	4.54E+07
25	71.0	45.2	7.14E+07	5.02E+07	5.07E+07
25	92.2	43.9	8.10E+07	5.83E+07	5.62E+07
25	120	42.6	9.17E+07	6.75E+07	6.20E+07
25	155	41.2	1.03E+08	7.78E+07	6.81E+07
25	202	39.8	1.16E+08	8.93E+07	7.45E+07
25	262	38.5	1.30E+08	1.02E+08	8.11E+07
25	340	37.1	1.46E+08	1.16E+08	8.78E+07
25	442	35.7	1.62E+08	1.32E+08	9.48E+07
25	574	34.3	1.80E+08	1.49E+08	1.01E+08
25	745	32.9	2.00E+08	1.68E+08	1.08E+08

$c = 50\%$

Temperature [°C]	Frequency [Hz]	Phase Angle [°]	Complex Modulus [Pa]	Storage Modulus [Pa]	Loss Modulus [Pa]
25	0.00161	80.0	4.92E+04	8.51E+03	4.85E+04
25	0.00210	79.9	6.19E+04	1.09E+04	6.09E+04
25	0.00274	79.7	7.79E+04	1.40E+04	7.66E+04
25	0.00357	79.4	9.81E+04	1.81E+04	9.64E+04
25	0.00466	79.0	1.24E+05	2.36E+04	1.21E+05
25	0.00607	78.6	1.56E+05	3.09E+04	1.53E+05
25	0.00792	78.1	1.97E+05	4.06E+04	1.93E+05
25	0.0103	77.6	2.49E+05	5.35E+04	2.44E+05
25	0.0135	77.0	3.14E+05	7.05E+04	3.06E+05
25	0.0176	76.4	3.96E+05	9.28E+04	3.85E+05
25	0.0229	75.8	4.97E+05	1.22E+05	4.82E+05
25	0.0299	74.8	6.96E+05	1.82E+05	6.72E+05
25	0.0390	74.3	8.19E+05	2.22E+05	7.88E+05
25	0.0509	73.7	1.06E+06	2.98E+05	1.02E+06
25	0.0664	73.0	1.25E+06	3.64E+05	1.19E+06
25	0.0865	72.6	1.58E+06	4.72E+05	1.51E+06
25	0.113	71.7	1.89E+06	5.95E+05	1.80E+06
25	0.147	71.3	2.37E+06	7.57E+05	2.24E+06
25	0.192	70.1	2.88E+06	9.80E+05	2.70E+06
25	0.251	69.8	3.54E+06	1.22E+06	3.32E+06
25	0.327	69.2	4.31E+06	1.53E+06	4.03E+06
25	0.426	68.0	5.30E+06	1.99E+06	4.91E+06
25	0.556	67.8	6.37E+06	2.40E+06	5.89E+06
25	0.725	65.9	7.88E+06	3.21E+06	7.19E+06
25	0.946	65.5	1.01E+07	4.17E+06	9.14E+06
25	1.23	63.7	1.18E+07	5.21E+06	1.06E+07
25	1.61	64.1	1.40E+07	6.13E+06	1.26E+07
25	2.10	63.1	1.64E+07	7.44E+06	1.46E+07
25	2.74	62.0	1.99E+07	9.33E+06	1.76E+07
25	3.57	60.7	2.34E+07	1.14E+07	2.04E+07
25	4.66	59.6	2.80E+07	1.42E+07	2.42E+07
25	6.07	58.9	3.32E+07	1.71E+07	2.84E+07
25	7.92	56.9	3.91E+07	2.14E+07	3.27E+07
25	10.3	56.1	4.60E+07	2.57E+07	3.82E+07
25	13.5	53.6	5.42E+07	3.21E+07	4.36E+07
25	17.6	52.7	6.32E+07	3.83E+07	5.02E+07
25	22.9	49.8	7.45E+07	4.81E+07	5.68E+07
25	29.9	50.4	8.47E+07	5.40E+07	6.52E+07
25	39.0	48.9	9.80E+07	6.44E+07	7.39E+07
25	50.9	47.3	1.13E+08	7.63E+07	8.29E+07
25	66.4	45.8	1.30E+08	9.03E+07	9.28E+07
25	86.6	44.1	1.48E+08	1.06E+08	1.03E+08
25	113	42.4	1.68E+08	1.24E+08	1.13E+08
25	147	40.6	1.91E+08	1.45E+08	1.24E+08
25	192	38.9	2.15E+08	1.67E+08	1.35E+08
25	251	37.1	2.42E+08	1.93E+08	1.46E+08
25	327	35.3	2.70E+08	2.20E+08	1.56E+08
25	426	33.5	3.01E+08	2.51E+08	1.66E+08
25	556	31.7	3.34E+08	2.84E+08	1.75E+08
25	725	29.9	3.69E+08	3.20E+08	1.84E+08

APPENDIX B TEST DATA FOR MASTER CURVE OF HMA MIXTURE

Air voids = 2.78%

Temperature [°C]	Frequency [Hz]	Phase Angle [°]	Dynamic Modulus [Pa]
25	2500	10.7	1.76E+10
25	2000	11.1	1.71E+10
25	1000	12.3	1.57E+10
25	500	13.6	1.42E+10
25	200	15.5	1.24E+10
25	100	17.1	1.10E+10
25	50	18.9	9.70E+09
25	25	22.0	8.63E+09
25	20	21.3	8.05E+09
25	20	22.5	8.23E+09
25	10	23.1	6.94E+09
25	10	24.4	7.01E+09
25	5	26.4	5.90E+09
25	2	29.0	4.57E+09
25	1	29.3	3.88E+09
25	1	30.9	3.67E+09
25	0.5	32.5	2.88E+09
25	0.4625	29.9	3.18E+09
25	0.37	30.7	2.88E+09
25	0.2	34.2	2.02E+09
25	0.185	32.0	2.18E+09
25	0.1	35.0	1.52E+09
25	0.0925	33.3	1.60E+09
25	0.037	34.8	1.01E+09
25	0.0185	35.9	6.83E+08
25	0.01	35.5	5.55E+08
25	0.00925	36.2	4.79E+08
25	0.0037	36.4	2.95E+08
25	0.00185	36.4	2.06E+08
25	0.000185	33.9	7.51E+07

Air voids = 3.91%

Temperature [°C]	Frequency [Hz]	Phase Angle [°]	Dynamic Modulus [Pa]
25	500	14.3	1.26E+10
25	400	14.8	1.22E+10
25	200	16.3	1.09E+10
25	100	17.8	9.70E+09
25	40	20.0	8.15E+09
25	25	22.3	7.55E+09
25	20	21.8	7.08E+09
25	20	22.9	7.19E+09
25	10	23.5	6.06E+09
25	10	24.8	6.11E+09
25	5	26.7	5.10E+09
25	4	25.9	4.83E+09
25	2	27.5	4.01E+09
25	2	29.3	3.94E+09
25	1.625	31.1	4.03E+09
25	1.3	31.4	3.77E+09
25	1	31.0	3.17E+09
25	0.65	32.9	3.02E+09
25	0.5	32.5	2.52E+09
25	0.325	34.2	2.34E+09
25	0.2	32.7	1.87E+09
25	0.2	34.2	1.79E+09
25	0.13	35.6	1.60E+09
25	0.1	35.1	1.36E+09
25	0.065	36.7	1.16E+09
25	0.0325	36.8	8.35E+08
25	0.013	36.8	5.31E+08
25	0.01	36.5	4.87E+08
25	0.0065	36.6	3.74E+08
25	0.00065	33.5	1.32E+08

Air voids = 5.74%

Temperature [°C]	Frequency [Hz]	Phase Angle [°]	Dynamic Modulus [Pa]
25	875	12.7	1.18E+10
25	700	13.1	1.14E+10
25	350	14.6	1.03E+10
25	175	16.1	9.28E+09
25	70	18.4	7.92E+09
25	35	20.4	6.92E+09
25	25	23.5	6.58E+09
25	20	24.1	6.27E+09
25	17.5	22.4	5.98E+09
25	10	26.1	5.29E+09
25	7	25.2	4.82E+09
25	5	28.1	4.40E+09
25	3.5	27.2	4.05E+09
25	2	30.6	3.33E+09
25	1	32.4	2.63E+09
25	0.5	33.8	2.04E+09
25	0.5	35.3	2.29E+09
25	0.4	36.5	2.04E+09
25	0.35	33.8	1.88E+09
25	0.2	35.3	1.41E+09
25	0.2	37.2	1.53E+09
25	0.1	36.1	1.05E+09
25	0.1	38.1	1.09E+09
25	0.04	38.7	6.95E+08
25	0.02	39.5	4.69E+08
25	0.01	36.4	3.63E+08
25	0.01	39.1	3.29E+08
25	0.004	38.9	2.00E+08
25	0.002	38.9	1.37E+08
25	0.0002	35.7	4.74E+07

Air voids = 7.91%

Temperature [°C]	Frequency [Hz]	Phase Angle [°]	Dynamic Modulus [Pa]
25	1250	14.7	9.57E+09
25	1000	15.1	9.23E+09
25	500	16.6	8.26E+09
25	250	18.4	7.32E+09
25	100	20.9	6.14E+09
25	50	22.8	5.30E+09
25	25	24.8	4.51E+09
25	25	25.4	4.59E+09
25	20	26.1	4.33E+09
25	10	27.4	3.57E+09
25	10	28.0	3.59E+09
25	5	29.2	2.95E+09
25	5	30.1	2.94E+09
25	2	32.5	2.19E+09
25	1	34.0	1.71E+09
25	0.5	35.1	1.35E+09
25	0.5	35.1	1.32E+09
25	0.5	36.0	1.53E+09
25	0.4	37.5	1.35E+09
25	0.2	35.9	9.14E+08
25	0.2	37.5	1.01E+09
25	0.1	36.1	6.87E+08
25	0.1	37.6	7.33E+08
25	0.04	37.9	4.66E+08
25	0.02	38.0	3.25E+08
25	0.01	35.7	2.50E+08
25	0.01	37.4	2.32E+08
25	0.004	37.3	1.45E+08
25	0.002	39.7	9.97E+07
25	0.0002	24.9	4.18E+07

**APPENDIX C EXAMPLES OF COMPUTER PROGRAM FOR PREDICTION
OF DYNAMIC (SHEAR) MODULI OF ASPHALT MASTIC AND HMA
MIXTURE**

Computer Program Example 1: Model 1 for prediction of dynamic shear modulus of asphalt mastic with the viscoelastic method

```

#Define the coefficients of Prony Series
rou:=Array([0.0001,0.001,0.01,0.1,1,10,100]):
E:=Array([76008149,22764192,8418004,1688698,275211.7,18910.2,445.1214]):
Ee:=1000:
#Define the Carson Transform
fEstar:=s->Ee+(s*rou[1]*E[1])/(s*rou[1]+1)+(s*rou[2]*E[2])/(s*rou[2]+1)+(s*rou[3]*E
[3])/(s*rou[3]+1)+(s*rou[4]*E[4])/(s*rou[4]+1)+(s*rou[5]*E[5])/(s*rou[5]+1)+(s*rou[6]
*E[6])/(s*rou[6]+1)+(s*rou[7]*E[7])/(s*rou[7]+1):

Fmax:=31: #Number of loading frequencies
Freq:=Array([0.00001,0.00002,0.00005,0.0001,0.0002,0.0005,0.001,0.002,0.005,0.01,0.0
2,0.05,0.1,0.2,0.5,1,2,5,10,20,50,100,200,500,1000,2000,5000,10000,20000,50000,10000
0]):

E2:=50000:      #Modulus of aggregate, in MPa
V1:=0.4:        #Poisson's ratio of pure asphalt cement,
V2:=0.2:        #Poisson's ratio of mineral filler,
V0:=0.3:        #Poisson's ratio of asphalt mastic,

# Define the complex shear modulus of pure asphalt binder
for i from 1 to Fmax do
Estar_as[i]:=evalf(fEstar(2*Pi*Freq[i]*I)/10^6): #10^6,Unit Changed to MPa
end do:

# Convert from G to E for pure binder
for i from 1 to Fmax do
Estar_as[i]:=Estar_as[i]*2*(1+V1):
end do:

# Calculate the complex shear modulus of mastic
ETA:=0.50:      #ETA = n = volume concentration
x1:=0.5*ETA*(1+V1)+(1-2*V1):
x2:=0.5*(1+V1)+ETA*(1-2*V1):

for i from 1 to Fmax do
E0[i]:=evalf(Estar_as[i]*(1-ETA)*(1-2*V0)/(x1-9*E2*ETA*(1-V1)*(1-
V1)/(Estar_as[i]*(1-ETA)*(4-8*V2)+4*E2*x2)):
end do:

# Convert from E to G for mastic
for i from 1 to Fmax do
E0[i]:=E0[i]/2/(1+V0):

```

```
end do:

# Print the complex G of mastic
for i from 1 to Fmax do
xmod[i]:=Re(E0[i]):
ymod[i]:=Im(E0[i]):
rmod[i]:=abs(E0[i]):
end do:
for i from 1 to Fmax do
xmod[i];
end do;
for i from 1 to Fmax do
ymod[i];
end do;
for i from 1 to Fmax do
rmod[i];
end do;
```

Computer Program Example 2: Model 1 for prediction of dynamic modulus of HMA mixture with mastic-aggregate system method

```
#First Time Equivalence
#Define aggregate gradation
No_of_sieve:=9:          #Number of Sieves
Size_of_sieve:=Array([16,12.5,9.5,4.75,2.36,0.6,0.3,0.15,0.075]):
Percent_passing_sieve:=Array([100,98.5,85,58.85,42.45,19.65,10.2,6.45,4.65]):

#Number of division btw neighboring sieve or size for refinery of gradation of aggregate
and air void distribution
Nmax:=10:

#Refine the aggregate gradation
for i from 1 to No_of_sieve-1 do
  Size1[i][Nmax+1]:=Size_of_sieve[i]:
  Size1[i][1]:=Size_of_sieve[i+1]:
  Percent1[i][Nmax+1]:=Percent_passing_sieve[i]:
  Percent1[i][1]:=Percent_passing_sieve[i+1]:
end do:
for i from 1 to No_of_sieve-1 do
  delta_size:=(Size1[i][Nmax+1]-Size1[i][1])/Nmax:
  delta_percent:=(Percent1[i][Nmax+1]-Percent1[i][1])/Nmax:
  for j from 2 to Nmax do
    Size1[i][j]:=Size1[i][1]+(j-1)*delta_size:
    Percent1[i][j]:=Percent1[i][1]+(j-1)*delta_percent:
  end do:
end do:

#Input the volume fractions of different phases
f3_in:=0.04:          #Air voids
f1_in:=0.12:         #Volume fraction of asphalt
f2_in:=1-f3_in-f1_in: #volume fraction of aggregate

#Recalcualte the volume fractions of different phases
f3:=f3_in:           #Volume fraction of air voids
f1:=f1_in+f2_in*Percent_passing_sieve[No_of_sieve]/100: #Volume fraction of mastic
f2:=1-f3-f1:        #volume fraction of aggregate

#Define function calculating asphalt film thickness
a0:=0:
a1:=0:
a2:=0:
a3:=0:
for i from 1 to No_of_sieve-1 do
```

```

for j from 1 to Nmax do
  a0:=a0+(Percent1[i][j+1]-Percent1[i][j]):
  a1:=a1+3*(Percent1[i][j+1]-Percent1[i][j])/(Size1[i][j]/4+Size1[i][j+1]/4):
  a2:=a2+3*(Percent1[i][j+1]-Percent1[i][j])/(Size1[i][j]/4+Size1[i][j+1]/4)^2:
  a3:=a3+(Percent1[i][j+1]-Percent1[i][j])/(Size1[i][j]/4+Size1[i][j+1]/4)^3:
end do:
end do:
#Function calculating exact thickness
g1:=x->(a0+a1*x+a2*x^2+a3*x^3)/(100-Percent_passing_sieve[No_of_sieve])-(f1+f2)/f2;
sol1:={solve(g1(x)=0,x)}; # Exact thickness
if type(sol1[1],nonreal) then
  if type(sol1[2],nonreal) then
    thickness1:=sol1[3]: # Exact thickness: thickness1
  else
    thickness1:=sol1[2]:
  end if;
else
  thickness1:=sol1[1]:
end if:
thickness1:=thickness1;

#Calculate the modulus corresponding to individual size particle
#Define the coefficients of Prony Series
rou:=Array([0.0001,0.001,0.01,0.1,1,10,100]):
E:=Array([171755261,58814471,20880482,3990591.3,633802.82,41138.916,3565.1405]):
Ee:=1667:
#Define the Carson Transform
fEstar:=s->Ee+(s*rou[1]*E[1])/(s*rou[1]+1)+(s*rou[2]*E[2])/(s*rou[2]+1)+(s*rou[3]*E[3])/(s*rou[3]+1)+(s*rou[4]*E[4])/(s*rou[4]+1)+(s*rou[5]*E[5])/(s*rou[5]+1)+(s*rou[6]*E[6])/(s*rou[6]+1)+(s*rou[7]*E[7])/(s*rou[7]+1):

Fmax:=31: #Number of frequencies
Freq:=Array([0.00001,0.00002,0.00005,0.0001,0.0002,0.0005,0.001,0.002,0.005,0.01,0.02,0.05,0.1,0.2,0.5,1,2,5,10,20,50,100,200,500,1000,2000,5000,10000,20000,50000,100000]):

E2:=50000: #Modulus of aggregate, in MPa
V1:=0.3: #Poisson's ratio of asphalt mastic,
V2:=0.2: #Poisson's ratio of aggregate,
V0:=0.25: #Poisson's ratio of Equivalent HMA mixture,

for i from 1 to Fmax do
  Estar_as[i]:=evalf(fEstar(2*Pi*Freq[i]*I)/10^6): #10^6,Unit Changed to MPa

```

```

end do:
for k from 1 to Fmax do
  for i from 1 to No_of_sieve-1 do
    for j from 1 to Nmax+1 do
      ETA:=(Size1[i][j]/2)^3/(Size1[i][j]/2+thickness1)^3: #radius: diameter divided by 2
      x1:=0.5*ETA*(1+V1)+(1-2*V1): # ETA = n in paper
      x2:=0.5*(1+V1)+ETA*(1-2*V1):
      E0[i][j][k]:=evalf(Estar_as[k]*(1-ETA)*(1-2*V0)/(x1-9*E2*ETA*(1-V1)*(1-
V1)/(Estar_as[k]*(1-ETA)*(4-8*V2)+4*E2*x2))):
    end do:
  end do:
total:=0:
  for i from 1 to No_of_sieve-1 do
    for j from 1 to Nmax do
total:=total+evalf((Percent1[i][j+1]-Percent1[i][j])*(E0[i][j][k]+E0[i][j+1][k])/2):
    end do:
  end do:
  Modulus1[k]:=evalf(total/(100-Percent_passing_sieve[No_of_sieve]]):
end do:

```

#Second Time Equivalence

#Air void distribution

No_of_voids:=11:

Size_of_voids:=Array([6,5,4,3,2,2,1.5,1,0.64,0.384,0.256,0.128]):

Percent_passing_voids:=Array([100,99.76,99,96.65,87,76,58,38.4,23.7,15.35,8.74]):

#Refine air void distribution

```
for i from 1 to No_of_voids-1 do
```

```
  Size2[i][Nmax+1]:=Size_of_voids[i]:
```

```
  Size2[i][1]:=Size_of_voids[i+1]:
```

```
  Percent2[i][Nmax+1]:=Percent_passing_voids[i]:
```

```
  Percent2[i][1]:=Percent_passing_voids[i+1]:
```

```
end do:
```

```
for i from 1 to No_of_voids-1 do
```

```
  delta_size:=(Size2[i][Nmax+1]-Size2[i][1])/Nmax:
```

```
  delta_percent:=(Percent2[i][Nmax+1]-Percent2[i][1])/Nmax:
```

```
  for j from 2 to Nmax do
```

```
    Size2[i][j]:=Size2[i][1]+(j-1)*delta_size:
```

```
    Percent2[i][j]:=Percent2[i][1]+(j-1)*delta_percent:
```

```
  end do:
```

```
end do:
```

#Calculate the equivalent thickness around air bubble

F1:=f1+f2: #Volume fraction of equivalent medium #Uppercase letter for the second part calc

```

F2:=f3: #volume fraction of air voids
total:=0:
  for i from 1 to No_of_voids-1 do
    for j from 1 to Nmax do
      total:=total+(Percent2[i][j+1]-Percent2[i][j])/(Size2[i][j]+Size2[i][j+1]):
    end do:
  end do:
total:=total/(100-Percent_passing_voids[No_of_voids]):
thickness_2:=F1/(12*F2*total); #Thickness of equivalent medium

#Define function calculating exact thickness around air bubble
a0:=0:
a1:=0:
a2:=0:
a3:=0:
for i from 1 to No_of_voids-1 do
  for j from 1 to Nmax do
    a0:=a0+(Percent2[i][j+1]-Percent2[i][j]):
    a1:=a1+3*(Percent2[i][j+1]-Percent2[i][j])/(Size2[i][j]/4+Size2[i][j+1]/4):
    a2:=a2+3*(Percent2[i][j+1]-Percent2[i][j])/(Size2[i][j]/4+Size2[i][j+1]/4)^2:
    a3:=a3+(Percent2[i][j+1]-Percent2[i][j])/(Size2[i][j]/4+Size2[i][j+1]/4)^3:
  end do:
end do:
g2:=x->(a0+a1*x+a2*x^2+a3*x^3)/(100-Percent_passing_voids[No_of_voids])-(F1+F2)/F2;
#Function calculating exact thickness
sol2:={solve(g2(x)=0,x)}; # Exact thickness
if type(sol2[1],nonreal) then
  if type(sol2[2],nonreal) then
    thickness2:=sol2[3]:
  else
    thickness2:=sol2[2]:
  end if;
else
  thickness2:=sol2[1]:
end if:
thickness2:=thickness2;

#Calculate the modulus corresponding to individual air bubble
V1:=0.25: #Poisson's ratio for 1st time equivalent HMA mixture,
V0:=0.25: #Poisson's ratio for 2nd time equivalent HMA mixture,
for k from 1 to Fmax do
  for i from 1 to No_of_voids-1 do
    for j from 1 to Nmax+1 do
      ETA:=(Size2[i][j]/2)^3/(Size2[i][j]/2+thickness2)^3:
    end do:
  end do:
end do:

```

```

x1:=0.5*ETA*(1+V1)+(1-2*V1);    # ETA = n in paper
E0[i][j][k]:=evalf(Modulus1[k]*(1-ETA)*(1-2*V0)/x1);
  end do:
  end do:
total:=0:
  for i from 1 to No_of_voids-1 do
    for j from 1 to Nmax do
total:=total+evalf((Percent2[i][j+1]-Percent2[i][j])*(E0[i][j][k]+E0[i][j+1][k])/2):
      end do:
    end do:
Modulus2[k]:=evalf(total/(100-Percent_passing_voids[No_of_voids]));

```

VITA

Xiang Shu was born in China in 1970. He attended Tongji University, Shanghai, China in 1988, where he received his Bachelor's degree in Inorganic and Nonmetallic Materials in 1993, his Master's degree in Inorganic and Nonmetallic Materials in 1996, and his Ph.D. in Geotechnical Engineering in 1999. After almost five years' teaching as a lecturer at Tongji University, he went to the University of Tennessee, Knoxville, in 2004, to pursue his Ph.D. in Civil and Environmental Engineering. He received his Doctor of Philosophy degree in Civil Engineering with concentration in Infrastructure Materials in August, 2007.